Exploring the role of TET family DNA demethylases in hyperglycaemia-induced endothelial dysfunction

Green, Hannah

Awarding institution:
King's College London

Exploring the role of TET family DNA demethylases in hyperglycaemia-induced endothelial dysfunction.

Hannah Louise Hoskins Green

School of Cardiovascular and Metabolic Medicine & Sciences

BHF Centre of Research Excellence

King's College London

December 2022

Submitted for the Degree of Doctor of Philosophy

Supervisors:

Dr Alison C Brewer

Dr Aleksandar Ivetic

Declaration

I declare that I am the sole author of this thesis and that the work contained within it is my own unless otherwise stated.

Hannah Louise Hoskins Green

Abstract

Hyperglycaemia in diabetes mellitus participates in the development of endothelial dysfunction, which typically precedes cardiovascular diseases. This hyperglycaemia-induced endothelial dysfunction may involve epigenetic mechanisms including DNA methylation. Ten-Eleven-Translocation (TET) enzymes catalyse the successive oxidation of 5-methylcytosine during DNA demethylation. TET2 is associated with functions in immune and vascular cells and decreased TET2 activity in hyperglycaemia has been observed in diabetic patient monocytes. However, the role of TETs in endothelial cells (ECs) is not fully understood. It was hypothesised that dysregulation of TET activity in ECs by hyperglycaemia contributes to endothelial dysfunction and impairs vascular function. RNA sequencing showed that TET2 silencing upregulated genes involved in interferon responses and cholesterol biosynthesis in ECs. TET2 silencing impaired the resolution of interferon responses, whilst TET3 silencing dampened their activation. Little overlap was observed between genes dysregulated by TET silencing and by high glucose culture, but intermittent high glucose culture of ECs dysregulated interferon responses in a similar manner to TET2 silencing. Data suggested that TET2-mediated regulation of CH25H expression may link interferon signalling and cholesterol homeostasis in ECs. A cytokine assay revealed increased levels of the interferon-induced T cell chemoattractants CXCL10 and CXCL11 in the supernatant of TET2-silenced ECs compared to controls. A significant decrease in permeability of EC monolayers was also observed in the absence of TET2, but HL-60 cell adhesion to ECs was not affected. To assess vascular function in the absence of endothelial TET2, tension generated by aortae from control and diabetic EC-specific TET2 knockout and wildtype mice was measured in response to vasoactive stimuli. No significant alteration in the control of vascular tone was observed. RNA sequencing was also performed on pulmonary ECs from these mice. Consistent with *in vitro* data, IRF7 and interferon-sensitive genes were upregulated by TET2 knockout, in addition to altered expression of genes associated with leukocyte recruitment. These pathways were similarly dysregulated in diabetic mice. Together, these data provide evidence that TET2 is functionally important in ECs, regulating interferon signalling and cholesterol homeostasis at the transcriptional level, with impacts on permeability and cytokine release. Disruption of these processes could contribute to endothelial dysfunction in vascular disease.

Acknowledgements

Firstly, I would like to thank Dr Alison Brewer for being an exceptional PhD supervisor whose scientific expertise, guidance and belief in me has made this work possible. I am so grateful to have had her support and mentorship throughout this PhD, alongside the freedom to explore my own ideas. I would also like to thank Dr Aleksandar Ivetic, my second supervisor, for his technical advice and discussions which have been incredibly helpful. I am very grateful to the British Heart Foundation for providing the funding to make this research possible.

I extend my thanks to Richard Thompson, Dr Helena Zhang, Dr Min Zhang and Dr Asjad Visnagri for training me in the *in vivo* and *ex vivo* aspects of this project and to the Denmark Hill BSU staff for all their work to facilitate the study.

I have been fortunate to have had so many kind and helpful colleagues, both past and present, during my time here. Thank you to Brewer lab members Dr Nermina Lamadema and Valeria León Kropf for advice and help with experiments and to Tom York, Hashum Sum and Michelle Sebele for contributing qPCR data to this thesis. Thank you to Yue Yang for isolating bone marrow cells for my adhesion assay and Angeliki Ntorla for helping with 5hmC profiles. Thank you to colleagues from the 3rd floor James Black Centre for training and advice, lending me reagents, equipment and protocols and for our fun lunchtimes and socials! Special thanks to Valeria León Kropf, Christina Reumiller and Jie Shen for sharing the PhD journey with me from the start.

Thank you to my friends and communities outside the lab. To Anies, Daisy, Jenny, Katie, Laura, Rebecca and Rowan and friends at St Anne's & St James – thank you for always being there to listen and laugh. To Melissa, Dan and everyone at London City Runners and Project Awesome – running has been a big part of my life outside the PhD and you have been a big part of that, as well as being great friends, for which I'm incredibly grateful.

Finally, and very importantly, a big thank you to my family especially my parents Sue and Rob and my brothers Sam and Dan. From listening to my experiment plans and 'biology facts' to rating my day in the lab out of 10 and PhD-advice-coffee-chats, I'm grateful for all your support.

Table of Contents

Table of figures

Table of tables

Abbreviations

2-HG	2-hydroxyglutarate
2-OG	2-oxoglutarate
25-HC	25-hydroxycholesterol
2OGDDs	2-oxoglutarate dependent dioxygenase
5azaC	5-aza-2'-deoxycytidine
5caC	5-carboxylcytosine
5fC	5-formylcytosine
5hmC	5-hydroxymethylcytosine
5mC	5-methylcytosine
ABCA1	ATP binding cassette subfamily A member 1
ABCG1	ATP binding cassette subfamily G member 1
ACCORD	Action to Control Cardiovascular Risk in Diabetes
ACh	Acetylcholine
ADP	Adenosine diphosphate
ADVANCE	Action in Diabetes and Vascular Disease: Preterax and Diamicron Modified Release Controlled Evaluation
AGE	Advanced glycosylation end products
AMPK	AMP-activated protein kinase
ANOVA	Analysis of variance
ATP	Adenosine triphosphate
BER	Base excision repair
BMDC	Bone marrow derived cells
BSA	Bovine serum albumin
cAMP	Cyclic adenosine monophosphate
Cas9	CRISPR-associated protein 9
cGMP	Cyclic guanosine monophosphate
CH25H	Cholesterol 25-hydroxylase
CRISPR	Clustered regularly interspaced short palindromic repeats
CXCL	Chemokine (C-X-C motif) ligand
DHCR7	7-Dehydrocholesterol Reductase
DNA	Deoxyribonucleic acid
DNMT	DNA methyltransferase
EC	Endothelial cell
EDHF	Endothelium-derived hyperpolarising factor
EGF	Epidermal growth factor
eNOS	endothelial nitric oxide synthase
ESAM	Endothelial cell-selective adhesion molecule
ESC	Embryonic stem cell
ET-1	Endothelin-1
FCS	Fetal calf serum
FGF	Fibroblast growth factor

FITC	Fluorescein isothiocyanate
GAPDH	Glyceraldehyde 3-phosphate dehydrogenase
GAS	Gamma activated sequence
GLUT-1	Glucose transporter 1
GM-CSF	Granulocyte-macrophage colony-stimulating factor
GTP	Guanosine triphosphate
HDAC	Histone deacetylase
HFD	High fat diet
hMeDIPseq	hydroxymethylated DNA immunoprecipitation
HMG-CoA	3-hydroxy-3-methylglutaryl coenzyme A
HMGCR	3-hydroxy-3-methylglutaryl-CoA reductase
HMGCS1	3-hydroxy-3-methylglutaryl-CoA synthase 1
HMOX1	Haemoxygenase 1
HSC	Haematopoietic stem cell
HUVEC	Human umbilical vein endothelial cells
ICAM	Intercellular adhesion molecule
IFIT	Interferon-induced protein with tetratricopeptide repeats
IFITM1	Interferon-induced transmembrane protein 1
IFN	Interferon
IL	Interleukin
IPA	Ingenuity pathway analysis
IRF	Interferon response factor
ISG15	Interferon-stimulated gene 15
ISRE	Interferon-sensitive response element
JAK	Janus kinase
JAM	Junctional adhesion molecule
KLF4	Kruppel-like factor 4
KO	Knockout
LDL	Low density lipoprotein
LFA-1	Lymphocyte function-associated antigen 1
LINE-1	Long interspersed nuclear element
lncRNA	long non-coding RNA
LPS	Lipopolysaccharide
LSS	Lanosterol synthase
Mac-1	Macrophage-1 antigen
MAD5	Melanoma differentiation-associated protein 5
MADCAM1	Mucosal vascular addressin cell adhesion molecule 1
MCP1	Monocyte chemoattractant protein-1
MHC	Major histocompatibility complex
miRNA	microRNA
MLEC	Mouse lung endothelial cells
MMP	Matrix metalloproteinase
MSMO1	Methylsterol monooxygenase 1

MX1	MX Dynamin Like GTPase 1
MYOCD	Myocardin
NAPDH	Nicotinamide adenine dinucleotide phosphate
NFkB	Nuclear factor kappa B
NO	Nitric oxide
NOS	Nitric oxide synthase
NOX	NADPH oxidase
OAS	Oligoadenylate synthetase
PAF	Platelet activating factor
PAI-1	Plasminogen activator inhibitor-1
PAMP	Pathogen associated molecular pattern
PBMC	Peripheral blood mononuclear cell
PDL1	Programmed death ligand 1
PE	Phenylephrine
PHD	Prolyl hydroxylase
PI3K	Phosphoinositide 3-kinase
piRNA	piwi RNA
PKA	Protein kinase A
PKR	Protein kinase R
PRR	Pattern recognition receptor
PSGL-1	P-selectin glycoprotein ligand-1
qPCR	quantitative polymerase chain reaction
RAGE	Receptor for AGEs
RBP4	Retinol binding protein 4
RIG-I	Retinoic acid-inducible gene I
RNA	Ribonucleic acid
ROS	Reactive oxygen species
RPLPO	Ribosomal protein lateral stalk subunit P0
RSAD2	Radical S-adenosyl methionine domain containing 2
SAM	S-adenosylmethionine
SDF1a	Stromal cell-derived factor 1a
SEM	Standard error of the mean
shRNA	short hairpin RNA
siRNA	small interfering RNA
SLE	Systemic lupus erythematosus
SNP	Single nucleotide polymorphism
SNP	Sodium nitroprusside
SQLE	Squalene epoxidase
SREBP	Sterol regulatory element-binding protein
SRF	Serum response factor
SSC	Trisodium citrate
STAT	Signal transducer and activator of transcription
t-PA	tissue plasminogen activator

TCA	Tricarboxylic acid
TDG	Thymine DNA glycosylase
TEER	Transendothelial electrical resistance
TET	Ten-Eleven Translocation
TET2 endo KO	Endothelial-specific TET2 knockout
TFPI	Tissue factor pathway inhibitor
TLR	Toll-like receptor
TNF	Tumour necrosis factor
TRITC	Tetramethylrhodamine
TxA2	Thromboxane A2
u-PA	urokinase plasminogen activator
UDP-GlcNAc	Uridine diphosphate N-acetylglucosamine
VCAM	Vascular cell adhesion molecule
VE-cadherin	Vascular endothelial cadherin
VEGF	Vascular endothelial growth factor
VLA4	Very late antigen 4
WT	Wild-type
ZO	Zonula occluden

1. General introduction

1.1 Diabetes mellitus and its vascular complications

Diabetes mellitus (diabetes) is characterised by hyperglycaemia and either impaired secretion of insulin by the pancreas (type 1 diabetes) or insulin resistance (type 2 diabetes) [1]. The incidence of diabetes is increasing worldwide and is a major source of morbidity and mortality. Diabetes affects approximately 415 million adults worldwide and this incidence is predicted to reach 642 million by 2040 [2]. People with diabetes often go on to develop vascular complications, affecting the microvasculature of the eyes, kidneys and nerves (diabetic retinopathy, nephropathy and neuropathy), or macrovasculature (atherosclerosis, peripheral artery disease, myocardial infarction and stroke) [2]. Partly due to the increased likelihood of developing cardiovascular diseases, diabetes is associated with a decreased life expectancy. Type 2 diabetics are reported to have a two to six-fold greater risk of death from cardiovascular diseases than non-diabetics [3, 4] and similar increased cardiovascular risks are reported for type 1 diabetics [5]. In addition, clinical trials and animal studies have shown that offspring of diabetic pregnancies (whether pre-existing type 1 or type 2 diabetes, or gestational diabetes which is first diagnosed during pregnancy and usually transient) are at increased risk of developing diabetes, obesity and cardiovascular diseases later in life [6, 7]. In the UK, 10% of the NHS budget is spent managing diabetes and its complications [8]. Thus, it is more important than ever to understand the molecular underpinnings of diabetes and its cardiovascular complications in order to design therapies to ameliorate these conditions. An early stage in the pathogenesis of many cardiovascular diseases is thought to be the dysfunction of endothelial cells and there is strong evidence to suggest that hyperglycaemia is a major contributor to the development of endothelial dysfunction in diabetes [9-16].

1.2 Endothelial cell functions

Vascular endothelial cells form the one cell thick innermost lining of blood vessels called the endothelium. The endothelium is comprised of heterogeneous populations of endothelial cells depending on the vessel type and the tissue in which they reside, allowing for diverse endothelial cell phenotypes [17]. This vast cell population spans the vascular network, performing functions that act to maintain vascular homeostasis [18]. Located at the interface between blood and underlying tissues, endothelial cells are uniquely situated to regulate the diffusion of solutes and extravasation of immune cells by acting as a semi-permeable barrier [19]. In addition to this important function regulating blood vessel permeability, endothelial cells are also involved in the control of vascular tone, haemostasis, innate immunity, inflammation and the formation of new blood vessels [20-24].

1.2.1 The role of endothelial cells in regulating vascular tone

The endothelium plays an important role in the regulation of vascular tone by releasing vasoactive substances which act to induce either vasodilation (*e.g.* nitric oxide, prostacyclin and endothelial-derived hyperpolarising factor) or vasoconstriction (*e.g.* endothelin-1 (ET-1), thromboxane A2 (TxA2)) [20]. Nitric oxide (NO) is produced by nitric oxide synthase (NOS), of which endothelial NOS (eNOS) is the primary isoform in endothelial cells [20]. NO is produced constitutively but its production can be increased when endothelial cells are exposed to increased shear stress or stimulated by agonists such as acetylcholine, adenosine triphosphate (ATP), adenosine diphosphate (ADP) or bradykinin [20]. These agonists increase intracellular Ca^{2+} levels, enabling eNOS to dissociate from caveolin and bind calmodulin. In this activated state, eNOS catalyses the production of NO from L-arginine [20]. eNOS is also regulated by phosphorylation and at the transcriptional level, both of which can be initiated by increased shear stress [20]. NO diffuses to the underlying smooth muscle cells where it binds soluble guanylyl cyclase to facilitate conversion of guanosine triphosphate (GTP) to cyclic guanosine monophosphate (cGMP), decreasing

cytosolic Ca^{2+} and resulting in reduced smooth muscle cell contraction [18]. Another vasodilator produced by the endothelium is prostacyclin, which is synthesised by cyclooxygenase-2. It binds prostacyclin receptors (IP receptors) on smooth muscle cells to activate adenylyl cyclase which catalyses the production of cyclic adenosine monophosphate (cAMP) to activate protein kinase A (PKA) and induce vasorelaxation [18]. Hyperpolarisation of vascular smooth muscle cells can also be mediated by endothelium-derived hyperpolarising factors [18]. Vasodilators released from the endothelium, particularly NO, are important in maintaining a basal level of vasodilation as well as for adapting to increased blood flow [18, 20].

The action of vasodilators is opposed by vasoconstrictors such as ET-1 and TxA2 produced by endothelial cells. These bind to receptors on vascular smooth muscle cells and cause an increase in intracellular Ca^{2+}, inducing smooth muscle cell contraction and vasoconstriction [18]. The balance of vasodilators and vasoconstrictors produced by the endothelium is vital for homeostatic regulation of tissue perfusion and is an important determinant of blood pressure [20].

1.2.2 The role of endothelial cells in haemostasis

In a healthy state, the endothelium maintains a non-thrombogenic surface by continuously producing factors that inhibit platelet activity and coagulation pathways [25]. Examples of anti-platelet factors include NO and prostacyclin (which are also potent vasodilators, described above) [18]. NO diffuses into platelets where it activates guanylyl cyclase and increases cGMP production to prevent the elevation of cytosolic Ca^{2+} concentrations which is required for platelet activation and aggregation [18]. Prostacyclin binding to its receptors on platelets results in adenylyl cyclase-mediated production of cAMP and subsequent PKA activation which inhibits cytosolic Ca^{2+} elevation [18]. Endothelial cells also limit the exposure of platelets to ATP and ADP which promote aggregation, by expressing ectonucleotidases on their surface which hydrolyse them into adenosine monophosphate (AMP) and adenosine [18]. In

addition to these anti-platelet agents, the endothelium synthesises anticoagulants to oppose the clotting process – a cascade of enzyme-catalysed reactions culminating in the generation of thrombin, which generates fibrin, the main non-cell component of clots [21]. Examples of anticoagulants produced by endothelial cells include tissue factor pathway inhibitor (TFPI) (to limit the action of tissue factor which generates thrombin), thrombomodulin (a membrane-bound receptor which reduces the activity and circulating levels of thrombin) and endothelial protein C receptor (which facilitates the interaction between protein C, another anti-coagulant, and thombin-thrombomodulin complexes) [21].

Upon injury to the vessel, the endothelium shifts the balance to favour a pro-thrombotic, pro-coagulant state and suppress anti-platelet and anti-coagulant pathways [18]. This enables the formation of a clot to maintain the integrity of the vessel wall and prevent blood loss. Activated endothelial cells release Von Willebrand Factor from Weibel-Palade bodies, which tethers the exposed subendothelial collagen to platelets via the platelet glycoprotein 1bα (GP1bα) receptor [25]. In addition, endothelial cells release platelet activating factor (PAF) which promotes platelet aggregation [25]. The coagulation system is also impacted by endothelial cells, as exposure to thrombin and various inflammatory stimuli can cause expression of tissue factor at the endothelial surface to initiate clotting [18]. In the resolution phase, endothelial cells synthesise factors such as tissue plasminogen activator (t-PA) and urokinase plasminogen activator (u-PA) involved in fibrinolysis for dissolution of the clot [21].

1.2.3 The role of endothelial cells in angiogenesis

The growth of new blood vessels from pre-existing vessels, termed angiogenesis, requires endothelial cells to respond to environmental cues to form new sprouts to expand the vascular network. This process is vital during physiological processes such as during embryogenesis, wound healing and the menstrual cycle, but dysregulation

of angiogenesis can contribute to pathological processes including cancer, atherosclerosis and diabetic retinopathy [22, 26-29]. In adulthood, endothelial cells are typically in a quiescent state and scarcely proliferate but retain their capacity to do so when activated by angiogenic stimuli [22]. The major angiogenic stimulus is Vascular Endothelial Growth Factor (VEGF) [28]. Upon sensing VEGF (released by cells upon nutrient and oxygen depletion), endothelial cells proteolytically degrade the basement membrane and modulate contacts with adjacent endothelial cells and pericytes [28]. Two specialised endothelial phenotypes, 'tip' and 'stalk' cells, emerge during angiogenesis as a result of VEGF and Notch signalling [30]. Tip cells at the distal end of each sprout extend filopodia to sense and migrate towards directional cues such as VEGFA, whilst stalk cells proliferate to elongate the sprout and form a lumen [22]. Tip cells of two sprouts anastomose upon contact with each other to form a new vessel and once the vessel is fully established, endothelial cells return to a quiescent state [22]. This intricate process is controlled by endothelial signalling pathways responding to biochemical messengers and physical properties of the surrounding microenvironment [31, 32].

1.2.4 The role of endothelial cells in regulating vascular permeability

Endothelial cells perform a crucial homeostatic role in maintaining a barrier between blood and underlying tissues and governing the passage of solutes and immune cells across the vessel wall. Adjacent endothelial cells are joined by three types of cell-cell junctions: tight junctions, adherens junctions and gap junctions [19]. Whilst gap junctions are primarily important for intercellular communication, tight junctions and adherens junctions form and regulate the endothelial barrier [33]. Tight junctions are typically associated with controlling permeability to small molecules and ions, whilst adherens junctions regulate permeability and provide mechanical stability to the cell junctions [19, 33]. Dynamic remodelling of these junctions allows paracellular permeability to be altered in response to stimuli when required.

The main components of endothelial tight junctions are zonula occludens (ZOs), claudins, occludin and junctional adhesion molecules (JAMs) [33] (Figure 1.1). ZOs are located in the cytoplasm where they connect the transmembrane components of tight junctions (and also some adherens junction components) to the actin cytoskeleton [19]. The JAM and claudin families contain multiple proteins, the distribution of which varies between endothelial cells in specific vascular beds [33]. The expression of occludin also depends on the region of the vasculature and reflects the permeability of that region, for example, occludin mRNA expression is 18-fold higher in arterial than venous endothelial cells and is highly expressed in brain endothelial cell tight junctions where permeability is limited compared to non-neural tissues [34, 35]. The main component of endothelial adherens junctions is vascular endothelial cadherin (VE-cadherin) [36] (Figure 1.1). VE-cadherin is a transmembrane protein and interacts with cytoplasmic catenins (β-catenin, p120-catenin and γ-catenin (pakoglobin)) to anchor to the actin cytoskeleton *via* α-catenin [19]. Although not part of tight junctions or adherens junctions, platelet endothelial cell adhesion molecule-1 (PECAM-1) is also important for the maintenance of the endothelial barrier [37] (Figure 1.1). There are many modulators of endothelial permeability, including VEGFA, angiopoietins, thrombin, histamine, bradykinin and inflammatory cytokines such as tumour necrosis factor (TNF)α, interferon (IFN)γ and interleukin (IL)-1 [33, 36, 38, 39]. Diverse signalling pathways are involved in their actions, some of which act upon junctional components to affect their stability (such as phosphorylation of VE-cadherin) and others disrupt junctional stability indirectly by altering actomyosin contractility [33, 36].

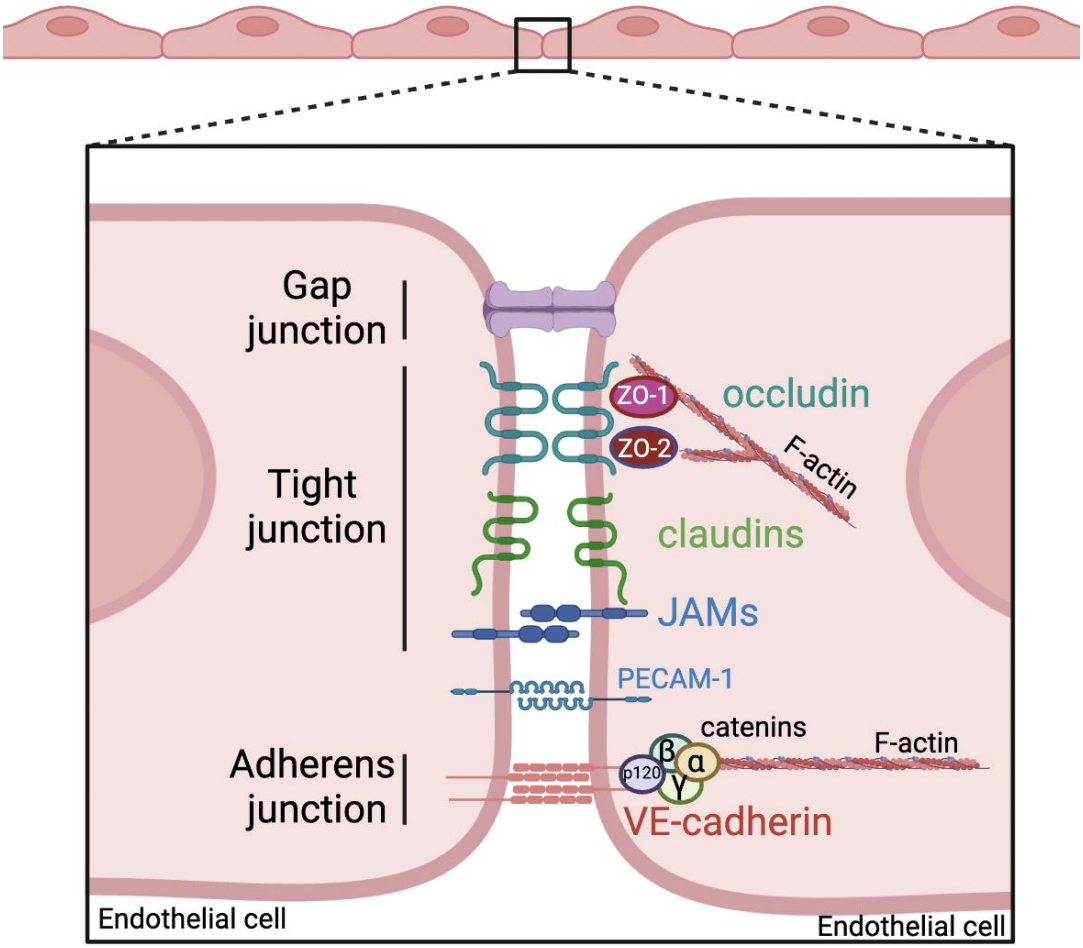

Figure 1.1: ***Schematic diagram of endothelial junctions****. Adjacent endothelial cells are connected by gap junctions, tight junctions and adherens junctions. Tight junctions consist of occludin, claudins, junctional adhesion molecules (JAMs) and zonula occludens (ZO) proteins which interact with the filamentous (F-)actin cytoskeleton. Adherens junctions consist of VE-cadherin and catenins which connect the junction to F-actin. Platelet Endothelial Cell Adhesion Molecule (PECAM)-1 is also present at endothelial junctions. These components are important regulators of endothelial barrier integrity.*

The endothelial junctions described above allow the passage of fluids and solutes (such as glucose, ions and metabolites) up to a radius of 3nm *via* the paracellular route (*i.e.* between adjacent endothelial cells) to underlying tissues [40]. In situations of acute or chronic inflammation, reorganisation of these junctions occurs to facilitate paracellular leukocyte transmigration (discussed in further detail below) [41]. For macromolecules such as albumin, insulin, lipids and hormones, trafficking across the endothelium relies on the transcellular route *i.e.* through the cell [40]. This often involves receptor binding at the luminal surface of the endothelial cell and caveolae-mediated transport across to the basolateral membrane, where the contents are

released by exocytosis [40]. Although controversial for some time, there is also evidence that leukocytes extravasate *via* the transcellular route [42, 43]. Endothelial cells actively regulate these processes at each stage to maintain homeostasis [40].

1.2.5 The role of endothelial cells in inflammation and immunity

In a quiescent state, endothelial cells prevent aberrant inflammation by releasing anti-inflammatory mediators such as prostacyclin, expressing low basal levels of adhesion molecules at their luminal surface and maintaining their barrier function to inhibit leukocyte extravasation [44]. Endothelial cells express pattern recognition receptors (PRRs) and receptors for various cytokines which enable rapid activation upon exposure to pathogen-associated molecular patterns (PAMPs) (*e.g.* lipopolysaccharide (LPS), a central component of the membrane of Gram-negative bacteria), damage-associated molecular patterns (DAMPs) (*e.g.* intracellular proteins or DNA), or inflammatory stimuli (*e.g.* TNFα, IFNγ or oxidised low density lipoprotein (LDL)) [23]. Upon activation, endothelial cells upregulate adhesion molecules (including E-selectin, P-selectin, intercellular adhesion molecule (ICAM)-1 and vascular cell adhesion molecule (VCAM)-1) at the cell surface and synthesise and release chemokines to trigger leukocytes to adhere to and cross the endothelium to reach the site of infection [24]. Leukocyte extravasation occurs by a multi-step process referred to as the 'leukocyte adhesion cascade' [24]. Figure 1.2 shows some of the key molecules involved in leukocyte-endothelial cell interactions at each stage, beginning with leukocyte tethering and rolling (mediated by selectins), which slows until arrest (mediated by ICAM-1 and VCAM-1 binding leukocyte integrins). Firmer adhesion occurs and the leukocyte spreads and crawls to the site of transmigration either *via* the paracellular or more rarely *via* the transcellular route (processes involving PECAM1) [24].

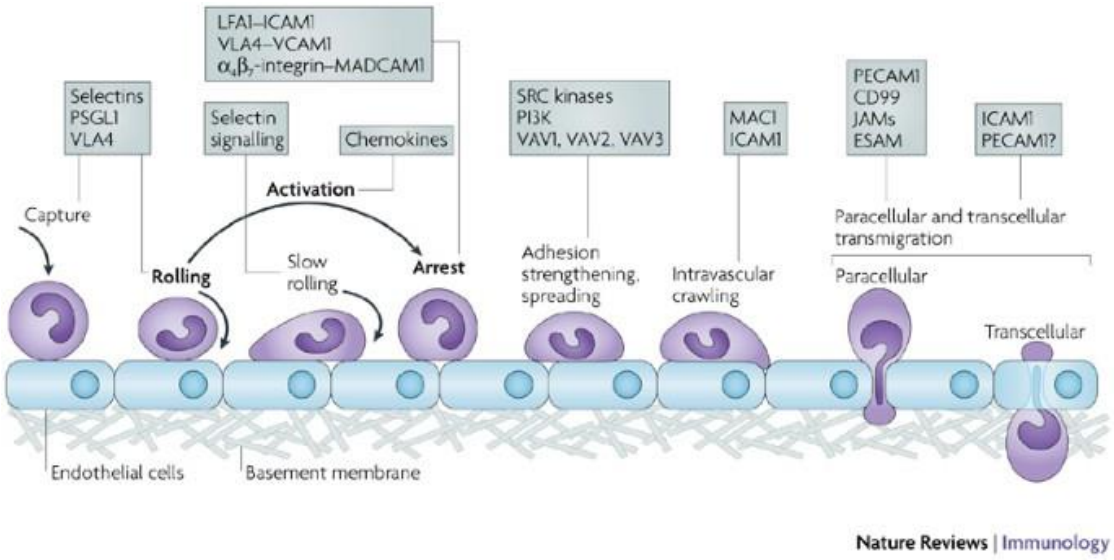

Figure 1.2: ***Schematic diagram of the multi-step leukocyte adhesion cascade.*** *Following initial capture, leukocytes roll along endothelial cells and slow until arrest. Leukocyte-endothelial cell adhesion is strengthened and leukocytes spread and crawl to their site of transmigration, either at endothelial junctions (paracellular) or through the cell body (transcellular). Key molecules involved in each stage are shown in boxes. Abbreviations: endothelial cell-selective adhesion molecule (ESAM), intercellular adhesion molecule 1 (ICAM- 1), junctional adhesion molecule (JAM), lymphocyte function-associated antigen 1 (LFA-1), macrophage antigen 1 (Mac-1), mucosal vascular addressin cell-adhesion molecule 1 (MADCAM1), P-selectin glycoprotein ligand 1 (PSGL-1), platelet/endothelial-cell adhesion molecule 1 (PECAM1), phosphoinositide 3-kinase (PI3K); vascular cell-adhesion molecule 1 (VCAM1), very late antigen 4 (VLA4). Figure reproduced from [24]*

In recent years, there has been an increasing appreciation that although not traditionally considered part of the innate or adaptive immune system, endothelial cells perform many functions that could classify them as innate immune cells [23, 45]. Endothelial cells are well-positioned to act as sentinels within the vasculature, being one of the first cell types to interact with circulating PAMPs *via* their PRRs [45]. They sense and respond to cytokines, in addition to secreting cytokines and chemokines themselves to amplify the immune response by recruiting leukocytes to the site of inflammation [45]. Although endothelial cells are not professional antigen-presenting cells like dendritic cells and macrophages, they express major histocompatibility complex (MHC) class I (found on all nucleated cells) and can induce MHC class II expression (restricted to antigen-presenting cells) upon IFNγ stimulation [23, 46]. This enables endothelial cells to present antigens to (and influence the function of) T cells [47], thus linking endothelial cells to initiation of the adaptive immune response. For successful resolution of an immune response, endothelial cells must downregulate

surface cell adhesion molecules, restore basal levels of permeability and decrease pro-inflammatory cytokine release [48].

The endothelial functions described in this section have been shown to be perturbed in the microvascular or macrovascular complications of diabetes. For example, key features of diabetic retinopathy include inflammation, a dysregulated angiogenic response and impairment of endothelial barrier function due to excessive upregulation of VEGF [49]. In atherosclerosis, increased endothelial permeability and excessive inflammation enables accumulation of LDL, monocytes and other immune cells in the intima [50]. The expression of pro-coagulant mediators can trigger thrombosis and cause occlusion of the vessel or plaque rupture [50]. Plaque growth can be supported by angiogenesis of the vasa vasorum (the microvasculature that supplies large blood vessels) but this can also lead to destabilisation and plaque rupture, potentially leading to consequences such as myocardial infarction and stroke [29].

1.3 Endothelial dysfunction

In a healthy state, activation of the endothelium is transient and after responding to the stimulus, endothelial cells return to a quiescent state where inflammation, thrombosis and angiogenesis are suppressed and an appropriate vascular tone is maintained [51]. However, this restoration of quiescence can be disrupted in some pathological contexts including diabetes, leading to a persistent activated state termed endothelial dysfunction [52]. Endothelial dysfunction is characterised by a reduced bioavailability of NO, resulting in impaired vasodilation [51, 52]. It also features dysregulation of homeostatic processes, leading to a pro-inflammatory, pro-thrombotic state, altered permeability and abnormal proliferation. Dysfunction of endothelial cells can also include a loss of endothelial characteristics and differentiation to a mesenchymal phenotype, termed endothelial-to-mesenchymal transition (EndoMT), further exacerbating vascular dysfunction (for example, by

contributing to neointima formation during atherogenesis) [53]. These characteristics are summarised in Figure 1.3. Endothelial dysfunction is a preceding factor in many cardiovascular diseases and is an independent predictor of future cardiovascular events [54-56]. Understanding the causes of endothelial dysfunction may be key to designing therapies for early intervention to prevent the progression of cardiovascular diseases.

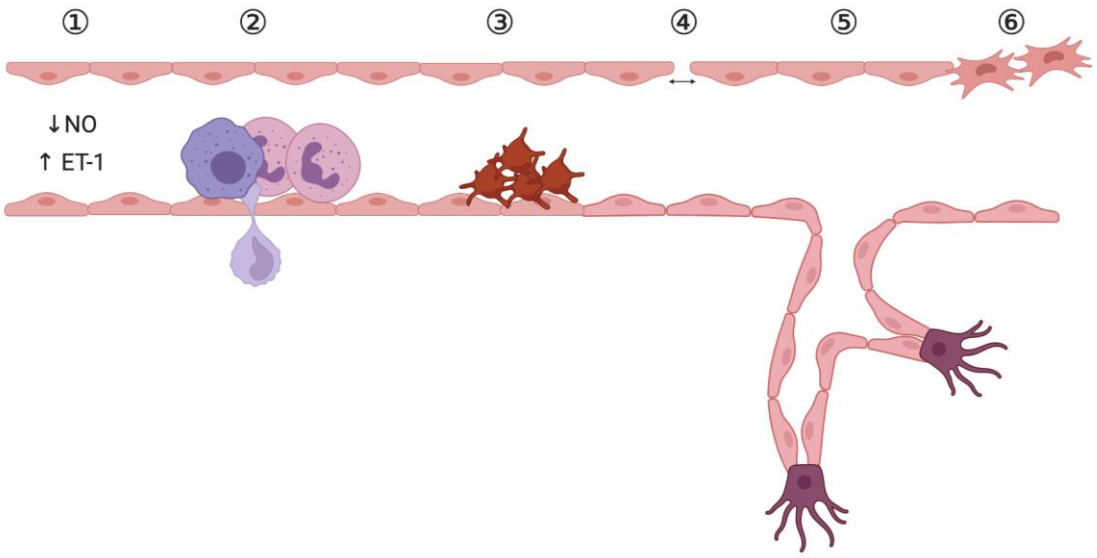

Figure 1.3: ***Characteristics of endothelial dysfunction.*** *Endothelial dysfunction is characterised by: ① A decreased bioavailability of nitric oxide (NO) and increased production of vasoconstrictors such as endothelin-1 (ET-1); ② Increased production of pro-inflammatory cytokines and adhesion molecules which promote leukocyte recruitment and transmigration; ③ A pro-thrombotic environment; ④ increased endothelial permeability; ⑤ Abnormal angiogenesis; ⑥ Endothelial-to-mesenchymal transition.*

1.3.1 Causes of endothelial dysfunction in diabetes

High glucose concentrations are directly damaging to endothelial cells due to alteration of their metabolism, increased reactive oxygen species (ROS) generation and the production of advanced glycosylation end products (AGEs) [57-62], discussed in detail in the next section. Indirect damage can also occur by paracrine actions of other cell types affected by hyperglycaemia, for example, persistent activation of endothelial cells by pro-inflammatory cytokines released by leukocytes and adipocytes. In type 2 diabetes, insulin resistance (a lack of insulin sensitivity in tissues)

is an additional cause of damage to the endothelium, causing a pathway-specific impairment. PI3K pathway activation downstream of insulin binding to the insulin receptor on endothelial cells is impaired, leading to a decrease in the production of NO [63, 64] (Figure 1.4). Compensatory hyperinsulinaemia appears to favour increased activation of the MAPK pathway, leading to increased expression of endothelin-1 and potentiation of adhesion molecule upregulation in response to growth factors, contributing to vasoconstriction and inflammation [63-65] (Figure 1.4). The endothelium can be further damaged by dyslipidaemia, which contributes to impaired insulin signalling, oxidative stress, inflammation and apoptosis of endothelial cells [66].

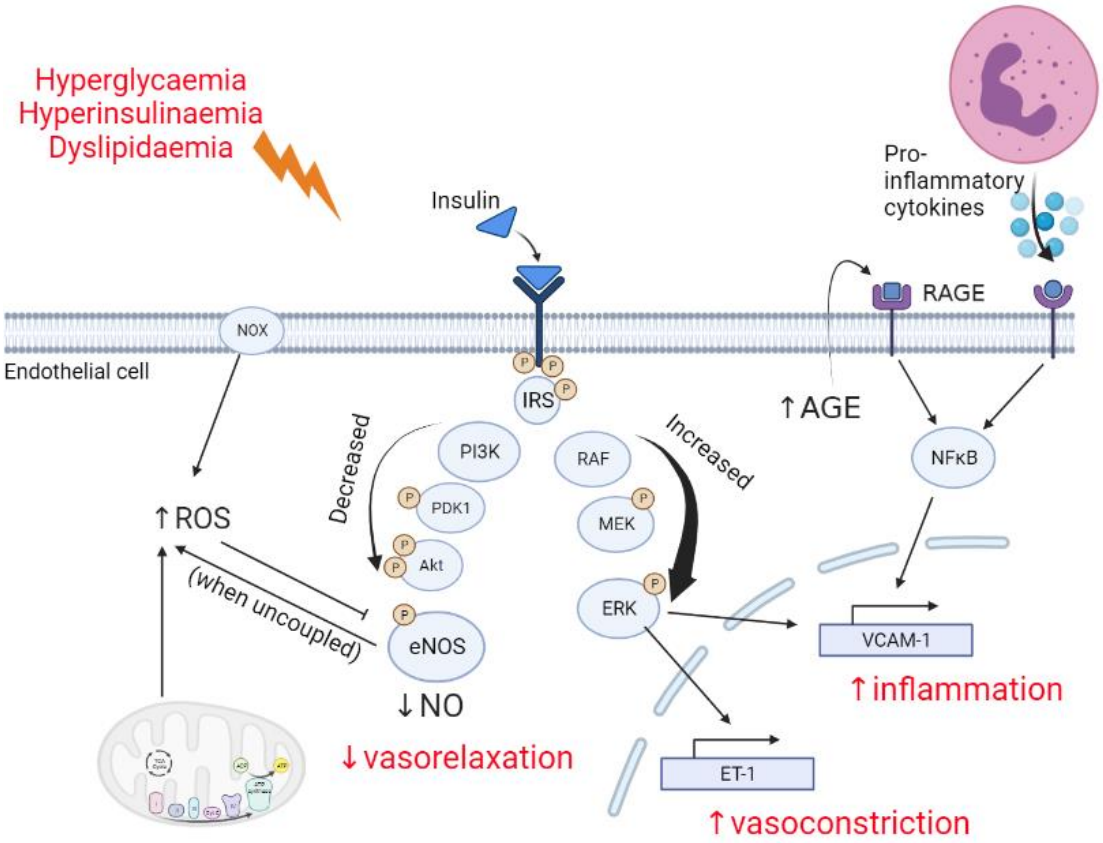

Figure 1.4: ***Examples of signalling pathways involved in endothelial dysfunction in diabetes****. Hyperglycaemia, hyperinsulinaemia and dyslipidaemia contribute to endothelial dysfunction. A selective insulin-resistance causes decreased PI3K pathway signalling and increased MAPK signalling, decreasing NO production and increasing ET-1 production. ROS production is elevated due to a hyperglycaemia-induced increase in NOX activity and mitochondrial damage, as well as superoxide production by uncoupled eNOS. Hyperglycaemia and dyslipidaemia together increase AGE formation which activates NFκB signalling via RAGE, upregulating adhesion molecules. Paracrine signalling by other cells such as leukocytes also contributes to inflammatory pathway activation and endothelial dysfunction. Abbreviations: Advanced glycosylation end product (AGE), receptor for AGE (RAGE), nicotinamide adenine dinucleotide phosphate oxidase (NOX), insulin receptor substrate (IRS), phosphoinositide 3-kinase (PI3K), phosphoinositide-dependent kinase-1 (PDK1), endothelial nitric oxide synthase (eNOS), nitric oxide (NO), endothelin-1 (ET-1), vascular cell adhesion molecule 1 (VCAM-1), reactive oxygen species (ROS), nuclear factor kappa B (NFκB).*

1.3.2 Hyperglycaemia and endothelial dysfunction

Given that the endothelium is directly exposed to changing blood glucose levels, it is understandable that this cell type is significantly affected by hyperglycaemia. Indeed, it is well documented by *in vitro* studies that hyperglycaemia alone is sufficient to induce endothelial dysfunction, evidenced by decreased eNOS activity [9], transcriptional changes in inflammation-related genes [67], enhanced monocyte adhesion [10], EndoMT [11], activation of prothrombotic signalling [12] and increased apoptosis [13]. *In vivo* evidence also supports this, as rodent models of type 1 diabetes (induced by streptozotocin injection) and type 2 diabetes (induced by a high fat diet) display impaired vasorelaxation in response to acetylcholine and enhanced noradrenaline- or phenylephrine-mediated vasoconstriction [14, 15]. In humans, measurements of brachial artery flow mediated vasodilatation indicate the presence of macrovascular endothelial dysfunction in healthy individuals and people with cardiometabolic diseases when exposed to acute hyperglycaemia following oral glucose loading [16]. Together, these studies support the notion that hyperglycaemia *per se* compromises endothelial function.

Some of the molecular mechanisms underlying hyperglycaemia-induced endothelial dysfunction have been characterised, including the accumulation of ROS, formation of AGEs and the redirection of glucose to non-glycolytic pathways (Figure 1.5). ROS are partial reduction products of molecular oxygen (O_2), such as superoxide anion and peroxides. Excessive ROS levels that overwhelm cellular antioxidant defences (termed oxidative stress) is associated with many pathologies including atherosclerosis and diabetes and has been associated with endothelial dysfunction in animal models of diabetes [59, 60]. This can result, in part, from the reaction of superoxide anion with NO, which reduces NO bioavailability and produces peroxynitrite which can damage cellular contents [68]. Increased production of superoxide anion in diabetic vessels has been suggested to result from increased xanthine oxidase and nicotinamide adenine dinucleotide phosphate (NADPH) oxidase (NOX) activity [69], eNOS uncoupling [59] and mitochondrial damage in hyperglycaemia [70].

AGEs are formed when proteins or lipids are non-enzymatically glycated in the presence of excess sugars including glucose, first to Schiff bases and Amadori products and then to AGEs [62]. Their production is elevated in diabetes due to hyperglycaemia [62]. AGEs can form aberrant cross-links between extracellular matrix components, alter protein conformation and can signal *via* Receptor for AGEs (RAGE) to activate the nucleus factor κB (NFκB) pathway, leading to increased endothelial permeability and leukocyte adhesion [62, 71, 72]. AGEs can also induce a pro-thrombotic phenotype in endothelial cells with upregulation of tissue factor and decreased activity of thrombomodulin [73, 74]. In addition, AGEs have been shown to influence mediators of vascular tone by quenching NO and upregulating ET-1 in endothelial cells [75, 76].

Various metabolites produced as intermediates in glycolysis participate in other metabolic pathways, usually in small amounts, for example to produce nucleotides [57]. However, during hyperglycaemia, excessive glucose and intermediates produced in glycolysis are diverted in larger amounts to alternative pathways including the hexosamine and polyol pathways [57, 58]. These generate AGEs [61] and uridine diphosphate N-acetylglucosamine (UDP-GlcNAc), respectively [77, 78]. Aberrant protein glycosylation resulting from increased UDP-GlcNAc levels has been linked to endothelial dysfunction and disrupted insulin signalling [77, 78]. Pentose phosphate pathway flux has been reported to decrease in high glucose conditions due to inhibition of glucose-6-phosphate dehydrogenase, leading to reduced NADPH production, a major cellular reductant and cofactor for eNOS [79].

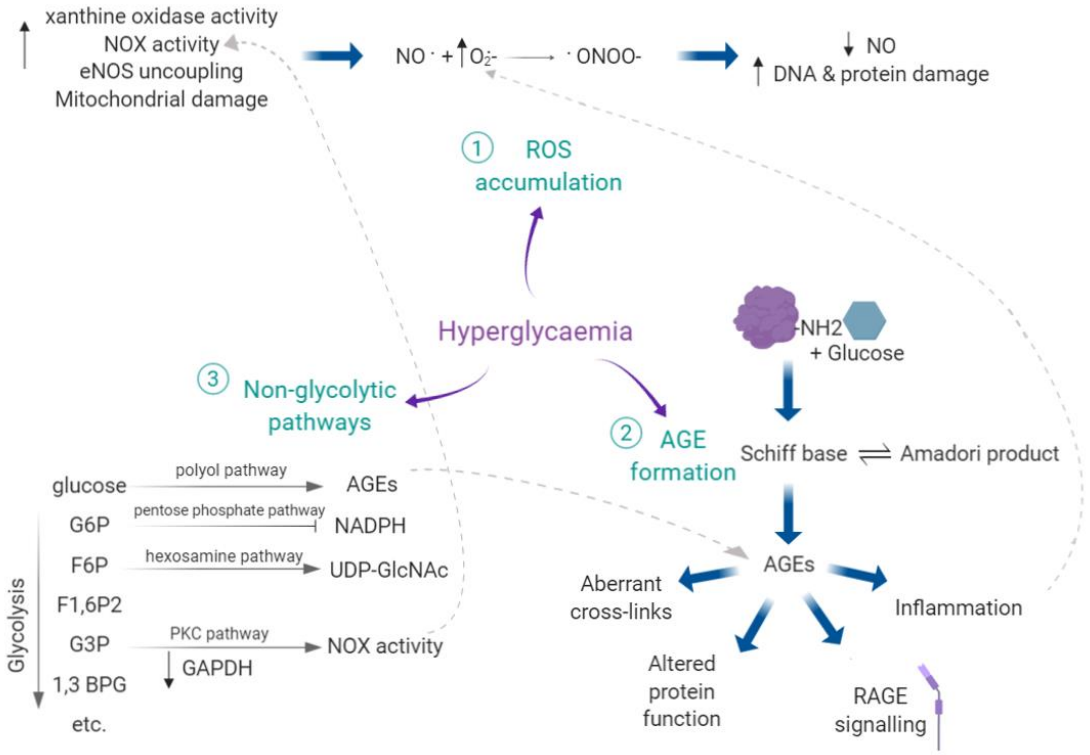

Figure 1.5: ***Mechanisms of hyperglycaemia-induced endothelial dysfunction.*** *1 Hyperglycaemia induces reactive oxygen species (ROS) formation by increasing xanthine oxidase and Nicotinamide adenine dinucleotide phosphate (NADPH) oxidase (NOX) enzyme activity, uncoupling of endothelial nitric oxide synthase (eNOS) and mitochondrial damage. This generates superoxide anion (.O2) which reacts with nitric oxide (NO) to generate the highly reactive and cytotoxic peroxynitrite radical (.ONOO-). 2 Advanced glycosylation end products (AGEs) are formed when aldose sugars react with the amino group of a protein. This forms the intermediate Schiff bases and Amadori products which are subsequently converted to AGEs. AGEs bind to receptors of AGE (RAGE), alter protein function, form cross-links between extracellular matrix components and promote inflammation. 3 A reduction in glyceraldehyde 3-phosphate dehydrogenase (GAPDH) activity in hyperglycaemia stalls glycolysis. Glycolytic intermediates are redirected into alternative pathways including polyol, hexosamine and protein kinase C (PKC) pathways, generating AGEs, Uridine diphosphate N-acetylglucosamine (UDP-GlcNAc) and increasing NOX activity. Flux through the pentose phosphate pathway is inhibited by decreased glucose-6-phosphate dehydrogenase levels. Some interactions between these pathways are indicated by dotted lines. Abbreviations: glucose-6-phosphate (G6P), fructose-6- phosphate (F6P), Fructose-1,6-diphosphate (F1,6P2), glyceraldehyde-3-phosphate (G3P), 1,3-bisphosphoglycerate (1,3 BPG).*

1.4 Hyperglycaemic memory

Whilst these mechanisms go some way to explaining hyperglycaemia-induced endothelial dysfunction, they do not fully explain reports of a long-lasting impact of transient hyperglycaemia on the cardiovascular system. In large clinical trials: Action in Diabetes and Vascular Disease: Preterax and Diamicron MR Controlled Evaluation (ADVANCE) and Action to Control Cardiovascular Risk in Diabetes (ACCORD), intensive

therapy targeting HbA1c <6.5% (ADVANCE) or <6% (ACCORD) through regular glucose monitoring and administration of glucose-lowering drugs was not found to reduce cardiovascular events significantly compared to standard therapy [80, 81]. In the ACCORD trial, intensive therapy was in fact associated with an *increased* mortality relative to the standard therapy group (target HbA1c 7-7.9%) in the ACCORD trial [80].

This phenomenon of 'hyperglycaemic memory' or 'metabolic memory' has also been observed in animal studies. For example, after inducing diabetes in dogs, good glycaemic control was reinstated after 2.5 years and diabetic retinopathy progression was assessed 5 years after diabetes onset [82]. Despite the lengthy period of good glycaemic control (consisting of twice daily insulin injection and specific measured food intake), retinopathy progressed during this period, suggesting that the initial hyperglycaemic period had lasting vascular effects [82]. This may suggest the need for early control of hyperglycaemia to limit the extent of vascular complications. In another study, diabetes was induced (by streptozotocin injection) in rats and poor glycaemic control was maintained for either 2 or 6 months, followed by 7 months of good glycaemic control. Retinal oxidative and nitrative stress were evident after hyperglycaemia and this was only partially improved when good glycaemic control was reinstated after only 2 months. When good glycaemic control was delayed to 6 months after onset of diabetes, fewer improvements in diabetic retinopathy features were observed [83]. Similar findings have been observed for diabetic nephropathy in rats [84]. These studies support the idea that re-establishment of good glycaemic control is not necessarily effective in reversing the vascular complications of diabetes.

Hyperglycaemic memory is also exemplified by the intergenerational 'priming' of metabolic and cardiovascular phenotypes, independently of genetic risk [85, 86]. Offspring of mothers with gestational diabetes have been observed to have a greater tendency towards obesity, impaired glucose tolerance, reduced insulin sensitivity, impaired pancreatic β-cell function and higher blood pressure, all of which are cardiovascular risk factors [85, 86]. Accordingly, population-based cohort studies have

demonstrated that maternal diabetes during pregnancy is associated with early onset of cardiovascular disease in offspring [87-89]. This is supported by rodent studies where it has been shown that either streptozotocin- or diet-induced diabetes during pregnancy results in impaired vascular reactivity in offspring [90, 91]. This suggests that intrauterine exposure to hyperglycaemia may be causal in the persistence of cardiovascular risk across generations.

In addition to the observation of hyperglycaemic memory *in vivo,* evidence from *in vitro* studies supports the existence of such memory at the cellular level. Increased generation of ROS and increased apoptosis were observed in human umbilical vein endothelial cells (HUVEC) cultured in high glucose for 48h, which persisted following restoration of normal glucose concentrations for 48h [92]. Over a longer time period, the finding of persistently increased ROS generation was replicated and markers of high glucose-induced stress (fibronectin, protein kinase C-beta, NOX subunit p47phox, BCL-2-associated X protein, 3-nitrotyrosine, poly(ADP-ribose)) were observed in HUVEC cultured in high glucose conditions for 2 weeks, followed by 1 week in normal glucose conditions [93]. In another study, it was shown that high glucose-induced increases in fibronectin and collagen IV expression in HUVEC continued to exceed that of control HUVEC significantly for over a week after returning to normal glucose levels [94]. Furthermore, using atomic force microscopy it was demonstrated that cells from the EA.hy926 endothelial cell line cultured under high glucose showed persistently increased stiffness when returned to normal glucose levels, to a similar degree to those cultured continuously in high glucose conditions [95]. In a transient model of hyperglycaemia involving 16h incubation of bovine and human aortic endothelial cells in a high glucose concentration, the NFκB subunit p65 was found to be upregulated in both cell types after continued culture under normal glucose concentrations for 6 days [67].

1.5 Epigenetics

The precise molecular mechanisms that underlie hyperglycaemic memory are not known, however, epigenetic mechanisms have been suggested to play a role [96]. The term epigenetics was coined by embryologist Conrad Waddington in 1942, referring to the notion that "between genotype and phenotype, and connecting them to each other, there lies a whole complex of developmental processes" [97]. He described the 'epigenome' as "concatenations of processes linked together in a network, so that a disturbance at an early stage may gradually cause more and more far reaching abnormalities in many different organs and tissues" [97]. Later, Waddington published an often-cited visual representation of an "epigenetic landscape" (Figure 1.6), depicting a ball rolling down a branching landscape of valleys as a metaphor for the determination of cell fate during development. At each stage, the paths diverge, indicating the progressive restriction of developmental potential for the cell as it commits to a particular cell fate: a process determined by the action of genes which underlie the landscape [98].

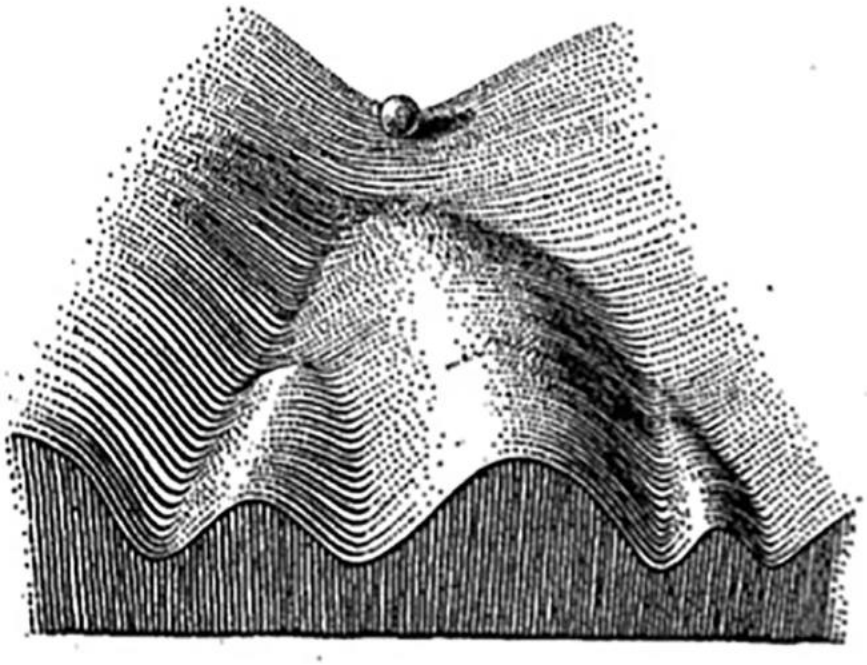

*Figure 1.6: **Waddington's epigenetic landscape**. In 1957, Conrad Waddington introduced the concept of an 'epigenetic landscape' using an illustration of a ball rolling down a branching landscape of valleys as a metaphor for the determination of cell fate during development. Figure reproduced from [99].*

The usage and definition of the term epigenetics has been altered and refined over time and a popular contemporary definition of epigenetics is the study of mitotically and/or meiotically heritable changes to gene expression that do not involve changes to the DNA sequence [100]. Many epigenetic studies today relate to chemical or structural modifications to chromatin, altering its conformation to be 'open' (euchromatin) or 'closed' (heterochromatin) to transcription machinery such as transcription factors and RNA polymerase [101]. Thus, epigenetic alterations involve stable modifications which remodel chromatin, subsequently altering gene expression patterns and hence phenotypes, either as part of normal development, or in response to environmental factors [102]. This can account for the vastly different cell types which can be observed in an organism, despite each cell having an identical DNA sequence. The epigenetic signature is inherited across cell divisions, thus maintaining the transcriptional profile and cellular 'identity' of daughter cells [102]. However, epigenetic modifications are reversible so they can also be dynamically altered in response to environmental changes [102]. It is increasingly appreciated that epigenetic modifiers can alter cell phenotypes in a temporal manner [103]. Epigenetic modifications include changes to histone covalent post-translational modifications, DNA methylation patterns and the action of non-coding RNAs (Figure 1.7).

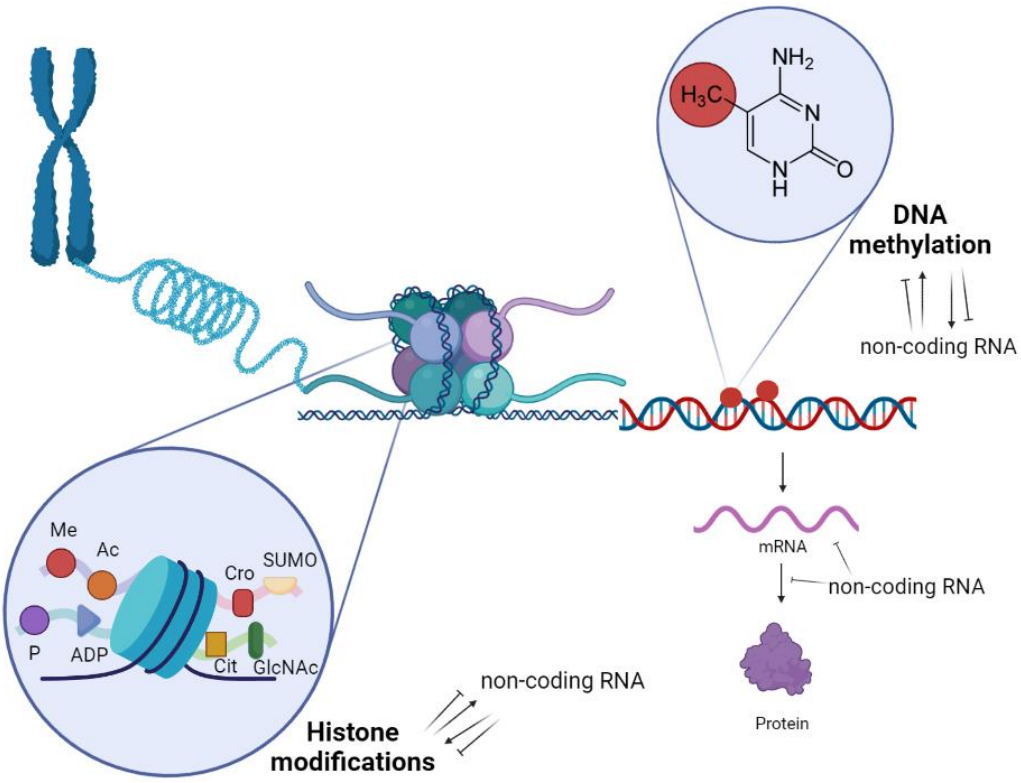

Figure 1.7: ***Epigenetic modifications.*** *Histone tails can be post-translationally modified by methylation (Me), acetylation (Ac), crotonylation (Cro), SUMOylation (SUMO), GlcNAcylation (GlcNAc), ubiquitination (Ub), citrullination (Cit), poly-ADP-ribosylation (ADP) or phosphorylation (P) to alter the interaction between DNA and histone proteins of the nucleosome. DNA methylation typically occurs at the 5th carbon of cytosine and is associated with transcriptional repression. Non-coding RNAs can influence epigenetic machinery and can also be regulated by epigenetic modifications. They can also regulate gene expression by altering mRNA stability or translation.*

1.5.1 Histone modifications

Within the nucleus, DNA is found in a complex with histone proteins. A nucleosome is a structural unit consisting of 147 base pairs of DNA wrapped around a tetramer of H3 and H4 and two H2A-H2B dimers [104]. Nucleosomes are separated by linker DNA in a 10nm fibre resembling 'beads on a string', which folds to form progressively higher order chromatin structures [104]. The N-terminal tails of histone proteins which protrude from the nucleosome can be post-translationally modified by acetylation, methylation, phosphorylation, crotonylation, ubiquitination, citrullination, poly-ADP-ribosylation, SUMOylation or O-GlcNAcylation to facilitate re-organisation of chromatin and thereby alter the accessibility of particular regions of DNA [104-106]. The presence of histone modifications depends on the opposing actions of 'writers'

and ‘erasers’ of the marks. For example, histone methylation is conferred by transfer of a methyl group from the universal methyl donor s-adenosyl methionine (SAM) to lysine or arginine residues, catalysed by a ‘writer’ enzyme in the histone methyltransferase family [101]. The methyl group can be removed by ‘erasers’ belonging to the Lysine-specific demethylase or Jumonji C demethylase families [107, 108]. Phosphorylation of histone proteins occurs at serine, threonine and tyrosine residues by the transfer of a phosphate group from ATP by kinases; this modification can be removed by phosphatases [105]. Histone acetylation occurs predominantly at lysine residues, where it is added by histone acetyltransferases and removed by histone deacetylases [105]. Lysine residues can also be modified by crotonylation, ubiquitination and SUMOylation [105, 106]. Citrullination occurs at arginine residues, poly-ADP-ribosylation at arginine and glutamate residues and O-GlcNAcylation at serine and threonine residues [105], demonstrating the specificity of each modification.

The type and position of histone modification influences whether it facilitates or represses gene transcription. For example, histone acetylation is typically associated with transcriptional activation due to its neutralisation of positively-charged lysine residues which disrupts electrostatic interactions between DNA and histones [105]. The effect of histone methylation on gene expression is more complex, being associated with transcriptional activation in some cases (trimethylation of histone H3 lysine 4) and transcriptional repression in others (trimethylation of histone H3 lysine 9 or 27) [105]. The role of other histone modifications in regulating transcription is less well-defined but each is likely to influence either the gross structure of chromatin and/or the binding of specific ‘reader’ proteins which specifically bind to the modified histones.

1.5.2 Non-coding RNA

Non-coding RNAs are not translated into proteins but instead perform infrastructural roles (*e.g.* small nuclear and ribosomal RNAs) or regulatory roles (*e.g.* microRNAs

(miRNAs), long non-coding RNAs (lncRNAs), small interfering RNAs (siRNAs) and piwi-interacting RNAs (piRNAs) [109]. Regulatory non-coding RNAs can influence gene expression by multiple mechanisms. The most-studied of these are miRNAs, which are approximately 22 nucleotides in length and associate with argonuate (Ago) 2 to form part of the RNA-induced silencing complex (RISC) to bind to and repress the expression of target mRNAs [110]. piRNAs (approximately 30 nucleotides in length) also bind to Ago proteins to form complexes involved in repression of transposable elements in germ cells [110]. lncRNAs have various functions that enable modulation of gene expression. They have been reported to guide transcription factors to particular gene loci, regulate mRNA stability and translation and act as a scaffold for the assembly of protein complexes [110]. Furthermore, miRNAs and lncRNAs can contribute to chromatin remodelling by regulating histone modifiers and enzymes involved in DNA methylation [111]. Roles for piRNAs have also been described in directing DNA methylation and heterochromatin formation [111]. Thus, non-coding RNAs can be considered epigenetic regulators. Furthermore, non-coding RNAs can, themselves, be regulated by epigenetic modifications, forming feedback loops to regulate gene expression [112]. Increasingly, roles are being described for non-coding RNAs in various physiological and pathological contexts including cardiovascular disease and their potential utility as biomarkers and therapeutic targets is being explored [109, 110].

1.5.3 DNA methylation

DNA methylation is one of the most studied epigenetic modifications. In eukaryotes, the majority of methylation occurs at CpG dinucleotides, where the 5th carbon of a cytosine residue is modified by the transfer of a methyl group from SAM, catalysed by a DNA methyltransferase (DNMT) to form 5-methylcytosine (5mC) [110]. DNA methylation is abundant in the mammalian genome (60-80% of CpG dinucleotides are methylated) [113]. However, at regulatory regions such as promoters and enhancers, regions of densely clustered CpG dinucleotides called ‘CpG islands’ can often be found and these are usually devoid of methylation [114]. When promoter-associated CpG

islands are methylated, this is typically associated with transcriptional repression of the affected gene [114]. DNA methylation patterns have garnered interest in the field of cancer research, as it is often observed that cancer cells display global DNA hypomethylation alongside aberrant site-specific hypermethylation of certain promoter CpG islands, which has been hypothesised to contribute to the downregulation of tumour suppressor genes [115].

5mC can be recognised by various proteins containing methyl-CpG-binding domains, which recruit complexes to repress transcription [110]. DNMT3A and DNMT3B are described as '*de novo*' DNMTs, as they establish methylation patterns during development, whereas DNMT1 is responsible for maintaining methylation during DNA replication, ensuring faithful reproduction of the epigenetic marks throughout successive cell divisions. DNMTs have been shown to be vital both in embryonic development (deletion of DNMT1 or DNMT3A/B in mice results in embryonic lethality [116, 117]) and maintenance of genomic stability throughout life (aberrant methylation is observed in cancers where DNMTs are mutated [118]). The function of DNA methylation patterns within gene bodies is less well characterised than promoter methylation, but has been observed to be positively correlated with gene expression [119].

Ordinarily, DNA methylation of a CpG site is symmetrical – that is, both strands possess 5mC. During DNA replication, the hemi-methylated DNA is recognised by DNMT1 (or other proteins which recruit DNMT1), which methylates cytosine on the daughter strand to match the parent strand [120]. Thus, DNA methylation is maintained across cell divisions. DNA methylation was thought previously to be irreversible and thus to silence gene transcription permanently unless passively lost through failure to copy the modification during DNA replication (e.g. if DNMT1 or SAM availability was low) [121]. However, in 2009, a new understanding of the regulation of DNA methylation was provided by the discovery that Ten-Eleven Translocation (TET) enzymes catalyse successive oxidation of 5mC to form intermediates which can be removed by base

excision repair machinery [103]. The methylation status of DNA is therefore also determined by the opposing action of enzymes belonging to the DNMT and TET families.

1.6 DNA methylation in diabetes

Multiple studies have demonstrated that diabetes is associated with changes in DNA methylation in particular genes, which correlate with differential expression of these genes [122-126]. Furthermore, a number of these differentially-expressed genes have been associated with functions relevant to diabetes aetiology, indicating that DNA methylation changes may play a causal role in the disease [122-126]. Methylation patterns have been studied in a variety of tissues relevant to diabetes, including pancreatic islets, adipose tissue, liver tissue and peripheral blood [122, 126-128]. In a genome-wide study of DNA methylation comparing type 2 diabetic pancreatic islets to those of healthy controls, 853 genes were found to be differentially-methylated (97% of these were hypermethylated in diabetic islets). By using bioinformatic tools, it was identified that 102 of the 853 differentially-methylated genes were also differentially-expressed in type 2 diabetic compared to non-diabetic islets. Differentially-methylated genes were associated with functions including insulin and glucagon secretion [122]. Further associations have been made in various diabetic tissues between altered methylation levels at promoter regions and dysregulation of genes relating to insulin resistance, body mass index, HbA1c and inflammation [123-126]. Assessments of global levels of DNA methylation have also been made using long interspersed nuclear element-1 (LINE-1) methylation as a surrogate marker [129]. LINE-1 retrotransposons account for 17% of the genome and are highly repetitive sequences which are typically methylated [129]. Reports of global methylation levels assessed by measuring LINE-1 methylation in type 2 diabetic patient peripheral blood have been inconsistent, with reports of worsened carbohydrate metabolism associated with hypomethylation [128] and increased fasting blood glucose concentrations associated with hypermethylation [130].

Although associations have been made between changes in methylation status and features of diabetes pathogenesis, it is much more difficult to establish whether DNA methylation changes are causal in the disease. One prominent example of causality of DNA methylation in disease is evidenced by the Agouti mouse model [131]. Eumelanin production by melanocytes contributes to a black coat colour [131]. However, depending on the extent of methylation of the Agouti gene promoter, the Agouti signalling protein can initiate a switch from eumelanin to phaeomelanin synthesis, which causes yellow coat colouring and a predisposition to diabetes, obesity and tumours [131]. The epigenetic modification and corresponding phenotype are inherited by offspring and can be influenced by maternal diet [132]. Administration of a methyl donor (folic acid) to pregnant dams was shown to increase offspring Agouti promoter methylation, thus suppressing phaeomelanin production and lessening the severity of the phenotype [132]. This example highlights how altered patterns of DNA methylation can strongly influence phenotypes including diabetes and that this can be influenced by environmental factors such as diet.

1.7 DNA methylation in endothelial cells under high glucose conditions

There is limited understanding of how DNA methylation patterns of endothelial cells are influenced by hyperglycaemia and the relevance of this to vascular diseases, but some methylation changes in response to high glucose culture have begun to be characterised *in vitro*. The vasoconstrictor ET-1 has been shown to be hypomethylated and upregulated following culture of human retinal endothelial cells in high glucose conditions [133]. ET-1 expression could be further increased by complete blockade of DNA methylation using 5-azacytidine, suggesting methylation-dependent expression of this gene which can be altered by high glucose conditions [133]. High glucose culture of bovine retinal endothelial cells has been associated with increased DNMT activity and hypermethylation of a subunit of mitochondrial DNA polymerase, possibly contributing to mitochondrial damage and apoptosis in retinal endothelial cells [134]. Furthermore, increased DNMT1 expression following transient high glucose conditions has been reported to induce endothelial dysfunction by hypermethylation and repression of angiopoietin-1, leading to persistent NFκB pathway induction [135].

Beyond investigating single players in endothelial dysfunction, some studies have employed whole-genome analyses to investigate how glucose concentrations affect endothelial cell methylation. A genome wide study of human aortic endothelial cells exposed to high glucose concentrations identified differentially-methylated CpG sites at the transcriptional start sites of genes, which were inversely correlated with histone acetylation, a marker of transcriptional activation [136]. These sites were, in many cases, associated with differential gene expression. Bioinformatic analysis further showed association of hyperacetylation with genes involved in diabetes and inflammatory pathways and some of the differentially-expressed genes overlapped with single nucleotide polymorphisms (SNPs) for diseases including type 1 and type 2 diabetes, cardiovascular disease risk factors and metabolic syndrome [136].

A second study has explored how glucose concentrations in culture affected the genome-wide DNA methylation profile of human aortic endothelial cells [137]. In this study, genes showing differentially-methylated regions were associated with pathways including endothelin signalling, angiogenesis and insulin signalling, all of which are implicated in the pathology of diabetes or its vascular complications [137]. Some of the genes with altered methylation patterns upon high glucose culture correlated with those differentially-expressed in human endothelial precursor cells obtained from diabetic and non-diabetic individuals, such as VEGF and NOS3, supporting the possibility of glucose-dependent methylation changes in the regulation of their expression [137]. By contrast, in a study comparing DNA methylation changes induced by high glucose culture of endothelial cells, unsupervised clustering of the top 5% of CpG sites with the most variable methylation level showed no distinction between cells cultured under high or low glucose conditions [138]. In this study, the cell type (microvascular (human retinal endothelial cells) or macrovascular (HUVEC) endothelial cells) and duration of culture had a much greater impact on DNA methylation than glucose concentration [138].

Taken together, there is some evidence for high glucose-induced alterations in DNA methylation levels in endothelial cells in genes relevant to diabetes and its vascular complications. In some cases, this may be attributed to altered expression or activity of DNMTs in endothelial cells in hyperglycaemia [134, 135]. However, an area that has not yet been investigated is whether high glucose levels affect TET-mediated demethylation of DNA in endothelial cells.

1.8 Demethylation function of Ten-Eleven Translocation (TET) Proteins

TETs belong to the group of 2-oxoglutarate-dependent dioxygenases (2OGDDs). This means they require the tricarboxylic acid (TCA) cycle metabolite 2-OG and molecular oxygen as substrates and Fe^{2+} as a cofactor [103]. TETs modify 5-methylcytosine (5mC) by successive oxidation, forming the oxidative intermediates 5-hydroxymethylcytosine (5hmC), 5-formylcytosine (5fC) and finally 5-carboxylcytosine (5caC) (Figure 1.8) [139]. Unmethylated cytosine can be restored either passively, through loss of maintenance of the modified cytosine during DNA replication, or actively, by removal of 5fC or 5caC by thymine DNA glycosylase (TDG) and base excision repair machinery (Figure 1.8) [139]. 5hmC is stable but its abundance in the genome is approximately 10 to 100-fold lower than that of 5mC [140]. Unlike 5mC which is usually symmetrically positioned on both DNA strands due to maintenance by DNMT1, the positioning of 5hmC is typically asymmetrical, with only approximately 13% of sites displaying symmetrical 5hmC [141, 142]. In mouse ESCs, the abundance of 5fC is approximately 10-fold lower than 5hmC, and the abundance of 5caC is approximately 10-fold lower than 5fC [143]. In addition to being catalytic intermediates, it is now increasingly recognised that 5hmC, 5fC and 5caC could function as epigenetic marks in their own right, having distinct effects on transcription (Reviewed in [144]).

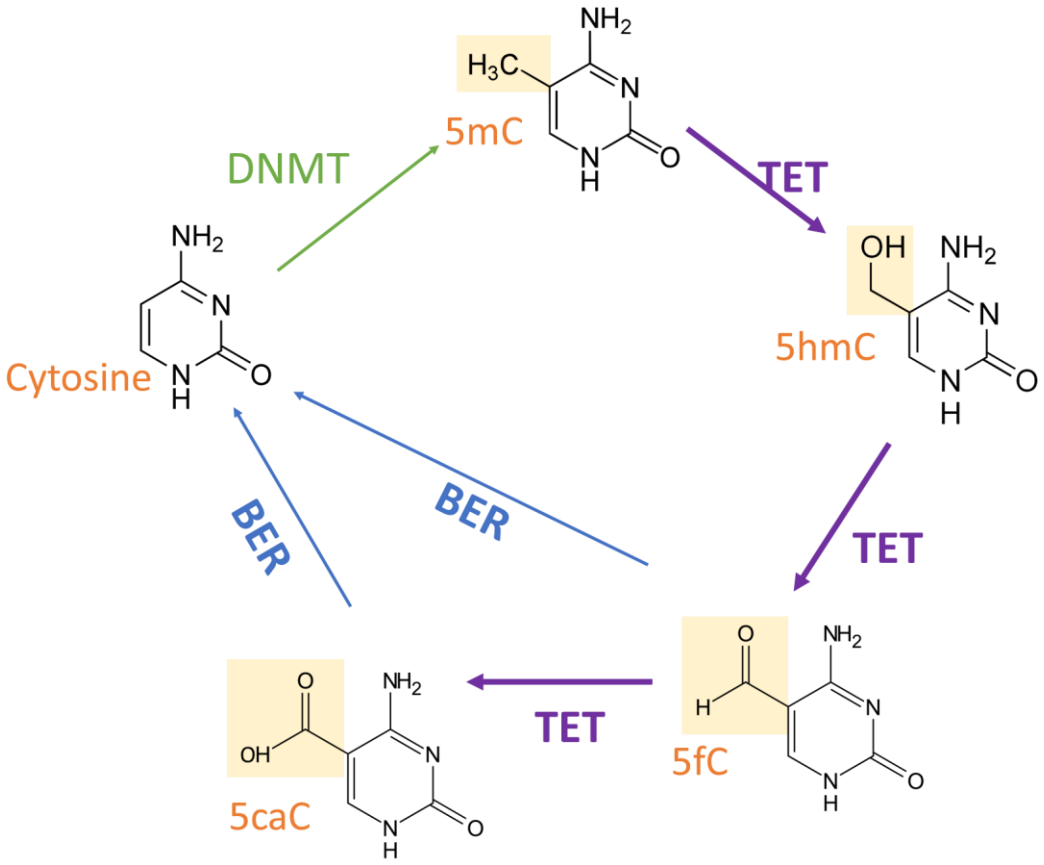

Figure 1.8: ***Methylation and active demethylation of cytosine****. DNA methylation typically occurs at position five of the cytosine ring in a reaction catalysed by a DNA methyltransferase (DNMT). Ten Eleven translocation (TET) enzymes mediate the successive oxidation of 5-methylcytosine (5mC) to 5-hydroxymethylcytosine (5hmC) and subsequently 5-formylcytosine (5fC) and 5-carboxylcytosine (5caC). 5fC and 5caC can be removed by thymine DNA glycosylase and replaced with unmethylated cytosine during base excision repair (BER).*

1.9 Structure of TET proteins

The TET family of proteins consists of three members: TET1, TET2 and TET3. They share a core catalytic domain at the C-terminus consisting of a cysteine-rich domain, a double stranded β-helix domain and Fe^{2+} and 2-oxoglutarate (2-OG) binding domains [145]. TET1 and TET3 both have a CXXC domain, which facilitates binding of the protein to CpG rich regions of chromatin [145]. TET2 instead partners with IDAX, a CXXC domain-containing protein which was originally encoded as part of the TET2 gene, but underwent a chromosomal inversion event during evolution which separated it from the TET2 catalytic domain (Figure 1.9) [146].

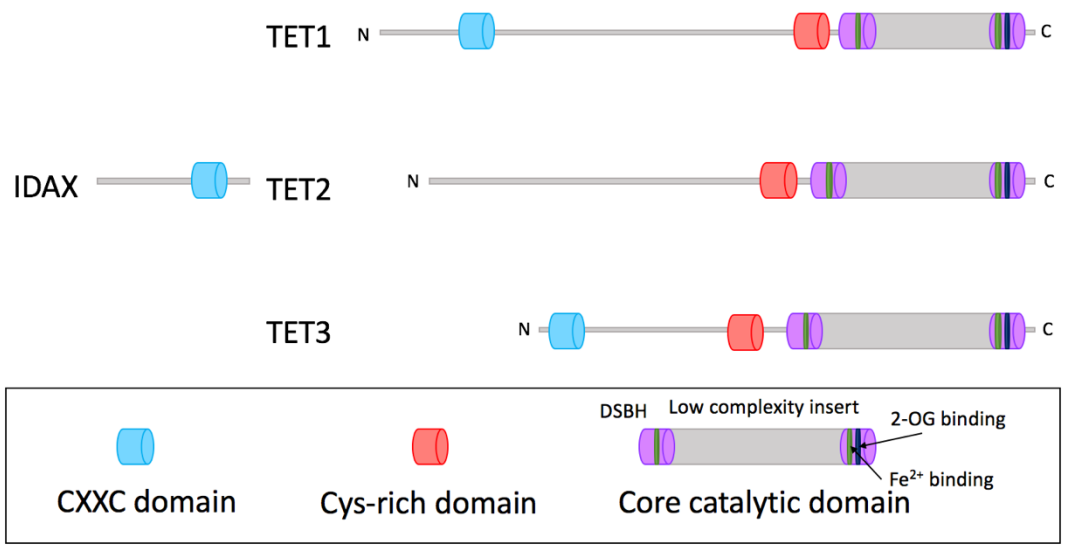

Figure 1.9: ***Structure of TET proteins.*** *The three members of the TET family share conserved structural features of a cysteine-rich domain and a core catalytic domain containing a double stranded beta helix (DSBH) region and binding sites for 2-oxoglurate (2-OG) and Fe^{2+}. Both TET1 and TET3 contain a CXXC domain, but TET2 instead partners with a separate CXXC domain containing protein called IDAX.*

1.10 Distinct functional roles of TETs

Although the three TETs are structurally similar and all possess methylcytosine dioxygenase activity, genetic ablation studies have shown that they perform distinct functional roles. The generation of TET1, TET2 and TET3 single knockout mice, as well as TET1/2 double knockout mice, has shed light on the physiological importance of these enzymes in development and in adult life. $TET1^{-/-}$ and $TET2^{-/-}$ mice can survive to adulthood, showing some reduction in body size and impairment of learning and memory (TET1) [147, 148], or haematopoietic malignancies (TET2) [149]. By contrast, $TET3^{-/-}$ mice display perinatal lethality, demonstrating its importance in development [150, 151]. Combined deficiency of TET1 and TET2 also causes perinatal lethality with a wide range of developmental defects in some cases, but a fraction of double knockout mice are viable and survive to adulthood, suggesting that loss of one or more TETs can, to some extent, be functionally compensated for by the remaining TET(s) [152]. During development, the expression of TETs is dynamically regulated [145, 153]. TET3 is highly expressed in oocytes and fertilised zygotes, but its expression declines

during cleavage. The expression of TET1 and TET2 is low in oocytes and fertilised zygotes, but increase during pre-implantation development, before TET1 expression declines again during later stages of differentiation [145, 153].

In adult tissues, multiple distinct roles for TETs have been described. In some cases, this relates to tissue-specific expression patterns. For example, TET3 is the most highly expressed of the TET proteins in the brain, where it is associated with functions in learning and memory [154]. TET1 is also functionally important in the adult brain [148]. TET2 is associated with functions in the vascular and haematopoietic systems, described in detail below [155-165].

1.11 Potential effects of hyperglycaemia on the regulation of TET activity by changes to cellular metabolism, redox and O_2 availability

By nature of their requirement for O_2, Fe^{2+} and 2-OG, TET function can be compromised when levels of these are altered. For example, in conditions of oxidative stress, TET activity is decreased, likely by loss of its cofactor by oxidation of Fe^{2+} to Fe^{3+} [166]. Conversely, TET activity is promoted by vitamin C which recycles Fe^{3+} to Fe^{2+} [167, 168]. The TCA metabolites fumarate and succinate can compete with 2-OG and thereby inhibit TETs (Figure 1.10) [169]. In addition, the 'oncometabolite' D-2-hydroxyglutarate (2-HG) (which is elevated in multiple cancers due to mutant gain-of-function isocitrate dehydrogenase) is thought to contribute to cancer pathogenesis, in part by competitive inhibition of TETs (Figure 1.10) [170]. O_2 availability is also a determinant of TET activity and is particularly relevant in cellular hypoxia or for differential regulation during embryogenesis where [O_2] is graded [171, 172]. There is good evidence to suggest that endothelial cell metabolism, redox state and O_2 availability may be altered in hyperglycaemic conditions in a manner that could potentially affect TET activity, which we have recently reviewed [173]. Some of the main points are discussed in brief below.

The O_2 consumption rate of endothelial cells has paradoxically been reported to *decrease* in high glucose conditions because ATP requirements can largely be met by glycolysis when glucose levels are high, decreasing the reliance on the TCA cycle and oxidative phosphorylation (referred to as the 'Crabtree effect') (Figure 1.10A) [174]. However, contrasting reports have suggested that exposure of endothelial cells (and other cell types) to hyperglycaemic conditions leads to cellular hypoxia, possibly involving increased mitochondrial ROS generation (Figure 1.10B) [175]. In either case, the activity of TETs may be affected by O_2 availability and by changes in metabolic flux. High glucose culture has been shown to increase lactate production in endothelial cells (due to increased glycolytic flux) [176]. An excess of pyruvate (resulting from lactate oxidation) has previously been suggested to inhibit another member of the 2-OGDD family, prolyl hydroxylase domain-containing protein 2 (PHD2), by competing with 2-OG [177]. Thus, it is plausible that a similar competitive substrate inhibition may decrease TET activity in hyperglycaemia. In hypoxic environments, the activity of lactate dehydrogenase-A is increased, leading to increased levels of the L-enantiomer of 2-HG [178]. As for the D-enantiomer mentioned above, L-2-HG inhibits TET activity [178]. Although it is not known precisely how excess glucose affects the production of TCA metabolites in endothelial cells, it has been shown that the succinate content of rat pancreatic islets increased by 40% upon culture in high glucose conditions [179]. Changes in metabolic flux in hyperglycaemia could therefore (by multiple mechanisms) potentially affect TET activity (Figure 1.10C).

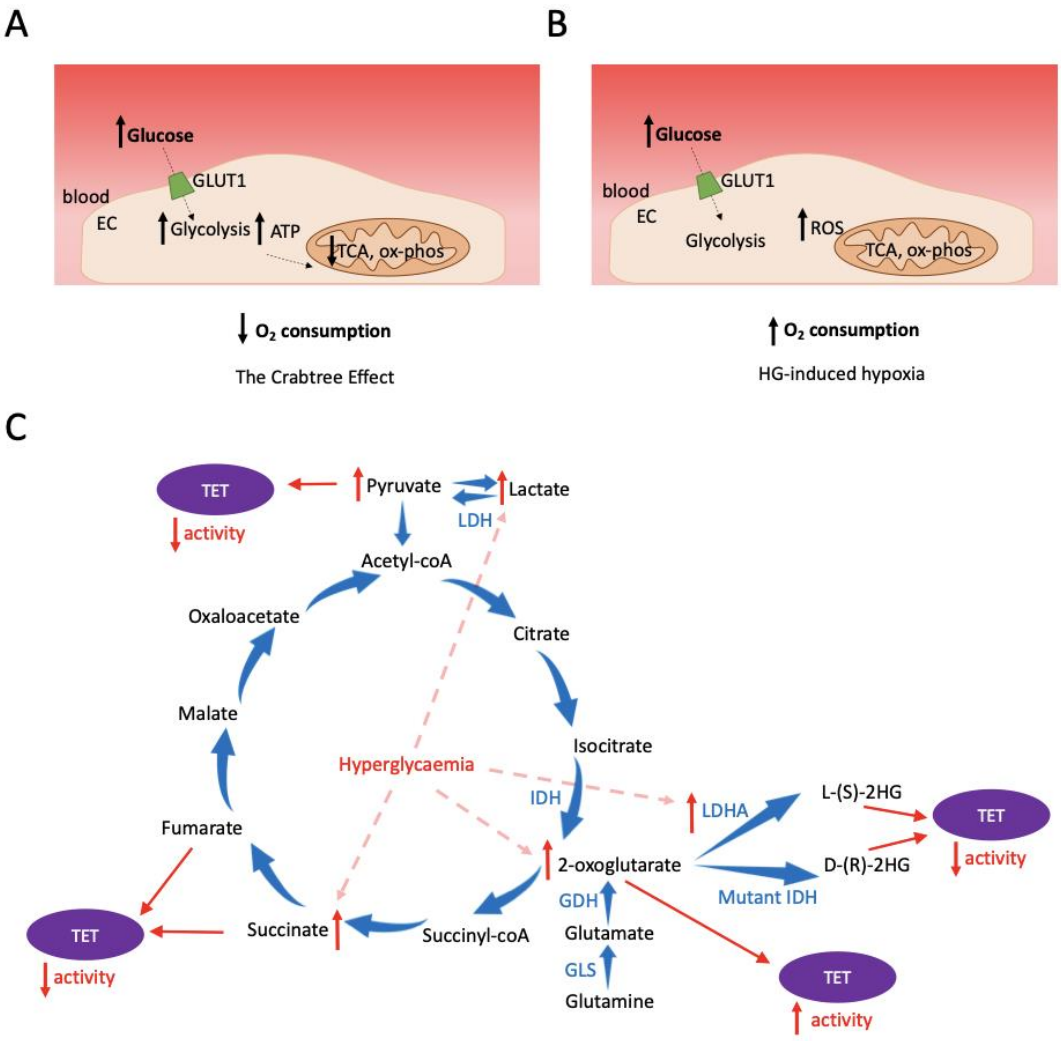

Figure 1.10: ***Potential effects of hyperglycaemia on cellular oxygen consumption and metabolite production****. A) Excess glucose has been reported to increase glycolytic flux and meet metabolic demands with a decreased reliance on oxidative phosphorylation, thus decreasing oxygen consumption. B) Excess glucose has been reported to increase oxygen consumption, increasing reactive oxygen species (ROS) and inducing hypoxia. C) Hyperglycaemia has been reported to increase levels of lactate and succinate, which have been reported to decrease 2-oxoglutarate dependent dioxygenase (2-OGDD) activity. Hyperglycaemia may increase flux through the tricarboxylic acid (TCA) cycle, which could alter intracellular levels of 2-oxoglutarate, fumarate and succinate, all known to affect TET activity. High levels of 2-hydroxyglutarate (2HG), formed by the action of lactate dehydrogenase (LDH)-A on glutamine-derived 2-OG, or by mutant isocitrate dehydrogenase (IDH), is also reported to inhibit TET activity. Abbreviations: glutamate dehydrogenase (GDH), glutaminase (GLS).*

Hyperglycaemia can result in excess production of ROS from various sources as described above (Figure 1.5). Furthermore, increased flux through the polyol pathway in hyperglycaemic conditions consumes NADPH and produces NADH [180]. As NADPH activity is required for glutathione reduction and glutathione (among many cellular functions) is responsible for reducing vitamin C, the balance of Fe^{2+} and Fe^{3+} may be influenced by hyperglycaemia (Figure 1.11) [180]. Cyclic AMP (cAMP) levels have also

been shown to influence Fe^{2+} availability and consequently alter TET activity [181]. Although hyperglycaemia-dependent changes in cAMP levels have not been quantified in endothelial cells, high glucose culture of mesangial cells (which, like endothelial cells, uptake glucose via glucose transporter 1 (GLUT-1)) has been associated with elevated cAMP levels (Figure 1.11) [182]. Hyperglycaemia may therefore affect iron homeostasis and lead to changes in TET activity. In addition to potential changes to TET activity as a result of altered O_2, Fe^{2+} and 2-OG levels, hyperglycaemia has been shown to influence post-translational modification of TET2 and impact its activity in peripheral blood mononuclear cells [183], which will be discussed below.

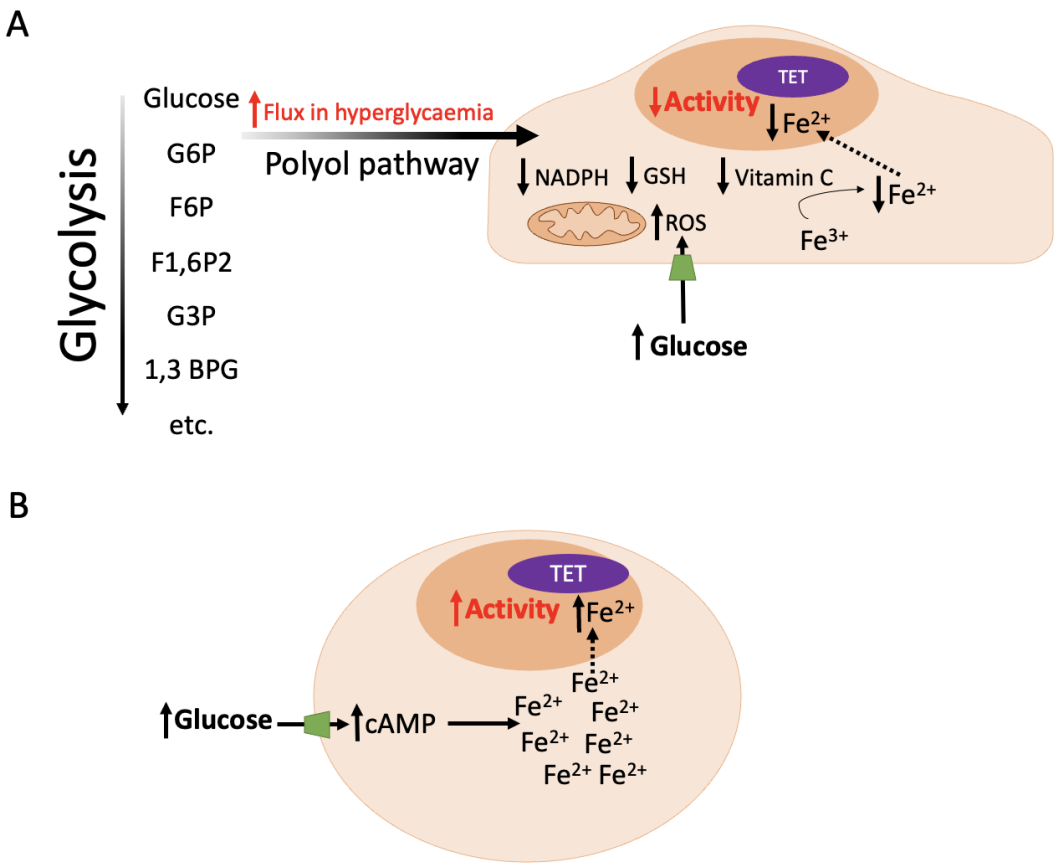

Figure 1.11: ***Hyperglycaemia may affect TET activity by altered availability of its cofactor Fe^{2+}.*** *A) In hyperglycaemia, excess glucose is diverted to the polyol pathway which consumes NADPH. The generation of reduced glutathione (GSH) requires reduced nicotinamide adenine dinucleotide phosphate (NADPH). A decrease in GSH levels may affect generation of the reduced form of vitamin C which regenerates Fe^{2+} for optimal TET activity. B) An increase in intracellular cyclic adenosine monophosphate (cAMP) levels in hyperglycaemic conditions may increase the intracellular labile Fe^{2+} pool and therefore increase TET activity. Abbreviations: glucose-6-phosphate (G6P), fructose-6-phosphate (F6P), Fructose-1,6-bisphosphate (F1,6P2), glyceraldehyde-3-phosphate (G3P), 1,3-bisphosphoglycerate (1,3 BPG).*

1.12 Non-catalytic roles and interaction partners of TETs

In addition to their catalytic activity, TETs have been shown to regulate transcription through non-catalytic mechanisms, acting as a binding partner for various transcription factors and chromatin modifiers. Table 1.1 shows examples of interaction partners identified for TET1, TET2 and TET3 and their functional role in cells. Functions that are independent of TET catalytic activity are indicated. These studies include a potential scaffolding role for TETs, enabling the recruitment of other epigenetic modifiers to alter the arrangement of chromatin and hence affect transcription without the involvement of cytosine demethylation.

TET enzyme involved	Interaction partner	Cell type	Function	Independent of catalytic activity?	Reference
TET1	PRC2	mESCs	PRC2-dependent recruitment of TET1 for demethylation of gene-regulatory elements during cell differentiation	No	[184]
TET1	OGT	HEK293T, mESCs	OGT promotes TET1 function during development	No	[185]
TET1	OGT	mESCs	TET1 is required for OGT recruitment to promoters where they regulate CpG island methylation in embryonic stem cells	No	[186]
TET1	SIN3A	mESCs	Sin3a interacts with TET1 to activate gene transcription for regulating pluripotency	No	[187]
TET1	Mbd3	mESCs	TET1 is required for Mbd3 binding to its genomic targets in embryonic stem cells	No	[188]
TET1	HIF-1a and HIF-2a	FADU, H1299	TET1 acts as a transcriptional co-activator with HIF-1a/2a for hypoxia-responsive genes involved in epithelial-mesenchymal transition	Yes	[189]
TET2	WT1	KG-1, HL-60, mESCs, mouse bone marrow cells	WT1 recruits TET2 to regulate its target gene expression and suppress leukemia cell proliferation	No	[190]
TET2	PU.1	Human PBMCs undergoing osteoclast differentiation	PU.1 recruits TET2 for demethylation of genes involved in the differentiation of monocytes to osteoclasts	No	[191]
TET2	OGT	HEK293T	TET2 promotes the association of OGT with chromatin to facilitate histone O-GlcNAcylation for regulation of gene transcription	Yes	[192]
TET2	OGT	HEK293T	TET2/3 promote O-GlcNAcylation of targets including host cell factor 1 which forms an essential component of the H3K4 methyltransferase SET1/COMPASS	Yes	[193]
TET2	IDAX	HEK293T	Facilitates TET2 binding to DNA, but also promotes caspase-dependent degradation of TET2	No	[146]
TET2	IκBζ and HDAC2 and HDAC1	Mouse BMDCs	IκBζ mediates targeting of TET2 to IL6 promoter where HDAC2, in a complex with HDAC1, represses its transcription by histone deacetylation	Yes	[158]
TET2	RUNX1	MEL	TET2 interacts with RUNX1 to regulate its transcriptional activity and expression of its target genes involved in osteoclast differentiation	No	[194]

TET2	SNIP1	HEK293T, MCF-7, U2OS	SNIP1 bridges TET2 to interact with various transcription factors including c-MYC, to regulate expression of genes involved in the DNA damage response	No	[195]
TET2	CXXC5	Mouse pDCs	CXXC5 recruits TET2 to maintain hypomethylation of genes including IRF7 involved in the antiviral response of plasmacytoid dendritic cells	No	[160]
TET2	AID	OCI-LY7	AID recruits TET2 to demethylate the FANCA promoter in diffuse large B cell lymphoma	No	[196]
TET2	STAT1	THP-1, B16-OVA	IFN-γ increased the interaction of STAT1 and TET2, enabling TET2-mediated hydroxymethylation of STAT1 target genes including chemokine and PD-L1 genes	No	[197]
TET2	p300, DNMT1	A2780	Acetylation of TET2 protein by p300 enhances its catalytic activity and DNMT1 binding capability, which stabilises it. Acetylation protects against abnormal DNA methylation during oxidative stress.	No	[198]
TET2	AMPK	PBMCs	AMPK-mediated phosphorylation of TET2 protein stabilises it and increases 5hmC levels. The AMPK-TET2-5hmC axis is important in TET2 tumour-supressor function	No	[183]
TET2	JAK2, KLF1	UT-7	JAK2 phosphorylates TET2, increasing its interaction with KLF1 to regulate genes involved in erythroid differentiation	No	[199]
TET2	FOXO3a	Mouse neural stem cells	FOXO3a interacts with TET2 and regulates the expression of genes related to adult neural stem cell proliferation	No	[200]
TET3	OGT	HEK293T	TET2/3 promote O-GlcNAcylation of targets including host cell factor 1 which forms an essential component of the H3K4 methyltransferase SET1/COMPASS	Yes	[193]
TET3	REST, NSD3	Mouse retina	REST recruits TET3 for transcriptional activation of neuronal genes during retinal maturation involving H3K36me3-induced chromatin remodeling by NSD3	No	[201]
TET3	Thyroid hormone receptors	HEK293T	TET3 stabilises thyroid hormone receptors and regulates their association with chromatin	Yes	[202]
TET3	HDAC1, SIN3A	HEK293T, mouse peritoneal macrophages	TET3 promotes the interaction of HDAC1 or SIN3A with the IFNb1 promoter to suppress its expression	Yes	[203]

Table 1.1: ***Interaction partners of TET enzymes and their functional roles.*** *TET1, TET2 and TET3 interact with a variety of proteins to elicit their cellular functions. Some of these functions involve the catalytic methylcytosine dioxygenase activity of TETs, whilst others are independent of their enzymatic activity.*

1.13 Roles of TET2 in vascular cells and disease

Of the three TETs, TET2 has been most often associated with functions in vascular and haematopoietic systems. TET2 is a tumour suppressor and one of the most frequently mutated genes in haematological cancers including acute myeloid leukaemia, chronic myelomonocytic leukemia and T-cell lymphomas [155]. Age-related somatic mutations of TET2 are also associated with non-malignant expansion of blood cells, termed clonal haematopoiesis [156]. Clonal haematopoiesis is relatively common in healthy elderly individuals, however, it has now been linked to an increased risk of all-cause mortality, partly attributed to an increased incidence of cardiovascular diseases [156, 204]. Animal studies have shown that inactivating mutations or knockout of TET2 in bone marrow cells causes clonal haematopoiesis and accelerates atherosclerosis [156, 157], exacerbates age- or obesity-induced insulin resistance [205] and worsens cardiac remodelling and function in models of heart failure [206]. These effects are associated with elevated IL-1β/NLRP3 inflammasome signalling in TET2-deficient cells [157, 205, 206].

In macrophages and dendritic cells, TET2 has been shown to be involved in the repression of IL-1β and IL-6 during the resolution phase of inflammatory responses [158, 159]. TET2 has also been shown to regulate antiviral responses in dendritic cells [160], regulate mast cell differentiation and proliferation [161] and contribute to the prevention of B cell hyperactivity and autoimmunity [162]. Thus, there are roles described for TET2 in both innate and adaptive immunity. In vascular smooth muscle cells, TET2 regulates plasticity by downregulating pro-contractile genes myocardin (MYOCD) and serum response factor (SRF), alongside upregulation of Kruppel-like factor (KLF)4 [163]. TET2 is therefore thought to act as a master regulator of the vascular smooth muscle cell phenotype, playing an important protective role against de-differentiation which is detrimental in atherosclerosis [163].

One of the first reports of a role for a TET protein in endothelial cells was that of Peng *et al.* in 2016 [164]. It was observed that TET2 expression and 5hmC levels were reduced progressively during the development of atherosclerotic lesions of ApoE$^{-/-}$ mice and that TET2 overexpression could rescue this. By investigating the impact of TET2 overexpression or short hairpin (sh)RNA-mediated silencing in HUVEC treated with oxidised LDL, the authors suggest that the protective effects of TET2 are mediated by its regulation of autophagy and the expression of inflammatory factors [164]. In 2017, the same group reported that shRNA-mediated silencing of TET2 in HUVEC increased the expression of ICAM-1 and VCAM-1, inhibited NFκB activation and decreased adhesion of THP-1 (monocyte-like) cells to the endothelium in response to oxidised LDL [165].

There are very few studies investigating TET function in the context of diabetes. However, an important study conducted in monocytes from type 2 diabetic patients has provided strong evidence that TET activity is altered by hyperglycaemia. Wu *et al.* observed that TET2 activity is reduced in monocytes of type 2 diabetic patients compared to healthy controls [183]. They found that under normal circumstances, AMP-activated protein kinase (AMPK) phosphorylates and thereby stabilises the TET2 protein, protecting it from calpain-mediated degradation. However, in the presence of excess glucose, AMPK activity is decreased, leading to destabilisation of TET2 and reduced global levels of 5hmC (a surrogate marker for TET activity). Decreased 5hmC levels were also observed in other cell types after exposure to high glucose culture conditions, including HUVEC [183]. This supports the notion that TET2 activity can be dysregulated as a direct consequence of hyperglycaemia.

Given the importance of endothelial cells to the pathophysiology of diabetic vascular complications, it is vital to understand the mechanisms by which they become dysfunctional in hyperglycaemia. The role of TETs in endothelial cell function and dysfunction remains largely unexplored but given that TET2 is involved in vascular functions and disease and TET2 has been shown to be dysregulated in cells from

diabetic patients, it may be hypothesised that TETs are involved in hyperglycaemia-induced endothelial dysfunction.

1.14 Hypothesis

TET enzymes act as cellular sensors of hyperglycaemia, altering the epigenetic and transcriptional landscape of endothelial cells. Dysregulation of TET activity by hyperglycaemia contributes to endothelial dysfunction and impairs vascular function in diabetes.

1.15 Aims

1. Investigate the relative contribution of TET1, TET2 and TET3 to the regulation of endothelial cell transcription.
2. Compare genes dysregulated by high glucose culture of endothelial cells to those differentially-expressed upon silencing of TET1, TET2 or TET3.
3. Explore the possible mechanisms underlying TET-mediated transcriptional regulation in endothelial cells.
4. Use *in vitro* assays to assess whether endothelial functions are compromised by silencing TET2 in endothelial cells in a similar manner to that observed upon exposure to high glucose concentrations.
5. Determine whether vascular reactivity of control or diabetic mice is altered by the endothelial-specific deletion of TET2.
6. Compare the abundance of plasma cytokines and the transcriptome of endothelial cells from these mice to explore whether characteristics of endothelial dysfunction are present and if this is influenced by the absence of TET2 in endothelial cells.

2. Materials and Methods

2.1 Reagents

All reagents were purchased from Sigma unless otherwise stated.

2.2 Cell culture

All cells were cultured in a 37^{o}C humidified incubator with 5% CO_2.

2.2.1 HUVEC culture

Human umbilical vein endothelial cells (HUVEC) from pooled donors (Lonza, #C2519A) were expanded in endothelial growth media-2 (EGM-2 #CC-3156 and #CC-3162) media (Lonza), in T75 flasks coated with 0.4% gelatin (Sigma, #G1393) in phosphate buffered saline (PBS). HUVEC were frozen in heat-inactivated fetal calf serum (FCS) (Sigma, #F9665) with 10% dimethyl sulfoxide (DMSO) and stored in liquid nitrogen at passage 3. HUVEC were thawed and cultured in EGM-2 media (Promocell, #C-22011) supplemented with 1% penicillin-streptomycin in 0.4% gelatin-coated T75 flasks. All HUVEC experiments were conducted at passage 4.

2.2.2 HL-60 cell culture

HL-60 cells stably expressing CXCR2 were cultured in RPMI 1640 medium (Sigma, #R0883) supplemented with 1% L-glutamine-penicillin-streptomycin solution (Sigma, #G1146) and heat-inactivated FCS (10%) and maintained at a density of 0.5x10^{6} cells/ml.

2.2.3 Differentiation of HL-60 cells

HL-60 cells were treated with 1.3% DMSO at a density of 1x10^{6} cells/ml for 4 days to promote differentiation to a neutrophil-like phenotype prior to adhesion assays.

2.2.4 HeLa cell culture and plasmid transfection

HeLa cells were cultured in Dulbecco's Modified Eagle Medium supplemented with 10% FCS and 1% penicillin/streptomycin/L-glutamine. HeLa cells were plated at a density of 400,000 cells per well of a 6-well plate. For each TET protein overexpression plasmid (Addgene 49792, 41710, 49449) and control plasmid pcDNA3.1, 8µg plasmid DNA was diluted in optimem to a volume of 400µl and mixed with 400µl optimem containing 4µl lipofectamine LTX reagent and 2µl plus reagent. After 10 minutes incubation at room temperature (RT), 200µl of the complex was added to cells in 3ml culture medium. Experiments were conducted after 48 hours.

2.3 HUVEC treatments

2.3.1 Glucose and mannitol treatments

To simulate hyperglycaemia, 20mM D-glucose was added to EGM-2 media for a final concentration of 25mM glucose. To control for osmotic effects, HUVEC in EGM-2 (5mM glucose) were supplemented with 20mM D-mannitol. Treatments were continued for 48h for RNA sequencing experiments. For intermittent glucose experiments, HUVEC were cultured for 2 weeks, changing between 5mM glucose and 25mM glucose media (or for controls, between 5mM glucose with or without the addition of 20mM mannitol) every 24h.

2.3.2 5-aza-2'-deoxycytidine treatment

Where indicated, HUVEC were treated with 5µM 5-aza-2'-deoxycytidine (5azaC) (Sigma #A3656) or 0.1% DMSO (as vehicle controls) in EGM-2 for 72 hours, refreshing the treatment every 24h.

2.3.3 Trichostatin A treatment

Where indicated, HUVEC were treated with 300nM Trichostatin A (Sigma, #T1952) or 0.1% DMSO in EGM-2 for 4h.

2.3.4 Tumour necrosis factor α (TNFα), interferon (IFN)α, IFNγ and lipopolysaccharide (LPS) treatments

1h prior to treatment with TNFα, IFNα, IFNγ or LPS, media was changed from EGM-2 to endothelial basal media-2 (EBM-2) supplemented with 2% FCS, 1μg/ml ascorbic acid and 22.5μg/ml heparin (referred to as 'basal media'). 10ng/ml recombinant human TNFα (RD systems #210-TA), 10ng/ml recombinant human IFNγ (Sigma #IF002), 1000U/ml recombinant human IFNα (Sigma #IF007) or 1μg/ml LPS (Sigma #L2880) was applied to the cells in basal media for the indicated time.

2.3.5 Synthechol®, atorvastatin and 25-hydroxycholesterol (25-HC) treatments

Where indicated, HUVEC were treated with 1x Synthechol® (Sigma #S5442), 5mM atorvastatin (or 0.01% DMSO control) or 2mM 25-hydroxycholesterol (or 0.02% ethanol control) in EGM-2 for the indicated time.

2.3.6 siRNA transfection of HUVEC

HUVEC were seeded at approximately $3x10^5$ cells per well of a 6-well plate in EGM-2 media. After 24 hours, media was replaced with optiMEM (Thermo Fisher Scientific #11058021) for 1h prior to transfection. Silencer™ Select siRNAs (Thermo Fisher Scientific, #4392420. TET1: s37193 TET2: s29441, TET3: s47238, HDAC1: s73 HDAC2: s6495) were mixed with lipofectamine™ RNAiMAX Transfection Reagent (ThermoFisher Scientific, #13778075) and diluted 1:1 with diluted lipofectamine RNAiMAX (1:100 in optiMEM). Mixtures were incubated at room temperature for 15 minutes before applying to cells in triplicate, to a final concentration of siRNA 20nM (TET2, HDAC1 and HDAC2 siRNA) or 100nM (TET1 and TET3 siRNAs) per well in 800μl optiMEM containing 8μl lipofectamine RNAiMAX. Silencer™ Select Negative Control No. 1 (ThermoFisher Scientific, #4390843) was used at an equivalent concentration to the respective targeting siRNA for control

samples. Media was replaced with EGM-2 after 7h. HUVEC were harvested >48h after transfection.

2.4 DNA analysis

2.4.1 DNA extraction

Phenol-chloroform extraction method

$1x10^6$ cells per sample were scraped into 350µl tail buffer (100mM Tris-HCl pH 8.0, 5mM EDTA pH 8.0, 0.2% SDS, 200mM NaCl) containing 350µg/ml proteinase K (Merck, #P5568) and digested overnight at 55°C. Samples were sonicated twice each for 10 seconds using a Branson sonifier, setting 2, before treating with 140µg/ml RNAse A (Qiagen, #19101) for 30 minutes at 55°C. An equal volume of phenol solution was added and mixed, samples were centrifuged at 9800 x g for 3 minutes and the aqueous phase retained. Phenol addition and centrifugation was repeated and the aqueous phase mixed with an equal volume of chloroform. The aqueous phase was retained and 0.8x the sample volume of isopropanol added. Centrifugation for 10 minutes at 14,000 x g pelleted precipitated DNA. DNA pellets were washed with 80% ethanol, re-pelleted and air-dried before resuspending in nuclease-free H_2O.

Monarch® Genomic DNA Purification Kit method

$1x10^6$ cells per sample were scraped into PBS and pelleted by centrifugation. DNA extraction was performed using the Monarch® Genomic DNA Purification Kit according to the manufacturer's instructions.

2.4.2 Dot blotting

1µg of DNA was diluted in nuclease-free H_2O to 70µl. DNA was denatured by addition of 5µl 1.5M NaOH and boiling at 95°C for 5 minutes. Samples were neutralised by the addition of 3.75µl 6.6M ammonium acetate and placed on ice. The dot blot manifold was assembled with a Hybond-N membrane and 3mm Whatman filter paper both pre-soaked in 6x saline sodium citrate (SSC). 75µl 6x SSC was loaded to each well and

allowed to pass through the membrane under vacuum pressure. 75µl sample was applied to each well and vacuum pressure applied. Wells were washed again with 6x SSC and the membrane removed and air-dried. UV cross-linking was performed for 5 minutes, followed by blocking for 1 hour in 10% milk powder (Marvel) in PBS/0.1% Tween (PBS-T). The membrane was incubated with 5hmC rabbit polyclonal antibody (Active Motif, #39769) diluted 1:10,000 in SignalBoost™ (Merck, #407207) overnight at 4^{o}C under constant agitation. Membranes were washed 3 times for 10 minutes with PBS-T under agitation, then incubated with donkey anti-rabbit 488 secondary antibody (LiCOR, C60322-02) diluted 1:15,000 in 10% milk powder in PBS-T for 1 hour under agitation. Following three 10-minute washes with PBS-T and one wash with PBS, 5hmC staining was visualised using a LiCOR Odyssey system and ImageStudio software. Methylene blue (0.04% w/v in 0.5M sodium acetate) was applied for 20 minutes and rinsed with H_2O to confirm equal loading of DNA.

2.4.3 Hydroxymethylated DNA immunoprecipitation sequencing (hMeDIPseq)

HUVEC were transfected with siRNA targeting TET2 or TET3 or a negative control siRNA as described above. In a separate experiment, HUVEC were cultured for 25h in basal media (as controls) or cultured in basal media for 1h and then treated with 10ng/ml IFNγ in basal media for 24h. In a third experiment, HUVEC were cultured for 2 weeks in media containing 25mM glucose or in media containing 5mM glucose and 20mM mannitol. For transfected HUVEC, genomic DNA was harvested by phenol-chloroform extraction after 48 hours. For all other HUVEC, genomic DNA was extracted using the Monarch Genomic DNA Purification Kit method. Successful silencing of TET2 and TET3 was confirmed by qPCR performed using RNA isolated from cells transfected and harvested at the same time as for DNA isolation. hMeDIPseq and initial bioinformatic analysis was carried out by ArrayStar using 3µg of DNA from duplicate negative control siRNA, TET2 siRNA and TET3 siRNA-treated HUVEC, or 5µg of DNA from control, IFNγ-treated, high glucose-treated or mannitol-treated HUVEC, using the following protocol:

DNA samples were fragmented to a size range of ~200-800bp with a Diagenode Bioruptor. Approximately 1µg of fragmented DNA was prepared for Illumina NovaSeq 6000 sequencing as the following steps: 1) End repair of DNA samples; 2) A single 'A' base was added to the 3' ends; 3) Ligation of Illumina's genomic adapters to DNA fragments; 4) hMeDIP to enrich hydroxymethylated DNA by anti-5-hydroxymethylcytosine antibody; 5) PCR amplification to enrich precipitated fragments; 6) Size selection of ~300-900bp DNA fragments using AMPure XP beads. The completed libraries were quantified by Agilent 2100 Bioanalyzer. The libraries were denatured with 0.1M NaOH to generate single-stranded DNA molecules, captured on Illumina flow cell, amplified in situ. The libraries were then sequenced on the Illumina NovaSeq 6000 following the NovaSeq 6000 S4 Reagent Kit (300 cycles) protocol. After sequencing images were generated, image analysis and base calling were performed using Off- Line Basecaller software (OLB V1.8). After passing Solexa CHASTITY quality filter, the clean reads were aligned to human genome (UCSC hg19) using Hisat2 software. Aligned reads were used for peak calling, long ncRNA, mRNA and small ncRNA associated hMeDIP enriched regions (peaks) with statistically significant were identified for each sample, using a q-value threshold of 10^{-4} by MACS2 software. Long ncRNA, mRNA and small ncRNA associated hMeDIP enriched regions (peaks) were annotated by the nearest gene using the newest UCSC RefSeq database. Long ncRNA, mRNA and small ncRNA associated differentially hydroxymethylated regions (DhMRs) within promoter between two samples/groups with statistically significant were identified by diffReps software (Cut-off: log2FC≥0.585, p-value≤0.001). Table 2.6 summarises experimental details and GSE identifiers for sequencing experiments conducted.

2.4.4 5hmC enrichment profiles across genomic regions

Graphs of 5hmC profiles across hg19 genomic regions were created from BAM files generated by hMeDIPseq using bamCoverage, computeMatrix and plotProfile tools within deepTools version 3.5.1 (https://deeptools.readthedocs.io/en/develop/index.html) using Python version

3.9.6. This generated 5hmC profiles for each condition across all genes (taking into account differences in gene length) and 3Kb upstream and downstream.

2.5 RNA analysis

2.5.1 RNA extraction

RNA was extracted using a Reliaprep™ kit (Promega, #Z6012), according to the manufacturer's instructions (with the exceptions that DNA was sheared with Qiashredders (Qiagen, #79656) before addition of isopropanol and that 1µl RQ1 RNase-free DNAse (Promega, #M6101) per sample was included in addition to DNase I in the incubation mix). RNA was eluted in nuclease-free H_2O and stored at -80^oC.

2.5.2 cDNA synthesis

Promega M-MLV reverse transcriptase method

1µg RNA was diluted to a volume of 13µl in nuclease-free H_2O with the addition of 1µl dNTPs (10mM) (Promega, #U1330) and 1µl oligodT (1µg/µl) and heated to 72^oC for 5 minutes. Samples were cooled to 4^oC and 4µl 5x M-MLV (Moloney murine leukaemia virus) reverse transcriptase buffer (Promega, #M531A), 0.5µl M-MLV reverse transcriptase enzyme (Promega, #M170B) and 0.5µl RNAsin (Promega, #N251B) were added. Samples were heated to 42^oC for 90 minutes, followed by 70^oC for 10 minutes and cooled to 4^oC. Samples were diluted to a final volume of 100µl with nuclease-free H_2O and stored at -20^oC. Negative controls were also prepared using equivalent amounts of RNA, dNTPs, oligodT and buffers in the absence of reverse transcriptase enzyme.

New England Biolabs LunaScript method

500ng RNA was diluted to a volume of 8µl in nuclease-free H_2O with the addition of 2µl 5X LunaScript RT SuperMix (New England Biolabs, #E3010L). Samples underwent primer annealing at 25^oC for 2 minutes, followed by cDNA synthesis at 55^oC for 10

minutes and then heat inactivated at 95°C for 1 minute. Negative controls were also prepared using equivalent amounts of RNA, H_2O and the No-RT Control Mix.

2.5.3 RT-qPCR

SYBR green method

Primer pairs were designed to span an intron in the corresponding genomic DNA using the NCBI Primer-BLAST online tool (https://www.ncbi.nlm.nih.gov/tools/primer-blast). RT-qPCR was performed with 10µl 10X SYBR green mastermix (PCR biosystems, #PB012612-04), 2µl each of forward and reverse primers (3µM), 4µl nuclease-free H_2O and 2µl cDNA per reaction using the StepOne Plus Real-Time PCR system (Applied Biosystems). Duplicate samples underwent denaturation for 10 minutes at 95°C, followed by amplification by 40 cycles of 95°C for 15 seconds, 60°C for 30 seconds and 72°C for 20 seconds. Melting profiles were also conducted to confirm specificity of primers by the appearance of a single melt curve peak indicating a single amplicon. Relative mRNA expression was calculated using the $2^{-\Delta\Delta CT}$ method.

Taqman method

For CH25H, pre-designed Taqman® primers/probes (Applied Biosystems) were used. Reactions consisted of 10µl 10X Taqman® Gene Expression MasterMix (Applied Biosystems, #4370048), 1µl 20x CH25H primer/probe mix and 7µl nuclease-free H_2O. Duplicate samples underwent denaturation for 10 minutes at 95°C, followed by amplification by 40 cycles of 95°C for 15 seconds, 60°C for 30 seconds and 72°C for 20 seconds. Relative mRNA expression was calculated using the $2^{-\Delta\Delta CT}$ method.

Species	Gene	Forward primer sequence (5’-3’)	Reverse primer sequence (5’-3’)
Human	β-actin (ACTB)	CCTCGCCTTTGCCGATCC	CGCGGCGATATCATCATCC
Human	RPLP0	CCATTCTATCATCAACGGGTACAA	TCAGCAAGTGGGAAGGTGTAATC
Human	TET1	CCGAATCAAGCGGAAGAATA	CCTGGAGATGCCTCTTTCAC
Human	TET2	GAAAGGAGACCCGACTGCAA	ATCTTGAGAGGGTGTGCTGC
Human	TET3	CAACGGCTGCAAGTATGCTC	CTCGTTGGTCACCTGGTTCT
Human	MX1	ATCAGCCTGCTGACATTGGG	CCACATTACTGGGGACCACC
Human	RSAD2	GTGCAACTACAAATGCGGCT	CTTGCCCAGGTATTCTCCCC
Human	OAS2	CCAGGATGCAGGCAAAAGAAA	CCAGAAGGCCCTGGTAACTA
Human	IFITM1	CGGCTCTGTGACAGTCTACC	CTGCTGTATCTAGGGGCAGG
Human	ISG15	ACAGCCATGGGCTGGGA	CCTTCAGCTCTGACACCGAC
Human	E-selectin (SELE)	CAGCTGCCAAAGCCTTGAATC	CCTCTAGTTCCCCAGATGCAC
Human	ICAM-1	AGCTTCGTGTCCTGTATGGC	TTTTCTGGCCACGTCCAGTT
Human	VCAM-1	TGCACAGTGACTTGTGGACAT	GGCCACCACTCATCTCGATT
Human	IRF7	GCAAGTGCAAGGTGTACTG	CACCAGCTCTTGGAAGAAGA
Human	STAT1	TCGACAGTCTTGGCACCTAA	AGTCAAGCTGCTGAAGTTCGT
Human	HDAC1	TGTCTACTGGTGGTTCTGTGG	ACCCTCTGGTGATACTTTAGCA
Human	HDAC2	TCTGCTACTACTACGACGGTGA	TCATTTCTTCGGCAGTGGCT
Human	HMGCR	GCCCTCAGTTCCAACTCACA	CAAGCTGACGTACCCCTGAC
Human	SQLE	CTATGGCAGAGCCCAATGCAA	AACAGTCAGTGGAGCATGGAG
Human	LSS	GTACGAGCCCGGAACATTCT	CCAGTCAGGAAACAGCCACA
Human	DHCR7	TATAACGAGGAAAGCCGCCC	TACTTGTTCACAACCCCTGC
Human	MSMO1	GCATGGGTGACCATTCGTTT	TGATGCCGAGAACCAGCATA
Human	HMGCS1	TCACGCTTGTGCCCGA	CCAGCAAGCTTCTGCATTCAA
Human	CH25H	*Taqman primer/probe set	*Taqman primer/probe set

Mouse	β-actin (ACTB)	CTTTGCAGCTCCTTCGTTGC	CCTTCTGACCCATTCCCACC
Mouse	L-selectin (SELL)	GTCACCGCATTCTCGGGGCT	TGTGGGAGATGCCTGCGTGT
Mouse	CXCL10	GCCCACGTGTTGAGATCATTGCC	GGGGTGTGTGCGTGGCTTC
Mouse	TNFA	CGGTCCCCAAAGGGATGAGAAGT	TGCTACGACGTGGGCTACAGG
Mouse	IL1B	TGCCACCTTTTGACAGTGATGAGA	TGCCTGCCTGAAGCTCTTGTT
Mouse	CD206	CCGGAGGGTGCAGACAAAGG	TCGTCCACAGTCCACCGAAAC
Mouse	IL6	CTGCAAGAGACTTCCATCCAG	AGTGGTATAGACAGGTCTGTTGG

Table 2.1: ***List of primers used for RT-qPCR.***

2.5.4 HUVEC RNA sequencing

HUVEC were treated with glucose or mannitol or transfected with siRNA targeting TET1, TET2 or TET3 or a negative control siRNA as described above. RNA was harvested after 48h. Triplicate samples of RNA were pooled in equal amounts to a final quantity of 1μg of RNA in 25μl nuclease-free H_2O. Library preparation, single-read sequencing (20 million sequence reads) and initial bioinformatic analysis was conducted by BGI using the DNBseq™ sequencing platform as follows:

RNA (approximately 1μg per sample) underwent quality control using an Agilent 2100 Bioanalyser to determine RNA concentration, RIN value, 28S/18S and fragment length distribution. Samples underwent mRNA enrichment, fragmentation and reverse transcription using N6 random primers. The synthesised cDNA was subjected to end-repair and then was 3' adenylated. Adaptors were ligated to the ends of these 3' adenylated cDNA fragments before PCR amplification. PCR products were heat denatured and cyclized by splint oligo and DNA ligase before sequencing using a DNBseq platform. Internal software was used to remove reads mapped to rRNA, reads with adaptors, reads with a high proportion of unknown bases (> 0.1%) or low quality reads. Clean reads were mapped to the reference genome (UCSC hg19) using Bowtie2, generating on average approximately 22.09 million clean reads per sample with an

average mapping ratio with the reference genome of 95.42%. Samples displayed uniform mapping suggesting that the samples are comparable. Gene expression levels were determined using RSEM software. Sequencing saturation analysis, read coverage and distribution analysis of the transcripts were used to confirm data quality prior to bioinformatic analysis. Differentially expressed genes were detected using PossionDis algorithms (based on the poisson distribution). Further differential gene expression analysis was performed using Ingenuity Pathway Analysis (IPA) software (Qiagen) applying thresholds of Log2FoldChange>|1| and false discovery rate <0.05. Table 2.6 summarises experimental details and GSE identifiers for sequencing experiments conducted.

2.6 Protein analysis

2.6.1 Nuclear and cytoplasmic fractionation

Nuclear and cytoplasmic fractionation of HUVEC was performed using the NE-PER kit (Thermo Fisher, #78833) according to the manufacturer's instructions, using 1-2 x 10^6 million cells per extraction.

2.6.2 Protein extraction, SDS-PAGE and western blotting

Cells were washed twice with PBS and lysed with 250µl NP40 lysis buffer (150mM NaCl, 5mM EDTA, 2mM EGTA, 0.5% (v/v) NP-40, 25mM Tris-HCl pH 7.4) containing 10µl per ml each of protease inhibitor cocktail II (Sigma, #P5726), cocktail III (Sigma, #P0044) and phosphatase inhibitor (Sigma, #P3840). Lysates were sonicated 3 times for 5 seconds using a Branson sonifier (setting 2). A 50µl aliquot of each sample was used for total protein quantification using a Pierce™ BCA Protein Assay Kit (Thermo Fisher Scientific, #23225) according to the manufacturer's instructions. Protein samples were diluted accordingly and mixed with 4X Bolt™ LDS Sample Buffer (Thermo Fisher Scientific, #B0007). 20µg of protein was loaded per well on a 4-12% gradient or 8% Bolt™ Bis-Tris Plus gel (Thermo Fisher Scientific, #NW04120) alongside a precision

plus all blue protein standard (Bio-Rad #1610373) and run at 190V using Bolt™ running buffer (Thermo Fisher Scientific B0002). Proteins were transferred to a nitrocellulose membrane (Thermo Fisher Scientific, #10600003) at 25V for 16h at 4°C in transfer buffer (25 mM Tris-base, 192 mM Glycine, 20% ethanol). Successful transfer was confirmed by Ponceau S staining (Merck, #P7170-1L) and membranes were blocked for 1 hour in 5% milk powder in TBST. Membranes were incubated with primary antibodies (Table 2.2) diluted in 5% milk powder in TBST overnight at 4^{o}C under agitation. Membranes were washed 3 times for 10 minutes under agitation at room temperature before incubation with secondary antibodies (Table 2.2) for 1h at room temperature under agitation. Blots were visualised using a LiCOR odyssey system and ImageStudio software.

Supplier	Catalogue number	Species raised in	Target	Detail	Dilution
Sigma	A1978	Mouse	β-actin	Primary	1:5000
Abcam	ab7291-100μg	Mouse	α-tubulin	Primary	1:1000
Sigma-Aldrich	ABE1034	Rabbit	TET1	Primary	1:1000
Active Motif	61990, clone 21F11	Mouse	TET2	Primary	1:1000
Abcam	ab139805	Rabbit	TET3	Primary	1:1000
Cell signalling tech	9172	Rabbit	STAT1	Primary	1:1000
Cell signalling tech	9167S (58D6)	Rabbit	phospho-STAT1 (Tyr 701)	Primary	1:1000
Cell signalling technology	18950 (D6B9Y)	Rabbit	TET2	Primary	1:1000
Cell signalling technology	2032	Rabbit	Lamin A/C	Primary	1:1000
LiCOR	926-32212	Donkey	Anti-Mouse IgG secondary antibody (800 CW)	Secondary	1:15,000
LiCOR	926-68072	Donkey	Anti-Mouse IgG secondary antibody (680 RD)	Secondary	1:15,000
LiCOR	926-32213	Donkey	Anti-Rabbit IgG Secondary Antibody (800 CW)	Secondary	1:15,000
LiCOR	926-68073	Donkey	Anti-Rabbit IgG Secondary Antibody (680 RD)	Secondary	1:15,000

Table 2.2: ***Table of antibodies used for western blotting****.*

2.6.3 HUVEC supernatant cytokine array

1.8ml of cell culture supernatants of TET2 siRNA- or negative control siRNA-treated HUVEC treated with 10ng/ml TNFα (4h), 10ng/ml IFNγ (24h) or 1000U/ml IFNα (4h) and untreated controls were collected from monolayers of HUVEC in 6-well plates and immediately frozen in liquid nitrogen. An array of 105 human cytokines was performed using a Proteome Profiler Human XL Cytokine Array Kit (Biotechne, #ARY022B) according to the manufacturer's instructions. Briefly, the membranes to

which capture antibodies were bound in duplicate were blocked for 1h at room temperature before overnight incubation with cell culture supernatants at 4°C. Membranes were washed 3 times for 10 minutes before addition of the detection antibody cocktail for 1h at room temperature. Washes were repeated and membranes were incubated with streptavidin-HRP for 30 minutes. Membranes were incubated with ECL reagent and developed using X-ray film.

2.7 Cell viability assay

HUVEC were transfected with siRNA targeting TET1, TET2 or TET3 or a negative control siRNA as described above. Cells were trypsinised, resuspended in EGM-2 and seeded at 1000 cells per well in a 0.4% gelatin-coated opaque white 96-well plate. Once cells had adhered, media was replaced with MT Cell Viability Substrate and NanoLuc® Luciferase (Promega RealTime-Glo MT Cell Viability Assay, #G9711) diluted 1:1000 in EGM-2. Luminescence was measured using a luminometer (Tristar2 S LB942 multimode reader, Berthold Technologies) at timepoints between 0-72 hours.

2.8 Cholesterol assay

TET2 siRNA- or negative control siRNA-treated HUVEC were treated with 10ng/ml IFNγ or 1000U/ml IFNα for 20 hours. Free and esterified cholesterol levels were measured using a Cholesterol/Cholesterol Ester-Glo™ Assay (Promega, #J3190) according to the manufacturer's instructions. Briefly, cells were washed twice with PBS, lysed and incubated at 37°C for 30 minutes. Lysates from each well of a 24-well plate were divided into two and cholesterol detection reagent with or without esterase was added and incubated at room temperature for 1 hour before measuring luminescence using a luminometer. Cholesterol levels were normalised to cell number (measured using Cell Titer Glo 2.0 kit (Promega, #G9241) according to the manufacturer's instructions) or total protein content (measured using a Pierce™ BCA Protein Assay Kit according to the manufacturer's instructions).

2.9 Animal studies

All studies were conducted in accordance with the Guidance on the Operation of the Animals (Scientific Procedures) Act, 1986 (UK Home Office) and with ethical approval from King's College London Animal Welfare Ethical Review Body. Mice were housed in individually ventilated cages in a temperature and humidity-controlled environment with a 12 hour light/dark cycle (light phase 7am-7pm) with access to food and water *ad libitum.*

2.10 Genotyping

Ear clips were taken from mice after weaning and digested with 300µl 50mM NaOH for 30 minutes at 95°C. Samples were vortexed before addition of 50µl 1M Tris-HCl and centrifugation at 16,000 x g for 5 minutes. 2µl of the resulting supernatant was mixed with 12.5µl GoTaq® G2 Master Mix (Promega, #M7823), 2µl of 10µM primers (GAPDH and Cre: see Table 2.3 for sequences) and 8.5µl H_2O. PCR amplification was performed as follows: 94°C 1 minute, 35 cycles (94°C 30s, 60°C 30s, 72°C 30s), 72°C 7 minutes, 4°C. 10µl PCR products were separated by size on a 1.5% agarose gel (containing Nancy 520 for visualisation) with 1x TAE buffer (Thermo Fisher Scientific, #B49) at 100V, alongside 5µl of 100bp ladder (New England Biolabs, #N0551S) to enable identification of band size. The presence or absence of a 200bp band was used to genotype mice as Cre^{+ve} or Cre^{-ve}. The presence of a GAPDH band at 342bp was confirmed in all samples as a housekeeping gene.

Gene name	Forward primer	Reverse primer
GAPDH	CCTAGACAAAATGGTGAAGG	GACTCCACGACATACTCAGC
Cre	TGCCAGGATCAGGGTTAAA	CCCGGCAAAACAGGTAGTT

Table 2.3: ***Primers used for genotyping mouse ear clips to identify the presence or absence of the Cre recombinase transgene.***

2.11 Diabetic mouse model

Experimental mice were generated by crossing $TET2^{fl/fl}$ mice [149] to tamoxifen-inducible, endothelial-specific Cre-expressing mice (Cdh5-CreERT2) [207] on a C57Bl/6J background. Male Cre^{+ve} $TET2^{fl/fl}$ mice and male Cre^{-ve} $TET2^{fl/fl}$ mice were injected intraperitoneally with 40mg/kg tamoxifen (MP Biomedicals, #0215673894) in peanut oil for 3 consecutive days at 6-8 weeks of age to induce Cre recombination or generate appropriate control animals. One week after tamoxifen injections, mice were fed a high fat diet (60% kcal from fat, TestDiet 58Y1) or continued a standard chow diet (13% kcal from fat, LabDiet 5053) *ad libitum* for 10 or 20 weeks (see details in Table 2.4). Body weights were measured at 4-week intervals.

LabDiet 5053 calories provided by…	TestDiet 58Y1 calories provided by…
Protein, % 24.5	Protein, % 18.1
Fat, % 13.1	Fat, % 61.6
Carbohydrates, % 62.4	Carbohydrates, % 20.3

Table 2.4: ***Percentage of calories in LabDiet 5053 and TestDiet 58Y1 derived from protein, fat and carbohydrates.***

2.12 Glucose tolerance tests

Glucose tolerance tests were performed at 9 weeks of high fat diet (or standard chow diet) feeding. Mice were fasted for 4 hours and blood was sampled from the tail vein using the needle-prick method. A baseline blood glucose concentration was measured using a Sinocare Safe-Accu 2 blood glucose monitor. Following intraperitoneal injection of D-glucose in saline (2g/kg dose), further blood samples were measured at 15, 30, 45, 60 and 120 minutes.

2.13 Tissue harvesting

After 10 or 20 weeks of high fat diet (or standard chow diet) feeding, mice were sacrificed by intraperitoneal injection of 300µl of 200mg/ml sodium pentobarbital and death was confirmed by cervical dislocation or exsanguination. Lung and heart tissue

were immediately frozen in liquid nitrogen and stored at -80°C for RNA or protein extraction. Blood was collected in potassium-EDTA anticoagulant tubes and centrifuged to collect plasma. Plasma was frozen in liquid nitrogen and stored at -80°C. The aorta was carefully removed, placed in ice cold Kreb's buffer (NaCl 6.95g/L, KCl 0.35g/L, KH_2PO_4 0.16g/L, $NaHCO_3$ 2.1g/L $MgSO_4.7H_2O$ 0.29g/L, Glucose 1.98g/L, $CaCl_2.2H_2O$ 0.37g/L) and dissected to clear perivascular fat and surrounding tissues whilst avoiding damage to the endothelium.

2.14 Organ bath experiments

3mm aortic rings were mounted onto wire triangles and suspended in an organ bath containing Kreb's buffer, maintained at 37°C and continuously aerated with 95% O_2 and 5% CO_2. Tension was increased from 0.5g to 3g gradually by 0.5g every 5 minutes and then allowed to reach a stable baseline. 40mM KCl was applied to test the constriction response, washed out and repeated once. Aortic rings which did not increase tension by ≥10% in response to the second application of KCl were excluded. Following 20 minutes of acclimatisation, aortic rings were pre-constricted by the addition of $3x10^{-9}$M phenylephrine and then exposed to an increasing dose of acetylcholine applied at 3-minute intervals between 10^{-9}M and 10^{-5}M. Aortic rings which failed to relax to >50% of the PE-induced constriction or relaxed by >140% were excluded to rule out vessels that may have been damaged during preparation. After washing and a 20-minute interval, phenylephrine-induced constriction was measured in a range of doses increasing from 10^{-9}M to 10^{-5}M. Finally, aortic rings were pre-constricted with $3x10^{-9}$M phenylephrine and a sodium nitroprusside relaxation curve was performed in a dose range between 10^{-11}M and 10^{-5}M.

2.15 Mouse plasma cytokine array

Plasma from n=8 mice was pooled in equal volumes. An array of 111 mouse cytokines was performed using a Proteome Profiler Mouse XL Cytokine Array Kit (Biotechne, #ARY028) according to the manufacturer's instructions. Briefly, the membranes to which capture antibodies were bound in duplicate were blocked for 1h at room

temperature before overnight incubation with plasma samples at 4°C. Membranes were washed 3 times for 10 minutes before addition of the detection antibody cocktail for 1h at room temperature. Washes were repeated and membranes were incubated with streptavidin-HRP for 30 minutes. Membranes were incubated with ECL reagent and developed using X-ray film.

2.16 RNA isolation from mouse heart tissue

20mg mouse heart tissue was homogenised in 500µl lysis buffer LBA+TG (Promega Reliaprep kit, #Z6112) in combination with lysing matrix D ceramic spheres, using a Precellys 24 homogeniser with a programme of 6000rpm for twice for 15 seconds. Subsequently, RNA was isolated using the Reliaprep tissue kit (Promega, #Z6112) according to the manufacturer's instructions.

2.17 Mouse lung endothelial cell (MLEC) isolation

3-9 week old $TET2^{fl/fl}$ Cre^{+ve} and $TET2^{fl/fl}$ Cre^{-ve} male and female mice were sacrificed by intraperitoneal injection of 300µl of 200mg/ml sodium pentobarbital and death was confirmed by cervical dislocation. Lungs were removed and washed twice with PBS containing 1% penicillin-streptomycin before finely mincing with scissors. Minced lung tissue was digested in 1mg/ml collagenase-dispase (Merck, #10269638001) in Dulbecco's Modified Eagle Medium (DMEM) for 45 minutes at 37°C with continuous shaking before passing through a 70µm nylon strainer followed by a 30µm nylon strainer, washing with PBS to ensure all cells passed through the filters. The cell suspension was centrifuged at 350 x g for 10 minutes, the supernatant discarded and the resulting cell pellet was resuspended in 5ml PBS before a further 5 minute centrifugation at 350 x g. The supernatant was removed and the cell pellet was resuspended in 90µl of 4°C MACS buffer (1:20 dilution of MACS BSA stock solution Miltenyi, #130-091-376 in autoMACS rinsing solution Miltenyi, #130-091-222). 10µl of anti CD31 antibody-conjugated microbeads (Miltenyi, #130-097-418) were added and incubated at 4°C for 15 minutes, followed by magnetic separation using a MACS separator and LS columns (Miltenyi #130-042-401). CD31+ cells were centrifuged at

350 x g for 5 minutes and resuspended in DMEM media containing 20% FBS, 1X endothelial cell growth supplements (Merck #211F-GS), 100μg/ml heparin (Merck #H3149-100KU) and 1% penicillin-streptomycin and plated onto a 12 well plate pre-coated with 0.1% fibronectin (Sigma, #F1141) and 0.4% gelatin. Media were refreshed the following day and cells were passaged when confluent. Cells were treated for 6 days with 5μM 4-hydroxytamoxifen, refreshing media after 3 days, to induce Cre recombination (or if cells were harvested from mice after intraperitoneal injection with 40mg/kg tamoxifen for 3 days, this step was not performed).

2.18 Confirmation of Cre recombination in MLEC

MLEC were digested in 150μl 50mM NaOH at 95°C for 30min. 25μl 1M Tris-HCl was added and samples were centrifuged at 16,000 x g for 5 minutes. 2μl of the resulting supernatant was mixed with 12.5μl GoTaq® G2 Master Mix (Promega, #M7823), 2μl of 10μM primers (see Table 2.5 for sequences and Figure 2.1 for genomic position) and 8.5μl H_2O. PCR amplification was performed as follows: 94°C 1 minute, 35 cycles (94°C 30s, 56°C 30s, 72°C 30s), 72°C 7 minutes, 4°C. 10μl PCR products were separated by size on a 1.5% agarose gel (containing Nancy 520 for visualisation) with 1x TAE buffer at 100V, alongside 5μl of 100bp ladder to enable identification of band size.

Target	Forward primer	Reverse primer
Floxed TET2	Tet2FloxF: AAGAATTGCTACAGGCCTGC	Tet2FloxR: TTCTTTAGCCCTTGCTGAGC
Knockout TET2	Tet2FloxF: AAGAATTGCTACAGGCCTGC	Tet2LoxP3R: TAGAGGGAGGGGGCATAAGT

Table 2.5: ***Primers used for confirming the presence of the floxed TET2 allele and successful Cre recombination in mouse lung endothelial cells.***

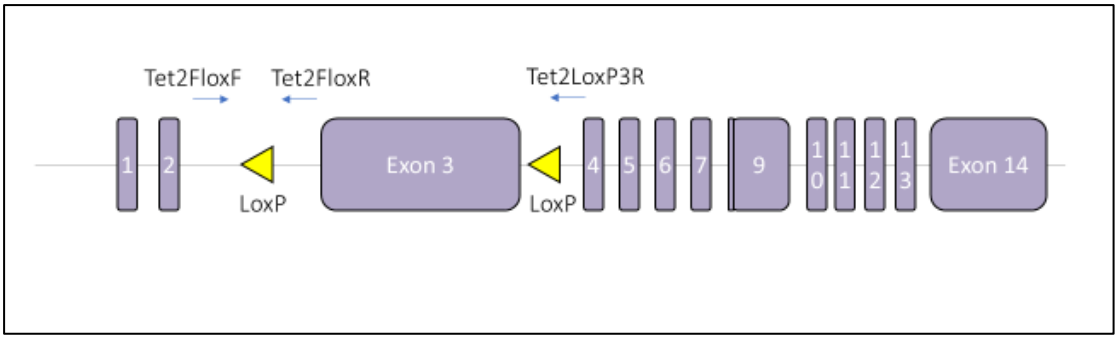

Figure 2.1: ***Schematic diagram of the location of LoxP sites flanking exon 3 of the TET2 gene.*** *Arrows above indicate the position of primers used to the presence of the floxed allele and confirmation of successful Cre recombination.*

2.19 MLEC RNA sequencing

RNA was prepared from MLEC immediately after isolation using the Reliaprep kit (Promega, #G9711). 350ng RNA from n=3 individual mice per group was used for library preparation, sequencing (50M reads) and initial bioinformatic analysis by Novogene, as follows:

mRNA was purified from total RNA using poly-T oligo-attached magnetic beads. After fragmentation, the first strand cDNA was synthesized using random hexamer primers, followed by the second strand cDNA synthesis. cDNA underwent end repair, A-tailing, adapter ligation, size selection, amplification, and purification. The library was checked with Qubit and real-time PCR for quantification and bioanalyzer for size distribution detection. Library preparations were sequenced on an Illumina platform and paired-end reads were generated. Raw data were firstly processed through in-house perl scripts to generate clean reads by removing reads containing adaptors, reads containing poly-N and low quality reads. Clean reads were aligned to the reference genome using HISAT2 software and gene expression was quantified using featureCounts software. Differential gene expression analysis was performed using the DESeq2 R package. The resulting P-values were adjusted using the Benjamini and Hochberg approach. Genes with an adjusted P-value <0.05 were assigned as differentially expressed. Further analysis was performed using Ingenuity Pathway Analysis (IPA) software (Qiagen) applying thresholds of Log2FoldChange>|1| and

adjusted P-value <0.05. Table 2.6 summarises experimental details and Gene Expression Omnibus (GEO) Series (GSE) accession numbers for sequencing experiments conducted.

Experiment	Cell type	Samples	Replicates	Company	GSE accession
RNA sequencing	HUVEC	siRNA control TET1 siRNA TET2 siRNA TET3 siRNA Media Mannitol Glucose	Single RNA sample for each condition (pooled from triplicate RNA samples)	BGI	GSE232279
hMeDIP-seq	HUVEC	siRNA control TET2 siRNA TET3 siRNA	Duplicate DNA samples for each condition	ArrayStar	GSE232145
hMeDIP-seq	HUVEC	Media IFNγ Media Mannitol Glucose	Duplicate DNA samples for each condition	ArrayStar	GSE232280
RNA sequencing	MLEC	WT-chow TET2 KO-chow WT-HFD TET2 KO-HFD	Individual RNA samples from n=3 mice per condition	Novogene	GSE232888

Table 2.6: ***List of sequencing experiments carried out.*** *Abbreviations: hydroxymethyl DNA immunoprecipitation sequencing (hMeDIP-seq), human umbilical vein endothelial cells (HUVEC), small interfering RNA (siRNA), interferon gamma (IFNγ), wild-type (WT), high fat diet (HFD), knockout (KO).*

2.20 Permeability assay

1.5 x10^5 HUVEC (untreated, treated with glucose or mannitol, or transfected as described above) or MLEC were seeded onto 10μg/ml fibronectin-coated 0.4μm pore polyester transwell inserts (Corning, #CC403) and cultured in EGM-2 for 24h. EGM-2 was changed to basal media for 1h prior to stimulation with IFNγ, LPS or TNFα for 4

or 24 hours as indicated. 10µl each of 300µg/ml fluorescein isothiocyanate (FITC)-dextran (Sigma, #46944-100MG-F) and tetramethylrhodamine (TRITC)-bovine serum albumin (BSA) (Sigma, #A2289-10MG) were added to the upper chamber and incubated at 37°C for 60 minutes. Lower chambers were mixed and 100µl aliquots were transferred to a black-walled 96-well plate for fluorescence readings at 490/525nm and 540/575nm using a fluorimeter.

2.21 Immunofluorescence

HUVEC or MLEC were grown on 10µg/ml fibronectin-coated glass coverslips (or transwell inserts, where immunofluorescence was performed after permeability assays) before fixation with 4% paraformaldehyde (Thermo Fisher Scientific, #28908) in PBS containing Ca^{2+} and Mg^{2+} for 10 minutes at 37°C. Cells were washed three times with PBS and then permeabilised with 0.4% Triton-X-100 for 5 minutes. After three PBS washes, cells were blocked in 3% BSA and 1% goat serum (Sigma, #G9023) in PBS (referred to as blocking solution) for 1h. Cells were incubated with a rabbit primary antibody to VE-cadherin (Cell Signalling Technology #2500 (D87F2)) diluted 1:400 in blocking solution overnight at 4°C. Cells were washed three times with PBS and then incubated at room temperature for 1h with 1:400 goat-anti-Rabbit 568 secondary antibody (Thermo Fisher Scientific, #A-11008), 1:200 phalloidin-488 (Abcam) and 2.5µg/ml DAPI in blocking solution. After three PBS washes, coverslips were mounted onto glass slides using Fluoromount (Sigma, #F4680) and images were obtained with an IX-81 or spinning disc confocal microscope. Mean cell area was measured using ImageJ software.

2.22 Isolation of mouse bone marrow cells

Mice were culled by schedule 1 methods. The femur and tibia of hind limbs were isolated and bone marrow was extracted by flushing Hank's Balanced Salt solution (Ca^{2+}/Mg^{2+} free) through the centre of each bone using a 27G needle. Cell suspensions were strained through a 40µm strainer and thoroughly resuspended before centrifugation at 450 x g. The cell pellet was haemolysed in 10ml 1X haemolysis buffer

(8.26g/L NH_4Cl, 1g/L K_2HCO_2, 0.037g/L EDTA) and centrifuged at 450 x g. The cell pellet was resuspended in PBS, centrifuged at 450 x g and the final cell pellet was resuspended in RPMI and stored on ice until use.

2.23 Leukocyte adhesion assay

Leukocyte adhesion assays were performed using the CytoSelect Leukocyte-Endothelium Adhesion Assay Kit (Cell Biolabs #CBA-210) according to the manufacturer's instructions. For HUVEC assays, differentiated HL-60 cells were used. For MLEC assays, bone marrow cells were used. Briefly, leukocytes were labelled with Leukotracker™ solution in serum-free RPMI media for 60 minutes. Labelled leukocytes were washed 3 times with serum-free RPMI. In a 48-well plate, monolayers of HUVEC or MLEC were washed once with serum-free RPMI, before replacing the media with a suspension of 1 x 10^5 leukocytes. Co-cultures were incubated at 37°C and 5% CO_2 for 60 minutes for leukocytes to adhere, before gentle washing 3 times with 1X wash buffer, followed by lysis with 150µl 1X lysis buffer. After 5 minutes shaking, 100µl of lysate was transferred to a 96-well black-walled plate and fluorescence was measured with 480nm excitation and 520nm emission.

2.24 Data analysis

Graphing and statistical analysis were performed using GraphPad Prism software (version 9). Data are presented as mean ± standard error of the mean (SEM). A Shapiro-Wilk test was conducted to determine whether data followed a normal distribution. Unpaired t-tests, one-way analysis of variance (ANOVA) or two-way ANOVA tests were used as appropriate. $p<0.05$ was considered statistically significant. Schematic diagrams were made using BioRender (https://biorender.com).

3. Results 1: A comparison of the effects of high glucose culture and silencing of TETs on the endothelial transcriptome.

3.1 Introduction

TET1, TET2 and TET3 all possess the ability to catalyse the successive oxidation of 5mC in the process of demethylation. However, whilst some genes are transcriptionally regulated by multiple TETs [208, 209], it has also been observed that the three TETs regulate the expression of distinct sets of genes [210-212]. Also reflecting distinct functional roles, the expression of the three TETs varies between cell types and throughout development. For example, TET1 and TET2 are much more highly expressed in embryonic stem cells than TET3, whereas TET3 is the most highly expressed TET enzyme in oocytes and neurones [213]. Of the three TETs, TET2 is most associated with roles in the blood and vasculature. TET2 is known to have an important role in haematopoietic stem cell differentiation [149], regulate the phenotype of vascular smooth muscle cells [163] and protect against oxidised LDL-induced endothelial dysfunction [165]. However, current literature lacks broad characterisation of the expression and functions of TETs in endothelial cells.

3.1.1 Aim

The aim of this chapter is to investigate the relative contribution of TET1, TET2 and TET3 to the regulation of endothelial cell transcription and identify potential functional roles for TETs in endothelial cells based on the biological pathways to which the TET-regulated genes belong. Pathways dysregulated by TET silencing are compared to those dysregulated by high glucose culture of endothelial cells, to explore whether there may be a potential role for dysregulation of TETs in hyperglycaemia-induced endothelial dysfunction.

3.2 Results

3.2.1 TET2 is the most highly expressed TET enzyme in HUVEC at the mRNA level

To determine which of the TETs is the most highly expressed in endothelial cells, qPCR was used to compare the relative mRNA expression of TET1, TET2 and TET3 in HUVEC (Figure 3.1). TET2 was, in all cases (Figure 3.1A-C), the most highly expressed of the three TETs and had an approximately 3.8-fold higher mRNA expression level than that of TET1 or TET3 (Figure 3.1D). In addition, TET2 protein expression was readily detectable in HUVEC lysates by western blotting and this could be abolished by targeting TET2 with siRNA (Figure 3.2). Although at a relatively weak signal: noise ratio, TET1 was also able to be detected in HUVEC at the predicted molecular weight by western blotting (Figure 3.2B). However, no band was visible at the predicted molecular weight of TET3, although various non-specific bands were observed (Figure 3.2C). Failure to detect endogenous TET3 using commercially available antibodies has been similarly reported by other researchers, highlighting a need for better tools for its study [202].

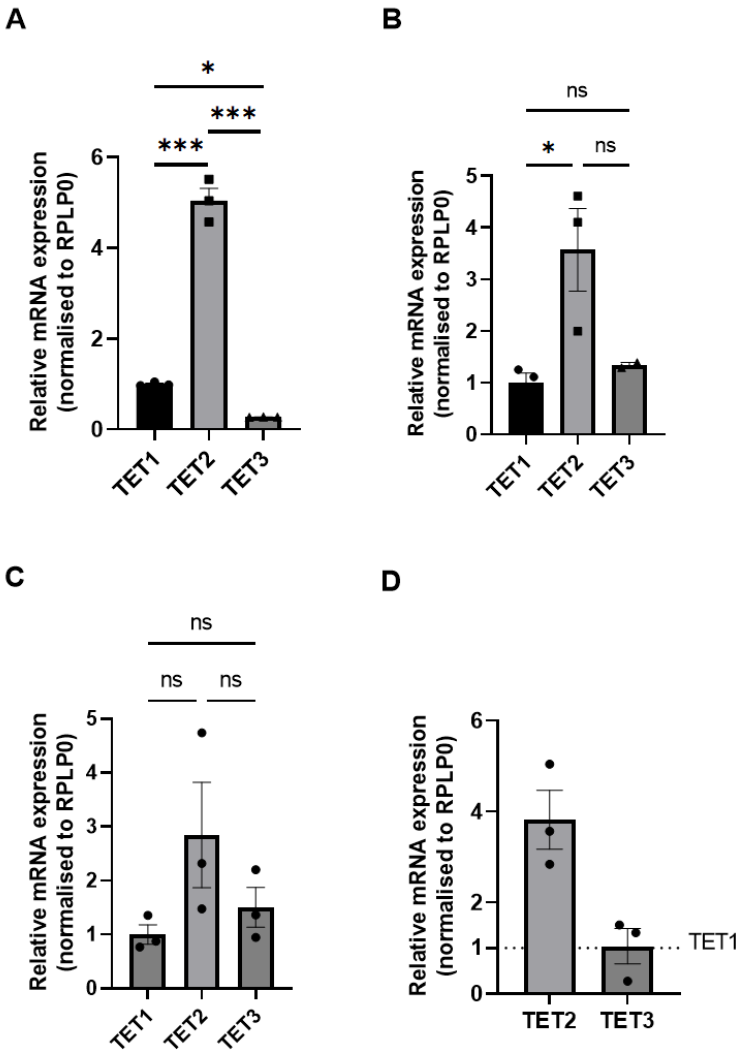

Figure 3.1: ***Relative mRNA expression of TET family members in human umbilical vein endothelial cells (HUVEC).*** *qPCR was performed to measure relative mRNA expression of each TET, normalised to the housekeeping gene RPLPO in three independent experiments (A-C). A Shapiro-Wilk test for normality was performed, followed by a one-way ANOVA with post-hoc Tukey's test. Data presented as mean ± SEM. n=3 triplicate samples.* denotes p<0.05, ** denotes p<0.01, *** denotes p<0.001. D) Fold change mRNA expression of TET2 and TET3 compared to TET1. Combined data from n=3 independent experiments. Data presented as mean ± SEM.*

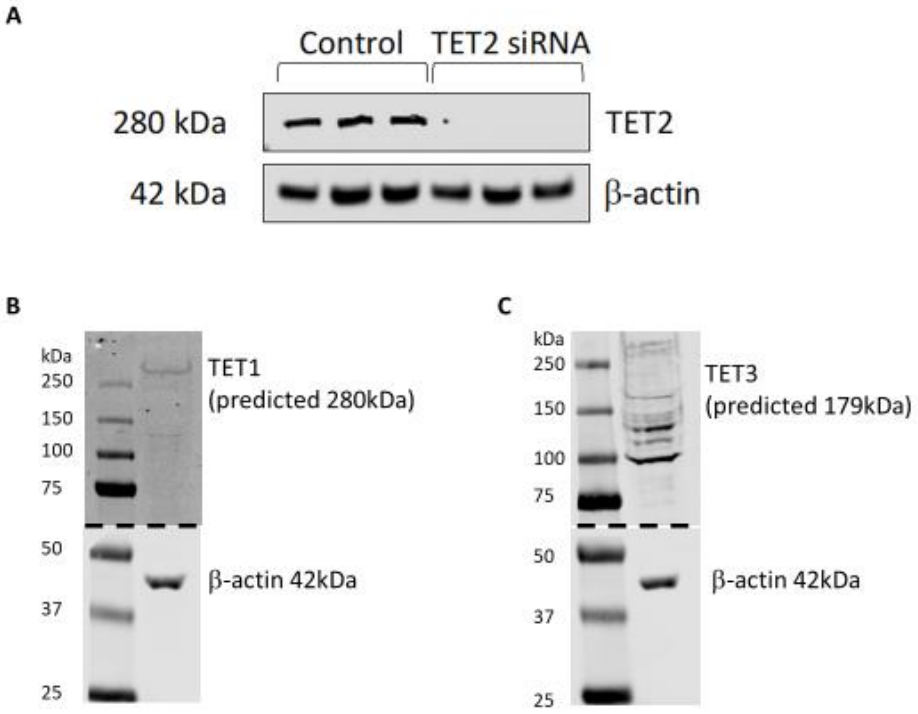

Figure 3.2: ***TET protein expression in HUVEC at baseline and following siRNA-mediated targeting of TET2.*** *A) HUVEC were transfected with negative control siRNA or siRNA targeting TET2. Western blotting was performed to measure TET2 protein expression. An anti-β-actin antibody was used to confirm equal loading. B) TET1 protein expression was probed by western blotting HUVEC lysate. An anti-β-actin antibody was used to confirm sufficient protein loading. C) TET3 protein expression was probed by western blotting HUVEC lysate. An anti-β-actin antibody was used to confirm sufficient protein loading.*

3.2.2 TET1 is downregulated but TET2 and TET3 expression are not affected by high glucose treatment

Next, the expression of the three TET family members was characterised in HUVEC cultured under high glucose (30mM) conditions, compared to HUVEC cultured under normal glucose (5mM) conditions, with the addition of 25mM mannitol as an osmotic control. After 24 hours of high glucose culture, the mRNA expression of TET1, TET2 and TET3 was not significantly different from mannitol-treated controls. After 48 hours, TET1 expression was significantly decreased but TET2 and TET3 expression remained unchanged (Figure 3.3).

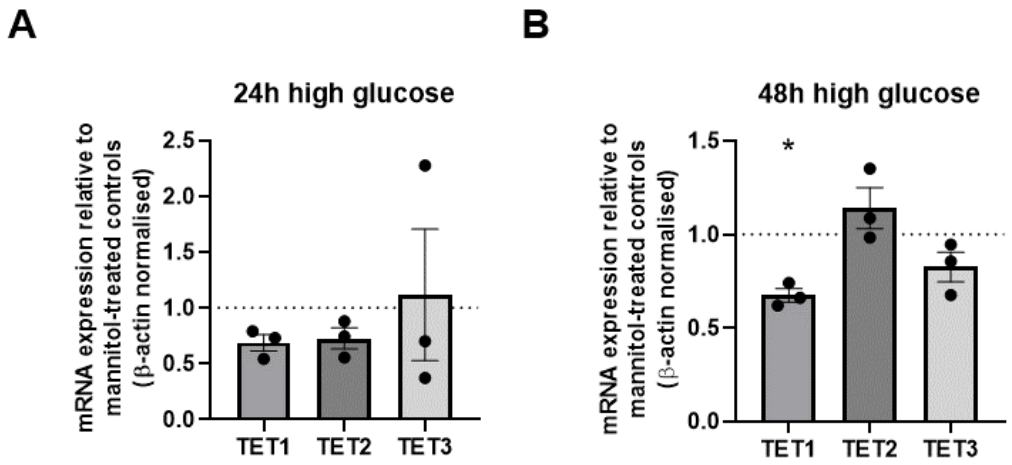

Figure 3.3: ***Expression of TETs in high glucose-treated HUVEC.*** *HUVEC were cultured for 24h (A) or 48h (B) in media containing a high glucose concentration (30mM) or normal glucose concentration (5mM) with the addition of 25mM mannitol as an osmotic control. qPCR was performed to measure relative mRNA expression of each TET, normalised to the housekeeping gene β-actin. A Shapiro-Wilk test for normality was performed, followed by an unpaired t-test comparing high glucose-cultured HUVEC to mannitol-treated controls (indicated by the dotted line at y=1). Data presented as mean ± SEM. n=3 triplicate samples. * denotes p<0.05.*

3.2.3 Hydroxymethylation patterns of HUVEC are affected by high glucose treatment

Next, it was questioned whether high glucose treatment of endothelial cells would alter global levels of 5hmC, the first intermediate produced by TETs by oxidation of 5mC, as a surrogate marker of TET catalytic activity. Previous literature has demonstrated a decrease in global 5hmC levels in peripheral blood mononuclear cells (PBMCs) from diabetic patients compared to healthy controls, detected by high performance liquid chromatography-mass spectrometry [183]. Similarly, when PBMCs, HUVEC or TF-1 cells were cultured in high glucose conditions (25mM compared to 5.5mM, duration not stated), a decrease in global 5hmC levels was detected by dot blotting [183]. A dot blot was used to measured 5hmC levels relative to total DNA content (assessed by methylene blue staining) in genomic DNA from high glucose-treated HUVEC, compared to HUVEC cultured in normal media (5mM glucose). In this experiment, no significant change in global 5hmC levels were observed at 30mM glucose for 24 or 48h, nor at a higher glucose concentration of 55mM glucose for 24h (Figure 3.4A). To confirm that the dot blot method can detect changes in global 5hmC, TET1, TET2 or TET3 were over-expressed in HeLa cells, which increased the abundance of 5hmC relative to 5mC, particularly upon TET1

overexpression (Figure 3.4B). However, the abundance of 5hmC in HUVEC may be insufficient to detect subtle changes by this method.

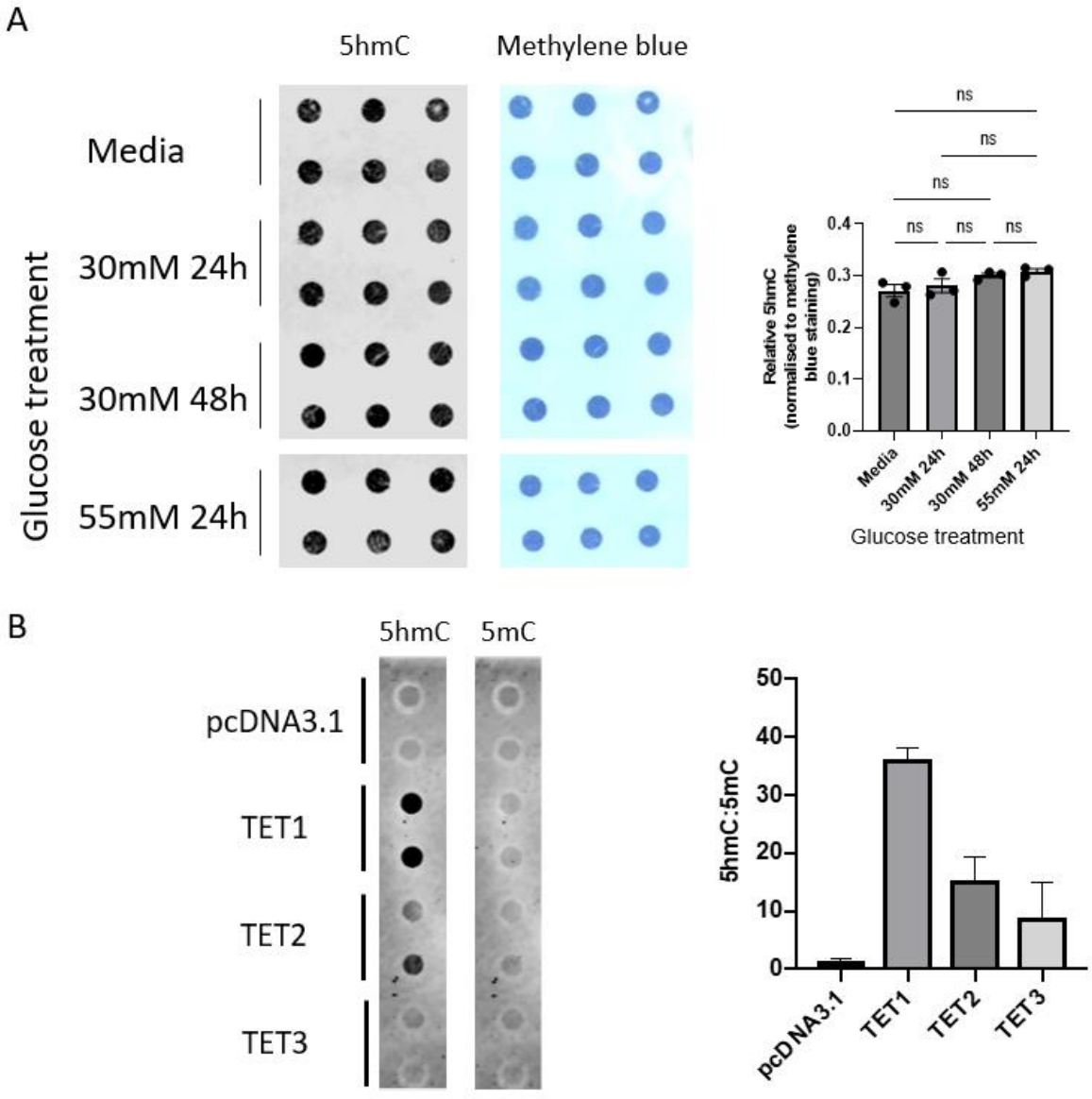

Figure 3.4: ***High glucose culture for 24h or 48h does not alter global 5hmC levels of HUVEC.*** *(A) Genomic DNA was extracted from HUVEC cultured in 5mM glucose media or treated for 24h or 48h with 30mM glucose, or for 24h with 55mM glucose. (B) HeLa cells were transfected with pcDNA3.1 plasmids to overexpress TET1, 2 or 3. pcDNA3.1 plasmids alone were transfected as a negative control. For each sample, 1μg DNA was applied to a nylon membrane by dot blotting and 5hmC signal was detected using an anti-5hmC antibody. 5hmC signal was analysed by densitometry and normalised to total DNA content assessed by methylene blue staining (A) or 5mC (B). Data presented as mean$\pm$SEM. n=3 samples (A) or n=1 samples (B) blotted in duplicate. A Shapiro-Wilk test for normality was performed, followed by an unpaired t-test.*

Although dot blotting did not detect altered global levels of 5hmC in HUVEC at these concentrations and durations of high glucose treatment, it was hypothesised that altered TET activity in high glucose conditions may instead alter the pattern of hydroxymethylation across the genome. To investigate this, hydroxymethylated regions of the genome in either high glucose-treated HUVEC or mannitol-treated controls (in this case, treated for 2 weeks) were immunoprecipitated using an antibody against 5hmC. The resulting fragments were sequenced and bioinformatic analysis was used to compare 5hmC enrichment across the genome in glucose-treated HUVEC compared to mannitol-treated controls. The profile of hydroxymethylation was broadly similar between the two treatments, with the majority of sites enriched for 5hmC being located within intergenic regions, with approximately 30% in gene bodies and 4% in promoter regions (Figure 3.5A & B). However, a decrease in 5hmC abundance was apparent in high glucose-treated HUVEC compared to mannitol-treated controls within gene bodies and the flanking 3Kb upstream and downstream, and peaks appear blunted in magnitude (Figure 3.5C). This suggests that TET activity in endothelial cells is decreased by high glucose levels, in agreement with published data [183]. Full lists of differentially hydroxymethylated regions can be accessed *via* the GEO database (GSE232280).

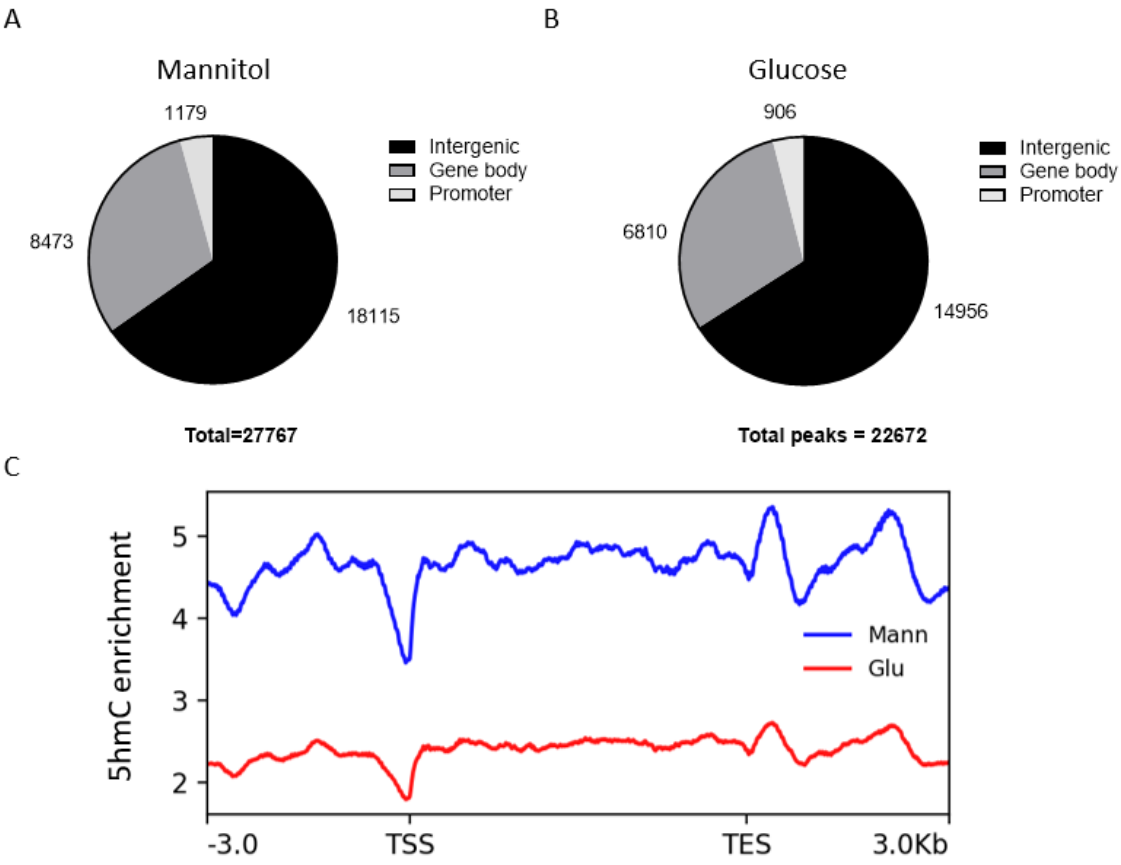

Figure 3.5: ***Differential hydroxymethylation is apparent in high glucose-treated HUVEC compared to controls.*** *Genomic DNA was prepared from HUVEC cultured for 2 weeks under high glucose conditions (25mM) and HUVEC cultured under normal glucose conditions (5mM) with the addition of 20mM mannitol as an osmotic control. Hydroxymethylated DNA immunoprecipitation was performed and resulting DNA fragments were sequenced. A) The proportion of 5-hydroxymethylcytosine (5hmC) enrichment peaks in high glucose-treated HUVEC (against input) present in intergenic, gene body and promoter regions. B) The proportion of 5hmC enrichment peaks in mannitol-treated HUVEC (against input) present in intergenic, gene body and promoter regions. C) 5hmC enrichment across gene bodies (between transcriptional start site TSS and transcriptional end site TES) and 3Kb upstream and downstream for all genes in the human genome assembly hg19, normalised to account for gene length in high glucose-treated HUVEC (Glu) and mannitol-treated controls (Mann).*

3.2.4 TET1, TET2 and TET3 transcriptionally regulate distinct sets of genes in HUVEC

To begin investigating the roles of TETs in endothelial cells, TET1, TET2 and TET3 were individually targeted by siRNA in HUVEC and compared to HUVEC transfected with a negative control siRNA. Successful silencing of TET expression was confirmed at the mRNA level using qPCR (Figure 3.6) and, where possible, at the protein level using western blotting (see, for instance, Figure 3.2A). Pooled RNA samples from each of these conditions were sequenced and differential gene expression analysis was performed to provide an unbiased transcriptome analysis comparing each TET-

silenced condition to the negative control siRNA. Applying a cut-off of Log2FoldChange>|1| and false discovery rate <0.05, 293, 258 and 138 downregulated genes and 179, 168 and 231 upregulated genes were identified upon TET1, TET2 and TET3 silencing, respectively (Figure 3.7). Volcano plots of differentially expressed genes compared to negative control siRNA-treated HUVEC are shown in Figure 3.7. Full lists of differentially expressed genes can be accessed *via* the GEO database (GSE232279). Of these differentially-expressed genes, 37 genes were common to all three conditions and additionally, a degree of overlap was observed between two of the three conditions: 83 genes were differentially-expressed in both TET1- and TET2-silenced HUVEC, 66 genes in both TET2- and TET3-silenced HUVEC and 43 in both TET1- and TET3-silenced HUVEC compared to controls (Figure 3.8). Interestingly, the vast majority of differentially-expressed genes were unique to a single TET, indicating that the three TETs are responsible for regulating the transcription of largely distinct sets of genes in endothelial cells, rather than performing overlapping or redundant roles.

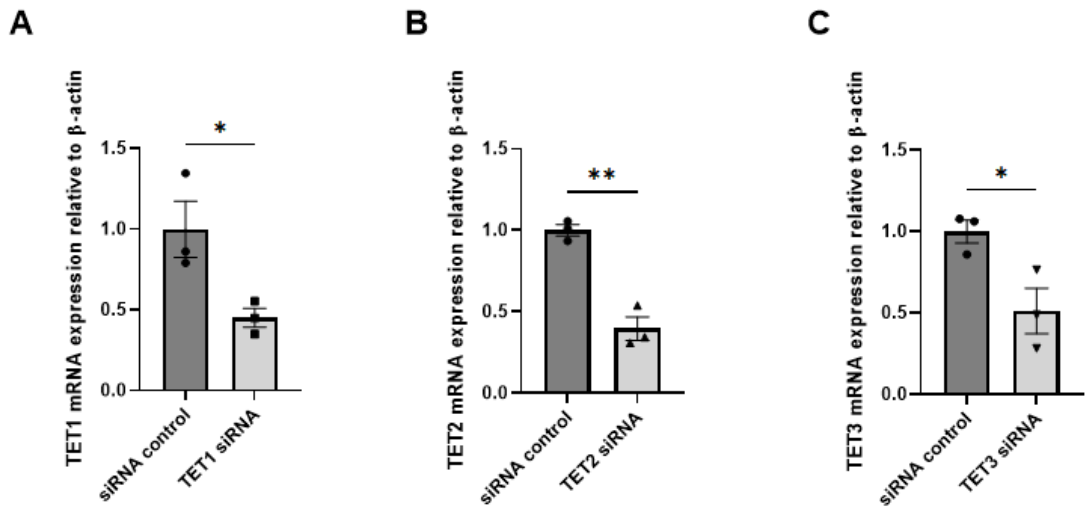

Figure 3.6: ***Confirmation of successful silencing of TET1, TET2 and TET3 by siRNA targeting in HUVEC.*** *HUVEC were transfected with negative control siRNA or siRNA targeting TET1, TET2 or TET3. qPCR was performed to measure relative mRNA expression of each TET, normalised to the housekeeping gene β-actin. A Shapiro-Wilk test for normality was performed, followed by an unpaired t-test. Data presented as mean ± SEM. n=3 triplicate samples. * denotes p<0.05. ** denotes p<0.01.*

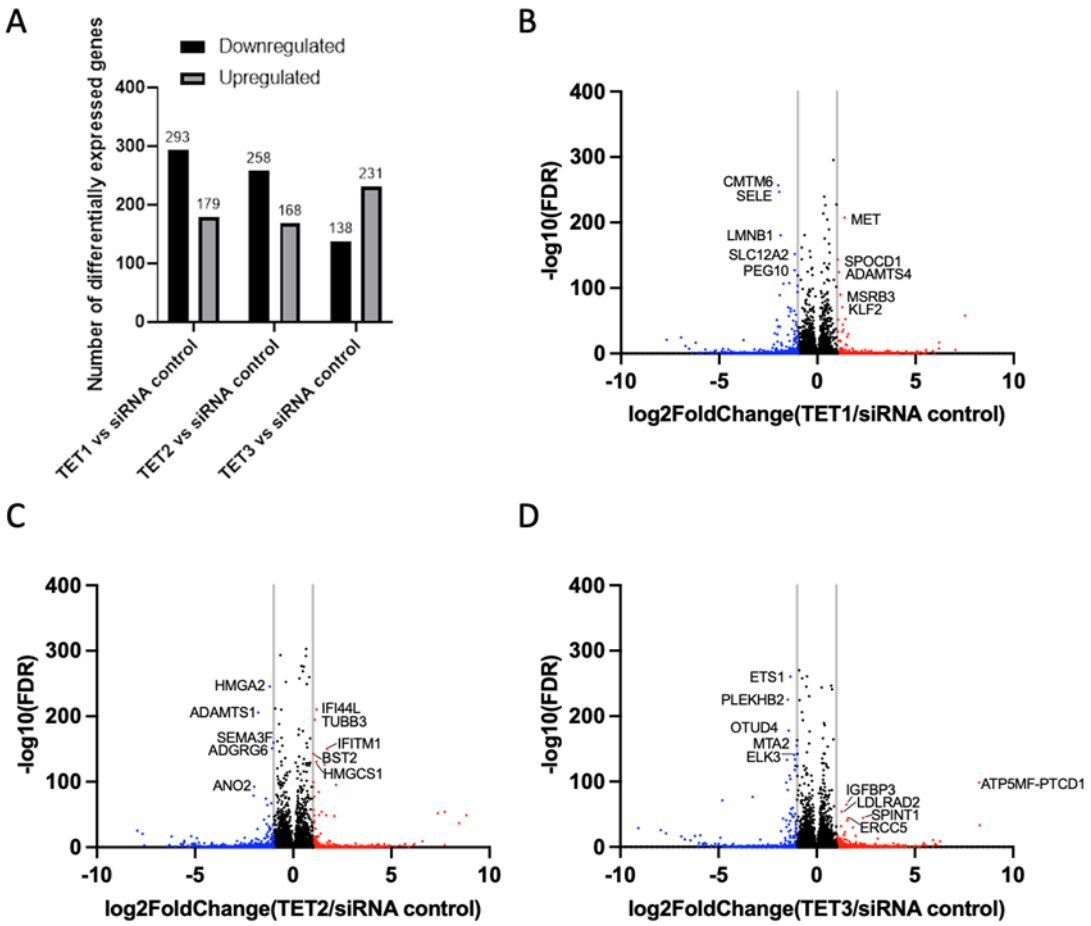

Figure 3.7: ***Differentially-expressed genes upregulated or downregulated by TET silencing in HUVEC.*** *RNA sequencing was performed on HUVEC treated with a negative control siRNA or siRNA targeting TET1, TET2 or TET3. (A) Graph displays the number of up- or down-regulated genes in siRNA control vs TET-silenced HUVEC applying cut-offs of Log2FoldChange>|1| and false discovery rate <0.05. (B-D) Volcano plots showing significantly differentially expressed genes in TET1- (B), TET2- (C) or TET3- (D) silenced HUVEC compared to siRNA control-treated HUVEC. The five genes with the most statistically significant upregulation and downregulation are labelled.*

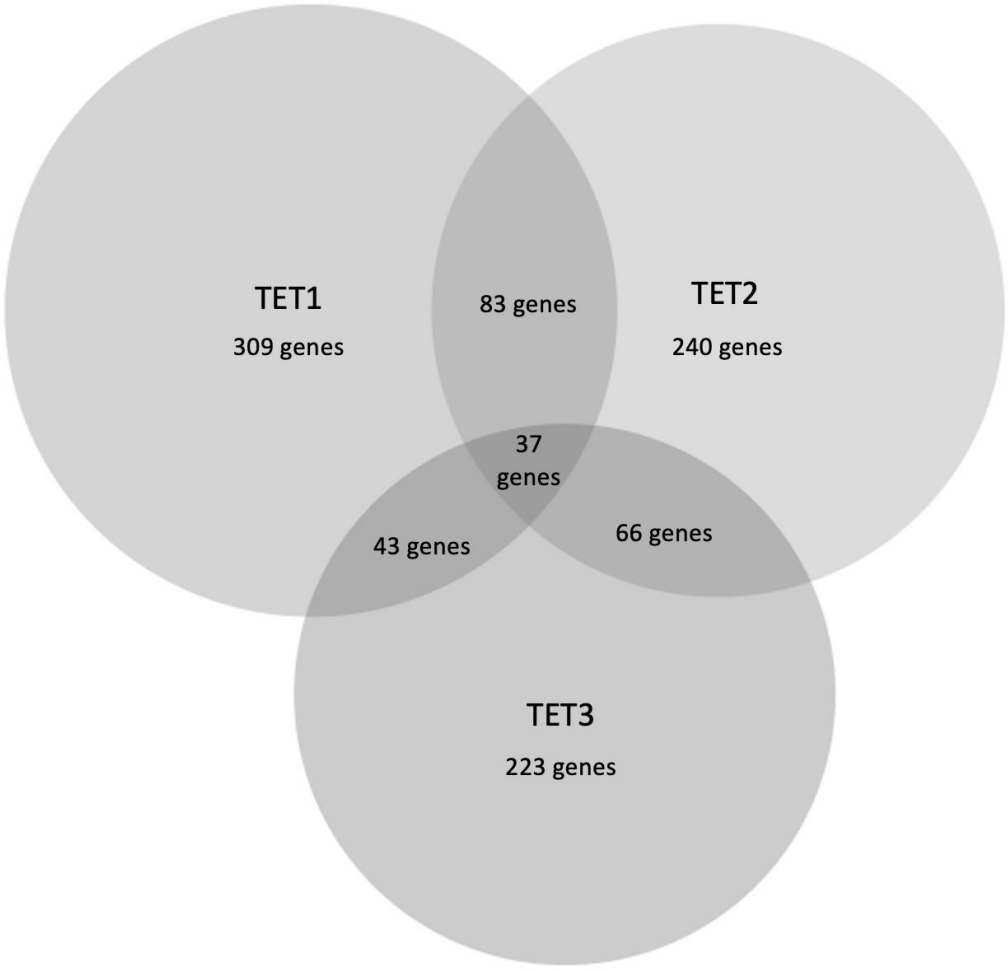

Figure 3.8: ***Venn diagram of differential gene expression in TET1-, TET2- or TET3-silenced HUVEC.*** *RNA sequencing was performed on HUVEC treated with a negative control siRNA or siRNA targeting TET1, TET2 or TET3. Venn diagram shows the number of uniquely and commonly differentially-expressed genes between TET-silenced and control HUVEC, applying cut-offs of Log2FoldChange>|1| and false discovery rate <0.05.*

3.2.5 TET2 and TET3 regulate biologically relevant pathways in endothelial cells

To begin exploring the potential functional roles of the TETs in endothelial cells, Ingenuity Pathway Analysis (IPA) software was used to group differentially-expressed genes into biological pathways, applying a cut-off of Log2FoldChange>|1| and false discovery rate <0.05. The Canonical Pathway Analysis within IPA ranks the pathways according to the statistical significance of the enrichment of the pathway using p-values calculated by Fisher's Exact Test. Put simply, a higher –log(p-value) indicates that the genes in the dataset overlap with genes belonging to the biological pathway significantly more than would be expected by random chance. P-values below p=0.05

(i.e. –log(p-value)<1.3) were considered statistically significant. In addition, a z-score was assigned to each pathway, indicating whether the pathway was predicted to be activated (positive z-score) or inhibited (negative z-score) based on the number and extent of up- or down-regulation of genes in the dataset. Absolute z-scores greater than 2 are considered statistically significant [214, 215]. Figure 3.9 shows the five most significantly altered pathways upon silencing of TET1 (Figure 3.9A), TET2 (Figure 3.9B) or TET3 (Figure 3.9C). Observing the –log(p-values), it is evident that the most significant changes in biological pathways resulted from TET2 silencing, with the top five pathways having –log(p-values) > 6, compared to those of TET3 silencing which were < 5 and TET1 silencing < 3. Furthermore, the absolute z-scores indicate that TET1 silencing did not significantly impact pathway activity. By contrast, significant activation of interferon signalling and cholesterol biosynthesis pathways were observed upon TET2 silencing and significant inhibition of interferon signalling and estrogen-mediated S-phase entry pathways were observed upon TET3 silencing (Figure 3.9). From this analysis, it appears that TET1 is less functionally important in regulating transcription within HUVEC than TET2 and TET3.

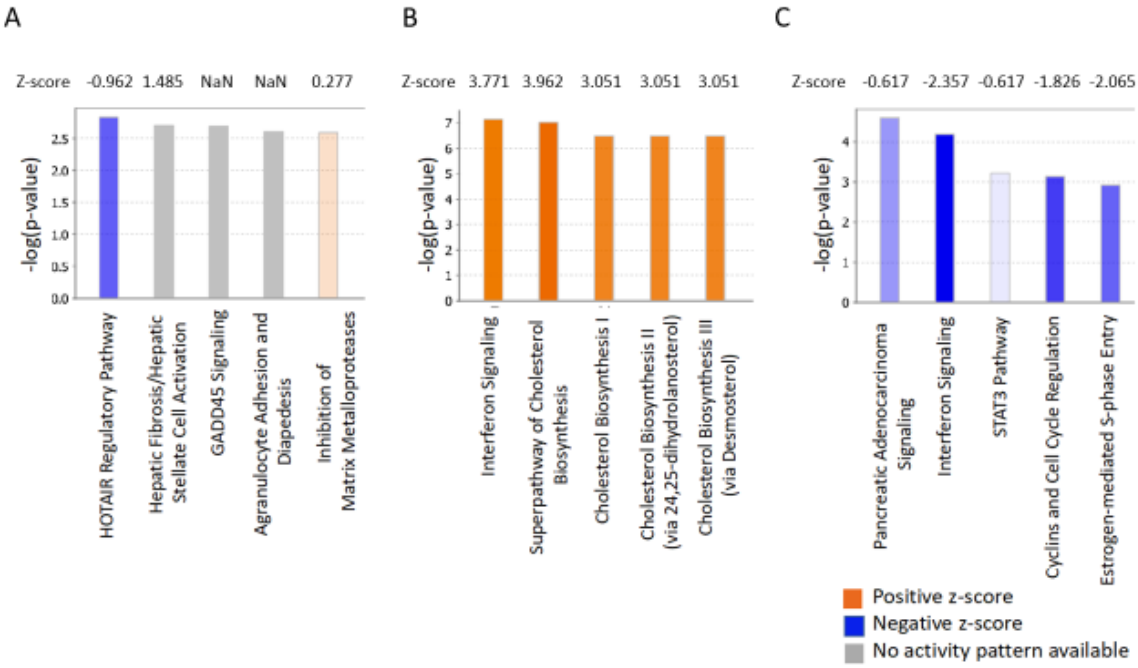

Figure 3.9: ***Pathway analysis of RNA sequencing of TET-silenced HUVEC****. RNA sequencing was performed on HUVEC treated with a negative control siRNA or siRNA targeting TET1, TET2 or TET3. Ingenuity Pathway Analysis was used to identify pathways containing significantly differentially-expressed genes between TET-silenced or control samples. Orange bars denote a positive z-score, indicating the pathway is overall predicted to be activated, and blue bars denote a negative z-score, indicating that the pathway is predicted to be inhibited. Grey bars indicate that no activity pattern prediction is available. In some cases, no Z-score was assigned (NaN – not a number). P-values were calculated by Fisher's Exact Test. –log(p-value)<1.3 and Z-scores >|2| are considered statistically significant.*

3.2.6 High glucose culture of HUVEC for 48h has little impact on the transcriptome

A comparison was made between the biological pathways dysregulated by TET silencing and those dysregulated by high glucose (30mM) culture of HUVEC, hypothesising that high glucose culture may dysregulate TET activity and therefore potentially lead to altered expression of similar pathways. Two control groups were included: HUVEC cultured in normal media, and HUVEC cultured in media with a normal glucose concentration (5mM) and the addition of 25mM mannitol as an osmotic control.

First, the number of genes that were up- or down-regulated in 48h high glucose-cultured HUVEC compared to mannitol-treated controls was quantified, applying cut-

off values of Log2FoldChange>|1| and false discovery rate <0.05. This revealed only a small number of differentially-expressed genes, with 38 genes upregulated and 44 genes downregulated by high glucose treatment (Figure 3.10A). Reasoning that the osmotic effects may also contribute to dysregulation of transcription in hyperglycaemia, high glucose-treated HUVEC were compared to HUVEC cultured in normal media. In this case, 61 genes were upregulated and 217 were downregulated (Figure 3.10A). Changes in gene expression are visualised as volcano plots with annotations of the 5 most significantly upregulated and downregulated genes (Figure 3.10B). Previous literature has suggested that short term exposure (12-48h) of human endothelial cells to high glucose levels (25-30mM) is sufficient to induce changes in transcription of genes with functions related to diabetes and inflammation [10, 67, 96]. However, genes which were previously reported in the literature to show altered expression in high glucose-cultured endothelial cells, such as haemoxygenase (HMOX)1, interleukin-8 (IL8), matrix metalloproteinase (MMP)10, cystine/glutamate transporter (SLCA11), MMP1, P65, monocyte chemoattractant protein (MCP)1 and VCAM1 [10, 67, 96], were not amongst the genes differentially-expressed upon high glucose treatment compared to mannitol-treated cells or cells in media alone. Full lists of differentially expressed genes can be accessed *via* the GEO database (GSE232279). Of the 82 genes identified as differentially-expressed in glucose-treated HUVEC compared to mannitol-treated HUVEC, 18 were also identified as containing differentially-hydroxymethylated regions by hMeDIPseq (Figure 3.10C). The mRNA expression and hydroxymethylation within regions of these genes are compared in Figure 3.10D.

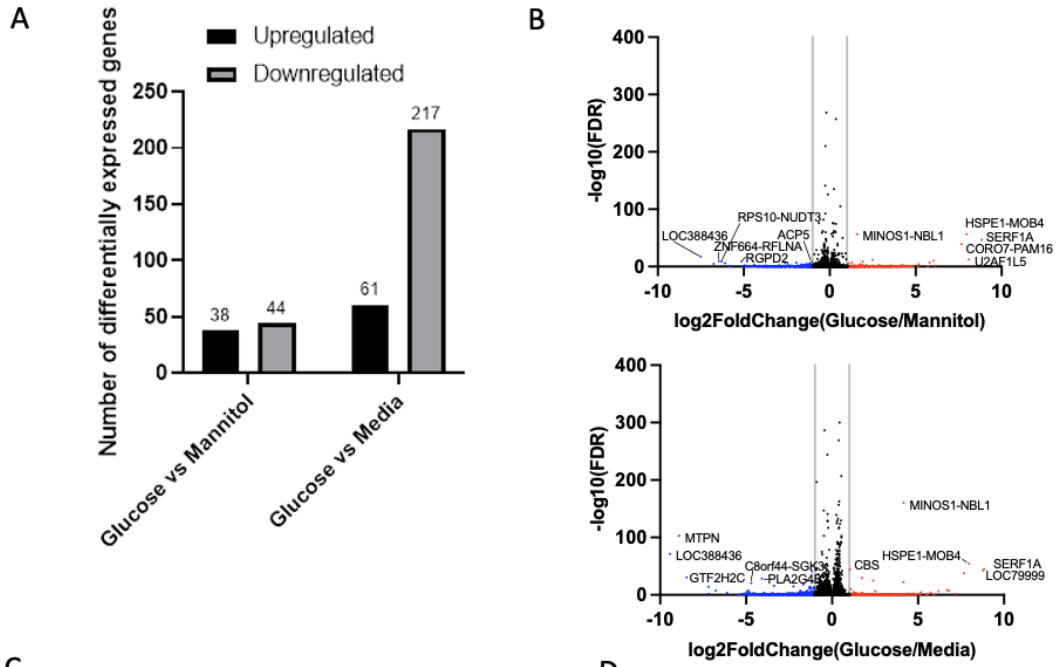

Gene	mRNA expression (Glucose vs Mannitol)	5hmC enrichment (Glucose vs Mannitol)
KCNJ3	↑	↑
CCDC152	↑	↑
STAB2	↓	↑
RGPD1	↑	↑
KCNAB1	↑	↑
RGPD6	↓	↑
GPR75	↑	↑
POLN	↑	↑
LOC79999	↑	↑
LOC388436	↓	↑
RGPD2	↓	↓
GOLGA8R	↑	↓
APOE	↓	↓
AIPL1	↑	↓
TTC39A	↓	↓
SPDYE2B	↑	↑↓
SPDYE2	↑	↑↓
HRASLS	↓	↑↓

Figure 3.10: ***Number of differentially-expressed genes upregulated or downregulated by high glucose or mannitol treatment of HUVEC and comparison with hydroxymethylation status.*** *RNA sequencing was performed on HUVEC cultured for 48h in normal media (5mM glucose) ('Media') or media containing a high glucose concentration (30mM) ('Glucose'), or a normal glucose concentration (5mM) with the addition of 25mM mannitol as an osmotic control ('Mannitol'). (A) Graph displaying the number of up- or down-regulated genes between the respective groups, applying cut-offs of Log2FoldChange>|1| and false discovery rate (FDR) <0.05. (B) Volcano plots showing significantly differentially expressed genes in glucose vs mannitol (upper) or glucose vs media (lower) datasets. The five genes with most statistically significant upregulation and downregulation are labelled. (C) Venn diagram displaying the overlap between differentially expressed genes (DEGs) and differentially hydroxymethylated regions (DHMRs) resulting from high glucose-treatment of HUVEC (compared to mannitol-treated controls). (D) A list of the 18 up- or down-regulated genes in high glucose vs mannitol treated HUVEC which showed concomitant changes in 5hmC enrichment. In some cases, regions of both hyper- and hypo-hydroxymethylation were identified within the same gene, indicated by ↑↓.*

3.2.7 High glucose culture of HUVEC for 48h does not induce similar transcriptomic changes to those resulting from TET-silencing

To investigate whether high glucose treatment induced transcriptomic changes in HUVEC that mirrored changes observed upon TET silencing, IPA software was used to group differentially-expressed genes into biological pathways, applying a cut-off of Log2FoldChange>|1| and false discovery rate <0.05. Comparing the high glucose-treated cells to mannitol-treated cells, EIF2 signalling (a pathway involved in regulating mRNA translation in response to stress [216]) was predicted to be significantly inhibited (Figure 3.11A). By contrast, this pathway was predicted to be significantly activated when comparing high glucose-treated cells to those cultured in normal media (Figure 3.11B). Oxidative phosphorylation was also predicted to be strongly activated in high glucose-treated cells compared to media only controls, which is perhaps expected due to increased substrate availability through metabolism of excess glucose (Figure 3.11B). Other pathways, although containing significantly differentially-expressed genes, were not directional in their regulation state. None of the pathways which were identified to be dysregulated by high glucose overlapped with those found to be dysregulated by silencing TET1, TET2 or TET3 in HUVEC (Figure 3.9).

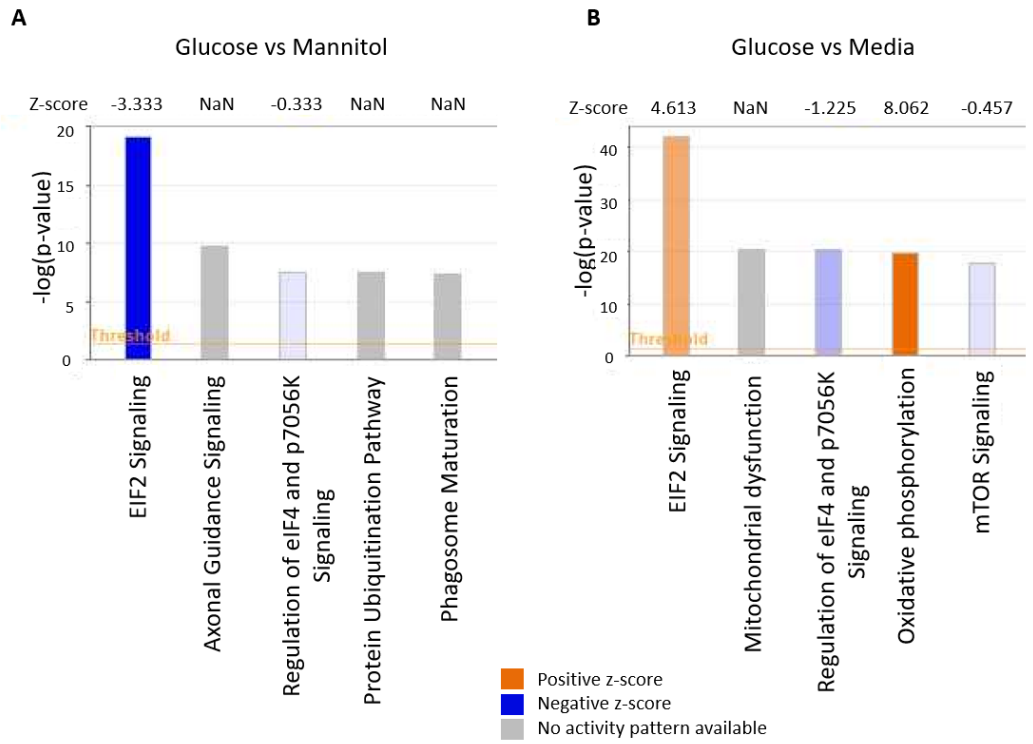

Figure 3.11: ***Pathway analysis of RNA sequencing of high glucose-cultured HUVEC****. RNA sequencing was performed on HUVEC cultured for 48h in normal media (5mM glucose) ('Media') or media containing a high glucose concentration (30mM) ('Glucose'), or a normal glucose concentration (5mM) with the addition of 25mM mannitol as an osmotic control ('Mannitol'). Ingenuity Pathway Analysis was used to identify pathways containing significantly differentially-expressed genes between Glucose and Mannitol cells (A) and between Glucose and Media cells (B). Orange bars denote a positive z-score, indicating the pathway is overall predicted to be activated, and blue bars denote a negative z-score, indicating that the pathway is predicted to be inhibited. Grey bars indicate that no activity pattern prediction is available. In some cases, no Z-score was assigned (NaN – not a number). P-values were calculated by Fisher's Exact Test. –log(p-value)<1.3 and Z-scores >|2| are considered statistically significant.*

Of the 82 mRNA transcripts that were differentially-expressed in high glucose-treated compared to mannitol-treated HUVEC, a subset were also differentially-expressed in TET-silenced compared to siRNA control-treated HUVEC (Table 3.1). However, many of the transcripts identified are readthrough transcripts and/or do not have well-characterised biological functions in endothelial cells. Perhaps a longer duration of high glucose culture or a variable glucose concentration would better model the *in vivo* setting and enable improved characterisation of the transcriptomic changes resulting from hyperglycaemia and whether they resemble the changes observed upon TET silencing.

Common to high glucose & TET1-silenced HUVEC			Common to high glucose & TET2-silenced HUVEC			Common to high glucose & TET3-silenced HUVEC		
Gene	log2FC (TET1-silenced vs siRNA control)	log2FC (glucose vs mannitol)	Gene	log2FC (TET2-silenced vs siRNA control)	log2FC (glucose vs mannitol)	Gene	log2FC (TET3-silenced vs siRNA control)	log2FC (glucose vs mannitol)
TBC1D3C	-6.7	-5.0	**URGCP-MRPS24**	-5.6	6.1	**TBC1D3C**	-6.7	-5.0
ZNF664-RFLNA	-5.7	-6.4	**SPP1**	-2	4.8	**ZNF664-RFLNA**	-5.7	-6.4
ZNF559-ZNF177	3.7	4.3	**TGIF2-C20orf24**	5.6	-6.8	**ZNF559-ZNF177**	5.5	4.3
CLEC18A	-4.7	4.3	**CORO7-PAM16**	1.1	7.7	**CORO7-PAM16**	1.9	7.7
RGPD1	-1.9	1.8	**HSPE1-MOB4**	-6.2	8	**HSPE1-MOB4**	-6.2	8.0
ASDURF	-1.2	-1.3	**PLA2G4B**	-5.2	-2.6	**PLA2G4B**	-5.2	-2.6
ACP5	1.2	-1.0	**U2AF1L5**	2.1	8.1	**U2AF1L5**	-9.1	8.1
NPIPB13	1.2	2.5	**RNF103-CHMP3**	-5.1	6	**RNF103-CHMP3**	1.5	6.0
RPS10-NUDT3	5.5	-6.3	**TMEM110-MUSTN1**	6.2	5.8	**TMEM110-MUSTN1**	6.0	5.8
URGCP-MRPS24	-5.6	6.2	**RGPD6**	-2.5	-1.9	**LOC79999**	-7.9	1.1
SPP1	-1.8	4.8	**SYT13**	-2.2	3.6	**SPDYE2B**	-5.6	1.7
TGIF2-C20orf24	5.6	-6.8	**TMEM189-UBE2V1**	-1.5	5.2	**SOGA3**	1.2	3.0
CORO7-PAM16	-6.9	7.7	**GOLGA8O**	-1.4	-2.4	**SV2A**	2.2	-1.8
HSPE1-MOB4	-6.2	8.0	**FAM72A**	-1.1	1.3	**GOLGA6L22**	4.1	-3.7
PLA2G4B	-5.2	-2.6	**SERF1A**	8.8	8.9	**LOC388436**	8.3	-7.5
U2AF1L5	-3.8	8.1	**LOC79999**	-7.9	1.1	**FSBP**	-5.9	-1.3
RNF103-CHMP3	1.6	6.0	**SPDYE2B**	-5.6	1.7	**FAM156A**	-5.8	-1.4
TMEM110-MUSTN1	5.9	5.8	**SOGA3**	1.2	3	**MINOS1-NBL1**	-4.8	1.6
			SV2A	1.6	-1.8	**APOE**	1.3	-1.5
			GOLGA6L22	4.6	-3.7	**OLFML3**	1.3	-1.6
			LOC388436	8.5	-7.5	**TBC1D3**	4.2	-5.0

Table 3.1: ***List of mRNA transcripts commonly differentially-expressed in high glucose vs mannitol-treated HUVEC and TET-silenced vs siRNA control-treated HUVEC.*** *RNA sequencing was performed on HUVEC cultured for 48h in media containing a high glucose concentration (30mM), or a normal glucose concentration (5mM) with the addition of 25mM mannitol as an osmotic control. RNA sequencing was also performed on HUVEC treated with a negative control siRNA or siRNA targeting TET1, TET2 or TET3. Table shows lists of genes commonly differentially-expressed by both high glucose treatment or TET silencing and their log2(fold-change) in expression.*

3.2.8 Type I and type II interferon signalling pathways

It was intriguing to note that both TET2 and TET3 were associated with dysregulation of genes involved in interferon signalling, but in opposing directions. Type I interferons (primarily IFNα and IFNβ) are released by many cell types early in the response to viral infection, following stimulation of pattern recognition receptors which sense pathogen-associated molecular patterns [217, 218]. Type II interferon (IFNγ) is mainly produced by natural killer (NK) cells and T cells [217, 218]. Cells respond to the binding of interferons to their cell surface receptors, IFNAR (type I IFN) or IFNGR (type II IFN) [219]. Upon receptor binding, downstream signalling *via* Janus kinase (JAK)/Signal transducer and activator of transcription (STAT) results in phosphorylation and nuclear translocation of STAT1-STAT2-IRF9 (in the case of type I interferon) or STAT1 homodimers (in the case of type II interferon) [219]. The complex binds to IFN-stimulated response elements (ISRE) or gamma activated sequences (GAS) in the promoter region of interferon-sensitive genes, activating their transcription (Figures 3.15 & 3.16) [219]. Many interferon-sensitive genes are associated with functions such as inhibition of viral entry, inhibition of viral replication, or are released as cytokines to attract or activate immune cells such as monocytes and NK cells [220]. Beyond the antiviral response, interferon signalling is known to regulate endothelial cell functions such as permeability, proliferation, angiogenesis and nitric oxide production [38, 221, 222].

3.2.9 siRNA/lipofectamine transfection *per se* activates interferon response pathways in HUVEC

An important consideration when interpreting these data is the method employed to silence TET2 or TET3. For this study, siRNA-mediated silencing was achieved by transfecting HUVEC using lipofectamine RNAiMax, a cationic lipid which complexes with the negatively-charged backbone of nucleic acids to facilitate their endocytosis. Although this is a widely used method to target genes of interest selectively by RNA interference, there have been few studies assessing the extent to which

lipofectamine/negative control siRNA-treated cell phenotypes differ from those of non-transfected cells. In the RNA sequencing datasets, it was observed that HUVEC transfected with the negative control siRNA had markedly increased expression of genes belonging to interferon signalling pathways, compared to non-transfected HUVEC (Figure 3.12). It is possible that the effects of TET2/3 silencing on expression of interferon-sensitive genes may be somewhat masked using this transfection method due to pre-existing interferon pathway activation.

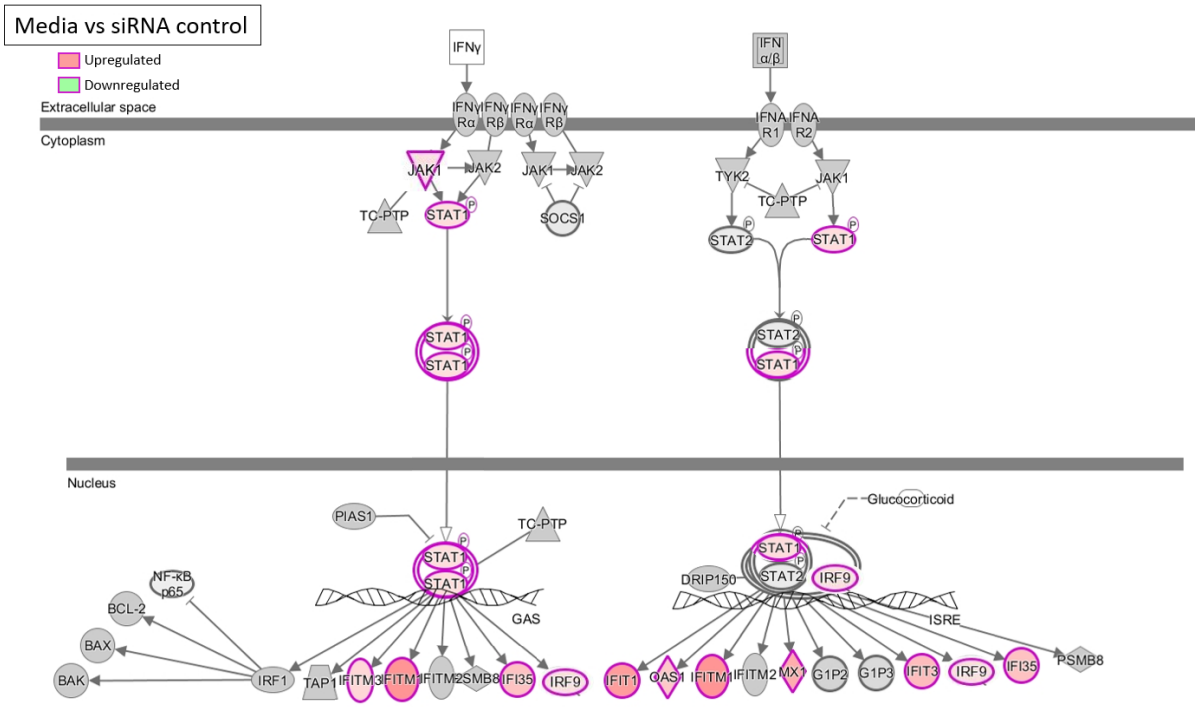

Figure 3.12: ***Type I and type II interferon signalling pathways showing genes differentially-expressed in negative control siRNA-treated HUVEC compared to non-transfected HUVEC.*** *RNA sequencing was performed on non-transfected HUVEC and HUVEC treated with a negative control siRNA. Schematic diagram of type I and type II interferon signalling pathways shows genes upregulated by negative control siRNA transfection in red.*

3.2.10 siRNA/lipofectamine transfection affects HUVEC morphology

To assess any general morphological differences between negative control siRNA-transfected HUVEC and non-transfected HUVEC, phase contrast and immunofluorescence staining with DAPI, phalloidin and VE-cadherin was performed to visualise nuclei, the actin cytoskeleton and cell-cell junctions, respectively (Figure 3.13). Although under both conditions, the HUVEC displayed the characteristic cobblestone morphology of endothelial cells under phase contrast (Figure 3.13A), a

striking increase in cell size was evident in transfected HUVEC compared to non-transfected HUVEC, with a mean cell area >2-fold higher (Figure 3.13B, C & D). Furthermore, a significantly higher proportion of transfected cells were binucleate than was observed in the non-transfected HUVEC, which could indicate impaired progression through the cell cycle (Figure 3.13E). This highlights the importance of considering to what extent transfection techniques employed routinely in laboratories cause cellular stress and deviate from the biological context and phenotypes they are used to investigate.

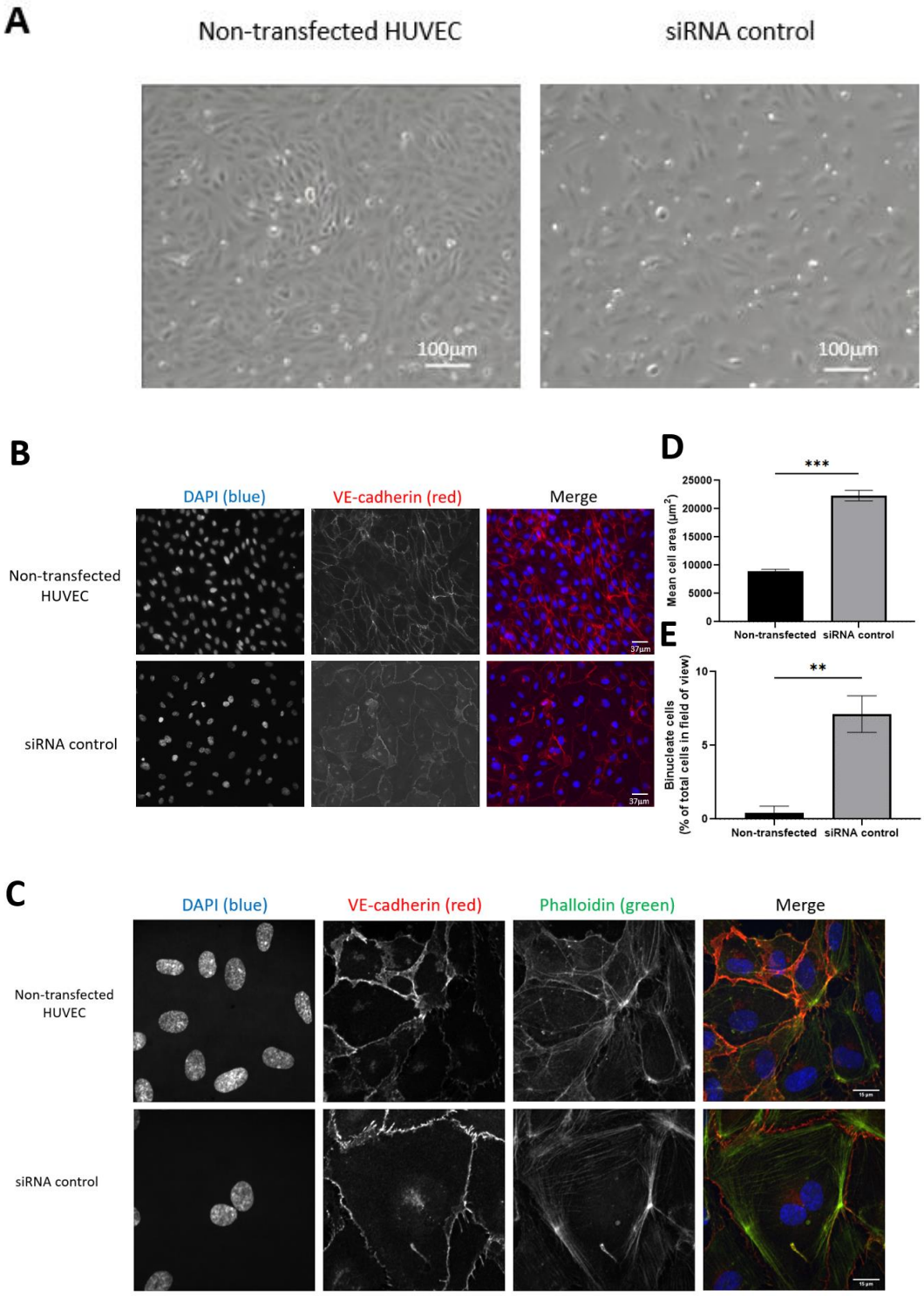

Figure 3.13: ***Negative control siRNA/lipofectamine transfection of HUVEC changes HUVEC morphology.*** *A) Phase contrast images of non-transfected and negative control siRNA-treated HUVEC acquired using an EVOS microscope. Scale bars represent 100µm. B) Fluorescence images of DAPI and VE-cadherin staining in non-transfected and negative control siRNA-treated HUVEC imaged using IX-81 microscope. Scale bars represent 37µm. C) Higher magnification images of DAPI, VE-cadherin and phalloidin staining in non-transfected and negative control siRNA-treated HUVEC imaged using a spinning disk confocal microscope. Scale bars represent 15µm. Quantification of mean cell area (D) and percentage of binucleate cells (E) observed in each field of view (at least 30 cells per image for each condition in triplicate) in non-transfected and negative control siRNA-treated HUVEC. Data presented as mean± SEM.*

To limit the impact of this, optimisation of the concentration and duration of lipofectamine and siRNA treatment was attempted. However, at shorter durations or lower concentrations of either reagent, silencing of TET2 or TET3 was inefficient (data not shown). As antibiotics and the presence of serum are also reported to affect transfection efficiency, conditions with or without these were also trialled. Although the manufacturer's protocol for the lipofectamine RNAiMax reagent states that complexes can be added to culture media containing serum and/or antibiotics and that it is not necessary to change media following transfection, this method did not successfully silence TET2 or TET3 in HUVEC when trialled (data not shown). Therefore, the protocol described in Materials & Methods (Chapter 2.3.6) was used throughout this work. Comparing TET2 siRNA-transfected cells to negative control siRNA-transfected cells, no significant differences in morphology, cell size or percentage of binucleate cells were observed (Figure 3.14).

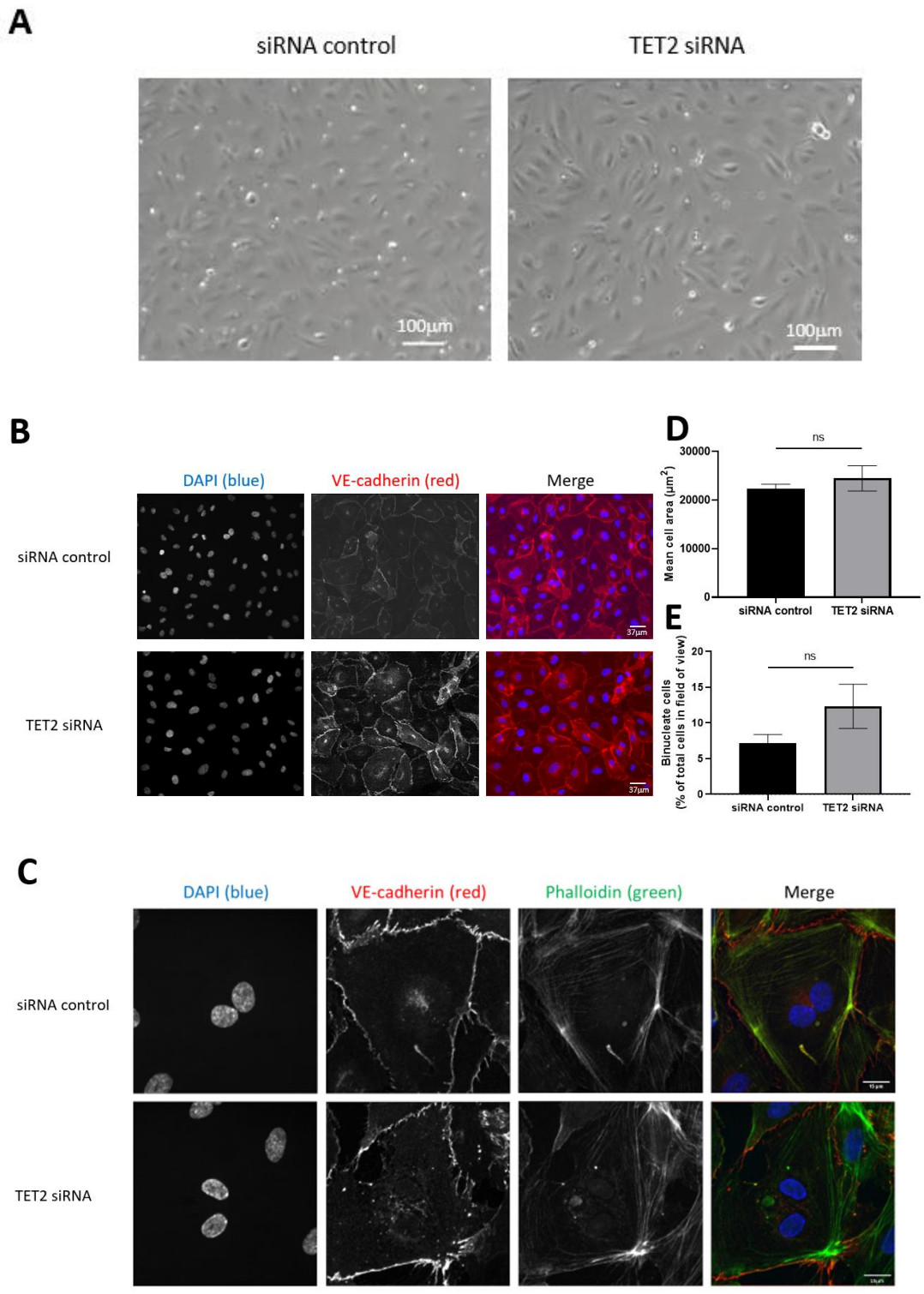

Figure 3.14: ***TET2 siRNA-transfected HUVEC are morphologically similar to negative control siRNA-transfected HUVEC.*** *A) Brightfield images of negative control siRNA- and TET2 siRNA-treated HUVEC acquired using an EVOS microscope. Scale bars represent 100µm. B) Fluorescence images of DAPI and VE-cadherin staining in negative control siRNA- and TET2 siRNA-treated HUVEC imaged using IX-81 microscope. Scale bars represent 37µm. C) Higher magnification images of DAPI, VE-cadherin and phalloidin staining in negative control siRNA- and TET2-siRNA-treated HUVEC imaged using a spinning disk confocal microscope. Scale bars represent 15µm. Quantification of mean cell area (D) and percentage of binucleate cells (E) observed in each field of view (at least 30 cells per image for each condition in triplicate) in negative control siRNA- and TET2 siRNA-treated HUVEC. Data presented as mean± SEM.*

3.2.11 TET2 and TET3 have reciprocal effects on interferon-sensitive gene expression in HUVEC under baseline conditions

To investigate the reciprocal relationship of TET2 and TET3 with interferon signalling, Ingenuity Pathway Analysis was used to visualise type I and type II interferon signalling pathways, highlighting genes that were dysregulated by TET2 (Figure 3.15) or TET3 (Figure 3.16) silencing. In many cases, the same interferon-sensitive genes were differentially-expressed in TET2- and TET3-silenced HUVEC compared to controls, but whereas the genes were upregulated by TET2 silencing, they were downregulated by TET3 silencing.

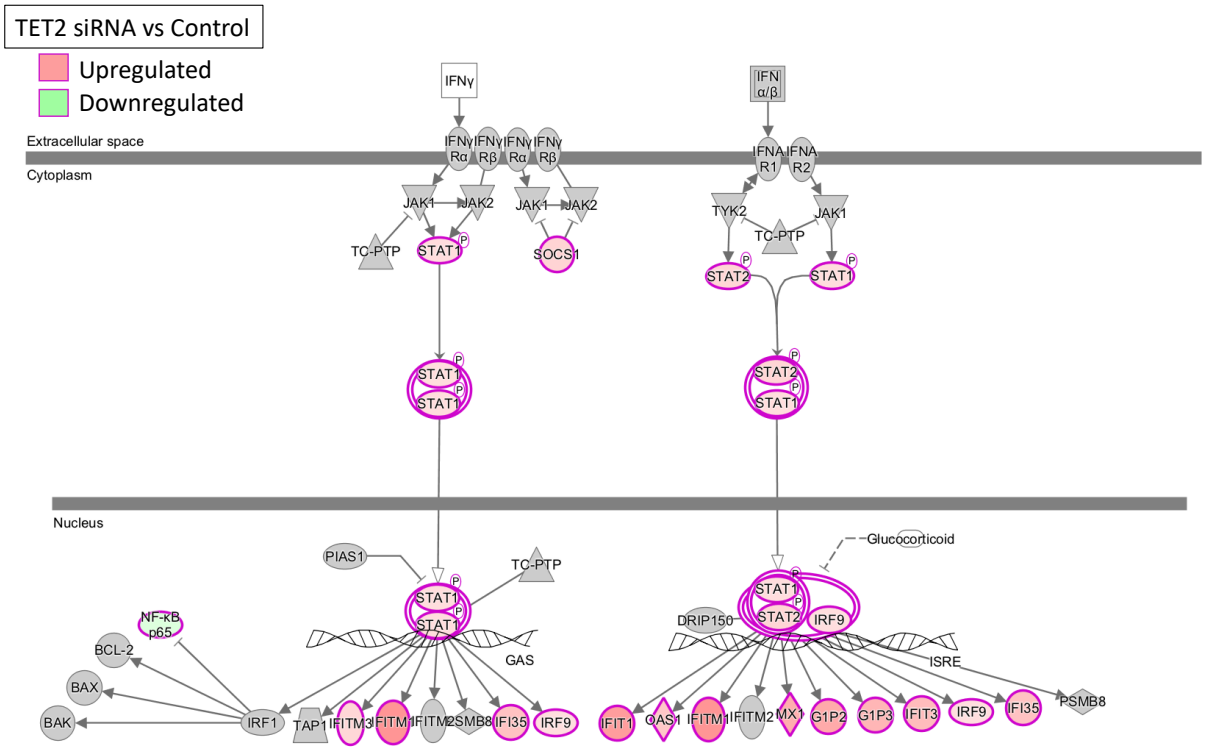

Figure 3.15: ***Type I and type II interferon signalling pathways showing genes differentially-expressed in TET2 siRNA-treated HUVEC compared to negative control siRNA-treated HUVEC.*** *RNA sequencing was performed on HUVEC treated with a negative control siRNA or siRNA targeting TET2. Schematic diagram of type I and type II interferon signalling pathways shows genes upregulated by TET2 silencing in red and genes downregulated by TET2 silencing in green.*

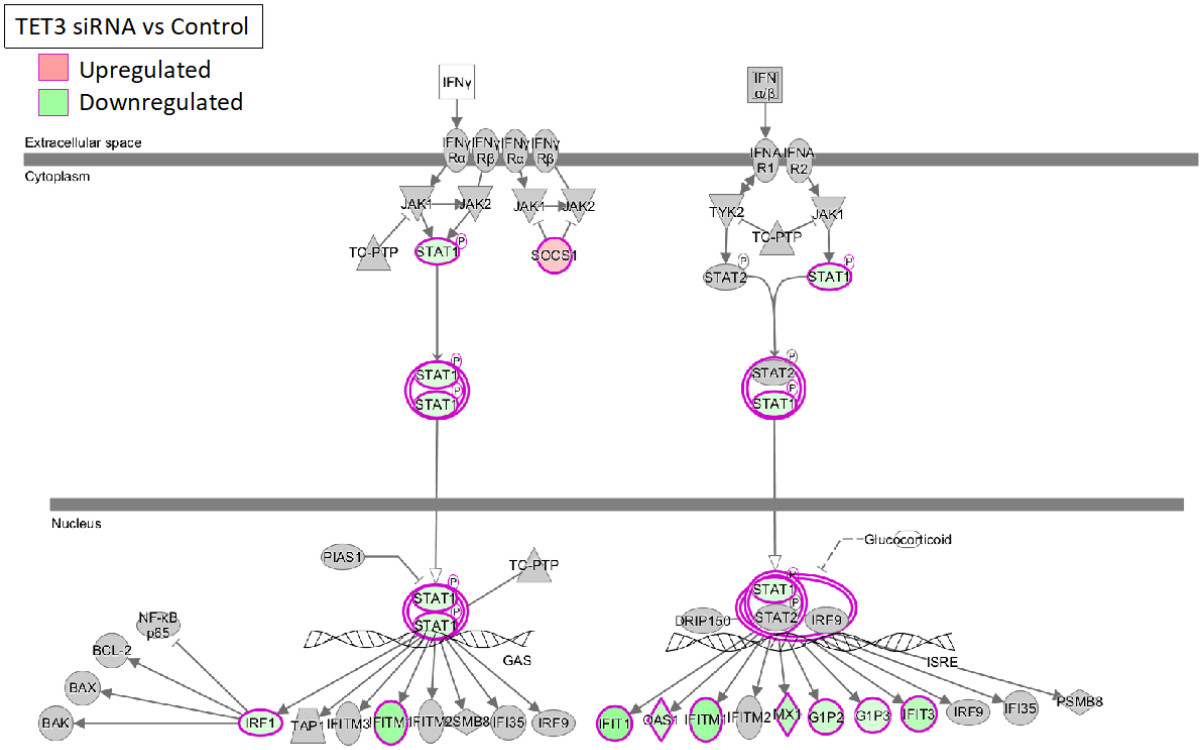

Figure 3.16: ***Type I and type II interferon signalling pathways showing genes differentially-expressed in TET3 siRNA-treated HUVEC compared to negative control siRNA-treated HUVEC.*** *RNA sequencing was performed on HUVEC treated with a negative control siRNA or siRNA targeting TET3. Schematic diagram of type I and type II interferon signalling pathways shows genes upregulated by TET3 silencing in red and genes downregulated by TET3 silencing in green.*

To validate the changes in gene expression identified by RNA sequencing, qPCR was performed on additional HUVEC samples using a small panel of interferon-sensitive genes dysregulated by both TET2 and TET3 silencing. Consistent with the RNA sequencing data, these genes followed a trend of upregulation in TET2-silenced HUVEC (Figure 3.17) and downregulation in TET3-silenced HUVEC (Figure 3.18). Significant changes were observed in MX dynamin like GTPase 1 (MX1), 2'-5'-oligoadenylate synthetase 2 (OAS2) and interferon-stimulated gene 15 (ISG15) expression following TET2 silencing, (Figure 3.17) and in MX1, radical S-adenosyl methionine domain containing 2 (RSAD2), OAS2 and interferon-induced transmembrane protein 1 (IFITM1) expression following TET3 silencing (Figure 3.18). This suggests that TET2 typically acts to repress transcription of interferon-sensitive genes in endothelial cells under basal conditions, whereas TET3 may function to increase their expression.

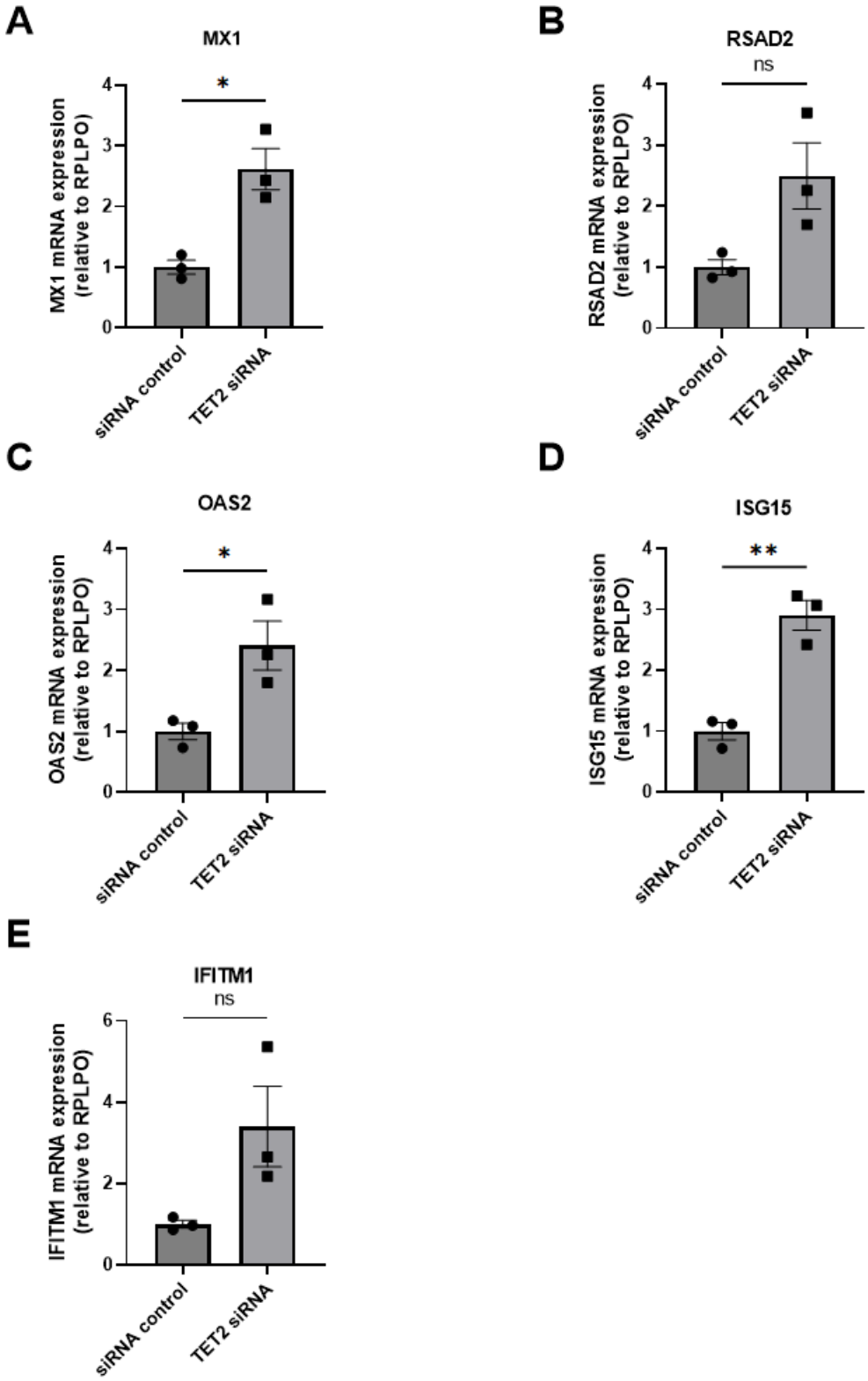

Figure 3.17: ***qPCR validation of differentially-expressed interferon pathway genes in TET2-silenced vs siRNA control HUVEC.*** *HUVEC were transfected with negative control siRNA or siRNA targeting TET2. qPCR was performed to measure relative mRNA expression of interferon-sensitive genes MX1 (A), RSAD2 (B), OAS2 (C), ISG15 (D) and IFITM1 (E), normalised to the housekeeping gene RPLPO. A Shapiro-Wilk test for normality was performed, followed by an unpaired t-test. Data presented as mean ±SEM. n=3 triplicate samples. * denotes p<0.05. ** denotes p<0.01.*

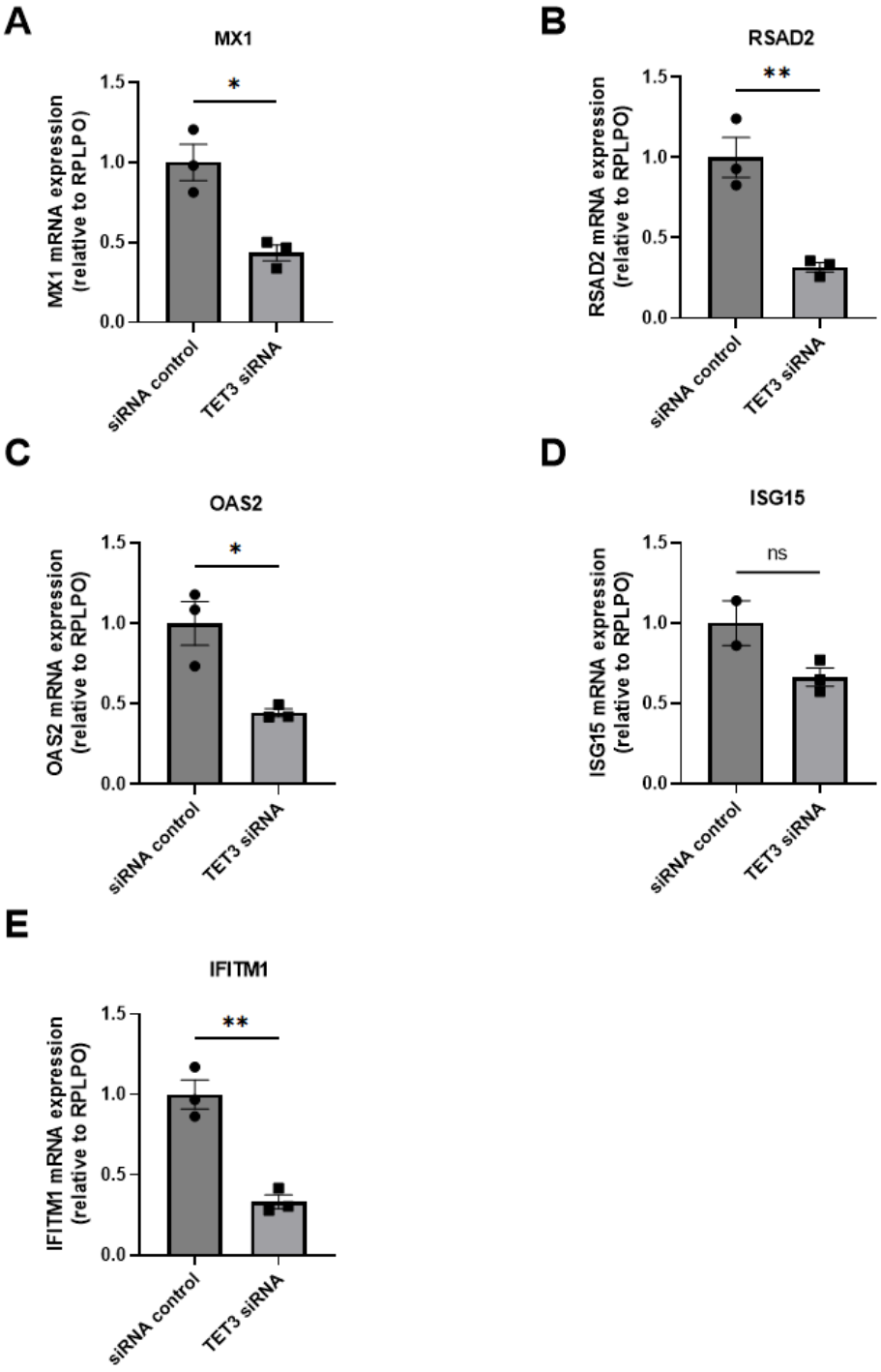

Figure 3.18: ***qPCR validation of differentially-expressed interferon pathway genes in TET3-silenced vs siRNA control HUVEC.*** *HUVEC were transfected with negative control siRNA or siRNA targeting TET3. qPCR was performed to measure relative mRNA expression of interferon-sensitive genes MX1 (A), RSAD2 (B), OAS2 (C), ISG15 (D) and IFITM1 (E), normalised to the housekeeping gene RPLPO. A Shapiro-Wilk test for normality was performed, followed by an unpaired t-test. Data presented as mean ± SEM. n=3 triplicate samples. * denotes p<0.05.*

3.2.12 TET2 and TET3 expression diverge at 4 hours of stimulation with interferon alpha or interferon gamma

The next experiments sought to elucidate the importance of TET2 and TET3 in the transcriptional response following stimulation with IFNα or IFNγ. In a preliminary experiment, the expression profiles of IFITM1 and ISG15 (as markers of the interferon response), TET2 and TET3 were determined in HUVEC by qPCR, during a timecourse of 1000U/ml IFNα (Figure 3.19) or 10ng/ml IFNγ (Figure 3.20) stimulation, ranging from 1 hour to 24 hours. Concentrations of IFN were selected based on observations of perturbed endothelial function in existing literature [38, 223]. In response to IFNα, the expression of IFITM1 and ISG15 rapidly increased, reaching over a 300-fold increase by 8 hours before plateauing. Intriguingly, a sharp increase in TET2 expression and a decrease in TET3 expression were observed at the 4-hour timepoint. In response to IFNγ, IFITM1 expression increased linearly to 300-fold by 24 hours. ISG15 was not as strongly upregulated by IFNγ as by IFNα, but its expression increased steadily to 24-fold over baseline by 24 hours. As for IFNα, the same opposing pattern of TET2 and TET3 expression was observed 4 hours after IFNγ stimulation.

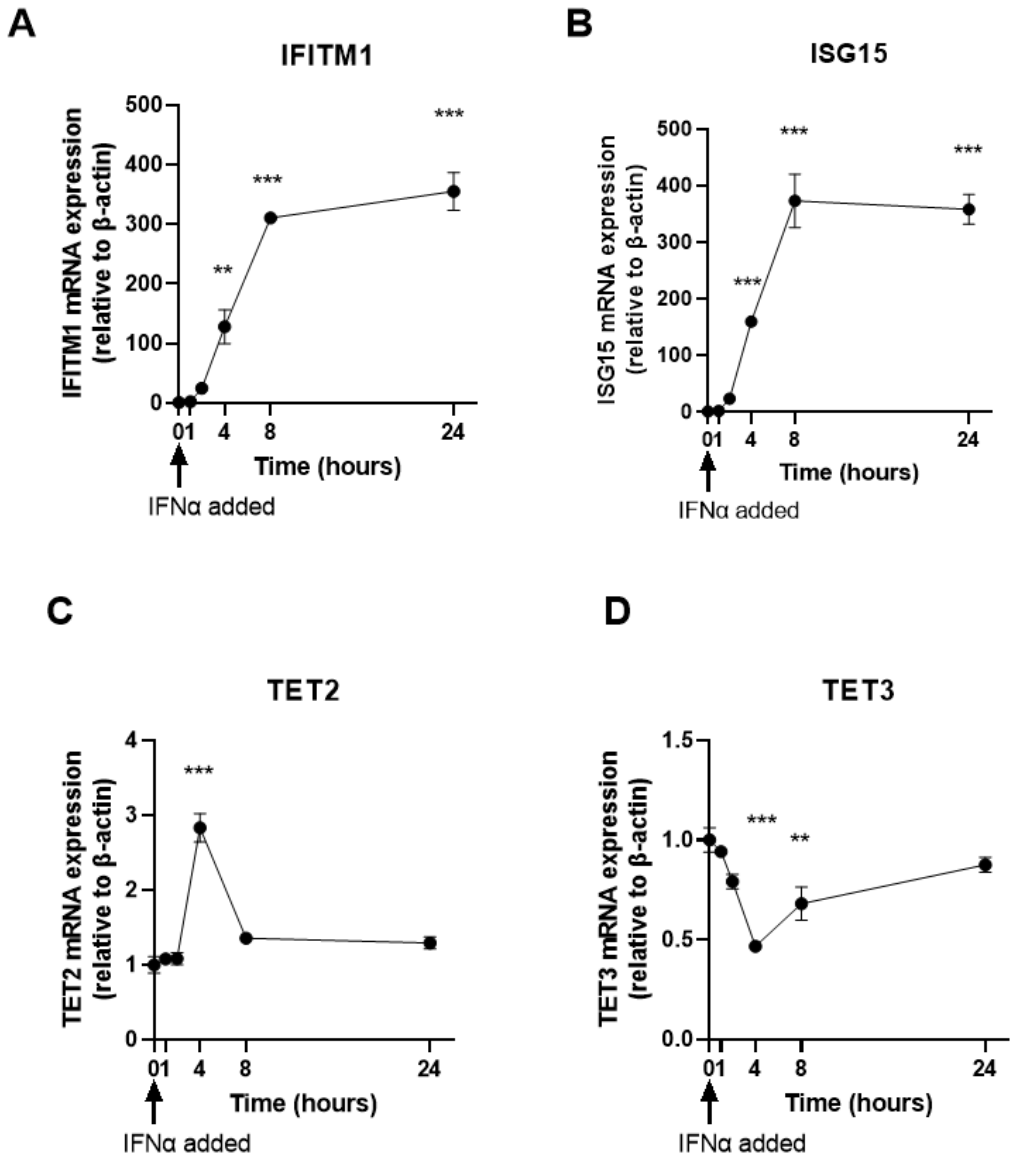

Figure 3.19: ***Expression of IFITM1, ISG15, TET2 and TET3 in a timecourse of IFNα stimulation of HUVEC.*** *cDNA was prepared from HUVEC treated with IFNα for 0, 1, 4, 8 or 24 hours. qPCR was performed to measure relative mRNA expression of IFITM1 (A), ISG15 (B), TET2 (C) and TET3 (D), normalised to the housekeeping gene β-actin. A Shapiro-Wilk test for normality was performed, followed by a one-way ANOVA with post-hoc Dunnett's test. Data presented as mean $\pm$SEM. n=3 triplicate samples. * denotes p<0.05. ** denotes p<0.01. *** denotes p<0.001.*

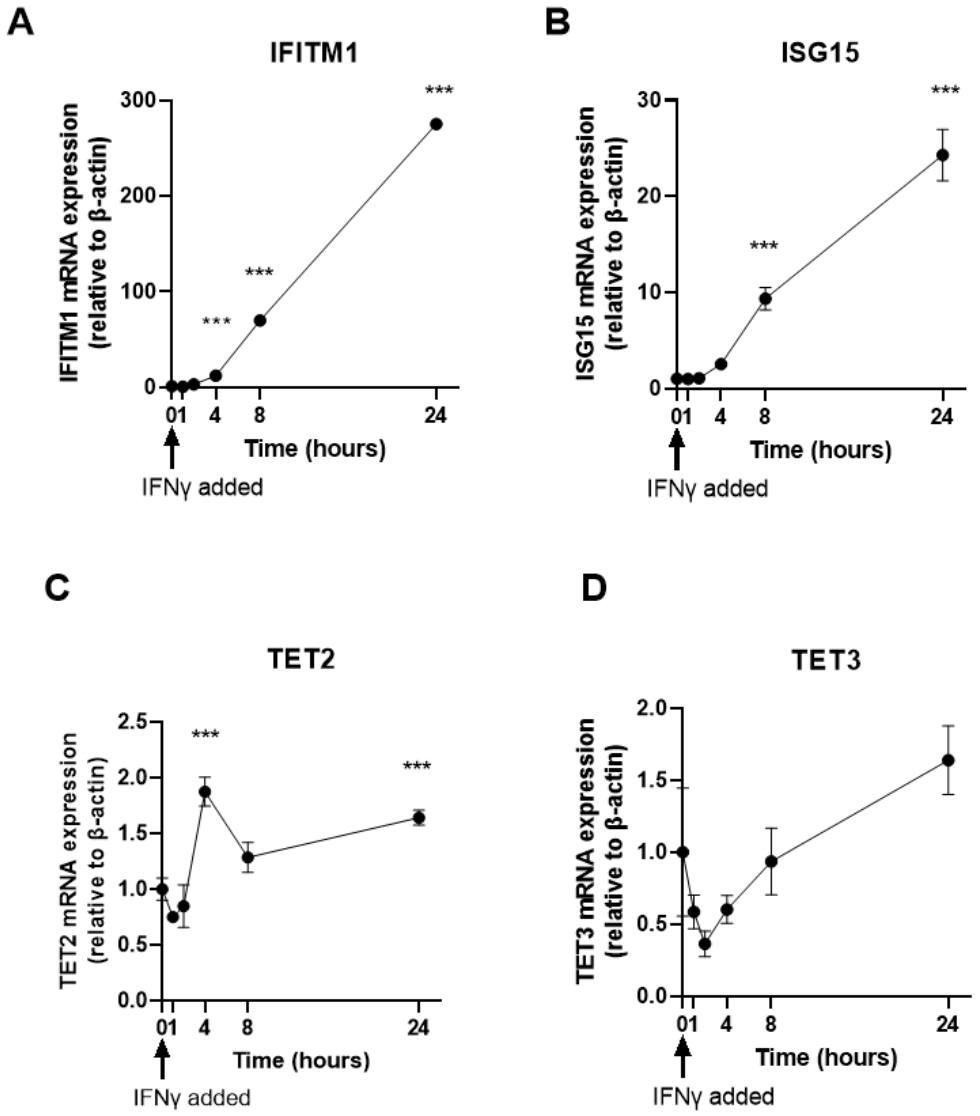

Figure 3.20: ***Expression of IFITM1, ISG15, TET2 and TET3 in a timecourse of IFNγ stimulation of HUVEC.*** *cDNA prepared from HUVEC treated with IFNγ for 0, 1, 4, 8 or 24 hours. qPCR was performed to measure relative mRNA expression of IFITM1 (A), ISG15 (B), TET2 (C) and TET3 (D), normalised to the housekeeping gene β-actin. A Shapiro-Wilk test for normality was performed, followed by a one-way ANOVA with post-hoc Dunnett's test. Data presented as mean ± SEM. n=3 triplicate samples. * denotes p<0.05. ** denotes p<0.01. *** denotes p<0.001.*

3.2.13 TET2 and TET3 expression diverge in the first 4 hours of resolution of the interferon response in HUVEC

Whilst the mechanisms underlying the activation of innate and adaptive immune responses and inflammatory pathways have been well characterised, an often overlooked aspect of the immune response is how these pathways are later suppressed to return to a quiescent state. TET2 has previously been shown *in vitro* and *in* vivo to have a role in the resolution of inflammatory responses in myeloid cells by

repression of IL-6, IL-1β and other inflammatory cytokines/chemokines [158, 159]. Therefore, the profile of interferon-sensitive gene expression was investigated in a 24-hour timecourse following the removal of the IFNα or IFNγ stimulus. IFITM1 and ISG15 expression declined in the 8 hours following IFNα removal towards baseline levels (Figure 3.21A & B). After 24 hours, IFITM1 expression had further decreased towards baseline, whereas a secondary increase in ISG15 expression was seen between 8 and 24 hours after IFNα removal (Figure 3.21A & B). Interestingly, TET2 expression increased sharply in the first 4 hours of resolution of the interferon response, whilst TET3 expression remained unchanged at this timepoint and subsequently increased (Figure 3.21C & D).

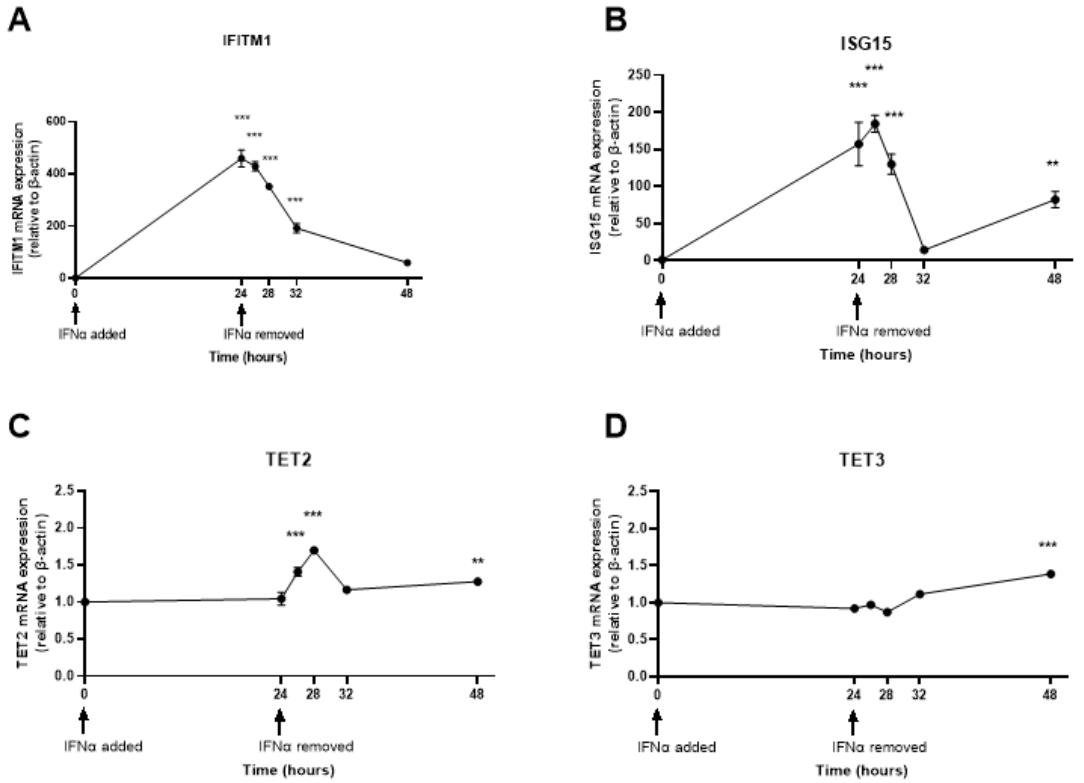

Figure 3.21: ***Expression of IFITM1, ISG15, TET2 and TET3 in a timecourse of recovery from IFNα stimulation of HUVEC.*** *cDNA was prepared from HUVEC treated with IFNα for 0 or 24 hours or treated with IFNα for 24 hours followed by removal for 1, 4, 8 or 24 hours. qPCR was performed to measure relative mRNA expression of IFITM1 (A), ISG15 (B), TET2 (C) and TET3 (D), normalised to the housekeeping gene β-actin. A Shapiro-Wilk test for normality was performed, followed by a one-way ANOVA with post-hoc Dunnett's test. Data presented as mean ±SEM. n=3 triplicate samples. * denotes p<0.05. ** denotes p<0.01. *** denotes p<0.001.*

Following removal of IFNγ, the profile of IFITM1 expression was similar to that seen after removal of IFNα, declining towards baseline (Figure 3.22). In this case, no secondary increase in ISG15 expression was observed, but it instead continued to decrease. An increase in TET2 expression and a slight decrease in TET3 expression was also evident at 4 hours post removal of IFNγ. This divergent pattern of expression of TET2 and TET3 observed during the early hours of activation and resolution of interferon responses, combined with the opposing effects of TET2 and TET3 silencing on interferon-sensitive gene expression supports distinct and opposing roles for these enzymes in the regulation of interferon signalling in endothelial cells.

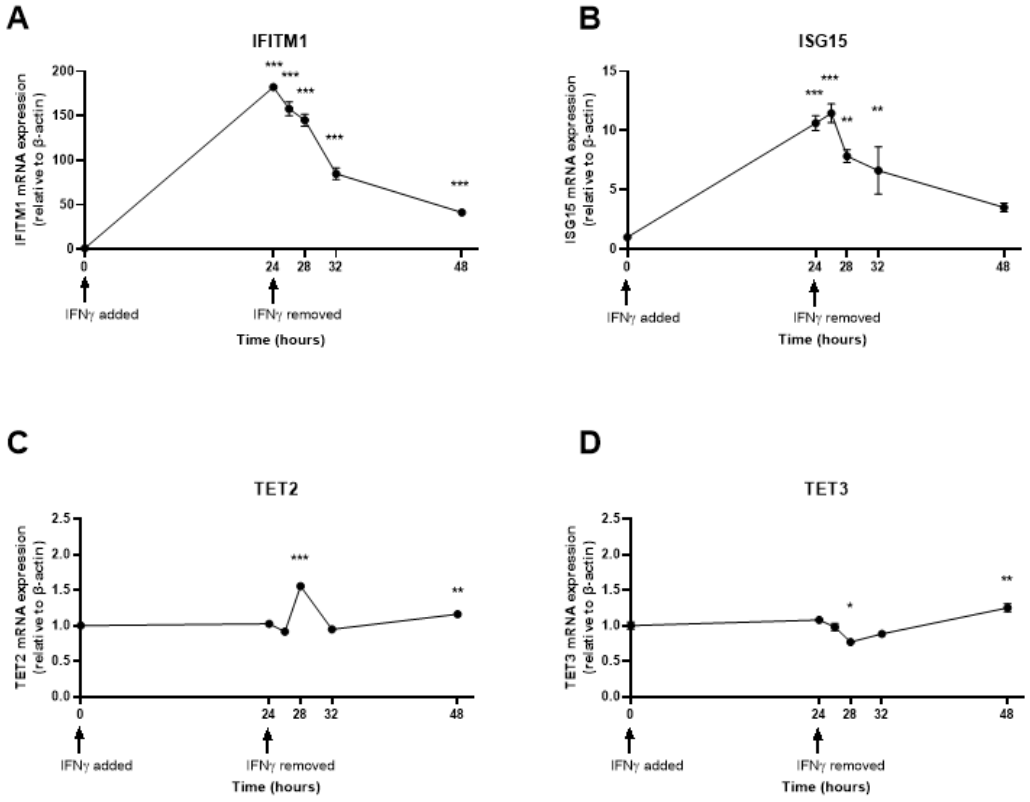

Figure 3.22: ***Expression of IFITM1, ISG15, TET2 and TET3 in a timecourse of recovery from IFNγ stimulation of HUVEC.*** *cDNA was prepared from HUVEC treated with IFNγ for 0 or 24 hours or treated with IFNγ for 24 hours followed by removal for 1, 4, 8 or 24 hours. qPCR was performed to measure relative mRNA expression of IFITM1 (A), ISG15 (B), TET2 (C) and TET3 (D), normalised to the housekeeping gene β-actin. A Shapiro-Wilk test for normality was performed, followed by a one-way ANOVA with post-hoc Dunnett's test. Data presented as mean ± SEM. n=3 triplicate samples. * denotes p<0.05. ** denotes p<0.01. *** denotes p<0.001.*

3.2.14 Silencing of TET2 impairs the resolution of type I and type II interferon responses in HUVEC

Next, the profiles of interferon-sensitive gene expression during and after interferon stimulation were examined following siRNA-mediated silencing of TET2. Given that TET2- silencing activated the interferon response under baseline conditions (Figures 3.9 & 3.17), it was hypothesised that upon stimulation with IFNα or IFNγ, the amplitude of the response may be increased and/or the resolution of the interferon response may be impaired. As markers of the interferon response, IFITM1 and ISG15 expression were measured at baseline, after 24h IFN stimulation and 4h or 24h after its removal.

At the 48h timepoint (*i.e.* 24h after removal of IFNα) IFITM1 expression was significantly higher in TET2-silenced HUVEC than in negative control siRNA-treated HUVEC (Figure 3.23). ISG15 expression was also higher in TET2-silenced HUVEC, but this did not reach statistical significance (Figure 3.23). Furthermore, 24h after removal of IFNγ, ISG15 expression was significantly higher in TET2-silenced HUVEC than in negative control siRNA-treated HUVEC and IFITM1 showed a trend towards increased expression (Figure 3.24). These data suggest that TET2 may be involved in the resolution of both type I and type II interferon response in endothelial cells.

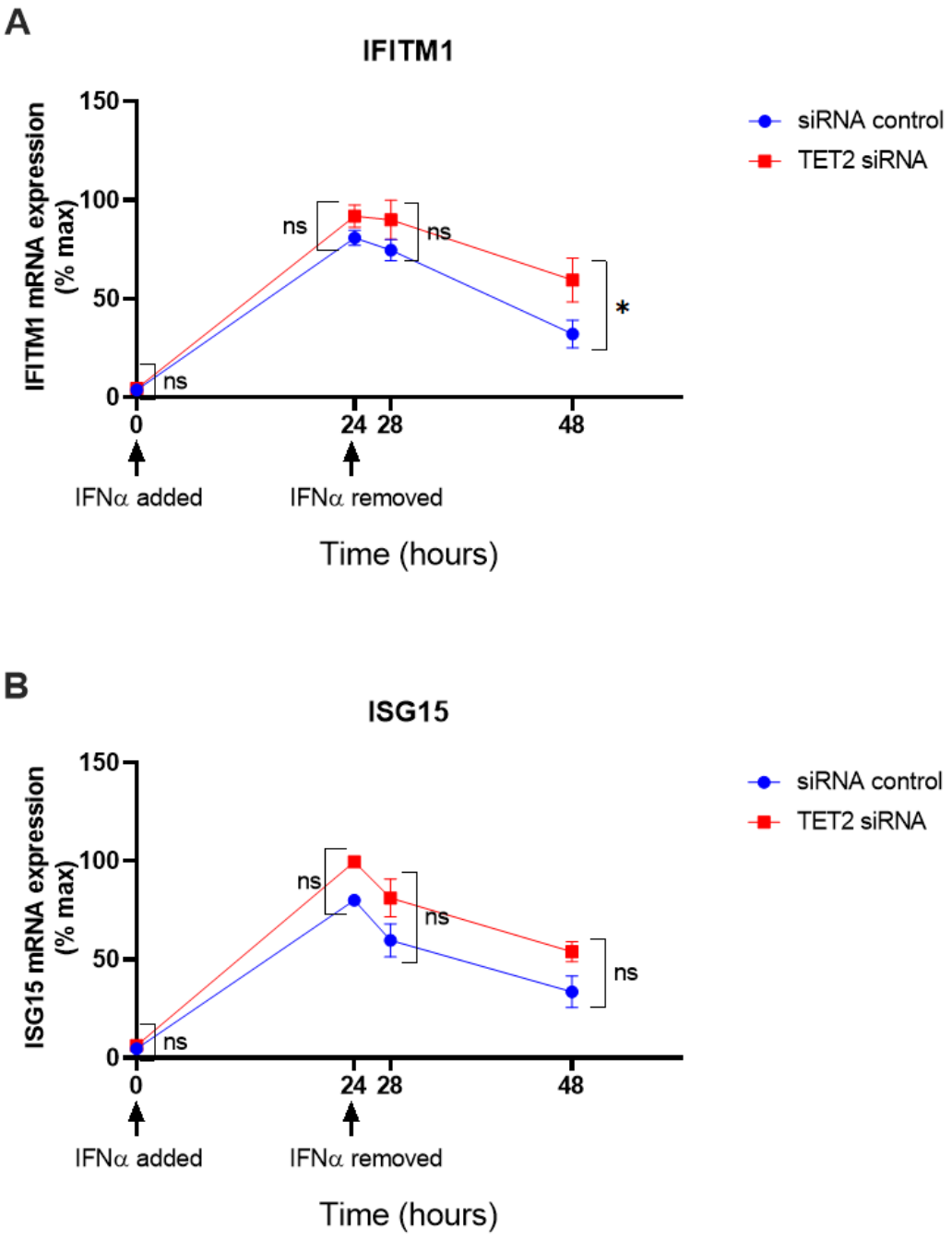

Figure 3.23: ***Profile of IFITM1 and ISG15 expression during IFNα activation and resolution in negative control siRNA or TET2-silenced HUVEC.*** *cDNA was prepared from HUVEC transfected with negative control siRNA or siRNA targeting TET2 and treated with IFNα for 0 or 24 hours or treated with IFNα for 24 hours followed by its removal for 4 or 24 hours. qPCR was performed to measure relative mRNA expression of IFITM1 (A) and ISG15 (B), normalised to the housekeeping gene β-actin. Owing to varied magnitudes of IFN response, 2-ΔΔCT values were expressed as a percentage of maximum expression in each experiment. A Shapiro-Wilk test for normality was performed, followed by an unpaired t-test at each timepoint. Data presented as mean ±SEM. n=3-4 independent experiments. * denotes p<0.05, ns = not significant.*

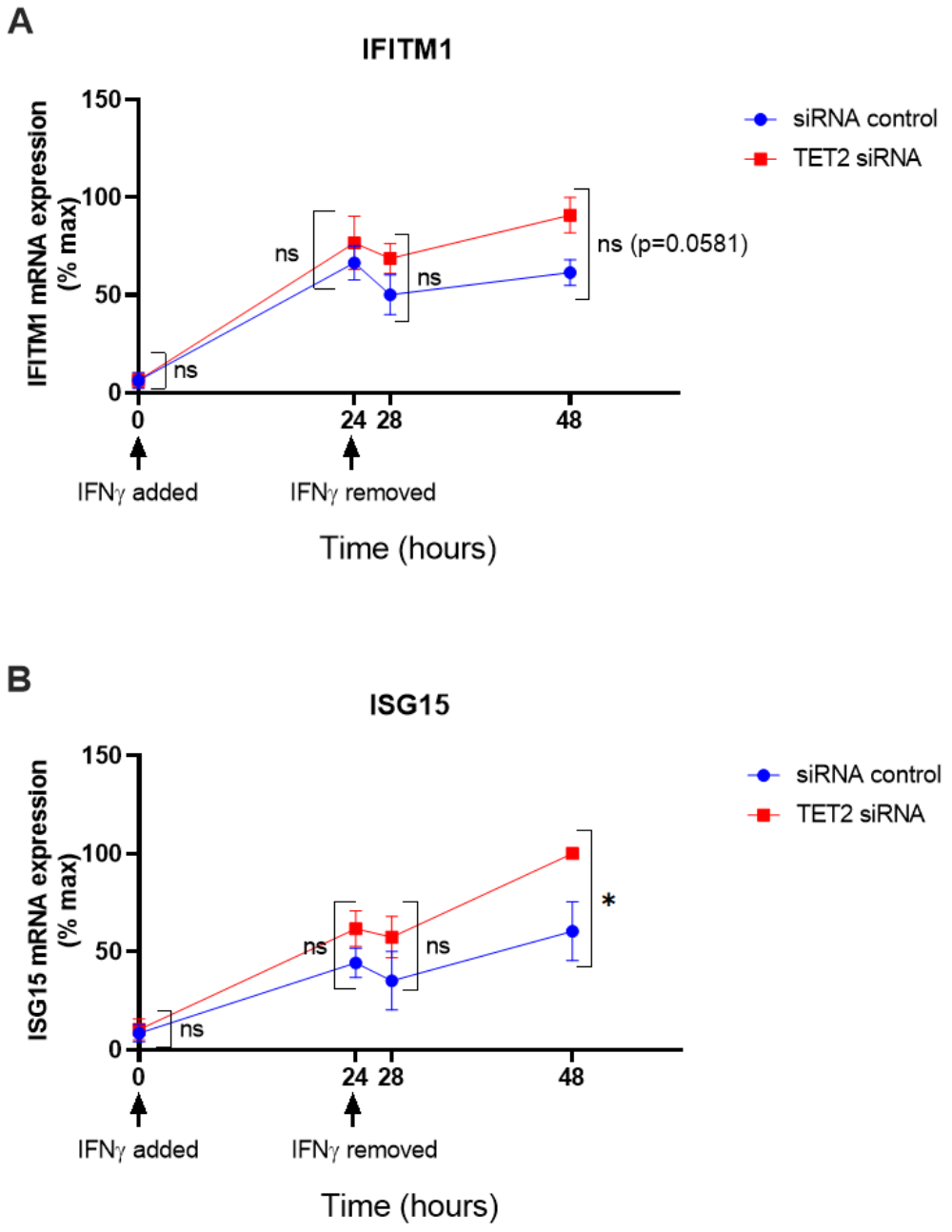

Figure 3.24: ***Profile of IFITM1 and ISG15 expression during IFNγ activation and resolution in negative control siRNA or TET2-silenced HUVEC.*** *cDNA was prepared from HUVEC transfected with negative control siRNA or siRNA targeting TET2 and treated with IFNγ for 0 or 24 hours or treated with IFNγ for 24 hours followed by its removal for 4 or 24 hours. qPCR was performed to measure relative mRNA expression of IFITM1 (A) and ISG15 (B), normalised to the housekeeping gene β-actin. Owing to varied magnitudes of IFN response, 2-ΔΔCT values were expressed as a percentage of maximum expression in each experiment. A Shapiro-Wilk test for normality was performed, followed by an unpaired t-test at each timepoint. Data presented as mean ±SEM. n=3-4 independent experiments. * denotes p<0.05, ns = not significant.*

3.2.15 Silencing of TET3 impairs the activation of type II but not type I interferon responses in HUVEC

To investigate the potential role for TET3 in regulating type I and type II interferon responses, IFITM1 and ISG15 mRNA expression levels were measured following 24h stimulation with IFNα or IFNγ and 24h after its removal in TET3-silenced HUVEC (Figures 3.25 & 3.26) and compared to control levels. TET3 silencing had no significant effect on the profile of IFITM1 and ISG15 expression in the response to IFNα (Figure 3.25), but these genes were less strongly upregulated by IFNγ in TET3-silenced HUVEC compared to scrambled controls and remained at a significantly lower expression level following its removal (Figure 3.26). These data support a positive role for TET3 in regulating the activation of type II interferon, but not type I interferon transcriptional responses in endothelial cells.

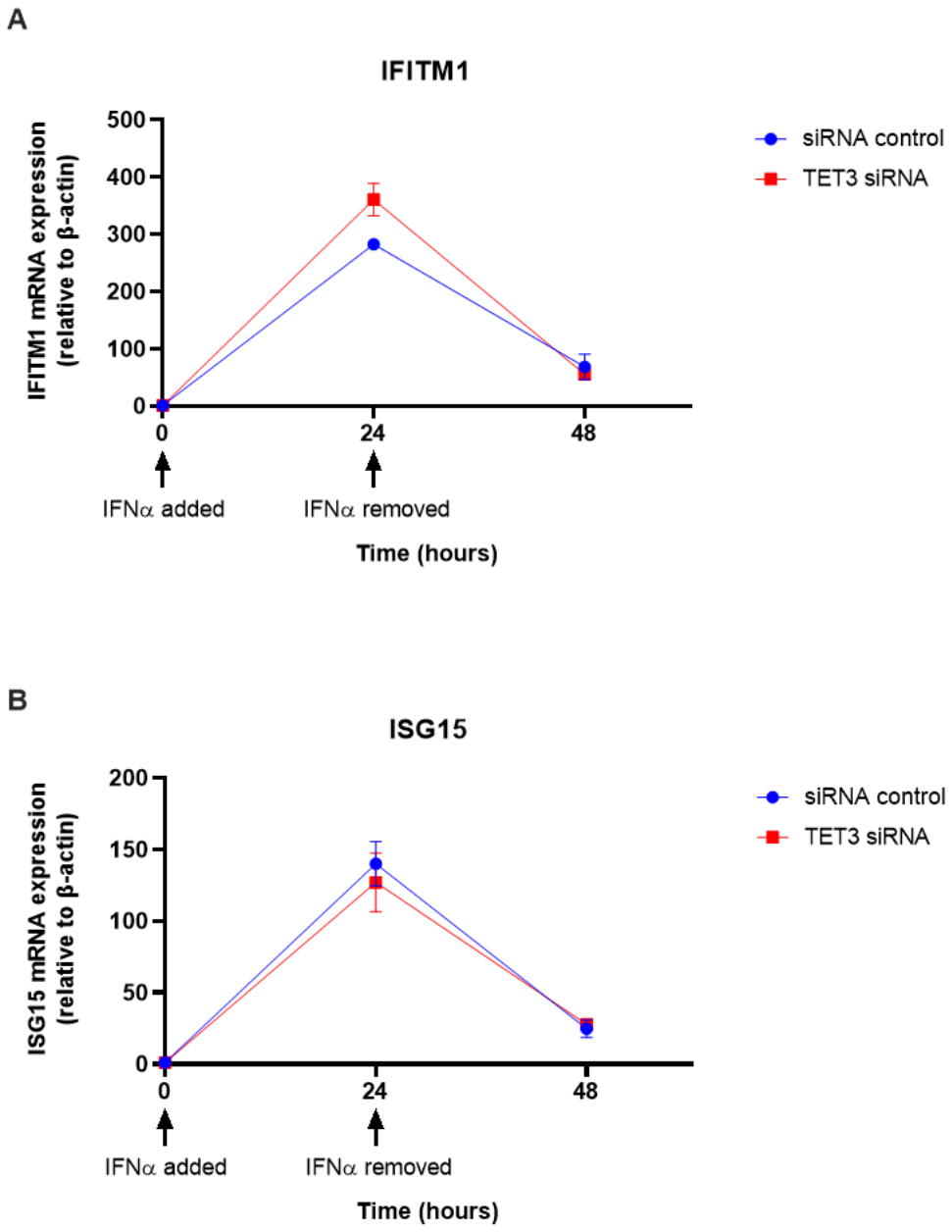

Figure 3.25: ***Profile of IFITM1 and ISG15 expression during IFNα activation and resolution in negative control siRNA or TET3-silenced HUVEC.*** *cDNA was prepared from HUVEC transfected with negative control siRNA or siRNA targeting TET3 and treated with IFNα for 0 or 24 hours or treated with IFNα for 24 hours followed by its removal for 4 or 24 hours. qPCR was performed to measure relative mRNA expression of IFITM1 (A) and ISG15 (B), normalised to the housekeeping gene β-actin. A Shapiro-Wilk test for normality was performed, followed by an unpaired t-test at each timepoint. Data presented as mean ±SEM. n=3 triplicate samples.*

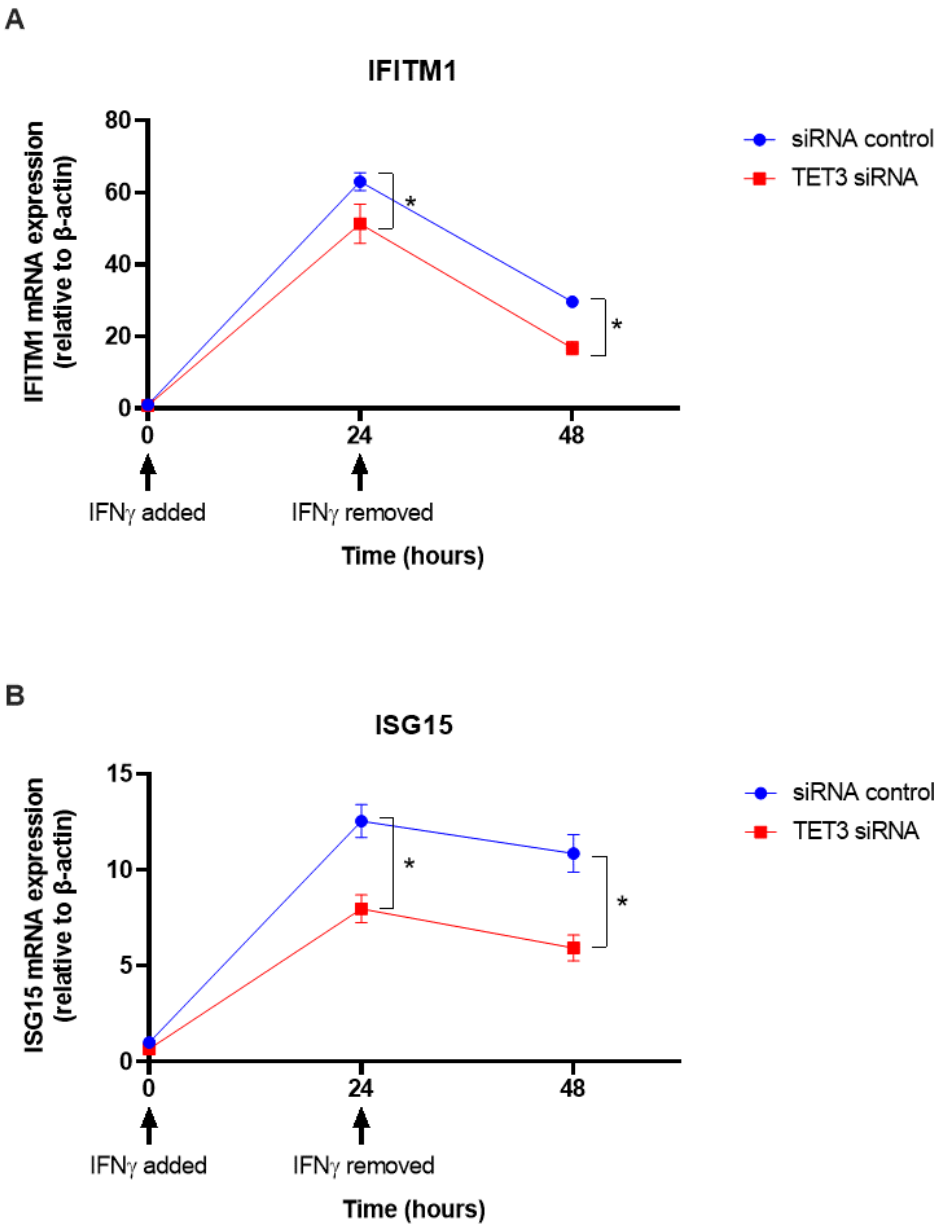

Figure 3.26: ***Profile of IFITM1 and ISG15 expression during IFNγ activation and resolution in negative control siRNA or TET3-silenced HUVEC.*** *cDNA was prepared from HUVEC transfected with negative control siRNA or siRNA targeting TET3 and treated with IFNγ for 0 or 24 hours or treated with IFNγ for 24 hours followed by its removal for 4 or 24 hours. qPCR was performed to measure relative mRNA expression of IFITM1 (A) and ISG15 (B), normalised to the housekeeping gene β-actin. A Shapiro-Wilk test for normality was performed, followed by an unpaired t-test at each timepoint. Data presented as mean ± SEM. n=3 triplicate samples. * denotes p<0.05.*

3.2.16 Exposure of HUVEC to intermittent high glucose augments type I and type II interferon responses

It would be interesting to explore whether exposure of endothelial cells to high glucose conditions perturbs the activation or resolution of interferon responses in a similar manner to TET2 or TET3 silencing. However, given that previous data showed very few transcriptional changes as a result of 48h high glucose culture (Figure 3.10) and that this was not associated with changes in global 5hmC levels (Figure 3.4), the *in vitro* model of hyperglycaemia was altered. For this study, intermittent high glucose was applied, varying from 5mM to 25mM glucose every 24h for 14 days. Control cells were maintained in 5mM glucose conditions but with the addition and removal of 20mM mannitol every 24h to control for osmotic effects. This was chosen because similar *in vitro* models have previously been shown to be more detrimental to endothelial cells than stable high glucose concentrations [224-229]. Upon stimulation with IFNγ, the expression of IFITM1 and ISG15 were significantly greater in glucose-treated HUVEC compared to mannitol-treated HUVEC (Figure 3.27). IFITM1 expression remained significantly higher following the removal of IFNγ and this trend was also observed for ISG15. Although not displaying the same profile of response and resolution, the sustained increased expression of IFITM1 and ISG15 in intermittent high glucose-cultured HUVEC is similar to that observed upon TET2 silencing. If TET2 activity is suppressed by hyperglycaemia, this trend would be expected.

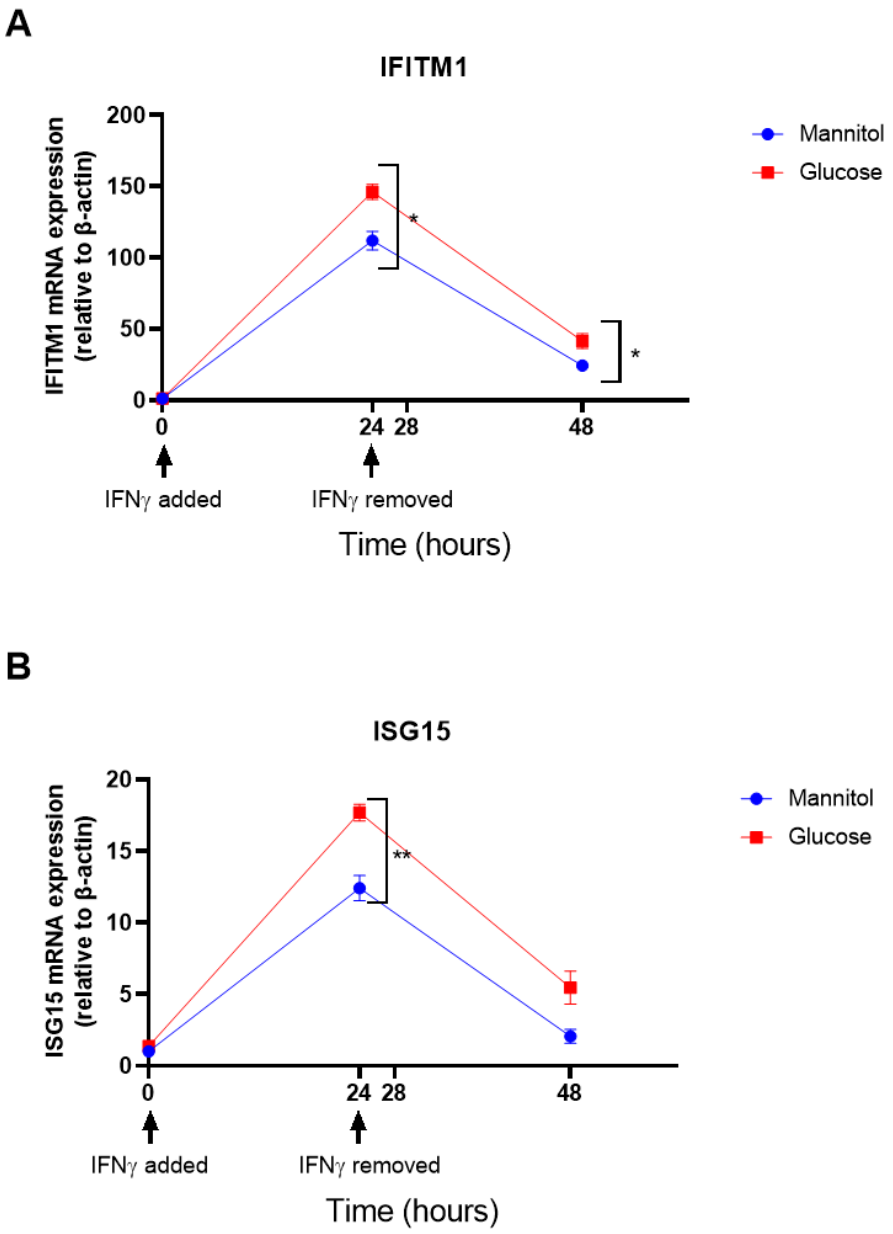

Figure 3.27: ***Profile of IFITM1 and ISG15 expression during IFNγ activation and resolution in intermittent glucose or mannitol-treated HUVEC.*** *cDNA was prepared from HUVEC cultured for 14 days in intermittent high glucose or mannitol and treated with IFNγ for 0 or 24 hours or treated with IFNγ for 24 hours followed by its removal for 24 hours. qPCR was performed to measure relative mRNA expression of IFITM1 (A) and ISG15 (B), normalised to the housekeeping gene β-actin. A Shapiro-Wilk test for normality was performed, followed by an unpaired t-test at each timepoint. Data presented as mean ±SEM. n=3 triplicate samples. * denotes p<0.05, * denotes p<0.01.*

3.2.17 TET2 silencing downregulates baseline expression of cell adhesion molecules but their TNFα-induced upregulation is not affected

The finding that TET2 is involved in the resolution of interferon signalling following IFNα or IFNγ stimulation in HUVEC led to the question of whether other inflammatory responses are regulated by TET2. Existing literature reports a role for TET2 in the regulation of cell adhesion molecules ICAM-1 and VCAM-1 in HUVEC treated with oxidised LDL [165]. Although no significant differences in VCAM-1 or ICAM-1 were identified in the RNA-sequencing data sets comparing TET2-silenced HUVEC to negative control siRNA-treated HUVEC at baseline, it was hypothesised that differences may be observed after stimulation with the pro-inflammatory mediator TNFα. Like oxidised LDL and IFNγ [165, 230], TNFα is known to be present in atherosclerotic lesions, where it strongly upregulates cell adhesion molecules and other genes involved in the leukocyte adhesion cascade [231]. Using qPCR, the expression of ICAM-1 and VCAM-1 and an additional cell adhesion molecule, E-selectin, were compared in TET2-silenced or negative control siRNA-treated HUVEC at baseline and following 4 hours of treatment with 10ng/ml TNFα. Without stimulation, the basal expression levels of E-selectin, VCAM-1 and ICAM-1 were significantly decreased in TET2-silenced cells, contrasting with the RNA sequencing data sets (Figure 3.28A-C). Upon TNFα stimulation, the expression of these adhesion molecules markedly increased as expected (Figure 3.28). However, unlike in the basal state, TNFα-stimulated expression of these adhesion molecules was not significantly altered by TET2 silencing (Figure 3.28D-F). TNFα did not affect TET2 expression at this timepoint (Figure 3.28G). These findings contrast with the involvement of TET2 in the inflammatory response to oxidised LDL reported by Peng *et al.,* where TET2 silencing increased adhesion molecule expression, perhaps reflecting a stimulus-specific role for TET2 in modulating inflammatory responses [165].

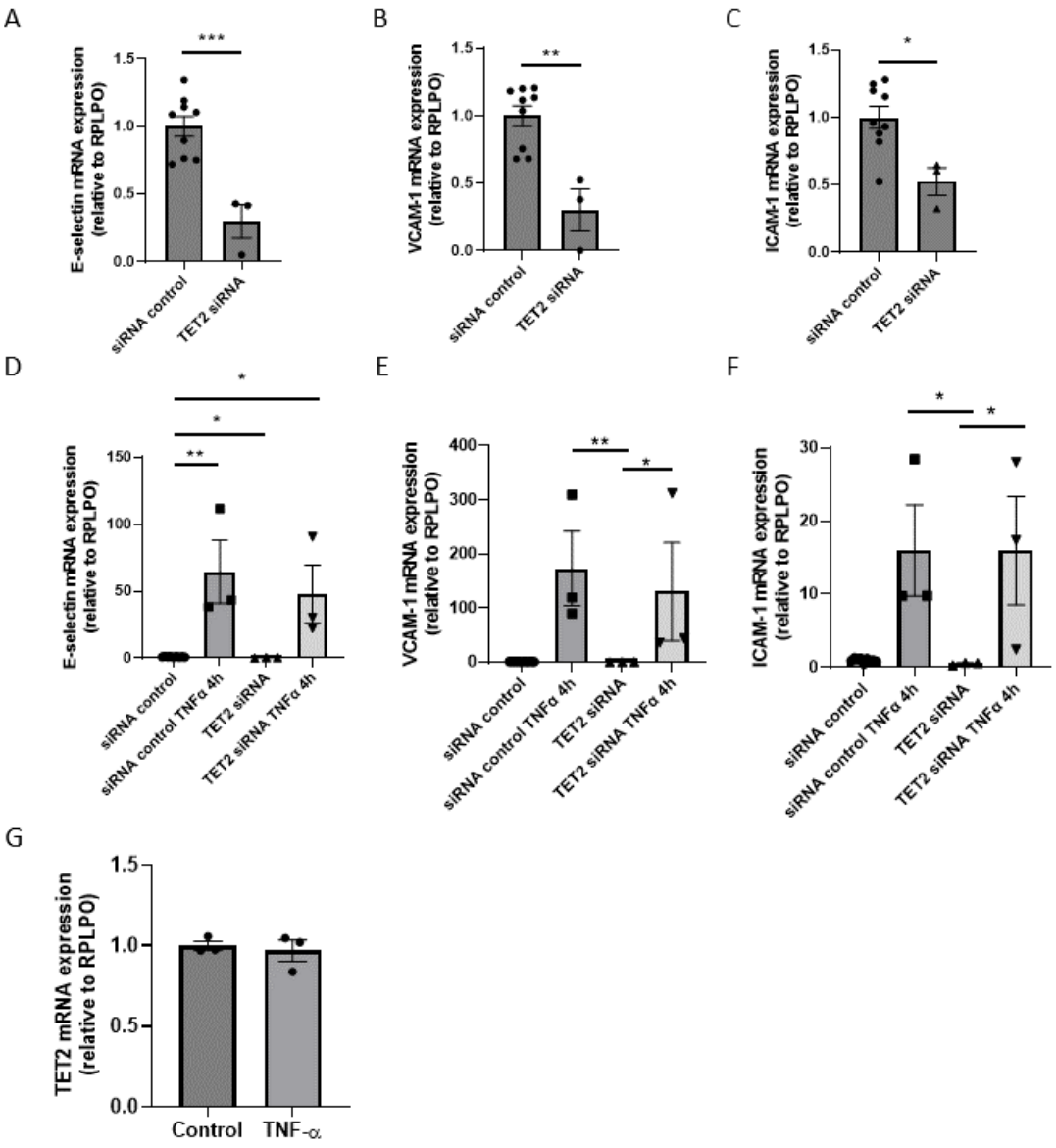

Figure 3.28: ***TET2 silencing decreases basal, but not TNFα-stimulated expression of adhesion molecules in HUVEC.*** *cDNA was prepared from HUVEC transfected with negative control siRNA or siRNA targeting TET2. qPCR was used to measure relative mRNA expression of E-selectin (A), VCAM-1 (B) and ICAM-1 (C), normalised to the housekeeping gene RPLPO. Expression of E-selectin (D), VCAM-1 (E) and ICAM-1 (F) were also measured in control or TET2 siRNA-treated HUVEC with or without 10ng/ml TNFα stimulation for 4 hours. (G) TET2 expression was measured in control HUVEC or HUVEC treated with 10ng/ml TNFα for 4 hours. A Shapiro-Wilk test for normality was performed, followed by an unpaired t-test (A-C, G) or one-way ANOVA and post-hoc Tukey's test (D-F). Data presented as mean ±SEM. n=3 independent experiments (A-F) or n=3 triplicate samples (G). * denotes p<0.05.*

3.2.18 TET2 silencing upregulates genes involved in the cholesterol biosynthesis pathway

The second most significant pathway identified by RNA sequencing to be dysregulated by TET2 silencing was the superpathway of cholesterol biosynthesis, which was predicted to be activated in the absence of TET2 (Figure 3.9). Cholesterol is a sterol produced by all nucleated animal cells [232]. It is a vital component of cell membranes accounting for approximately a quarter of plasma membrane lipids [233]. There, it regulates membrane fluidity and rigidity, as well as modulating cell signalling, cytoskeletal reorganisation and cell adhesion and migration [234]. This means that proper cholesterol homeostasis is vital for normal cell function.

Cholesterol biosynthesis occurs *via* a multi-step pathway involving many enzymes which catalyse the conversion of acetyl-coenzyme A to cholesterol. Figure 3.29 shows a summary of this process, listing some of the enzymes which catalyse intermediate reactions, with those significantly upregulated by TET2 silencing highlighted. It is clear that TET2 silencing affects the expression of genes encoding many of the enzymes that catalyse each step of the pathway (Figure 3.29). This indicates that TET2 may be involved in the regulation of cholesterol homeostasis in endothelial cells at many distinct levels. To confirm the RNA sequencing data, a panel of the differentially-expressed genes were validated by qPCR, with the addition of 3-hydroxy-3-methylglutaryl-CoA reductase (HMGCR) which is the rate-limiting step of the pathway (Figure 3.30). HMGCR, dehydrocholesterol reductase 7 (DHCR7) and 3-hydroxy-3-methylglutaryl-CoA synthase 1 (HMGCS1) were significantly upregulated by TET2 silencing, while squalene epoxidase (SQLE), lanosterol synthase (LSS) and methylsterol monooxygenase 1 (MSMO1) were not significantly changed, although a trend of upregulation was observed, consistent with the RNA sequencing data (Figure 3.30).

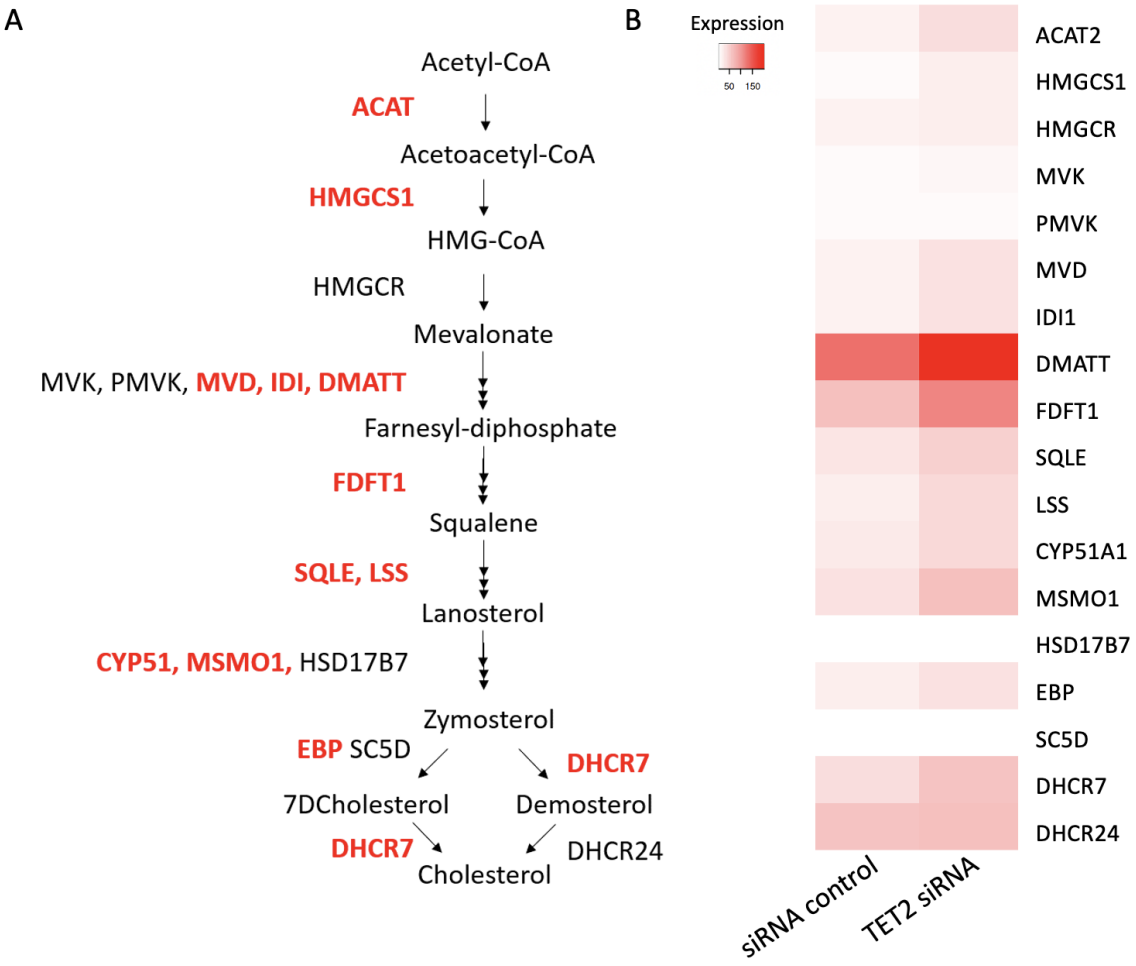

Figure 3.29: ***Schematic diagram of cholesterol biosynthesis pathway showing enzymes with differential gene expression following TET2 silencing in HUVEC.*** *RNA sequencing was performed on HUVEC treated with a negative control siRNA or siRNA targeting TET2. (A) Schematic diagram of the cholesterol biosynthesis pathway showing genes upregulated by TET2 silencing in red. (B) Heatmap showing expression level of genes in siRNA control and TET2 siRNA-treated HUVEC. Abbreviations: coenzyme A (CoA), HMG (3-hydroxy-3-methylglutaryl) ACAT (acetyl-CoA acetyltransferase), HMGCS1 (3-hydroxy-3-methylglutaryl-CoA synthase 1), HMGCR (3-hydroxy-3-methylglutaryl-CoA reductase), MVK (mevalonate kinase), PMVK (phosphomevalonate kinase), IDI (isopentenyl-diphosphate delta isomerase), DMATT (dimethylallyltranstransferase), FDFT1 (farnesyl-diphosphate farnesyltransferase 1), SQLE (squalene epoxidase), LSS (lanosterol synthase), CYP51 (Cytochrome P450 Family 51), MSMO1 (methylsterol monooxygenase 1), HSD17B7 (hydroxysteroid 17-beta dehydrogenase 7), EBP (emopamil binding protein), SC5D (sterol-C5-desaturase), DHCR (dehydrocholesterol reductase).*

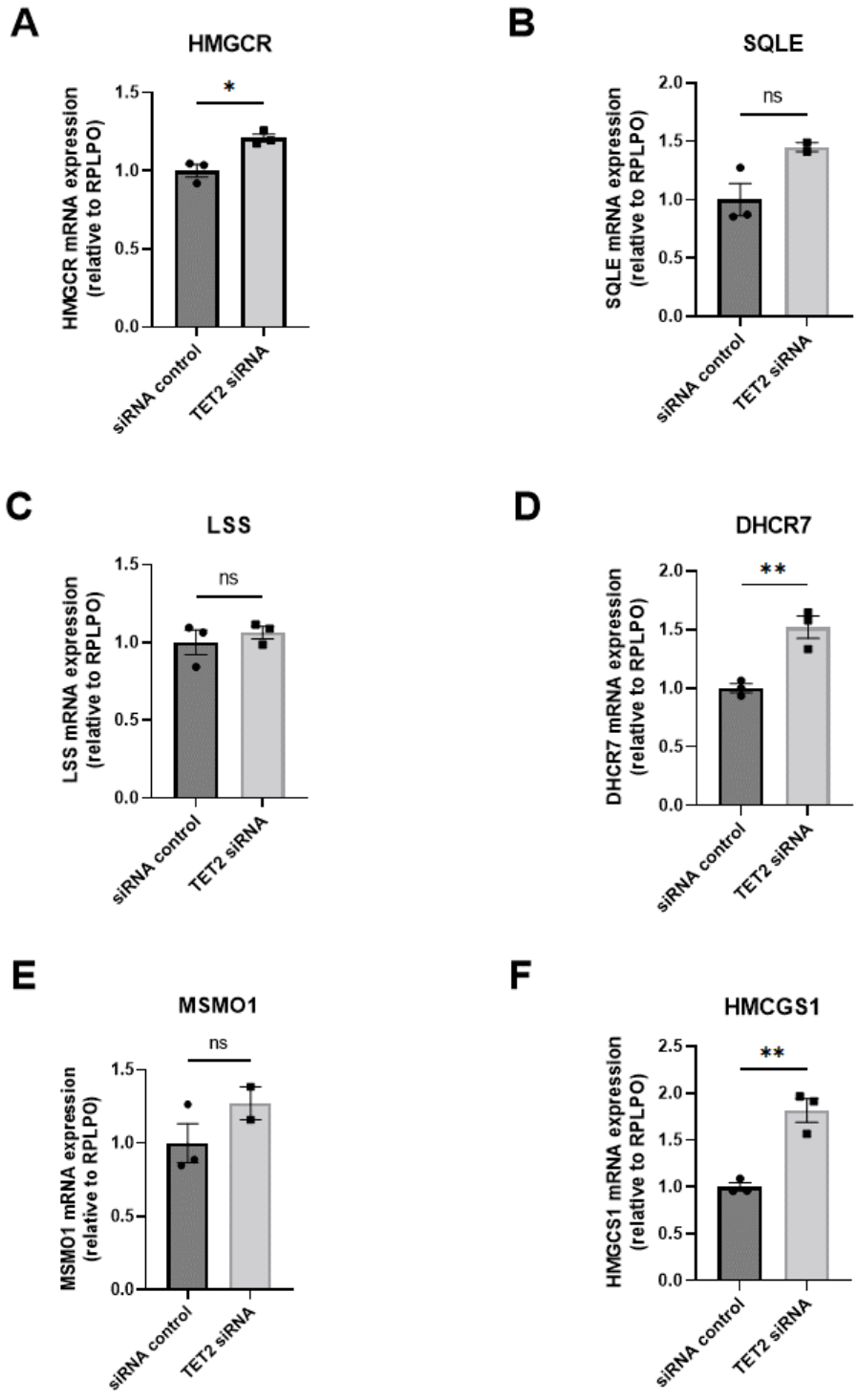

Figure 3.30: ***qPCR validation of differentially-expressed cholesterol biosynthesis pathway genes in TET2-silenced HUVEC.*** *HUVEC were transfected with negative control siRNA or siRNA targeting TET2. qPCR was performed to measure relative mRNA expression of cholesterol biosynthesis pathway genes 3-hydroxy-3-methylglutaryl-CoA reductase (HMGCR) (A), squalene epoxidase (SQLE) (B), lanosterol synthase (LSS) (C), dehydrocholesterol reductase 7 (DHCR7) (D), methylsterol monooxygenase 1 (MSMO1) (E) and 3-hydroxy-3-methylglutaryl-CoA synthase 1 (HMGCS1) (F), normalised to the housekeeping gene RPLPO. A Shapiro-Wilk test for normality was performed, followed by an unpaired t-test. Data presented as mean ±SEM. n=3 triplicate samples. * denotes p<0.05. ** denotes p<0.01.*

3.2.19 IFNγ induces CH25H expression and downregulates cholesterol biosynthesis genes

The transcriptional regulation of cholesterol biosynthesis genes is governed largely by the master transcription factor sterol regulatory element-binding protein 2 (SREBP-2) [235]. When cholesterol levels are high, SREBP-2 is sequestered in the endoplasmic reticulum by 25-hydroxycholesterol (25-HC), a sterol produced from cholesterol *via* the action of cholesterol 25-hydroxylase (CH25H) (Figure 3.31). When cholesterol levels decrease, 25-HC levels decrease which releases SREBP-2 to move to the Golgi for processing, followed by nuclear translocation (Figure 3.31) [236]. In the nucleus, SREBP-2 initiates transcription of cholesterol biosynthesis pathway genes, as well as genes influencing cholesterol import (Figure 3.31) [235]. Thus, 25-HC is a potent negative regulator of cholesterol biosynthesis. Intriguingly, CH25H, which catalyses the production of 25-HC, is itself reported in some cases to be an interferon-sensitive gene and 25-HC has been shown to have antiviral and immunomodulatory roles in myeloid cells [237-239]. As in the case of other interferon-sensitive genes (Figures 3.15 & 3.17), silencing of TET2 in HUVEC caused a significant upregulation of CH25H (Figure 3.32). It is therefore tempting to speculate that the regulation of both the cholesterol biosynthesis pathway and interferon signalling pathway by TET2 may be interlinked in endothelial (and perhaps other) cells.

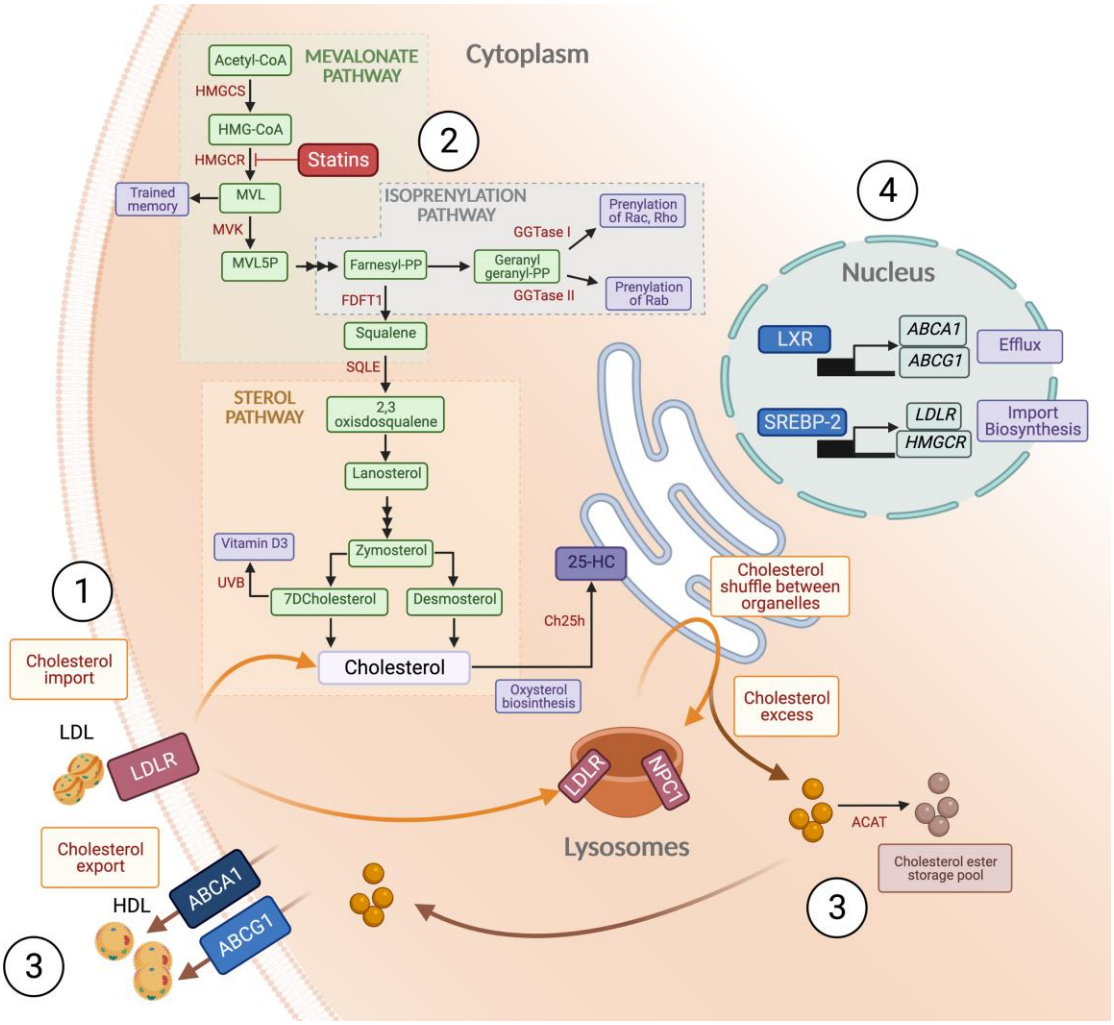

Figure 3.31: ***Schematic diagram of cellular cholesterol metabolism.*** *1) Cellular cholesterol is imported from LDL via LDLR. 2) Cholesterol biosynthesis is a multi-stage process. 3) Excess cholesterol can be esterified or exported via ABCA1 and ABCG1. 4) SREBP-2 and LXR transcription factors regulate the transcription of cholesterol biosynthesis genes and cholesterol transporters. Abbreviations: 25-hydroxycholesterol (25-HC), ATP-binding cassette transporter 1 (ABCA1), ATP-binding cassette subfamily G member 1 (ABCG1), acyl coenzyme A cholesterol acyltransferase (ACAT), cholesterol 25-hydroxylase (Ch25h), farnesyl diphosphate farnesyltransferase 1 (FDFT1), geranylgeranyl transferase (GGTase), 3-hydroxy-3-methylglutaryl-coenzyme A (HMG-CoA), 3-hydroxy-3-methylglutaryl-CoA synthase (HMGCS), 3-hydroxy-3-methylglutaryl-CoA reductase (HMGCR), low density lipoprotein (LDL), LDL receptor (LDLR), liver X receptor (LXR), mevalonate kinase (MVK), mevalonate (MVL), mevalonate-5-phosphate (MVL5P), Nieman-Pick C 1 (NPC1), squalene epoxidase (SQLE), sterol response element binding protein 2 (SREBP-2). Figure reproduced from [235].*

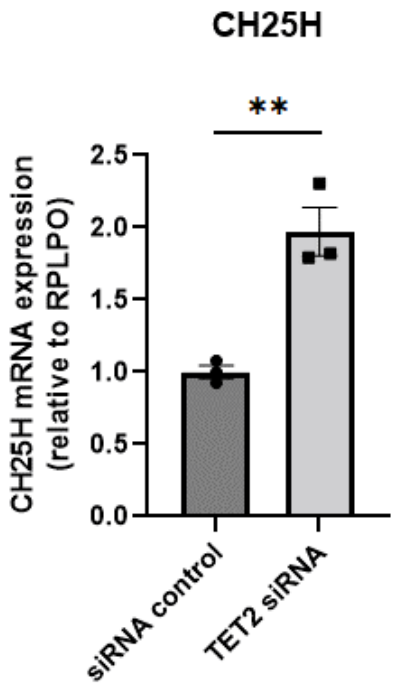

Figure 3.32: ***CH25H expression is increased in HUVEC upon TET2 silencing.*** *HUVEC were transfected with negative control siRNA or siRNA targeting TET2. qPCR was performed to measure relative mRNA expression of CH25H, normalised to the housekeeping gene RPLPO. A Shapiro-Wilk test for normality was performed, followed by an unpaired t-test. Data presented as mean ±SEM. n=3 triplicate samples. ** denotes p<0.01.*

To begin exploring this possibility, the expression of cholesterol biosynthesis genes DHCR7, HMGCS1 and HMGCR, as well as CH25H, were measured by qPCR in a timecourse of interferon activation. The expression of cholesterol biosynthesis genes decreased during IFNγ treatment, as might be expected if interferons negatively regulate cholesterol biosynthesis *via* CH25H (Figure 3.33A-C). This downregulation was not as apparent during IFNα treatment (Figure 3.33A-C). In agreement with suggestions that CH25H is an interferon-sensitive gene, CH25H expression increased with both IFNα and IFNγ treatment (Figure 3.33D). This occurred only very transiently for IFNα, peaking after 1 hour of treatment and returning to baseline, whereas CH25H expression increased up to 24 hours of treatment with IFNγ (Figure 3.33A-C), concomitant with the downregulation of cholesterol biosynthesis genes (Figure 3.33D). These data, although preliminary, confirm that CH25H is an interferon-sensitive gene in endothelial cells and demonstrates that the expression of cholesterol

biosynthesis genes decreases in response to IFNγ, supporting the link between interferon signalling and cholesterol biosynthesis in endothelial cells.

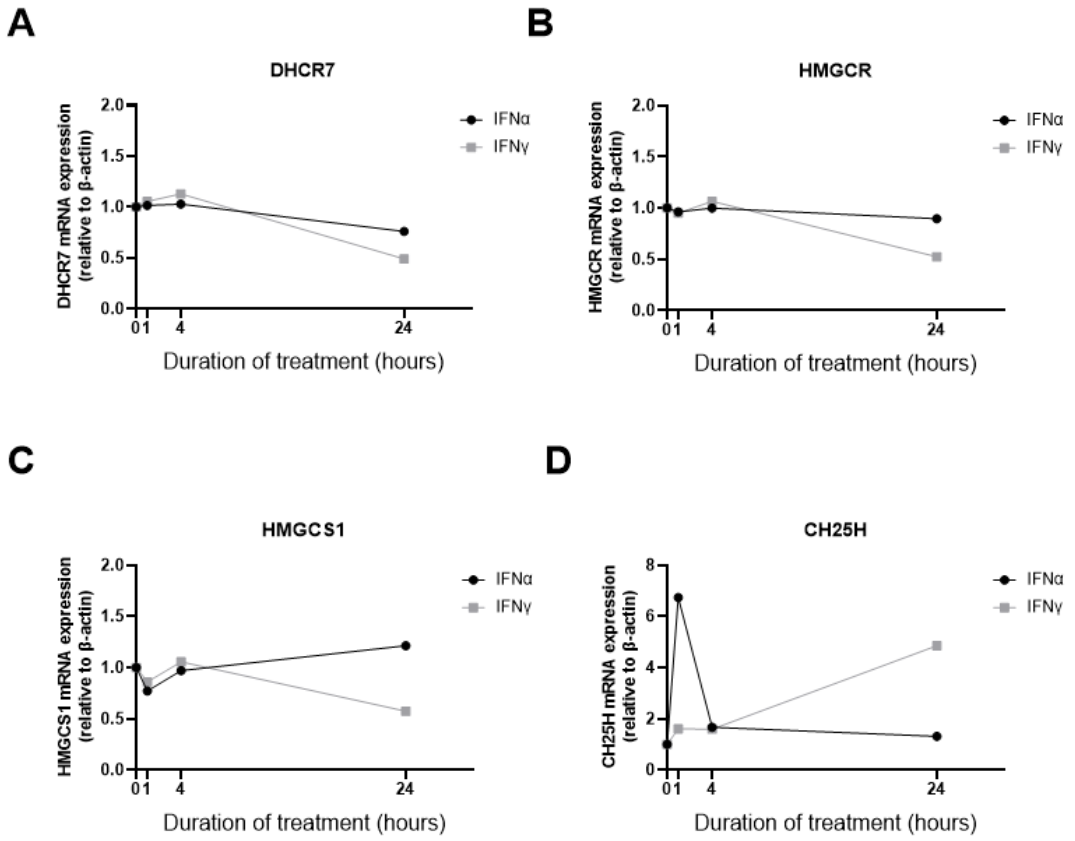

Figure 3.33: ***Expression of cholesterol biosynthesis genes in HUVEC in response to IFNα or IFNγ treatment.*** *HUVEC were transfected with negative control siRNA or siRNA targeting TET2 and treated for 0, 1, 4 or 24 hours with IFNα or IFNγ. qPCR was performed to measure relative mRNA expression of cholesterol biosynthesis pathway genes DHCR7 (A), HMGCR (B), HMGCS1 (C) and CH25H, normalised to the housekeeping gene β-actin. n=1.*

3.3 Discussion

3.3.1 Summary of findings

In this chapter, TET2 was identified as the most highly expressed TET enzyme in HUVEC, at least at the mRNA level. TET1, TET2 and TET3 were shown to regulate predominantly non-overlapping gene sets in HUVEC at the transcriptional level, with TET2 and TET3 showing a statistically significant association with biologically relevant pathways. However, little overlap was observed between genes dysregulated by TET silencing and genes dysregulated by high glucose culture. The cellular response to interferon appears to involve both TET2 and TET3 acting in opposing manners. The data presented here suggests that TET3 may be involved in the activation of type II interferon responses, whereas TET2 may play a role in the resolution of type I and type II interferon responses in endothelial cells. High glucose culture of HUVEC also dysregulated interferon responses. A divergence in TET2 and TET3 expression was observed 4 hours after stimulation with IFNα or IFNγ and again 4 hours after removal of the stimulus. This gives further support to the hypothesis that TET2 and TET3 are functionally important during the activation and resolution of interferon responses. Although TNFα-regulated cell adhesion molecule expression was decreased in TET2-silenced HUVEC at baseline, their expression was not significantly altered upon activation with TNFα compared to controls. RNA sequencing and qPCR validation also showed a significant upregulation of cholesterol biosynthesis genes in the absence of TET2. Preliminary data showed an increase in CH25H expression in response to interferon stimulation or TET2 silencing and downregulation of cholesterol biosynthesis genes in response to IFNγ, demonstrating an interplay between these two pathways.

3.3.2 Relative importance of TET1, TET2 and TET3 to endothelial cell function

Although these data show TET2 to be the most abundant TET at the mRNA level, it is important to note that mRNA transcript levels do not always correlate with protein

levels. All three TETs are known to be subject to regulation by microRNAs, which can degrade or prevent translation of mRNA transcripts [240-242]. Furthermore, post-translational modifications of TET proteins can affect their stability. For example, AMPK-mediated phosphorylation of TET2 has been demonstrated to increase its stability [183]. Although silencing of each of the three TETs altered the transcriptomic profile of HUVEC, TET2 and TET3 were associated with significantly greater changes in activation or inhibition of biological pathways compared to TET1, indicating that they are functionally more relevant in endothelial cells. For this study, HUVEC were chosen since they are tractable primary cells commonly used in the field to represent endothelial cells of the macrovasculature. This is a limitation, however, as methylation profiles are known to vary significantly between macro- and microvascular endothelial cells [138], raising the possibility that the action of DNA methylation regulators, including TETs, may differ depending on the source and type of endothelial cells studied.

3.3.3 The relationship of TET2/3 with immunity and inflammation

Existing evidence for a role for TET2 in endothelial inflammatory responses comes from the finding that TET2 overexpression lessened atherosclerotic lesion severity and decreased expression of cell adhesion molecules and pro-inflammatory cytokines and chemokines, both within the plaques of ApoE-/- mice and in HUVEC treated with oxidised LDL (and vice versa for shRNA-mediated silencing of TET2) [164]. ICAM-1 and VCAM-1 are endothelial-expressed cell adhesion molecules which promote leukocyte adhesion to the endothelium [18]. When TET2 was silenced in oxidised LDL-treated HUVEC, increased ICAM-1 and VCAM-1 expression and increased monocyte binding in a static adhesion assay were observed [165]. However, this finding does not seem to extend to TNFα-induced inflammatory responses in HUVEC, as increased ICAM-1 or VCAM-1 expression upon TET2 silencing in TNFα-treated HUVEC were not observed in the present study (Figure 3.28). This indicates that the repressive action of TET2 may depend on the inflammatory stimulus, even though both stimuli upregulate ICAM-1 and VCAM-1 *via* NFκB signalling [165, 243]. Unlike the reported effect of oxidised LDL,

TNFα stimulation did not affect TET2 expression (Figure 3.28G), which may account for these differences [165]. However, a decrease was seen in ICAM-1, VCAM-1 and E-selectin expression in the absence of TET2 at baseline in HUVEC, which supports the involvement of TET2 in the regulation of their transcription (Figure 3.28).

An interesting and novel finding from this work is the involvement of TET2 and TET3 in regulating interferon responses in endothelial cells. Type I and type II interferons are primarily known for their role in responding to viral infection. Many of the interferon-sensitive genes identified to be differentially-expressed upon TET silencing have functions associated with prevention of viral entry to the cell or inhibiting viral replication [220]. IFITM1 and ISG15 were used as markers of the interferon response in this study since they are both strongly induced by type I and type II interferon stimulation and have known roles in endothelial cell function or dysfunction [244, 245].

The finding that TET2 may be involved in the resolution of type I and II interferon responses is consistent with the growing number of publications suggesting that TET2 acts to repress pro-inflammatory mediators, thereby participating in the resolution of inflammatory responses or suppressing gene expression to prevent baseline activation of these pathways [158, 159, 162]. TET3 has previously been reported to be a negative regulator of type I interferon responses (specifically IFNβ) in peritoneal macrophages [203]. Although a role for TET3 in type I interferon responses (IFNα) in HUVEC was not found (Figure 3.25), a significant decrease in interferon-sensitive gene expression was observed in TET3-silenced HUVEC in response to IFNγ, compared to controls, suggesting that TET3 may be a positive regulator of type II interferon responses in endothelial cells (Figure 3.26). Interestingly, a decrease in TET3 expression was observed 4 hours after addition of IFNα or IFNγ, which may limit the effect of TET3-mediated upregulation of interferon-sensitive genes. A similar decrease in TET3 expression has been observed in murine bone marrow-derived macrophages

stimulated with poly(I:C) to induce type I interferon production [203]. However, the mechanism underlying this is unknown.

Beyond antiviral functions, diverse roles for both type I and type II interferon responses in homeostasis and disease are increasingly appreciated. *In vitro* findings suggest that type I interferon inhibits endothelial cell proliferation, abrogates VEGF-induced angiogenesis, decreases fibrinolytic activity and reduces production of nitric oxide [221]. Treatment of endothelial cells with IFNγ *in vitro* has been shown to increase permeability through actin cytoskeletal reorganisation [38], inhibit VEGF-mediated growth and tube-formation [222], increase adhesion molecule expression and alter glucose metabolism [246]. This is relevant not only in viral infection, but also in sterile injury such as atherosclerosis, where IFNγ is produced by CD4+ and CD8+ T lymphocytes [246]. Together, this gives a strong rationale for further exploring the finding that transcriptional responses of endothelial cells to type I or type II interferon involve regulation by TET2 and TET3, as this may lead to alterations in endothelial functions relevant to vascular disease.

3.3.4 Effect of high glucose culture on the HUVEC transcriptome

Surprisingly, in this study, 48h stable high glucose culture of HUVEC did not lead to many of the expected transcriptional changes (typically associated with inflammatory responses) described in previous literature [10, 67, 96]. However, mitochondrial damage and oxidative phosphorylation were identified as pathways containing differentially-expressed genes in high glucose-cultured HUVEC compared to HUVEC cultured in normal media (Figure 3.11). This is in agreement with existing reports that high glucose culture influences the aerobic metabolism of endothelial EA.hy926 cells and induces mitochondrial damage in bovine retinal endothelial cells [134, 247]. In the latter case, this was associated with altered DNA methylation of mitochondrial DNA polymerase [134]. However, the genes dysregulated by high glucose did not overlap with genes dysregulated by TET silencing to a large extent (Table 3.1) challenging the

hypothesis that dysregulation of TETs by hyperglycaemia alters endothelial gene expression. Although high glucose culture decreased TET1 mRNA expression (Figure 3.3), TET1 may not be as functionally important in endothelial cells as TET2 or TET3 (Figure 3.9), so this may not be expected to cause extensive transcriptional changes.

It was hypothesised that TET activity may be altered by hyperglycaemia. Using a dot blot to measure 5hmC levels in high glucose-cultured HUVEC as a surrogate marker of TET activity, no changes were observed after 24-48h stable high glucose culture. This contrasted with previous findings by Wu *et al.* showing that high glucose decreased 5hmC levels in HUVEC [183]. However, as the duration of exposure to high glucose concentrations was not reported in their study, it is possible that a longer duration of high glucose culture may be required to replicate the observed change in 5hmC levels. Alternatively, the dot blot method may not be sufficiently sensitive to detect subtle changes if the 5hmC abundance of HUVEC is low. This is likely, as 5hmC abundance has previously been shown to decrease with increasing passage number [248]. Using the more sensitive technique of hMeDIPseq, it was observed that 5hmC enrichment was generally decreased across gene bodies and the surrounding genomic regions of HUVEC treated with high glucose for 2 weeks compared to mannitol-treated controls (Figure 3.5), in agreement with Wu *et al*. [183]. HUVEC displayed both hyper- and hypo-hydroxymethylated promoter regions (Figure 3.5). This supports the idea that TET activity is altered by hyperglycaemia, although its relationship appears complex. Given that TET enzymes catalyse not only the reaction which yields 5hmC (*i.e.* oxidation of 5mC), but also the reaction that removes it (i.e. oxidation of 5hmC to 5fC and further to 5caC), this complex relationship is perhaps unsurprising.

Many studies have shown that intermittent exposure to high glucose concentrations causes more damage to endothelial cells than stable high glucose [224-229]. Acute fluctuations in blood glucose concentrations between post-prandial and inter-prandial states have also been associated with increased oxidative stress in diabetic patients compared to sustained hyperglycaemia [249] and glycaemic variability is inversely

correlated with endothelial function [250]. For these reasons, later studies involved a 2-week intermittent high glucose culture, changing media from 5mM glucose to 25mM glucose every 24h. Using this model, evidence was found to suggest that IFNγ responses in HUVEC are dysregulated by intermittent high glucose concentrations (Figure 3.27), in a somewhat similar manner to that observed upon silencing TET2 in HUVEC where IFITM1 and ISG15 mRNA expression increased to a greater extent than controls and remained higher following removal of IFNγ (Figure 3.24). Previous literature has shown an involvement of IFNγ or JAK-STAT signalling in endothelial dysfunction and the vascular complications of diabetes [251-254]. Whether or not the perturbations of endothelial interferon signalling in high glucose involve dysregulation of TET2 remains to be explored further.

3.3.5 Cholesterol homeostasis in endothelial cells and its relationship with interferon signalling

Cholesterol is a vital component of cell membranes and its association with cardiovascular disease is well known. The detrimental effect of perturbed cholesterol homeostasis is exemplified by the formation of foam cells in atherosclerosis, resulting from the uncontrolled intracellular accumulation of cholesterol, primarily by macrophages, but also vascular smooth muscle cells [255]. The regulation of cholesterol metabolism in endothelial cells in health and disease has not been extensively studied. In this chapter, it was identified that TET2-silenced HUVEC had elevated expression of multiple genes involved in the cholesterol biosynthesis pathway compared to controls (Figures 3.29 & 3.30). This appears to be the first evidence to suggest a role for an epigenetic regulator in regulating cholesterol synthesis in endothelial cells. Indeed, reports of epigenetic regulation of cholesterol synthesis in *any* cell type is largely limited to observation of altered expression of cholesterol biosynthesis pathway genes in cell lines by pharmacological inhibitors of histone deacetylases (trichostatin A or sodium butyrate) or DNA methylation (5-aza-2'-deoxycytidine) [256-258]. A role for TET2 in the regulation of cholesterol homeostasis has not been described previously.

Recently, the control of cholesterol metabolism has been positioned as a player in the induction and resolution of inflammatory responses in innate and adaptive immune cells [235]. This link is centred around the induction of 25-HC by type I interferon activation in response to pathogen sensing [235]. 25-HC is an oxysterol generated from cholesterol, which acts as part of a negative feedback loop, potently repressing cholesterol biosynthesis by sequestration of SREBP-2 in the endoplasmic reticulum [235]. More recently, 25-HC has been shown to have antiviral functions, blocking viral entry and replication in innate immune cells and regulating inflammasome activation [237-239, 259]. It is thought that downregulation of cholesterol synthesis functions to protect against pathogens utilising host cell cholesterol reserves for their own replication [235]. Upon pathogen sensing, the enzyme responsible for synthesis of 25-HC, CH25H, is induced by type I interferon *via* STAT1 in mouse bone marrow-derived macrophages [237]. However, there is some controversy in the literature regarding whether CH25H is an interferon-sensitive gene in humans [239, 260]. The data presented here suggest that CH25H is indeed an interferon-sensitive gene in HUVEC (Figure 3.33). Its regulation by type I and type II interferons appears highly dynamic and time-dependent, which may explain the discrepancy with previous reports. Consistent with interferon-mediated downregulation of cholesterol biosynthesis genes *via* 25-HC, upregulation of CH25H was observed, concomitant with downregulation of cholesterol biosynthesis genes in HUVEC, although this was apparent upon type II, rather than type I interferon stimulation (Figure 3.33). Intriguingly, TET2 appears to regulate the expression of CH25H in HUVEC (Figure 3.32), suggesting possible involvement of this epigenetic modifier linking interferon signalling and cholesterol biosynthesis in endothelial cells.

3.3.6 Methodological limitations

While investigating how the transcriptional regulation of HUVEC was altered by silencing TETs, it was noted that the transfection process itself, involving the addition of a negative control siRNA complexed with lipofectamine under temporary serum-

starved conditions, upregulated interferon-sensitive genes compared to non-transfected HUVEC (Figure 3.12). This may explain why the changes in expression of interferon-sensitive genes were less marked in negative control siRNA-treated HUVEC, compared to those observed in non-transfected HUVEC following stimulation with interferon. Thus the interferon-responsive pathway(s) may already be activated at baseline in transfected cells, diminishing the effects observed upon IFN addition (Figures 3.19, 3.2, 3.25 & 3.26).

It is perhaps unsurprising that siRNA transfection activated the interferon response, given that the response exists as an antiviral mechanism, of which sensing double stranded RNA is a core component [261]. Thus, when the double stranded siRNA is sensed by a cell, it is likely to stimulate production of interferon-sensitive genes *via* retinoic acid-inducible gene I (RIG-I)/melanoma differentiation-associated protein 5 (MAD5), protein kinase R (PKR) and toll-like receptor (TLR)-dependent pathways [261, 262]. This is an important consideration because, for the reasons discussed above, the HUVEC used as negative controls are likely to exhibit altered phenotypes as a result of interferon pathway stimulation so do not accurately reflect the quiescent state. Given that the concentration of siRNA required to silence TET2 and TET3 in HUVEC differed (20nM and 100nM, respectively), the concentration of negative control siRNA used to transfect control HUVEC for RNA sequencing was chosen to match that of the TET3-targeting siRNA (100nM). This has the limitation that it is not the ideal control for TET2-silenced HUVEC. However, if the activation of interferon response pathways is dependent on the concentration of siRNA, then those treated with a higher concentration of negative control siRNA would be anticipated to have an even greater degree of interferon pathway activation than at lower concentrations. The finding that TET2 silencing *upregulated* interferon-sensitive genes above that of the 100nM siRNA control is therefore even more striking, as differences are likely to be underestimated. In subsequent experiments including qPCR validation of RNA sequencing results, the appropriate respective concentrations of siRNA controls for TET2- and TET3-silenced HUVEC were used.

Unfortunately, transfection was accompanied by morphological changes including increased cell size and an increase in the proportion of cells with two nuclei compared to non-transfected cells (Figure 3.13). This could imply an impairment of cell cycle progression, perhaps due to the serum starvation during the transfection procedure. Although optimisation of transfection conditions was attempted to limit this effect, shortening the duration of serum starvation caused unsuccessful gene silencing. Given how extensively siRNA/lipofectamine-mediated silencing is used for *in vitro* studies, it is surprising how few publications discuss phenotypic changes resulting from its use. A recent publication has reported that lipofectamine 2000/negative control siRNA complexes induce autophagy and the endoplasmic reticulum unfolded protein response in HUVEC, indicating that transfection does indeed alter cellular functions and initiate a stress response [263]. In addition, the introduction of the cationic lipid lipofectamine has been shown to alter lipid metabolism in HepG2 cells, which is an important consideration with respect to changes in cholesterol biosynthesis pathway genes in this study [264]. Nonetheless, there is confidence in the validity of comparisons between HUVEC treated with siRNA targeting a gene of interest and HUVEC treated with negative control siRNA, as both are exposed to the same transfection conditions. In future studies, the use of other methods of gene silencing could be employed to validate and explore these findings further.

In summary, the data presented in this chapter support a role for TET2 and TET3 in regulating endothelial cell transcriptional responses to interferon. TET2 may also regulate cholesterol homeostasis in endothelial cells, a process that is interlinked with interferon signalling and inflammation. These may be relevant for endothelial cell homeostasis and protect against endothelial dysfunction in vascular diseases such as atherosclerosis.

4. Results 2: Investigating the mechanisms underlying TET-mediated transcriptional regulation and the functional impact of TET silencing in endothelial cells *in vitro.*

4.1 Introduction

In the previous chapter, a potential role for TET2 and TET3 in transcriptionally regulating interferon responses in endothelial cells was described. In addition, silencing of TET2 was shown to upregulate cholesterol biosynthesis genes and CH25H, the transcription of which were also affected by interferon stimulation. Although TET enzymes are well known for their catalytic function as methylcytosine dioxygenases, previous literature indicates that transcriptional regulation by TETs is also mediated through non-catalytic mechanisms, in some cases involving the recruitment of other epigenetic modifiers [158, 265]. Therefore, in this chapter, the possible involvement of catalytic and non-catalytic activities of TET enzymes in regulating the transcription of genes involved in interferon signalling and cholesterol homeostasis is explored. Interferon signalling has been suggested to play a role in many endothelial functions, including proliferation, angiogenesis, fibrinolytic activity and nitric oxide production [221]. Likewise, many cell functions could be compromised by aberrant cholesterol handling, as it is a vital component of cell membranes which participates in cell signalling as well as structural integrity [234]. Beyond protecting endothelial cells from oxidised LDL-induced dysfunction [165], the role of TET2 in endothelial cells remains largely unexplored. This chapter explores whether the altered endothelial transcriptome resulting from TET2 silencing is associated with impairment of endothelial functions such as the regulation of leukocyte adhesion and permeability. These functions have previously been shown to be dysregulated by hyperglycaemia [72, 266-268], so it stands to reason that if TET2 activity is dysregulated by hyperglycaemia, these functions could potentially be similarly perturbed by TET2 silencing or high glucose culture of HUVEC.

4.1.1 Aim

The aim of this chapter is firstly to gain an understanding of the possible mechanisms underlying TET-mediated transcriptional regulation of interferon signalling and cholesterol homeostasis in endothelial cells. Secondly, considering the findings of the previous chapter as well as existing literature, *in vitro* functional assays are used to assess whether endothelial proliferation, permeability, cytokine release or leukocyte adhesion are compromised by siRNA-mediated silencing of TET2 in HUVEC in a similar manner to that observed upon high glucose culture of HUVEC.

4.2 Results

4.2.1 Interferon-sensitive genes may be subject to regulation by DNA methylation

Both catalytic and non-catalytic roles for TET2 and TET3 have been previously described [158, 161, 193]. To investigate the potential involvement of a catalytic role for TETs in regulating the transcription of interferon-sensitive genes, DNA methylation was pharmacologically inhibited in HUVEC using 5-aza-2'-deoxycytidine (5azaC). 5azaC is a non-selective DNMT inhibitor that is routinely used *in vitro* to investigate whether the transcriptional regulation of a gene involves DNA methylation [133, 269]. It is expected that if a gene is subject to regulation by DNA methylation, then treatment with 5azaC will lead to its demethylation and transcriptional activation. Using this approach, the mRNA levels of MX1, RSAD2, IFITM1 and ISG15 were found to be upregulated (3-4 fold) in 5azaC-treated HUVEC compared to controls (Figure 4.1), indicating that DNA methylation may indeed be involved in their regulation.

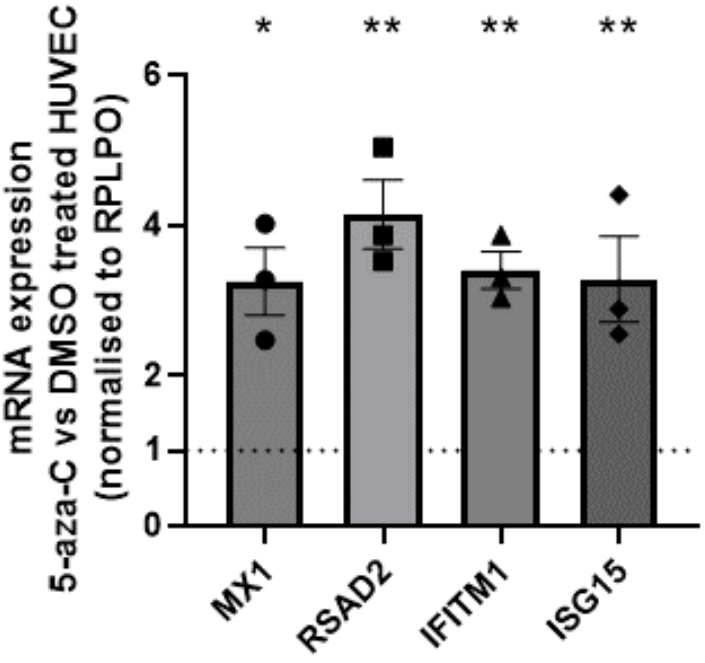

Figure 4.1: ***Interferon-sensitive genes MX1, RSAD2, IFITM1 and ISG15 are upregulated by inhibition of DNA methylation.*** *cDNA was prepared from HUVEC treated for 3 days with 5μM 5-aza-2'-deoxycytidine (5azaC) or 0.1% DMSO as a vehicle control. qPCR was used to measure relative mRNA expression of MX1, RSAD2, IFITM1 and ISG15, normalised to the housekeeping gene RPLPO, in 5azaC-treated vs DMSO-treated samples (denoted by the dotted line at y=1). Data presented as mean ± SEM. n=3 triplicate samples. Shapiro-Wilk tests were performed, followed by unpaired t-tests comparing DMSO- and 5azaC-treated samples for each gene. * denotes p<0.05, ** denotes p<0.01.*

4.2.2 Hydroxymethylation patterns of HUVEC are affected by interferon treatment

Given that TET2 and TET3 expression changed following interferon stimulation (Figures 3.19 & 3.2) and that interferon-sensitive gene expression is altered by TET2/3 silencing (Figures 3.17 & 3.18) and by inhibition of DNMTs (Figure 4.1), it was questioned whether treatment of HUVEC with interferon would measurably change global levels of 5hmC, a surrogate measure of TET activity. Using dot blotting to measure 5hmC levels relative to total DNA content (assessed by methylene blue staining), no change was identified following 24h IFNα or IFNγ treatment (Figure 4.2). Perhaps instead, locus-specific changes in 5hmC levels or a non-catalytic activity of TETs may be involved in interferon responses.

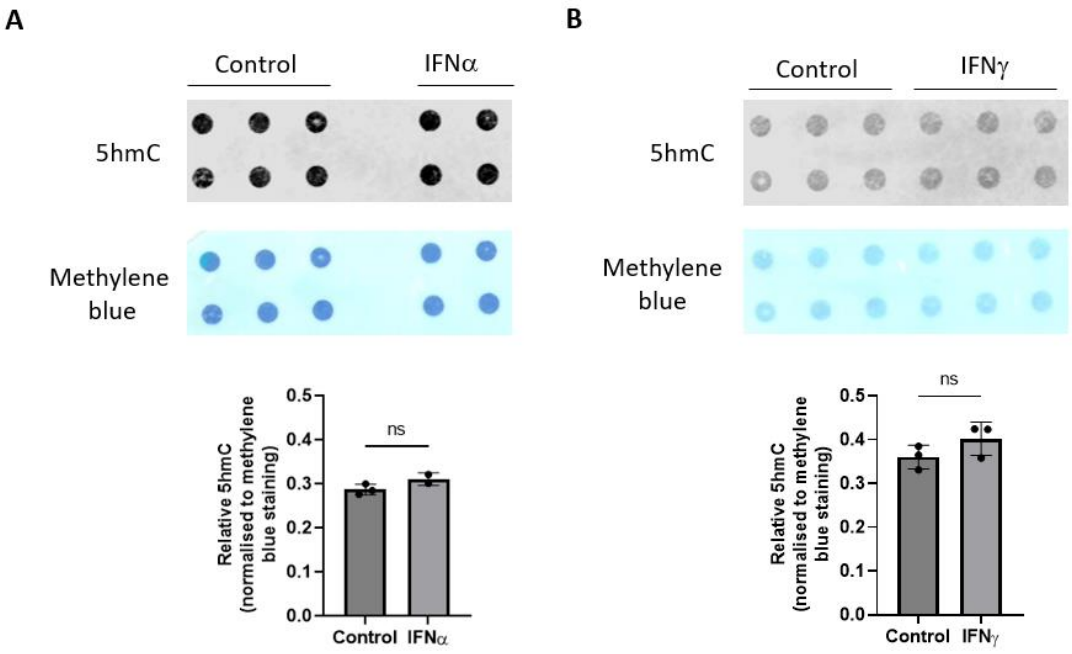

Figure 4.2: ***Interferon stimulation for 24h does not alter global 5hmC levels of HUVEC.*** *Genomic DNA was extracted from HUVEC cultured in basal media (Control) or treated for 24h with IFNα (A) or IFNγ (B). For each sample, 1μg DNA was applied to a nylon membrane by dot blotting and 5hmC signal was detected using an anti-5hmC antibody. 5hmC signal was analysed by densitometry and normalised to total DNA content assessed by methylene blue staining. A Shapiro-Wilk test for normality was performed, followed by an unpaired t-test.*

To investigate changes in 5hmC deposition across the genome upon interferon treatment, hMeDIPseq was performed (Figure 4.3). The majority of 5hmC peaks were within intergenic regions, with IFNγ-treated HUVEC displaying a slightly higher proportion of hydroxymethylation within gene bodies and promoter regions than control HUVEC (Figure 4.3A & B). Analysis of 5hmC profiles also showed that IFNγ-treated HUVEC have higher levels of 5hmC than control HUVEC within gene bodies and the flanking 3Kb upstream and downstream regions, with similarities in their pattern of deposition (Figure 4.3C). Full lists of differentially hydroxymethylated regions can be accessed *via* the GEO database (GSE232280).

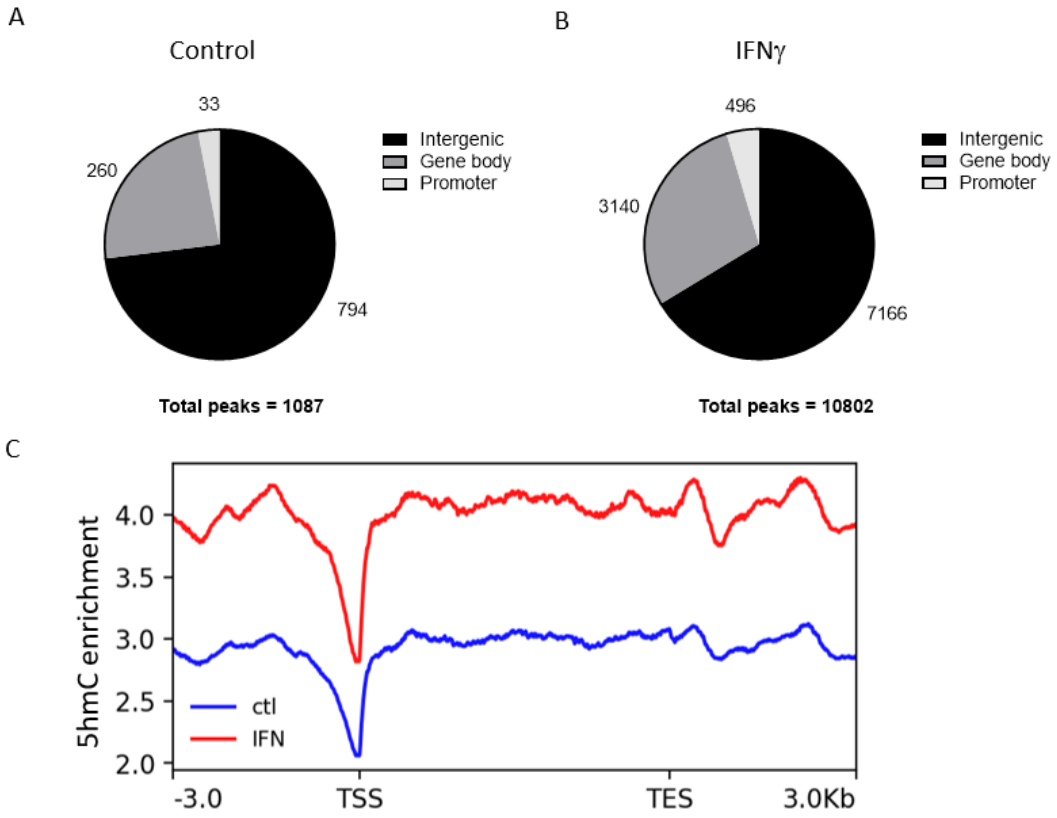

Figure 4.3: ***Differential hydroxymethylation is apparent in IFNγ-treated HUVEC compared to controls.*** *Genomic DNA was prepared from untreated HUVEC and HUVEC treated for 24h with 10ng/ml IFNγ. Hydroxymethylated DNA immunoprecipitation was performed and resulting DNA fragments were sequenced. A) The proportion of 5-hydroxymethylcytosine (5hmC) enrichment peaks in control HUVEC (against input) present in intergenic, gene body and promoter regions. B) The proportion of 5hmC enrichment peaks in IFNγ-treated HUVEC (against input) present in intergenic, gene body and promoter regions. C) 5hmC enrichment across gene bodies (between transcriptional start site TSS and transcriptional end site TES) and 3Kb upstream and downstream for all genes in the human genome assembly hg19, normalised to account for gene length in IFNγ-treated HUVEC (IFN) compared to untreated controls (ctl).*

Using the raw 5hmC signal from this hMeDIPseq experiment, the enrichment of 5hmC across the MX1, RSAD2, IFITM1 and ISG15 genes was compared in control and IFNγ-treated HUVEC, to give an indication of whether their upregulation may involve TET-mediated demethylation (Figure 4.4). Some subtle differences in 5hmC enrichment can be observed, primarily within introns (Figure 4.4).

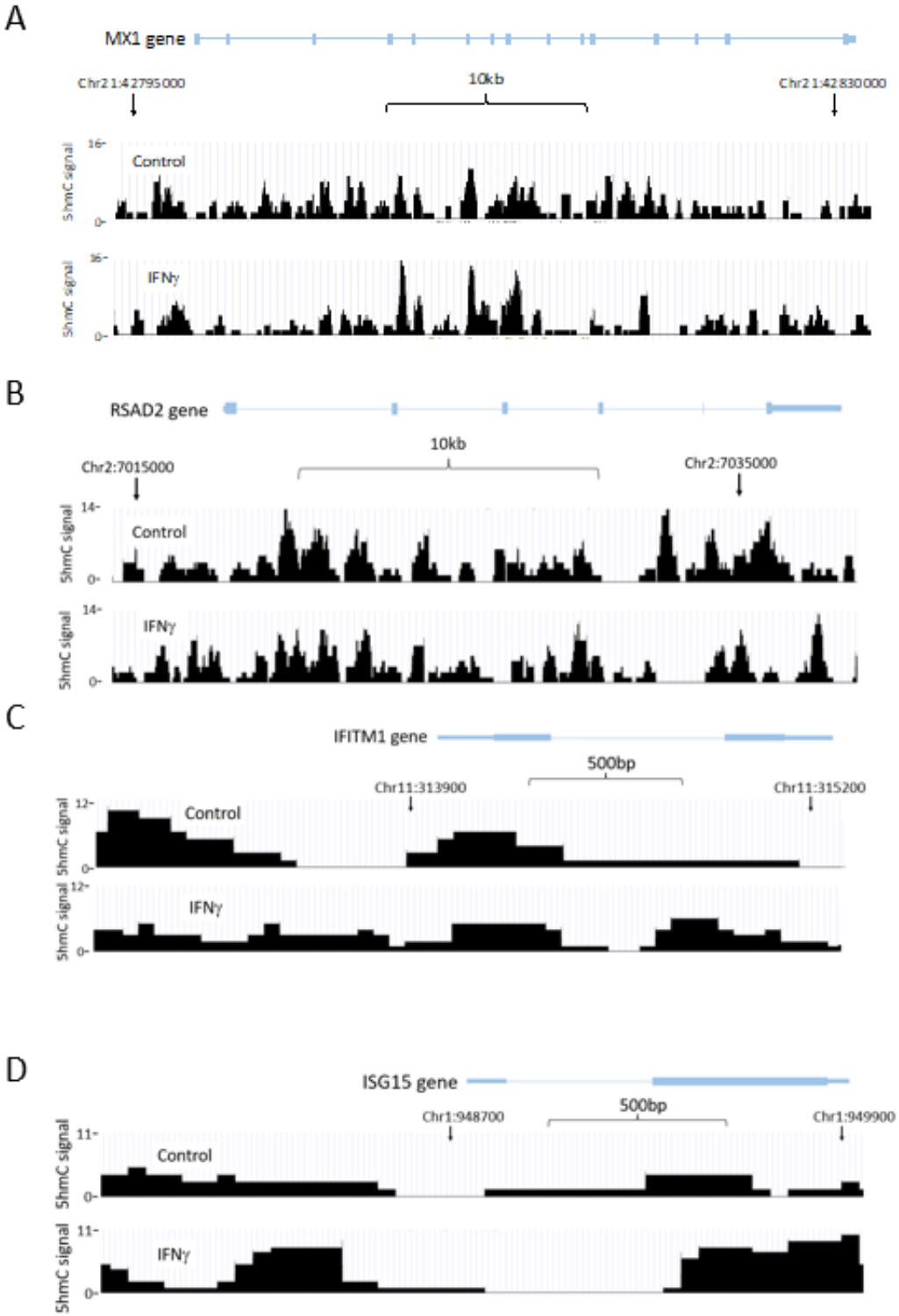

Figure 4.4: ***Raw signal of 5hmC enrichment at the MX1, RSAD2, IFITM1 and ISG15 gene loci in control and IFNγ-treated HUVEC.*** *Genomic DNA was prepared from untreated HUVEC and HUVEC treated for 24h with 10ng/ml IFNγ. Hydroxymethylated DNA immunoprecipitation was performed and resulting DNA fragments were sequenced. The raw signal profiles were visualised using the UCSC genome browser to assess 5hmC enrichment across the MX1 (A), RSAD2 (B), IFITM1 (C) and ISG15 (D) gene loci.*

4.2.3 STAT1, STAT2 and IRF7 are potential upstream regulators of interferon-sensitive genes differentially-expressed upon TET2/3-silencing in HUVEC.

Although it is possible that each individual interferon-sensitive gene may be subject to direct binding of, and demethylation by, TET2 or TET3, it is also plausible that TET2 or TET3 instead influence the expression of a transcriptional regulator common to all the interferon-sensitive genes, which in turn leads to the changes in their expression. To identify potential transcriptional regulators, the RNA sequencing datasets of TET2- and TET3-silenced HUVEC compared to controls were input into Ingenuity Pathway Analysis software. Using the Upstream Regulator analysis, known regulators of genes within the dataset were assessed according to the number of target genes present in the dataset and their predicted direction of change given the activation state (upregulated or downregulated by TET2/TET3 silencing compared to controls) of the regulator. From this analysis, STAT1 was identified as a potential upstream regulator of genes differentially-expressed upon TET2 silencing, accounting for 14 of the genes in the dataset (Figure 4.5). STAT2 and IRF7 were identified as potential upstream regulators of genes differentially-expressed by both TET2- and TET3-silencing (Figures 4.6 & 4.7). However, STAT2 accounted for only 8 genes differentially-expressed upon TET2 silencing and 4 genes differentially-expressed upon TET3 silencing (Figure 4.6).

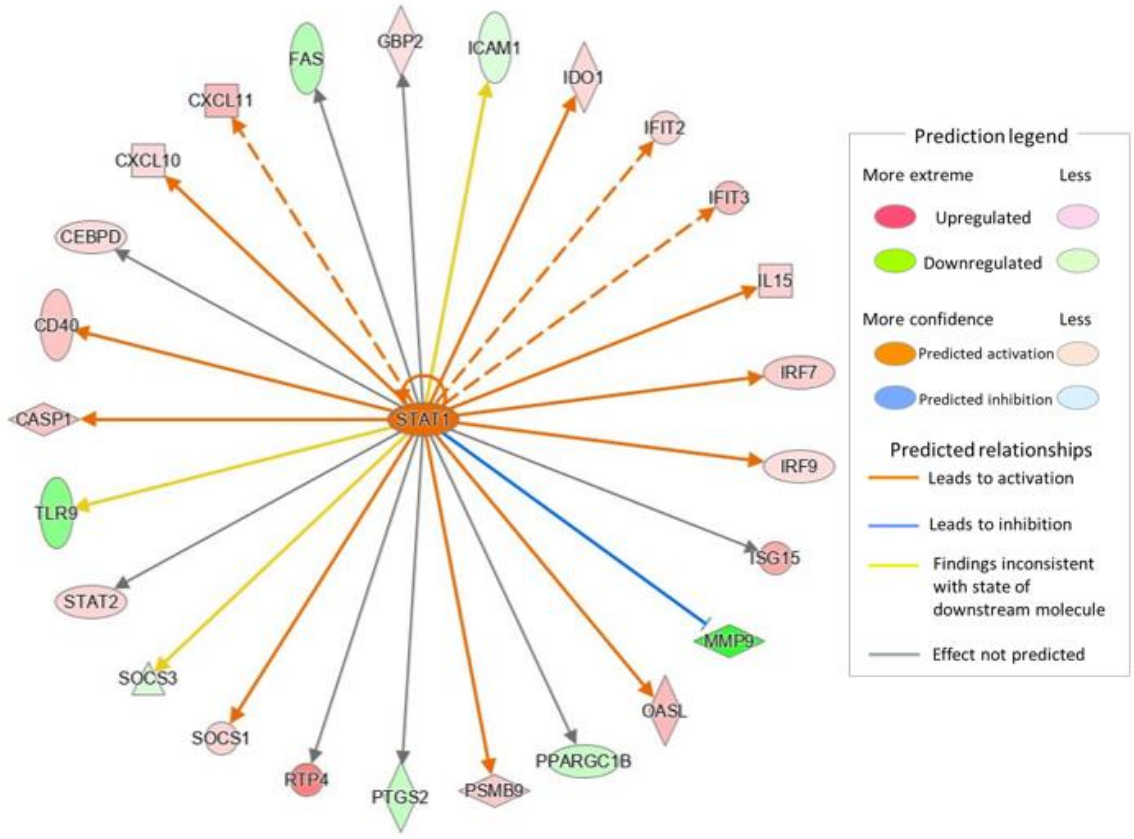

Figure 4.5: ***Ingenuity Pathway Analysis identifies STAT1 as an upstream regulator of genes differentially-expressed by TET2 silencing in HUVEC.*** *Schematic diagram of genes in the dataset regulated by STAT1. STAT1 is upregulated in TET2-silenced vs siRNA control cells. RNA sequencing was performed on HUVEC treated with a negative control siRNA or siRNA targeting TET2. Ingenuity Pathway Analysis software was used to predict upstream regulators of differentially-expressed genes, based on known interactions from existing literature Orange arrows indicate that activation of STAT1 is predicted to activate the target gene and that the target gene is upregulated in TET2-silenced vs siRNA control cells. Blue arrows indicate that activation of STAT1 is predicted to inhibit the target gene and that the target gene is downregulated in TET2-silenced vs siRNA control cells. Yellow arrows indicate that the expression of the target gene in the dataset is inconsistent with that predicted from STAT1 activation. Grey arrows indicate that no activity pattern is available. Dotted lines indicate an indirect relationship.*

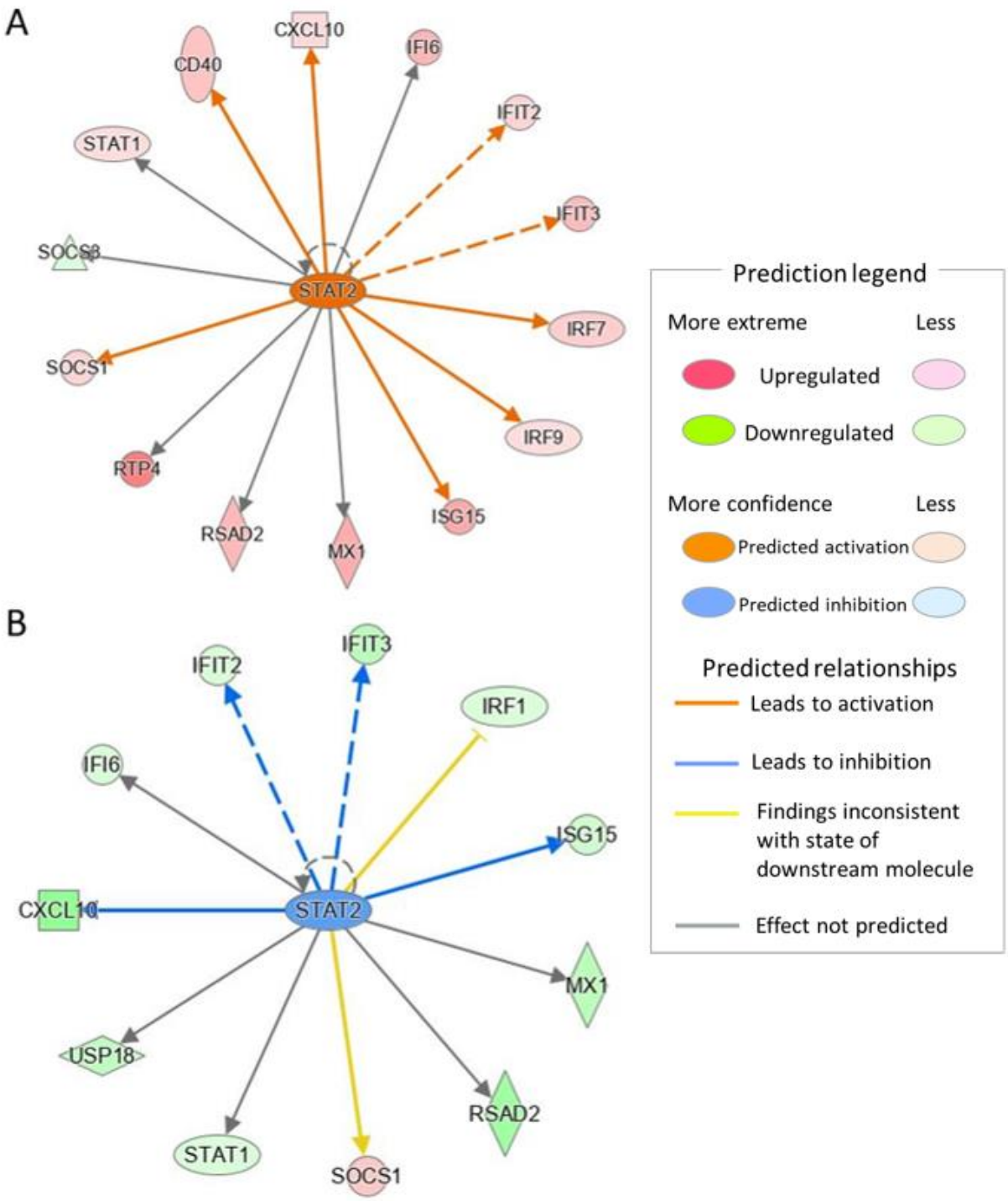

Figure 4.6: ***Ingenuity Pathway Analysis identifies STAT2 as an upstream regulator of genes differentially-expressed by TET2 or TET3 silencing in HUVEC.*** *Schematic diagram of genes in the dataset regulated by STAT2. RNA sequencing was performed on HUVEC treated with a negative control siRNA or siRNA targeting TET2 or TET3. Ingenuity Pathway Analysis software was used to predict upstream regulators of differentially-expressed genes, based on known interactions from existing literature. A) STAT2 is upregulated in TET2-silenced vs siRNA control cells. Orange arrows indicate that activation of STAT2 is predicted to activate the target gene and that the target gene is upregulated in TET2-silenced vs siRNA control cells. Grey arrows indicate that no activity pattern is available. Dotted lines indicate an indirect relationship. B) STAT2 is downregulated in TET3-silenced vs siRNA control cells. Blue arrows indicate that inhibition of STAT2 is predicted to inhibit the target gene and that the target gene is downregulated in TET3-silenced vs siRNA control cells. Yellow arrows indicate that the expression of the target gene in the dataset is inconsistent with that predicted from STAT2 inhibition. Grey arrows indicate that no activity pattern is available. Dotted lines indicate an indirect relationship.*

Interferon regulatory factor 7 (IRF7) was identified as a regulator of an extensive number of genes within both datasets and its activation state was highly consistent with the activation state of the target genes (Figure 4.7). IRF7 is expressed at low levels in most cells but can be induced by recognition of pathogens or type I interferons, resulting in a positive feedback loop to amplify interferon production (Figure 4.8) [270]. Accordingly, STATs and IRF7 can reciprocally induce the expression of one another, demonstrating the complex interplay of these signalling pathways (Figures 4.6-4.8).

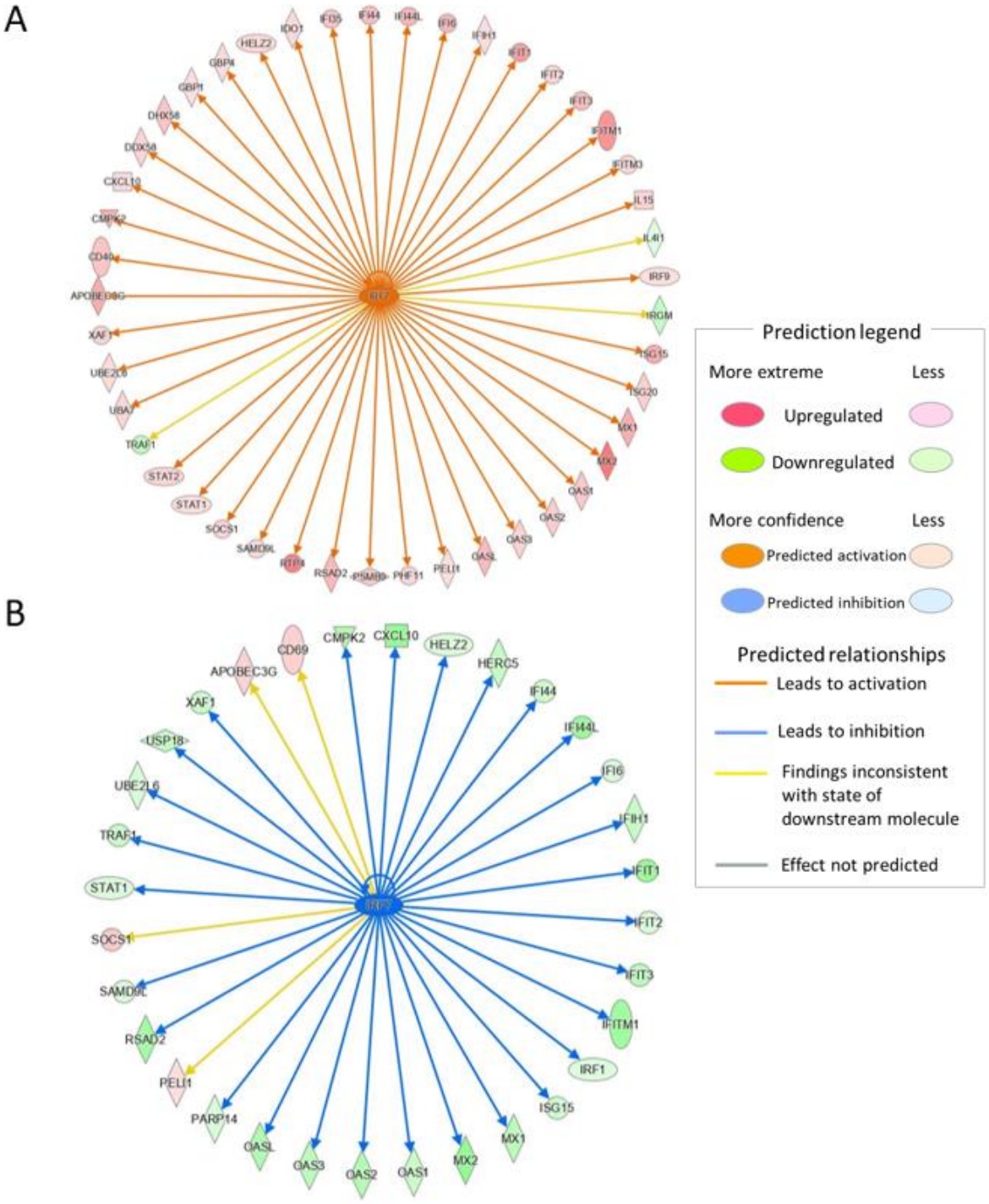

Figure 4.7: ***Ingenuity Pathway Analysis identifies IRF7 as an upstream regulator of genes differentially-expressed by TET2 or TET3 silencing in HUVEC.*** *Schematic diagram of genes in the dataset regulated by IRF7. RNA sequencing was performed on HUVEC treated with a negative control siRNA or siRNA targeting TET2 or TET3. Ingenuity Pathway Analysis software was used to predict upstream regulators of differentially-expressed genes, based on known interactions from existing literature. A) IRF7 is upregulated in TET2-silenced vs siRNA control cells. Orange arrows indicate that activation of IRF7 is predicted to activate the target gene and that the target gene is upregulated in TET2-silenced vs siRNA control cells. Yellow arrows indicate that the expression of the target gene in the dataset is inconsistent with that predicted from IRF7 activation B) IRF7 is downregulated in TET3-silenced vs siRNA control cells. Blue arrows indicate that inhibition of IRF7 is predicted to inhibit the target gene and that the target gene is downregulated in TET3-silenced vs siRNA control cells. Yellow arrows indicate that the expression of the target gene in the dataset is inconsistent with that predicted from IRF7 inhibition.*

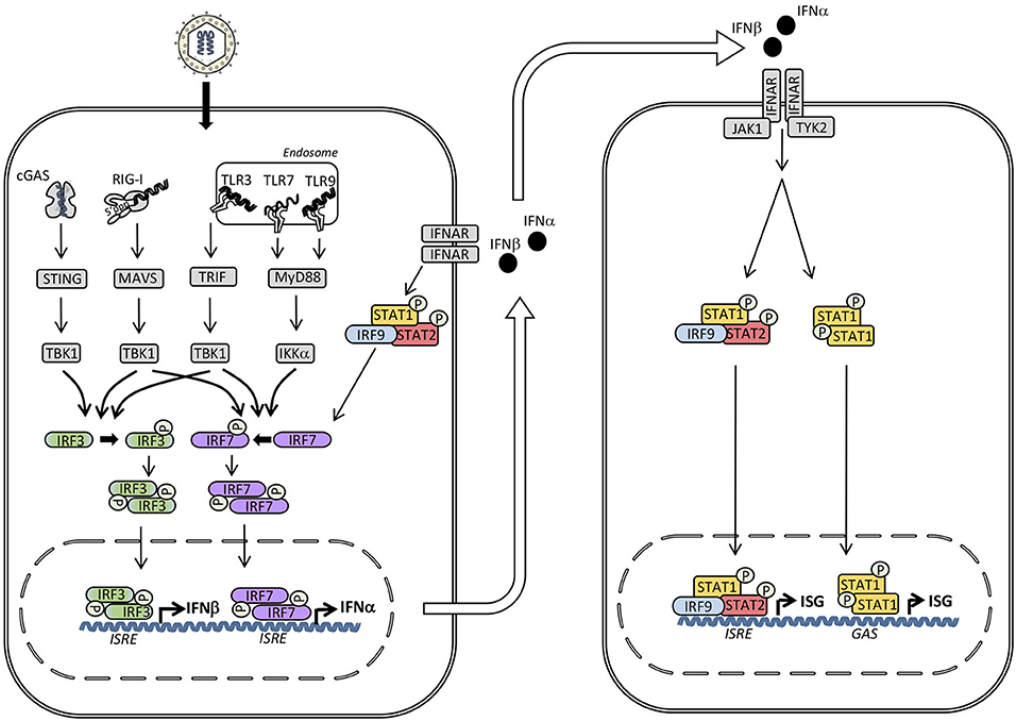

Figure 4.8: ***Schematic diagram of type I interferon induction by IRFs in response to pathogen recognition.*** *Pathogen sensing activates IRF7 downstream of TLR, RIG-I and IFNAR signalling. Phosphorylated dimers of IRF7 bind to ISRE and facilitate the transcription of type I interferons, which in turn are released and act on neighbouring cells to amplify the interferon response. Image reproduced from [270].*

4.2.4 IRF7 may be subject to regulation by DNA methylation and shows differential hydroxymethylation in TET2-silenced HUVEC compared to controls

As IRF7 was identified as an upstream regulator of the interferon-sensitive genes which were found to be upregulated by TET2 silencing, the potential for catalytic involvement of TET2 in its transcriptional regulation was explored. Firstly, HUVEC were treated with 5azaC and relative IRF7 expression was measured by qPCR to assess whether DNA methylation may be involved in the regulation of its transcription (Figure 4.9). IRF7 showed 2-fold greater expression in 5azaC-treated cells compared to controls, suggesting that this may be the case (Figure 4.9). Secondly, hMeDIPseq was performed to compare 5hmC enrichment in control and TET2-silenced HUVEC (Figure 4.10). It was hypothesised that in the absence of TET2, an altered distribution of 5hmC signal would be observed either in the gene body or regulatory regions of IRF7, indicating potential sites of TET2-mediated demethylation that could be involved in the transcriptional regulation of the gene. Comparing the raw signal profile of control

and TET2-silenced HUVEC, a decrease in 5hmC enrichment was observed across exons 4 and 10 of IRF7 compared to controls (Figure 4.10). Although this by no means proves a causal relationship between TET2-mediated demethylation and expression of IRF7 and its targets, the correlation between altered hydroxymethylation patterns and altered expression of IRF7 in TET2-silenced HUVEC, together with the upregulation of IRF7 by 5azaC treatment, supports the possible involvement of TET2 catalytic activity in its regulation. This is in agreement with previous literature identifying IRF7 as a target of TET2 catalytic activity in plasmacytoid dendritic cells [160].

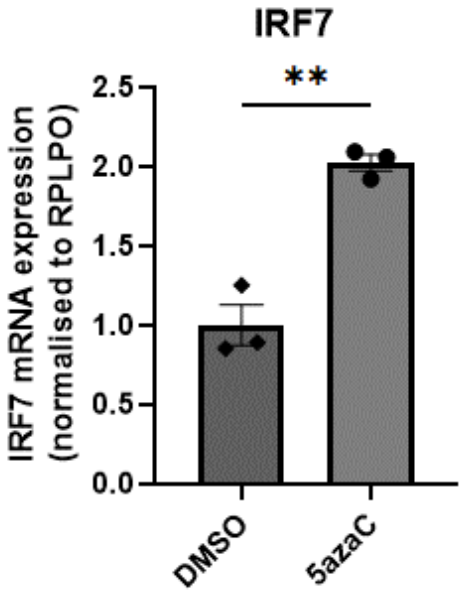

Figure 4.9: ***IRF7 is upregulated by inhibition of DNA methylation.*** *cDNA was prepared from HUVEC treated for 3 days with 5μM 5-aza-2'-deoxycytidine (5azaC) or 0.1% DMSO as a vehicle control. qPCR was used to measure relative mRNA expression of IRF7, normalised to the housekeeping gene RPLPO, in 5azaC-treated vs DMSO-treated samples. A Shapiro-Wilk test for normality was performed, followed by an unpaired t-test. Data presented as mean ± SEM. n=3 triplicate samples. ** denotes p<0.01.*

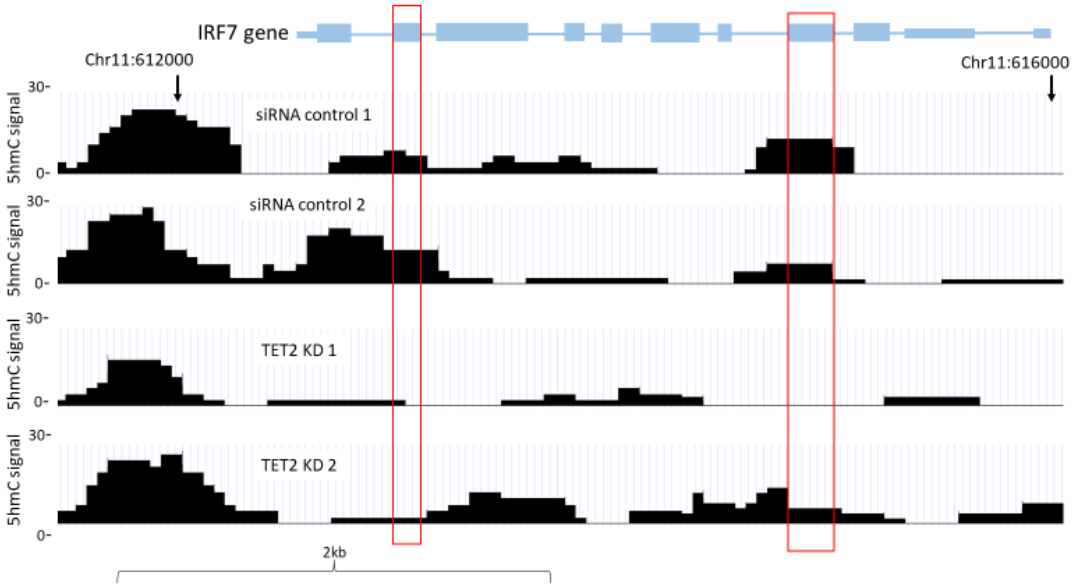

Figure 4.10: ***Raw signal of 5hmC enrichment at the Irf7 gene locus in siRNA control and TET2-silenced HUVEC.*** *Genomic DNA was prepared from HUVEC treated with a negative control siRNA or siRNA targeting TET2. Hydroxymethylated DNA immunoprecipitation was performed and resulting DNA fragments were sequenced. The raw signal profiles were visualised using the UCSC genome browser to assess 5hmC enrichment across the IRF7 gene. Red boxes denote regions of 5hmC enrichment present in both siRNA control cell samples that display less enrichment in both TET2 KD cell samples.*

The enrichment of 5hmC at the same genomic region was also compared in control and IFNγ-treated HUVEC. Hydroxymethylation was broadly similar in the two conditions and no differences were observed within the two exons identified to differ upon TET2 silencing. Instead, a peak was apparent in exon 12 in IFNγ-treated, but not control HUVEC. Although it would perhaps be expected that 5hmC enrichment would increase upon IFNγ treatment if interferon-induced upregulation of IRF7 is mediated by TET2, it is important to consider that transcriptional activation may occur at a specific timepoint after endothelial activation and that this dynamic temporal regulation may not be captured in the 24h timepoint used here.

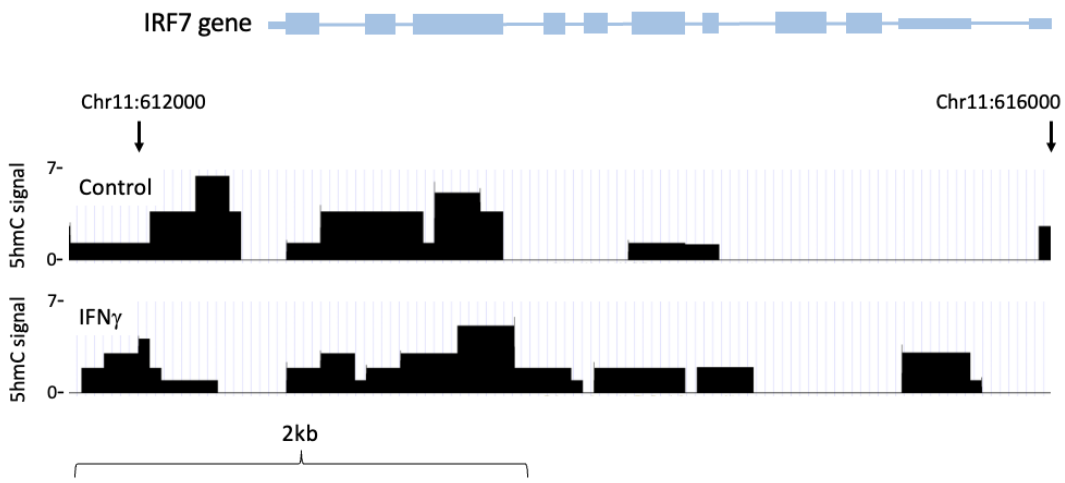

Figure 4.11: ***Raw signal of 5hmC enrichment at the IRF7 gene locus in control and IFNγ-treated HUVEC.*** *Genomic DNA was prepared from untreated HUVEC and HUVEC treated for 24h with 10ng/ml IFNγ. Hydroxymethylated DNA immunoprecipitation was performed and resulting DNA fragments were sequenced. The raw signal profiles were visualised using the UCSC genome browser to assess 5hmC enrichment across the IRF7 gene.*

4.2.5 STAT1 is unlikely to be regulated by DNA methylation and shows no differential hydroxymethylation in TET2-silenced HUVEC compared to controls

Given that STAT1 was also identified as a potential upstream regulator of interferon-sensitive genes which were upregulated by TET2 silencing, it was assessed for potential regulation by TET2 catalytic activity in the same manner. 5azaC treatment did not affect STAT1 mRNA expression in HUVEC (Figure 4.12). In addition, no obvious differences in 5hmC enrichment across the STAT1 gene locus were identified by hMeDIPseq in TET2-silenced, compared to control, HUVEC (Figure 4.13). This does not support the concept of regulation of STAT1 transcription by direct TET2-mediated demethylation activity.

In previous literature, TET2 and STAT1 have been shown to co-immunoprecipitate in THP-1 and B16-OVA cells [197]. TET2-STAT1 binding was detectable at baseline in these cells, but was strongly enhanced by IFNγ stimulation [197]. The authors conclude that STAT1 recruits TET2 to hydroxymethylate chemokine and programmed death ligand 1 (PDL1) genes in this context, resulting in their upregulation and improving

anti-tumour immunity and response to anti-PDL1 therapy *in vivo* [197]. This raises the possibility that TET2-STAT1 co-operation is involved in regulating the cellular response to interferon, but in a manner not involving TET-mediated demethylation of STAT1 itself.

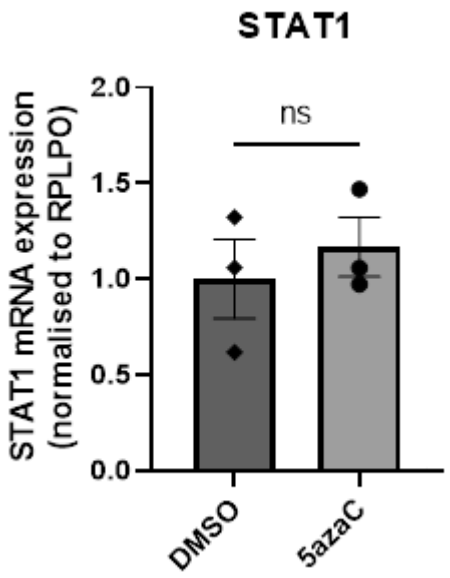

Figure 4.12: ***STAT1 expression is not altered by inhibition of DNA methylation.*** *cDNA was prepared from HUVEC treated for 3 days with 5μM 5-aza-2'-deoxycytidine (5azaC) or 0.1% DMSO as a vehicle control. qPCR was used to measure relative mRNA expression of STAT1, normalised to the housekeeping gene RPLPO, in 5azaC-treated vs DMSO-treated samples. A Shapiro-Wilk test for normality was performed, followed by an unpaired t-test. Data presented as mean ± SEM. n=3 triplicate samples.*

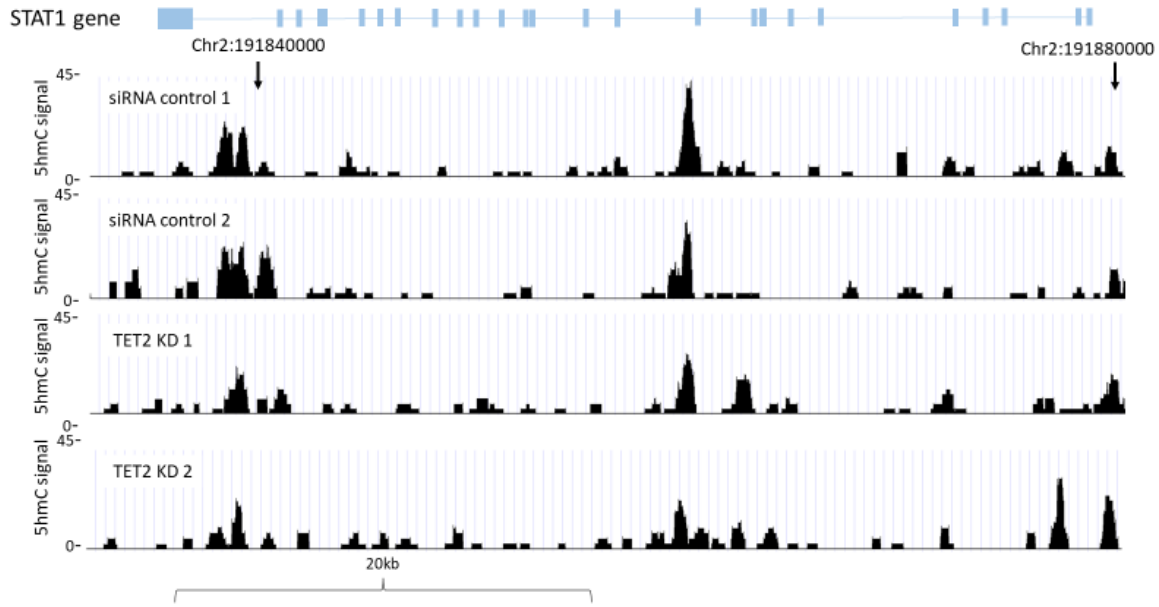

Figure 4.13: ***Raw signal of 5hmC enrichment at the STAT1 gene locus in siRNA control and TET2-silenced HUVEC.*** *Genomic DNA was prepared from HUVEC treated with a negative control siRNA or siRNA targeting TET2. Hydroxymethylated DNA immunoprecipitation was performed and resulting DNA fragments were sequenced. The raw signal profiles were visualised using the UCSC genome browser to assess 5hmC enrichment across the STAT1 gene.*

4.2.6 STAT1 is strongly upregulated by TET2 silencing and pSTAT1 is retained in the nucleus during the resolution of the interferon gamma response in TET2-silenced HUVEC

It is well established that dimers of STAT1 become phosphorylated upon IFNγ stimulation, enabling them to undergo nuclear translocation [219]. Thus, the activity of STAT1 may be regulated more at the post-translational level as opposed to the transcriptional level. Increased pSTAT1 levels in the nucleus in the absence of TET2 could potentially explain the upregulation of interferon-stimulated genes and perturbed resolution of interferon stimulation observed upon TET2 silencing (see Chapter 3 Figures 3.17, 3.23 & 3.24). Therefore, the hypothesis was tested that silencing of TET2 in HUVEC impacts on the phosphorylation or nuclear translocation of STAT1 during activation and resolution of the IFNγ response. To this end, nuclear and cytoplasmic cell fractions were harvested from control and TET2-silenced HUVEC at baseline, following 24h IFNγ treatment, or after 24h IFNγ treatment followed by its removal for 24h (Figure 4.14). A striking increase in unphosphorylated and

phosphorylated STAT1 was evident in the cytoplasmic fraction upon TET2 silencing both at baseline and following IFNγ stimulation (Figure 4.14). Although phosphorylated STAT1 (pSTAT1) levels in the nucleus were similar between both conditions at these timepoints, during the resolution of the response, 24h after removal of IFNγ, pSTAT1 levels in the nucleus remained higher in TET2 siRNA-treated HUVEC compared to negative control siRNA-treated HUVEC (Figure 4.14). Taken together, these findings, although preliminary and yet to be explored further, are suggestive of a possible non-catalytic role for TET2 in regulating the expression and activity of STAT1 in HUVEC. Increased pSTAT1 levels in the nucleus could explain the sustained high expression of interferon-sensitive genes in TET2-silenced HUVEC during the resolution of the type II interferon response (see Chapter 3 Figure 3.24).

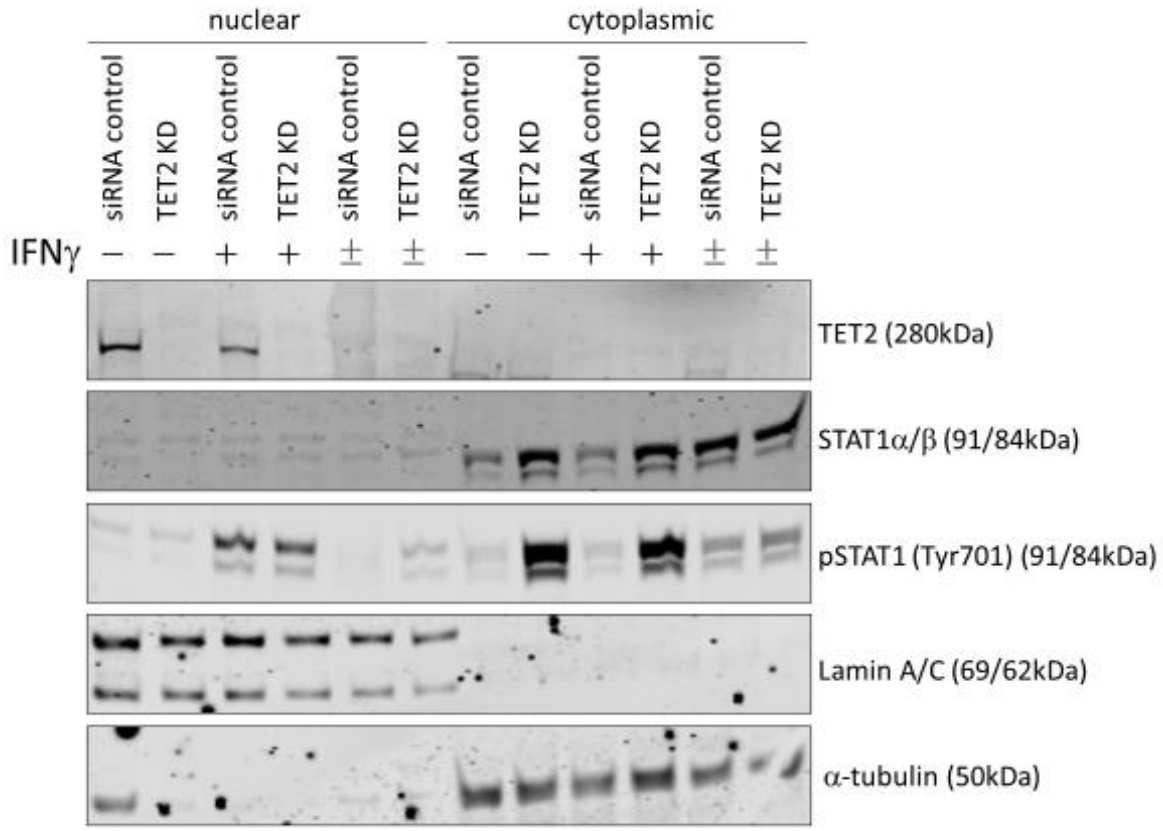

Figure 4.14: ***Western blot of TET2, STAT1 and pSTAT1 proteins in nuclear and cytoplasmic fractions of TET2-silenced or siRNA control HUVEC before, during and after IFNγ treatment.*** *HUVEC were treated with a negative control siRNA or siRNA targeting TET2.Nuclear and cytoplasmic fractions were collected at baseline (-), following 24h IFNγ treatment (+) or 24 hours after its removal (±). pSTAT1 was probed on a second blot with identical sample loading. Successful nuclear and cytoplasmic fractionation was confirmed with Lamin A/C and α-tubulin loading controls.*

4.2.7 Pharmacological inhibition of HDACs upregulates interferon-sensitive genes in HUVEC

A second potential non-catalytic mechanism of interest involves potential cross-talk between TET2 and HDACs. Recruitment of histone deacetylase (HDAC)2 by TET2 has been reported to repress IL-6 expression following LPS stimulation in bone marrow dendritic cells (BMDCs) and macrophages [158]. Although the authors attribute the deacetylation of the IL6 promoter during resolution of the LPS stimulation primarily to HDAC2, they also note that HDAC1 is present in the complex containing TET2 and HDAC2 and that it can compensate for loss of HDAC2 [158]. Interestingly, some of the genes identified by RNA sequencing to be upregulated in Tet2-deficient LPS-stimulated BMDCs were in common with those identified in TET2-silenced HUVEC in the RNA sequencing dataset (RSAD2, IFIT2, IFIT3) [158]. To begin exploring the possibility that TET2 co-operates with HDACs to mediate resolution of interferon responses in endothelial cells, HUVEC were treated with trichostatin A, a selective inhibitor of class I/class II HDACs. Trichostatin A treatment resulted in significant upregulation of IFITM1, ISG15 and STAT1 (Figure 4.15C, D & E). However, it cannot be concluded that these changes are a direct result of HDAC inhibition, as trichostatin A treatment also significantly downregulated TET2, which may account for their altered expression (Figure 4.15F).

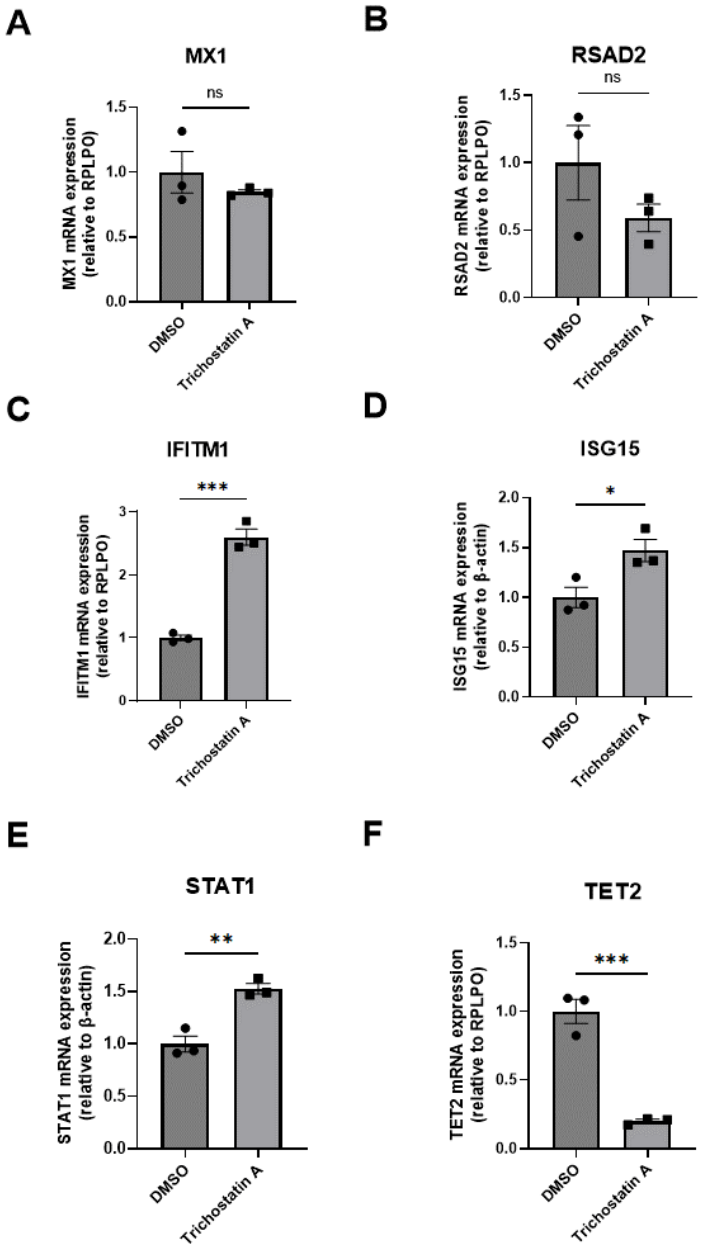

Figure 4.15: ***IFITM1, ISG15 and STAT1 are upregulated by inhibition of HDAC activity.*** *cDNA was prepared from HUVEC treated for 4h with 300nM Trichostatin A or 0.1% DMSO as a vehicle control. qPCR was used to measure relative mRNA expression of MX1 (A), RSAD2 (B), IFITM1 (C), ISG15 (D) and STAT1 (E), normalised to the housekeeping gene RPLPO (or β-actin). A Shapiro-Wilk test for normality was performed, followed by an unpaired t-test. Data presented as mean ± SEM. n=3 triplicate samples. * denotes p<0.05. ** denotes p<0.01. *** denotes p<0.001.*

4.2.8 siRNA-mediated silencing of HDAC1 and HDAC2 has opposite effects on the expression of interferon-sensitive genes in HUVEC

To examine the contribution of specific HDACs to the regulation of interferon-sensitive expression, siRNA was used to silence HDAC1 or HDAC2 in HUVEC. Silencing was highly efficient and selective (Figure 4.16A & B) and had little impact on TET2 and TET3 expression (although TET3 was significantly downregulated by HDAC1 silencing, the actual change in expression was minimal) (Figure 4.16C & D). Intriguingly, silencing of HDAC1 resulted in a trend towards upregulation of IFITM1 and ISG15 (mimicking that of TET2 silencing (Figure 3.17)), whereas HDAC2 silencing showed a trend towards downregulation of these genes (mimicking that of TET3 silencing (Figures 3.18, 4.16E & F)).

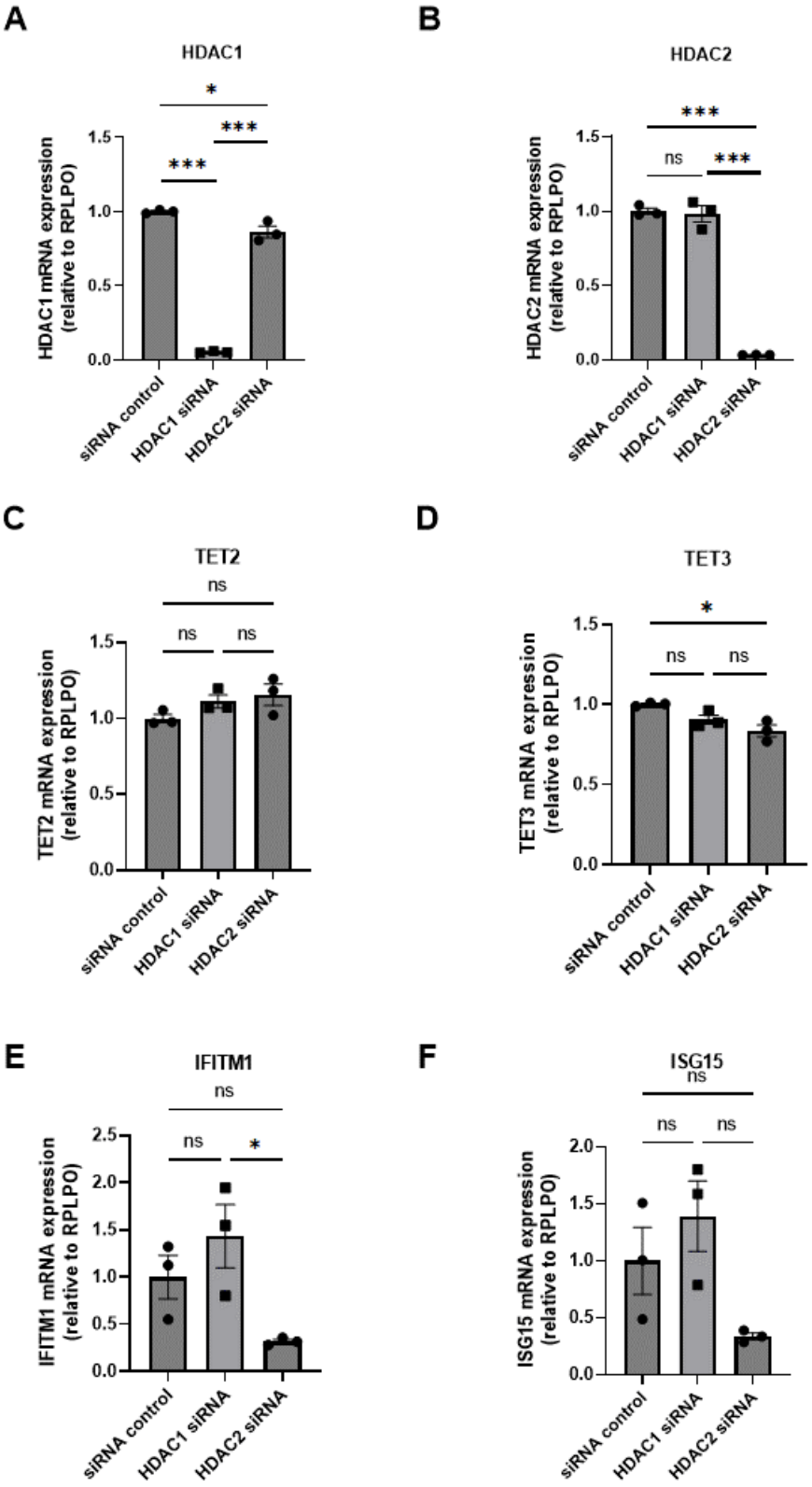

Figure 4.16: ***Trend towards upregulation of interferon-sensitive genes upon HDAC1 silencing and downregulation upon HDAC2 silencing in HUVEC.*** *HUVEC were transfected with negative control siRNA or siRNA targeting HDAC1 or HDAC2. qPCR was performed to measure relative mRNA expression of HDAC1 (A), HDAC2 (B), TET2 (C), TET3 (D), IFITM1 (E) and ISG15 (F), normalised to the housekeeping gene RPLPO. A Shapiro-Wilk test for normality was performed, followed by a one-way ANOVA with post-hoc Tukey's test. Data presented as mean ± SEM. n=3 triplicate samples. * denotes p<0.05. *** denotes p<0.001.*

The regulation of IFITM1 and ISG15 expression by HDACs was then explored upon IFNγ stimulation and following its removal (Figure 4.17). Silencing of HDAC1 resulted in a trend towards increased IFNγ-induced expression of IFITM1 and ISG15 and their expression remained higher following removal of IFNγ, suggesting that HDAC1 may be involved in suppressing interferon-sensitive gene expression. By contrast, HDAC2 silencing abrogated the upregulation of IFITM1 and ISG15 by IFNγ but their expression did not differ from controls during the resolution of the IFNγ response, suggesting that HDAC2 may be involved in the activation of interferon-sensitive gene transcription. Taken together, these data show similar patterns of expression of interferon-sensitive genes between HDAC1- and TET2-silenced HUVEC and between HDAC2- and TET3-silenced HUVEC. This raises the intriguing possibility that TETs and HDACs may co-operate to mediate transcriptional activation or repression of interferon-sensitive genes in endothelial cells, although further work is required to explore this hypothesis.

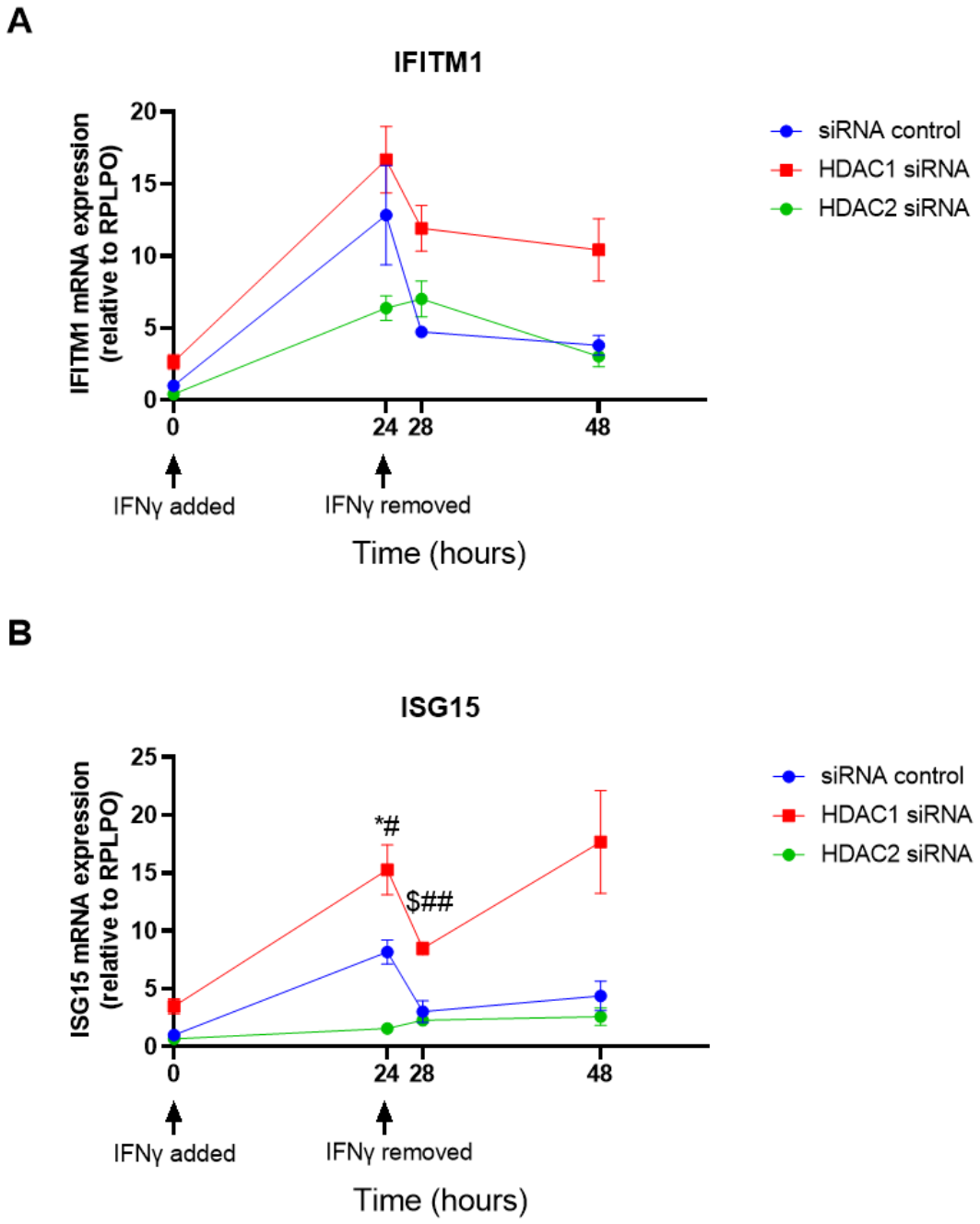

Figure 4.17: ***Profile of IFITM1 and ISG15 expression during IFNγ activation and resolution in negative control siRNA, HDAC1 or HDAC2 siRNA-treated HUVEC.*** *cDNA was prepared from HUVEC transfected with negative control siRNA or siRNA targeting HDAC1 or HDAC2 and treated with IFNγ for 0 or 24 hours or treated with IFNγ for 24 hours followed by its removal for 4 or 24 hours. qPCR was performed to measure relative mRNA expression of IFITM1 (A) and ISG15 (B), normalised to the housekeeping gene RPLPO. A Shapiro-Wilk test for normality was performed, followed by a two-way ANOVA and post-hoc Šidák's test. Data presented as mean ±SEM. n=3 triplicate samples. * denotes p<0.05 comparing siRNA control and HDAC2 siRNA. # denotes p<0.05 and ## denotes p<0.01 comparing HDAC1 siRNA and HDAC2 siRNA. $ denotes p<0.05 comparing siRNA control and HDAC1 siRNA.*

4.2.9 TET2-silenced HUVEC are not prevented from modulating cholesterol biosynthesis gene expression upon cholesterol excess or inhibition of HMGCR activity

In chapter 3, RNA sequencing and qPCR showed that genes involved in the cholesterol biosynthesis pathway, including DHCR7, HMGCS1 and HMGCR, were upregulated by silencing TET2 in HUVEC (Figures 3.29 & 3.30). It has previously been shown that downregulation of cholesterol synthesis is an important factor in the maintenance of cholesterol homeostasis of endothelial cells after cholesterol loading (as opposed to ATP-binding cassette protein A1 (ABCA1)-mediated cholesterol efflux which is a key factor in macrophages and other cell types) [255]. To investigate the importance of TET2 in the dynamic transcriptional regulation of cholesterol biosynthesis genes, a synthetic form of cholesterol (synthechol®) was added to the culture media of negative control siRNA-treated and TET2 siRNA-treated HUVEC. The expression of DHCR7, HMGCS1 and HMGCR was assessed in these HUVEC and under conditions without synthechol addition (Figure 4.18). It was hypothesised that if TET2 was required for the repression of cholesterol biosynthesis genes upon sensing excess cholesterol levels, then in the absence of TET2, the expression of these genes would not be downregulated upon addition of synthechol. Consistent with the data presented in chapter 3, TET2 silencing significantly increased the expression of DHCR7 and HMGCS1 (Figure 4.18). The impact of synthechol on cholesterol biosynthesis gene expression was subtle and not statistically significant, so it is difficult to draw conclusions about the impact of TET2 silencing in this setting. However, given that a similar fold-change in expression was observed upon synthechol addition in both siRNA control and TET2-silenced cells, it appears that TET2-silenced cells are not prevented from modulating cholesterol biosynthesis gene expression when intracellular cholesterol levels are high (Figure 4.18).

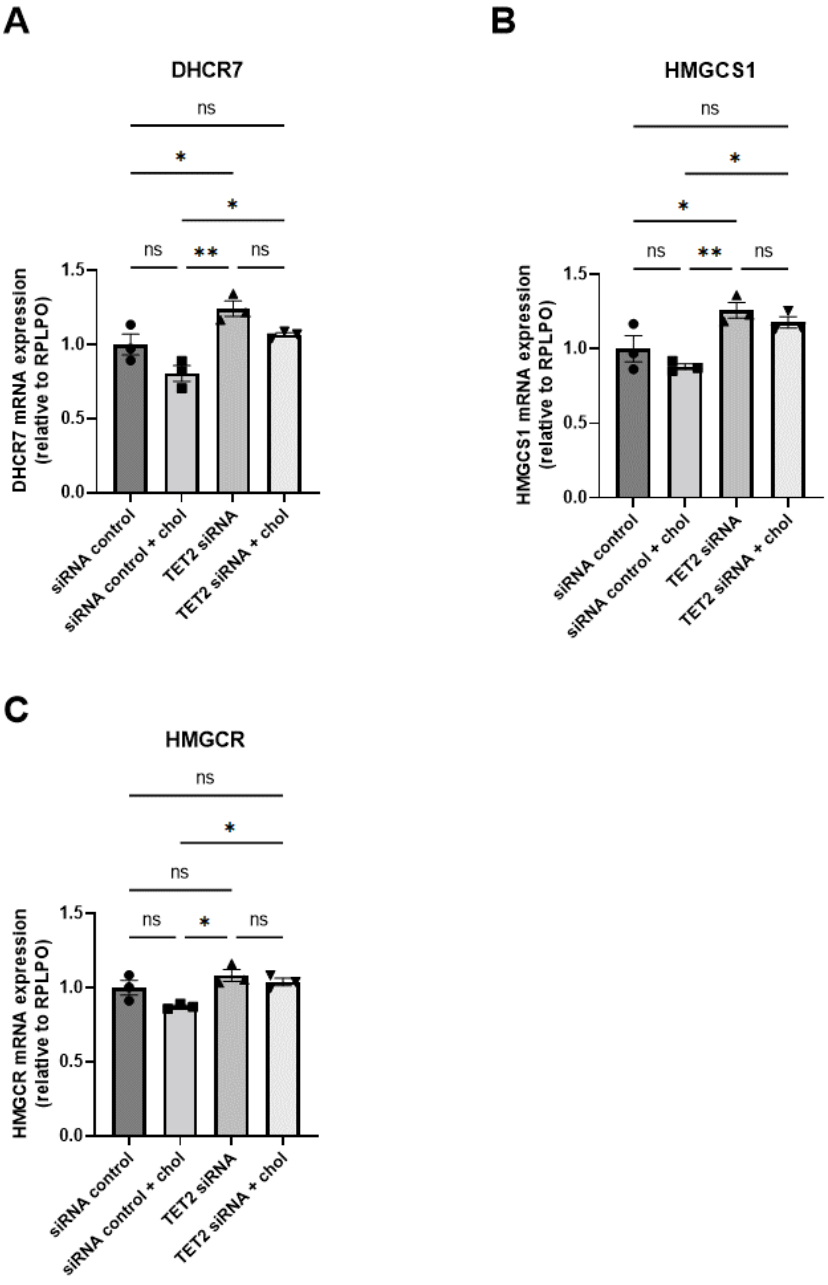

Figure 4.18: ***Expression of cholesterol biosynthesis pathway genes in siRNA control and TET2-silenced HUVEC upon addition of cholesterol.*** *cDNA was prepared from HUVEC transfected with negative control siRNA or siRNA targeting TET2 and treated with synthechol (chol) for 0 or 24 hours. qPCR was performed to measure relative mRNA expression of DHCR7 (A), HMGCS1 (B) and HMGCR (C), normalised to the housekeeping gene RPLPO. A Shapiro-Wilk test for normality was performed, followed by a one-way ANOVA and post-hoc Tukey's test. Data presented as mean ± SEM. n=3 triplicate samples. * denotes p<0.05. ** denotes p<0.01.*

To explore further the importance of TET2 in the dynamic transcriptional regulation of cholesterol biosynthesis genes, control and TET2-silenced HUVEC were treated with atorvastatin or DMSO as a vehicle control (Figure 4.19). Statins competitively inhibit the activity of HMGCR, preventing the rate-limiting step of cholesterol biosynthesis: conversion of 3-hydroxy-3-methylglutaryl coenzyme A (HMG-CoA) to mevalonate [271]. It was reasoned that addition of a statin would decrease cholesterol production, leading to upregulation of genes encoding enzymes that catalyse this and other stages of the cholesterol biosynthesis pathway. It was further hypothesised that TET2 may act to regulate the expression of cholesterol biosynthesis genes in situations of depleted cholesterol, so TET2-silenced HUVEC may display an altered expression level of DHCR7, HMGCS1 and HMGCR expression following statin treatment compared to negative control siRNA-treated HUVEC. However, this did not appear to be the case. Atorvastatin treatment significantly upregulated the cholesterol biosynthesis genes, but the fold-change of upregulation was similar in TET2-silenced and control HUVEC (Figure 4.19). These data indicate that TET2 is not required for the upregulation of cholesterol biosynthesis genes when low cholesterol levels are encountered in HUVEC.

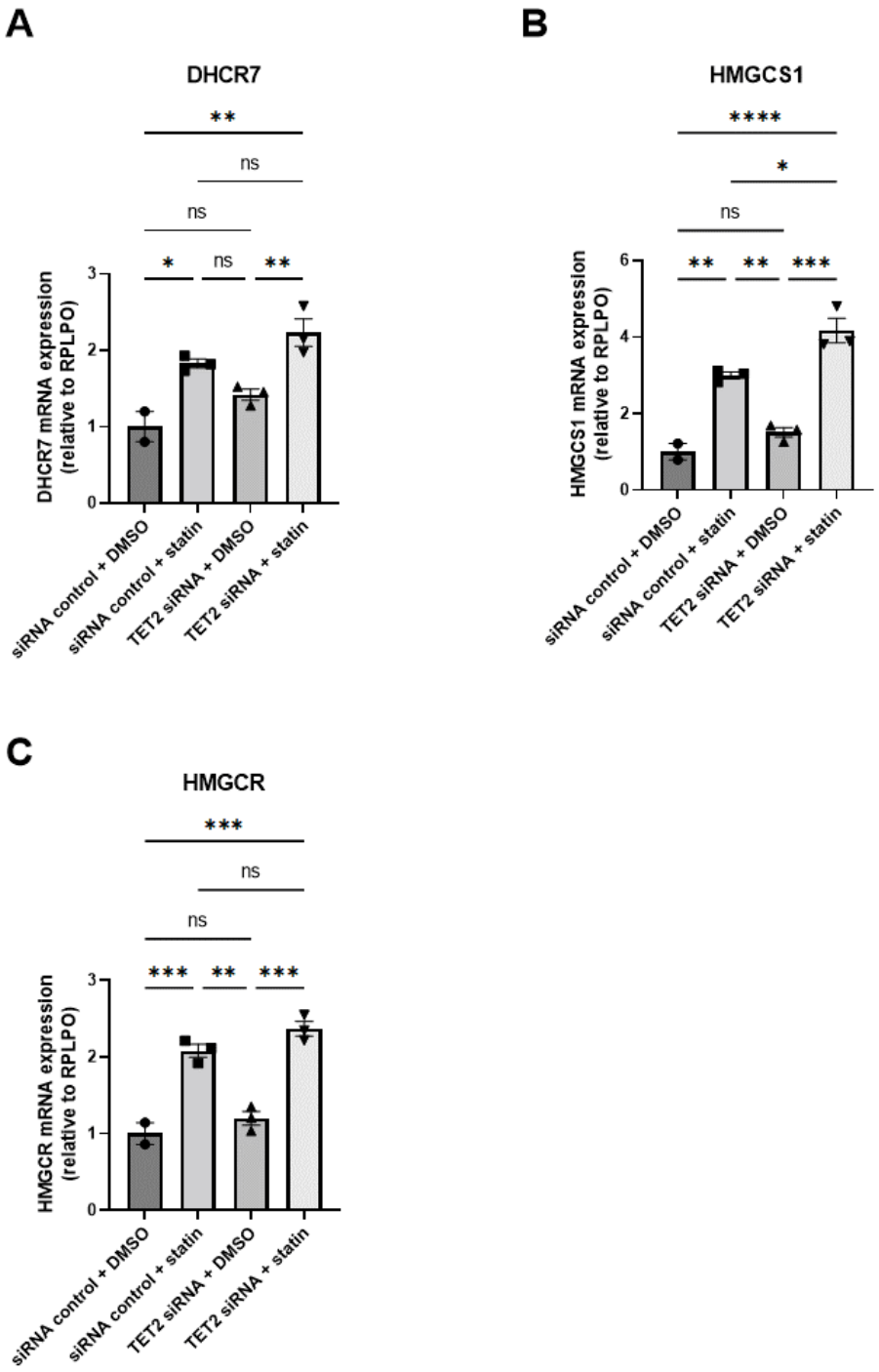

Figure 4.19: ***Expression of cholesterol biosynthesis pathway genes in siRNA control and TET2-silenced HUVEC upon addition of atorvastatin.*** *cDNA was prepared from HUVEC transfected with negative control siRNA or siRNA targeting TET2 and treated with atorvastatin (statin) or 0.01% DMSO vehicle control for 0 or 24 hours. qPCR was performed to measure relative mRNA expression of DHCR7 (A), HMGCS1 (B) and HMGCR (C), normalised to the housekeeping gene RPLPO. A Shapiro-Wilk test for normality was performed, followed by a one-way ANOVA and post-hoc Tukey's test. Data presented as mean ±SEM. n=3 triplicate samples. * denotes p<0.05. ** denotes p<0.01. *** denotes p<0.001.*

4.2.10 Treatment of TET2-silenced HUVEC with 25-hydroxycholesterol abolishes differences in cholesterol biosynthesis gene expression

As discussed in Chapter 3, there is an interplay between interferon signalling and cholesterol metabolism, at least in immune cells, centred around the type I interferon-inducible oxysterol 25-HC and the enzyme responsible for its production from cholesterol, CH25H [237-239]. CH25H was found to be upregulated by TET2 silencing or interferon signalling in HUVEC (Figures 3.32 & 3.33). This raises the possibility that TET2-dependent regulation of CH25H may be responsible for the increased expression of cholesterol biosynthesis genes observed in unstimulated HUVEC. To investigate this, 25-HC or vehicle was added to siRNA control and TET2-silenced HUVEC. It was hypothesised that if the regulation of DHCR7, HMGCS1 and HMGCR expression by TET2 is mediated *via* regulation of CH25H, then the changes in the expression of these genes would be abolished by the addition of 25-HC. In agreement with the findings of Chapter 3, TET2 silencing again significantly increased DHCR7 and HMGCS1 expression (Figures 3.30 & 4.20). Addition of 25-HC potently downregulated these genes as expected and abolished the difference in expression between siRNA control and TET2-silenced HUVEC (Figure 4.20). Taken together, these data suggest that although TET2 may not be involved in sensing changes in level of intracellular cholesterol in HUVEC, the genes encoding enzymes involved in cholesterol biosynthesis are subject to regulation by TET2 in some manner, possibly through regulation of CH25H modulating 25HC levels.

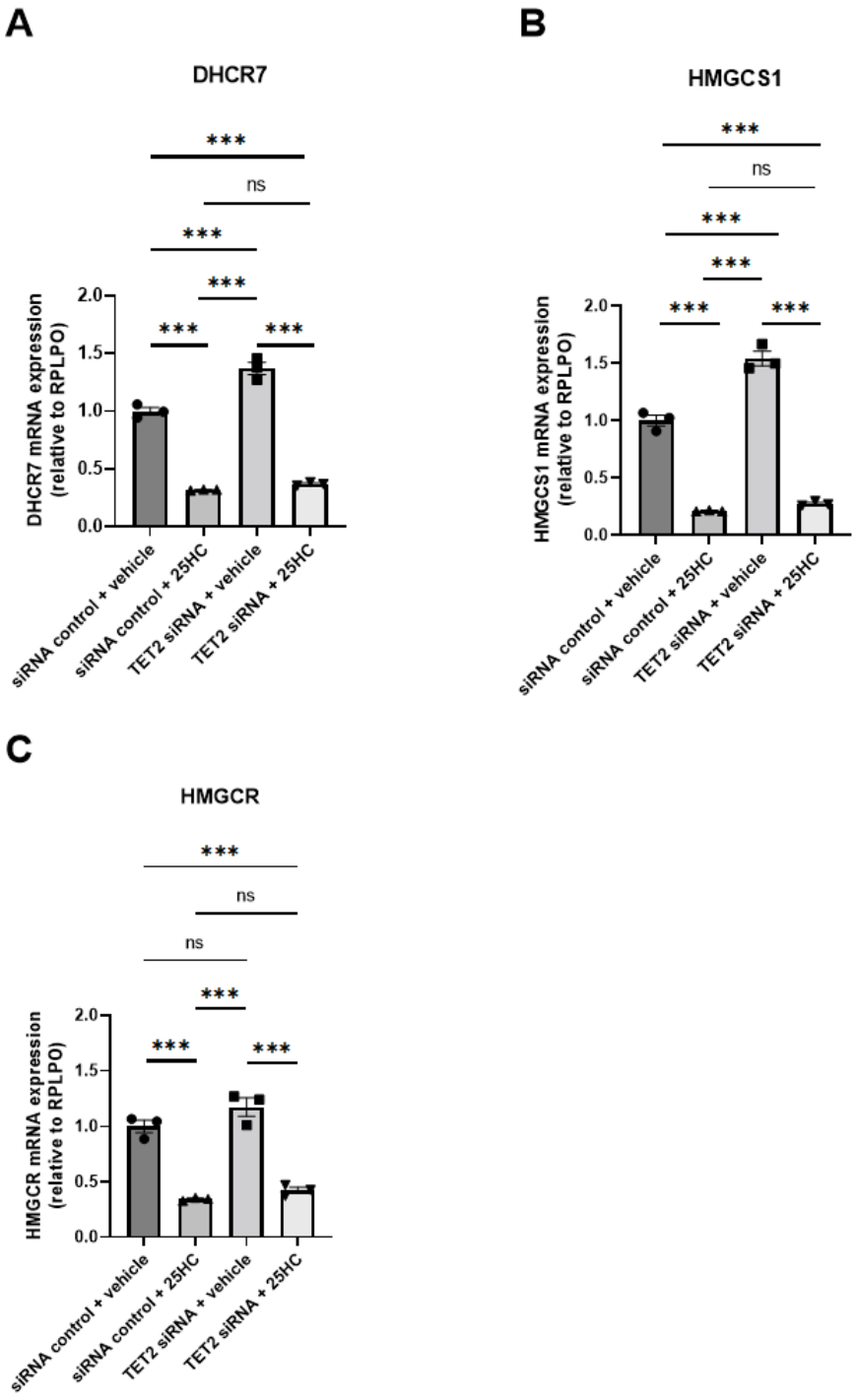

Figure 4.20: ***Expression of cholesterol biosynthesis pathway genes in siRNA control and TET2-silenced HUVEC upon addition of 25-hydroxycholesterol.*** *cDNA was prepared from HUVEC transfected with negative control siRNA or siRNA targeting TET2 and treated with 25-hydroxycholesterol (25-HC) or 0.02% DMSO vehicle control for 0 or 24 hours. qPCR was performed to measure relative mRNA expression of DHCR7 (A), HMGCS1 (B) and HMGCR (C), normalised to the housekeeping gene RPLPO. A Shapiro-Wilk test for normality was performed, followed by a one-way ANOVA and post-hoc Tukey's test. Data presented as mean ± SEM. n=3 triplicate samples. * denotes p<0.05. ** denotes p<0.01. *** denotes p<0.001.*

4.2.11 CH25H may be subject to regulation by DNA methylation and shows differential hydroxymethylation in TET2-silenced HUVEC compared to controls

To begin investigating whether transcriptional regulation of cholesterol biosynthesis genes involves TET2 catalytic activity, 5azaC was applied to HUVEC and the relative mRNA expression levels of HMGCR, SQLE, LSS, DHCR7, HMGCS1 and CH25H were compared to DMSO-treated controls (Figure 4.21). Only CH25H showed a significant upregulation upon 5azaC treatment, indicating possible involvement of DNA methylation in its regulation, unlike for HMGCR, SQLE, LSS, DHCR7 and HMGCS1 (Figure 4.21).

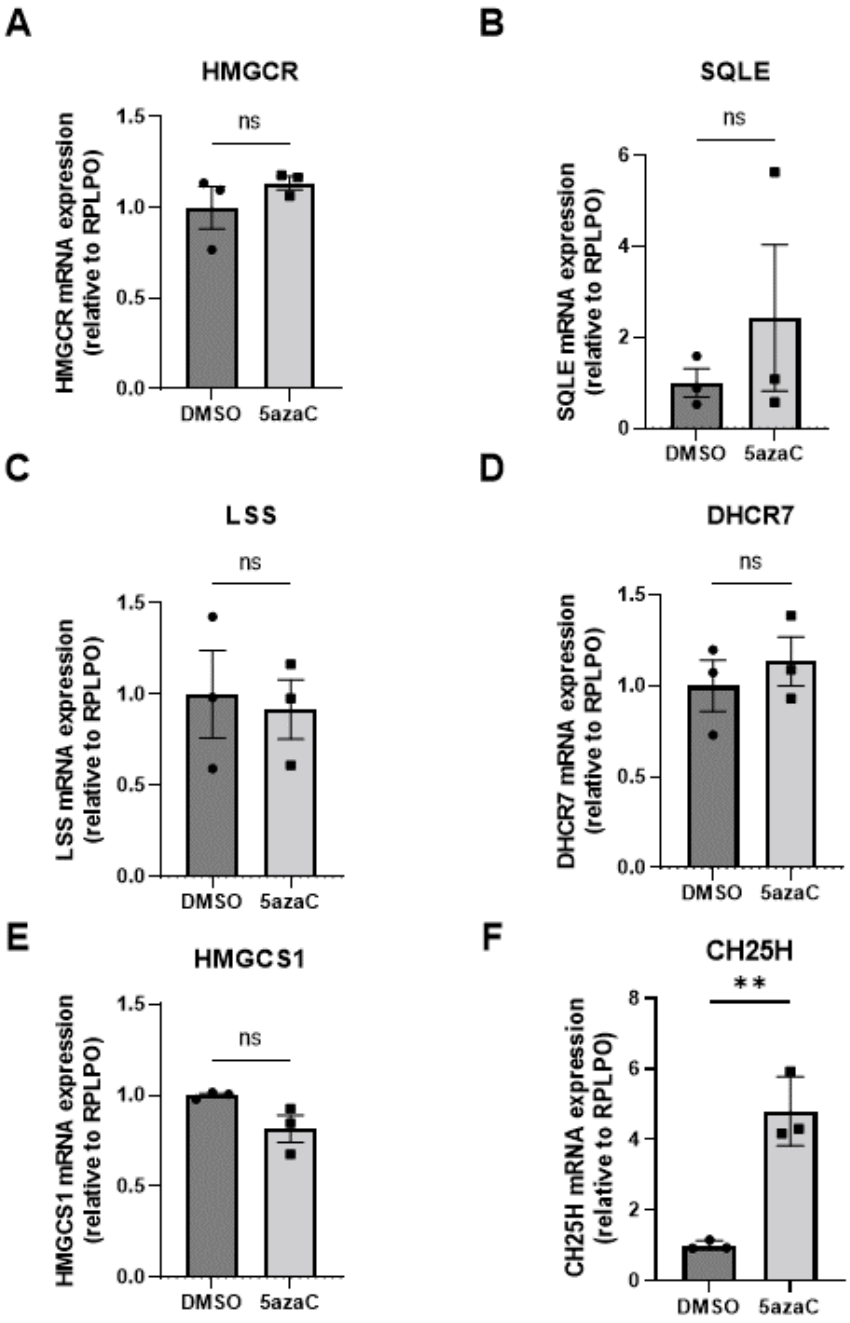

Figure 4.21: ***CH25H is upregulated by inhibition of DNA methylation.*** *cDNA was prepared from HUVEC treated for 3 days with 5μM 5-aza-2'-deoxycytidine (5azaC) or 0.1% DMSO as a vehicle control. qPCR was used to measure relative mRNA expression of HMGCR (A), SQLE (B), LSS (C), DHCR7 (D), HMGCS1 (E) and CH25H (F), normalised to the housekeeping gene RPLPO, in 5azaC-treated vs DMSO-treated samples. A Shapiro-Wilk test for normality was performed, followed by an unpaired t-test. Data presented as mean ± SEM. n=3 triplicate samples. ** denotes p<0.01.*

Next, the enrichment of 5hmC at the CH25H gene locus was assessed by hMeDIPseq, comparing siRNA control and TET2-silenced HUVEC (Figure 4.22). Although there was little 5hmC enrichment in this region in all samples and there was some inconsistency between duplicate samples, a 100-200bp region was identified which was enriched

for 5hmC in siRNA control HUVEC but devoid of 5hmC in TET2-silenced HUVEC (Figure 4.22). Although it cannot be concluded that this differentially-hydroxymethylated region in the gene body is necessarily important for TET2-mediated alteration of CH25H gene expression, changes in the 5hmC distribution of this gene in the absence of TET2 are intriguing and warrant further study.

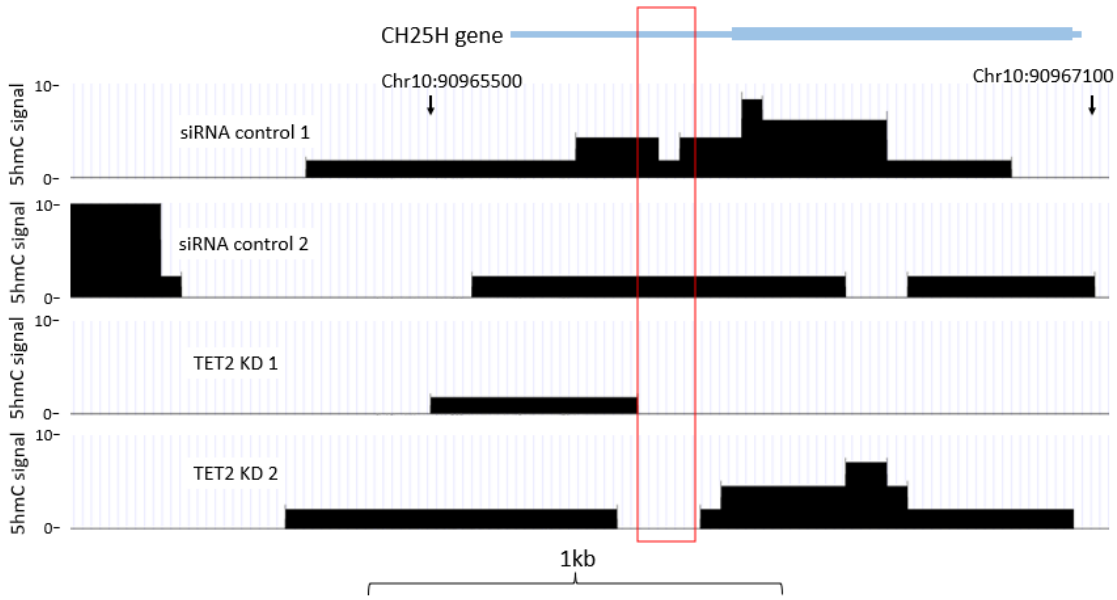

Figure 4.22: ***Raw signal of 5hmC enrichment at the CH25H gene locus in siRNA control and TET2-silenced (TET2 KD) HUVEC.*** *Genomic DNA was prepared from HUVEC treated with a negative control siRNA or siRNA targeting TET2. Hydroxymethylated DNA immunoprecipitation was performed and resulting DNA fragments were sequenced. The raw signal profiles were visualised using the UCSC genome browser to assess 5hmC enrichment across the CH25H gene. Red box denotes a region of 5hmC enrichment present in both siRNA control cell samples that is absent from both TET2 KD cell samples.*

4.2.12 Free and esterified intracellular cholesterol levels are increased by TET2 silencing in HUVEC

Having observed that TET2-silenced HUVEC demonstrated consistently higher expression levels of genes involved in the cholesterol biosynthesis pathway compared to negative control siRNA-treated HUVEC (Figures 3.30, 4.18 & 4.20), it was questioned whether this would lead to a measurable difference in intracellular cholesterol levels. Using a Cholesterol/Cholesterol Ester-Glo™ Assay, the cholesterol and cholesterol ester content of HUVEC were measured following treatment with a negative control-siRNA or siRNA targeting TET2 (Figure 4.23). A significant increase in

free cholesterol was identified in TET2-silenced HUVEC (Figure 4.23A). Similarly, although contributing only a small proportion to total cholesterol levels, the esterified cholesterol level was also significantly increased by TET2 silencing (Figure 4.23B & C). Together, this corresponds to a highly significant increase in total cholesterol content of HUVEC in the absence of TET2 (Figure 4.23C). In agreement with the gene expression data, this supports a role for TET2 in the regulation of cholesterol biosynthesis in endothelial cells.

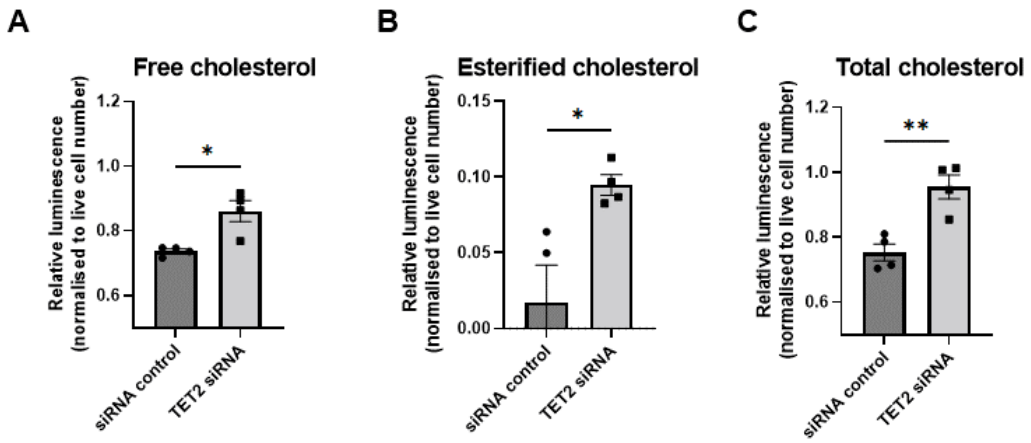

Figure 4.23: ***TET2 silencing in HUVEC increases intracellular free and esterified cholesterol levels.*** *HUVEC were transfected with a negative control siRNA or siRNA targeting TET2. A Cholesterol/Cholesterol Ester-Glo™ Assay was performed to measure free and esterified cholesterol levels relative to the number of live cells in each sample. A Shapiro-Wilk test for normality was performed, followed by an unpaired t-test. Data presented as mean ± SEM. n=4 technical replicates. * denotes p<0.05. ** denotes p<0.01.*

4.2.13 Opposite effects of type I and type II interferons on intracellular cholesterol levels in HUVEC

It has previously been suggested that downregulation of cholesterol synthesis by innate immune cells in response to type I interferon signalling functions to protect against pathogens utilising host cell cholesterol reserves for their own replication (115). Whether this extends to other cell types, including endothelial cells, is not known and neither is the impact of type II interferon signalling on endothelial cell cholesterol levels. Therefore, the free, esterified and total cholesterol levels were measured in HUVEC at baseline and following IFNα or IFNγ stimulation (Figure 4.24). Unlike in innate immune cells, free cholesterol levels in HUVEC were increased by type

I interferon stimulation (Figure 4.24A). Interestingly, the opposite effect was observed upon type II interferon stimulation (Figure 4.24A). Although slightly increased by both IFNα and IFNγ stimulation, esterified cholesterol levels were not significantly altered by interferon stimulation (Figure 4.24B & C).

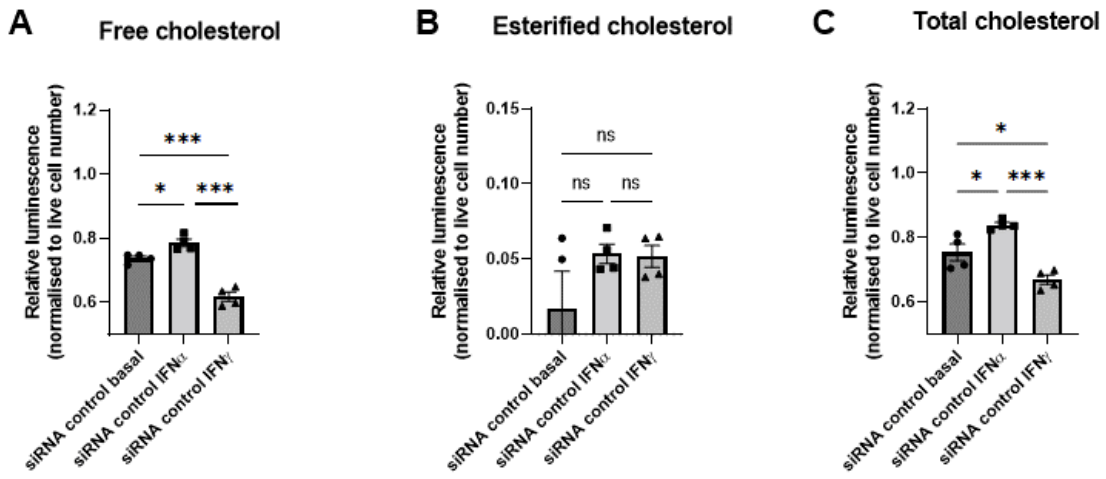

Figure 4.24: ***Opposing effects of type I and type II interferon stimulation on free cholesterol levels in HUVEC.*** *HUVEC were transfected with a negative control siRNA and treated for 20h with 1000U/ml IFNα or 10ng/ml IFNγ. A Cholesterol/Cholesterol Ester-Glo™ Assay was performed to measure free and esterified cholesterol levels relative to the number of live cells in each sample. A Shapiro-Wilk test for normality was performed, followed by a one-way ANOVA and post-hoc Tukey's test. Data presented as mean ± SEM. n=4 technical replicates. * denotes p<0.05. ** denotes p<0.01. *** denotes p<0.001.*

4.2.14 Effect of TET2 silencing on intracellular cholesterol levels at baseline and following IFNα or IFNγ stimulation

The differences in free cholesterol levels of endothelial cells following interferon stimulation are intriguing and novel findings. In chapter 3, data were presented supporting a role for TET2 in regulating interferon-sensitive genes, including CH25H - an enzyme thought to link interferon signalling and cholesterol metabolism in innate immune cells (Figures 3.17 & 3.32) [237-239]. Therefore, cholesterol levels were measured in control and TET2-silenced HUVEC at baseline and following interferon stimulation, to understand whether TET2 may be involved in the interferon-induced changes in cholesterol levels in HUVEC (Figure 4.25). In all cases, free cholesterol levels were significantly greater in TET2-silenced compared to negative control siRNA-

treated HUVEC (Figure 4.25A). At baseline, TET2 silencing also significantly increased the level of esterified cholesterol. However, no change was observed in TET2-silenced cells compared to siRNA controls upon the addition of IFNα or IFNγ (Figure 4.25B). This may indicate an involvement of TET2 in regulating intracellular esterified cholesterol levels in endothelial cells, however, further work is required to validate these preliminary findings.

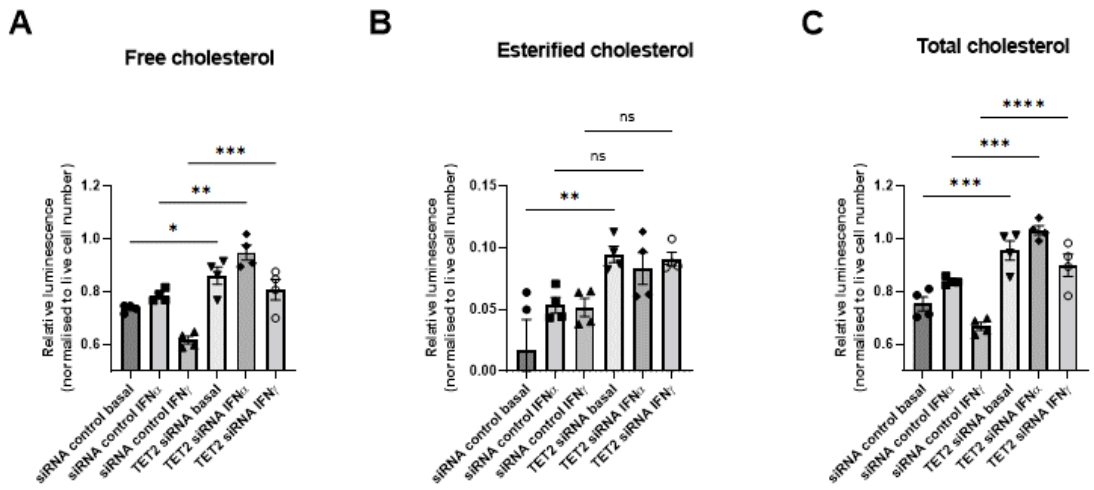

Figure 4.25: ***TET2 silencing in HUVEC increases intracellular free, but not esterified, cholesterol levels following IFNα or IFNγ stimulation.*** *HUVEC were transfected with a negative control siRNA or siRNA targeting TET2 and treated for 20h with 1000U/ml IFNα or 10ng/ml IFNγ. A Cholesterol/Cholesterol Ester-Glo™ Assay was performed to measure free and esterified cholesterol levels relative to the number of live cells in each sample. A Shapiro-Wilk test for normality was performed, followed by a one-way ANOVA and post-hoc Tukey's test comparing siRNA control to TET2 siRNA samples. Data presented as mean ± SEM. n=4 technical replicates. * denotes p<0.05. ** denotes p<0.01. *** denotes p<0.001.*

4.2.15 TET silencing does not affect the viability of HUVEC

After investigating the transcriptomic effects of TET silencing and their mechanistic underpinnings, an understanding of the importance of TET enzymes, particularly TET2, in endothelial cell functions was sought. Mutations of TET2 have been observed in haematological cancers and in age-associated clonal haematopoiesis where loss of TET2 offers haematopoietic stem cells a proliferative advantage [272, 273]. Therefore, whether endothelial proliferation would be influenced by TET silencing was questioned. As an initial experiment, the viability of siRNA control HUVEC was

compared to that of TET1-, TET2- or TET3-silenced HUVEC in the 3 days following transfection. No significant difference in cell viability was observed (Figure 4.26).

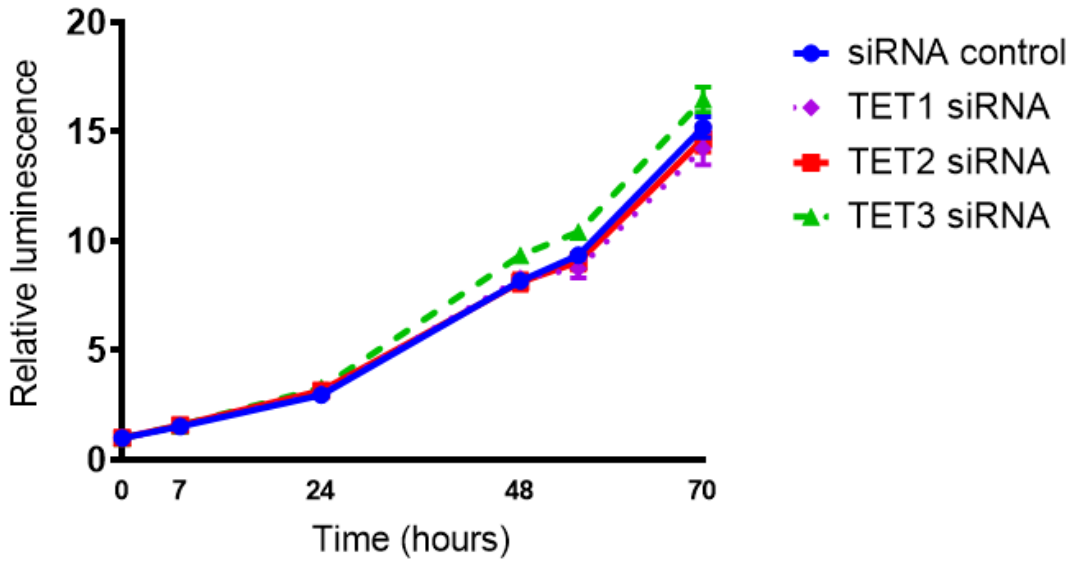

Figure 4.26: ***HUVEC viability is not affected by siRNA-mediated silencing of TET enzymes.*** *HUVEC were transfected with a negative control siRNA or siRNA targeting TET1, TET2 or TET3. Cell viability was measured using a luminometer following the addition of NanoLuc© enzyme and substrate. A Shapiro-Wilk test for normality was performed, followed by a one-way ANOVA and post-hoc Tukey's test at 70h. No significant difference between siRNA control or TET-silenced HUVEC viability was observed. Data presented as mean ± SEM. n=12 technical replicates.*

4.2.16 Silencing TET2 affects cytokine release by HUVEC

An important aspect of endothelial cell homeostasis is the appropriate activation and resolution of inflammatory responses, enabling the recruitment of immune cells to and across the endothelium when required to respond to infection or tissue damage. One facet of the endothelial cell inflammatory response is the release of pro- or anti-inflammatory cytokines and chemokines. Because the transcriptomic data suggested that TET2 may be involved in restraining interferon responses (Figures 3.15, 3.23 & 3.24), it was hypothesised that TET2 silencing would increase interferon-induced pro-inflammatory cytokine release. To begin investigating this, the abundance of cytokines were first compared in the cell culture supernatants of unstimulated HUVEC treated with negative control siRNA or siRNA targeting TET2 using a Proteome Profiler Human XL Cytokine Array (Figure 4.27). A small number of cytokines were more abundant in

the supernatant of TET2-silenced HUVEC. These included IL-24, a cytokine with diverse context-dependent pro- and anti-inflammatory effects (Figure 4.27C) [274]. Among those with decreased abundance were MMP-9, stromal cell-derived factor 1α (SDF-1α), resistin and granulocyte-macrophage colony-stimulating factor (GM-CSF) (Figure 4.27D). Consistent with its decreased abundance in the absence of TET2, MMP-9 is a known target of TET2 catalytic activity and TET2 expression has previously been shown to correlate with MMP-9 expression [275]. It functions to degrade extracellular matrix proteins and activates cytokines and chemokines through proteolysis [276]. SDF-1α (also known as CXCL12) is a chemokine with roles in haematopoiesis and angiogenesis, as well as chemoattraction of most leukocytes [277]. Resistin is an adipokine involved in insulin resistance and can itself impact cytokine release and induce endothelial dysfunction [278]. GM-CSF is a haematopoietic growth factor and has multiple roles in recruitment, survival and the activation of effector functions of myeloid cells at sites of infection [279]. Accordingly, changes in the abundance of these cytokines released from the endothelium in the absence of TET2 may be functionally important in inflammatory contexts.

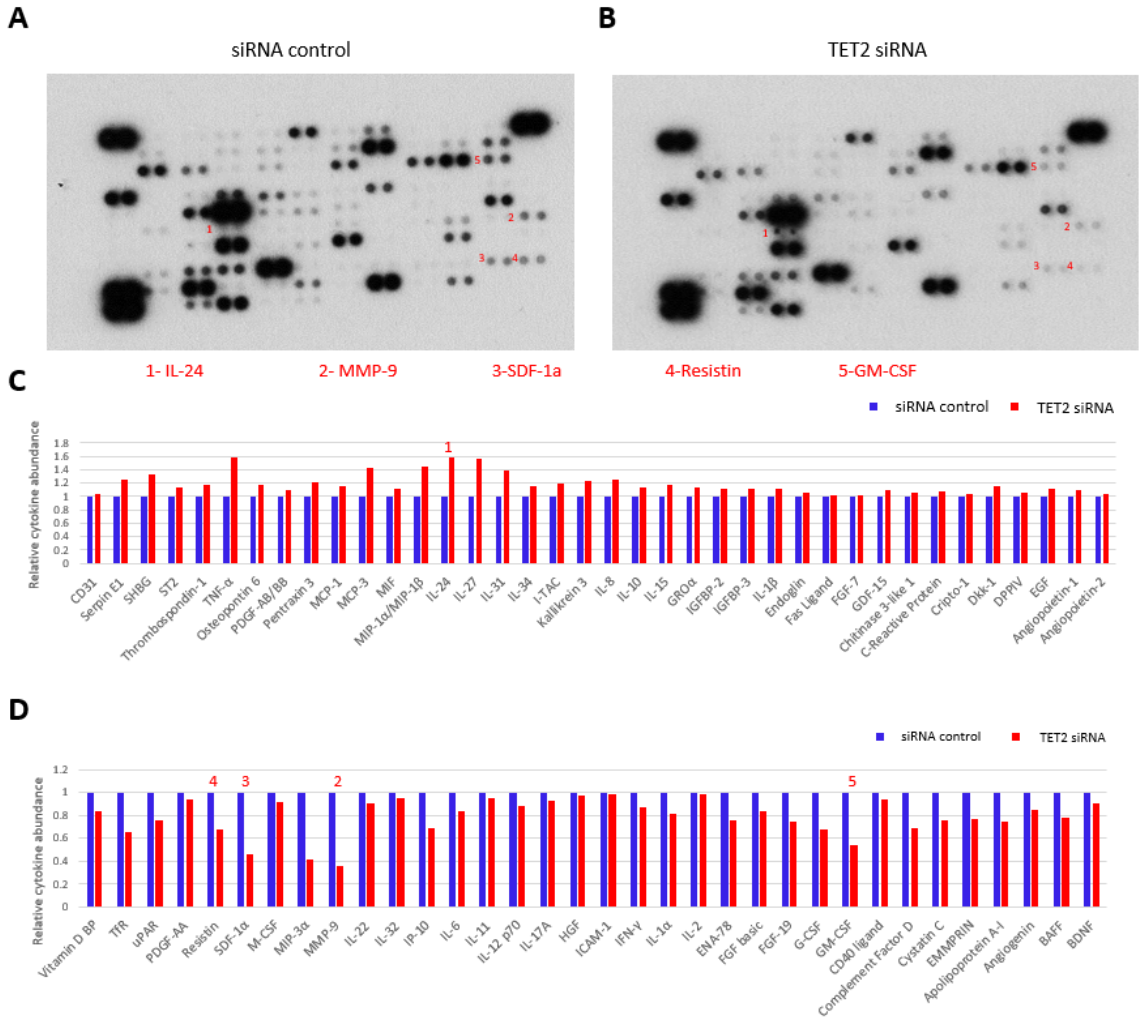

Figure 4.27: ***siRNA-mediated silencing of TET2 affects baseline cytokine release by HUVEC.*** *Cell culture supernatants were collected from negative control siRNA-treated (A) or TET2 siRNA-treated HUVEC (B) and cytokine abundance was measured using a Proteome Profiler Human XL Cytokine Array. The signals from each array were quantified by densitometry and the relative cytokine abundance was calculated. C) Cytokines with increased abundance in samples from TET2-silenced HUVEC compared to siRNA controls. D) Cytokines with decreased abundance in samples from TET2-silenced HUVEC compared to siRNA controls. Red numbers show the corresponding signal in each array.*

Perhaps even more relevant to inflammatory contexts than the baseline cytokine release, is the abundance of cytokines released from the endothelium when pro-inflammatory cytokines are encountered. To investigate the role of TET2 in this setting, siRNA control or TET2-silenced HUVEC were treated with IFNα, IFNγ or TNFα and the cytokine assay was performed on their cell culture supernatants (Figure 4.28). Figure 4.28 shows the subset of cytokines upregulated by IFNα (Figure 4.28A), IFNγ (Figure 4.28B), or TNFα (Figure 4.28C) and their relative abundance in control and TET2-silenced samples. IP-10 (CXCL10) and I-TAC (CXCL11) (both of which are T-

lymphocyte chemoattractants that bind to CXCR3) are known to be upregulated by interferon stimulation, particularly IFNγ [280]. Consistent with this, a strong increase in their release upon IFNα or IFNγ treatment was identified (Figure 4.28A & B). Interestingly, in both cases their abundance was greater still in TET2-silenced HUVEC (Figure 4.28A & B). This may suggest that TET2 functions to restrain CXCL10 and CXCL11 production by endothelial cells in response to interferon stimulation. There were no obvious differences in cytokine production between TET2-silenced and control cells treated with TNFα (Figure 4.28C).

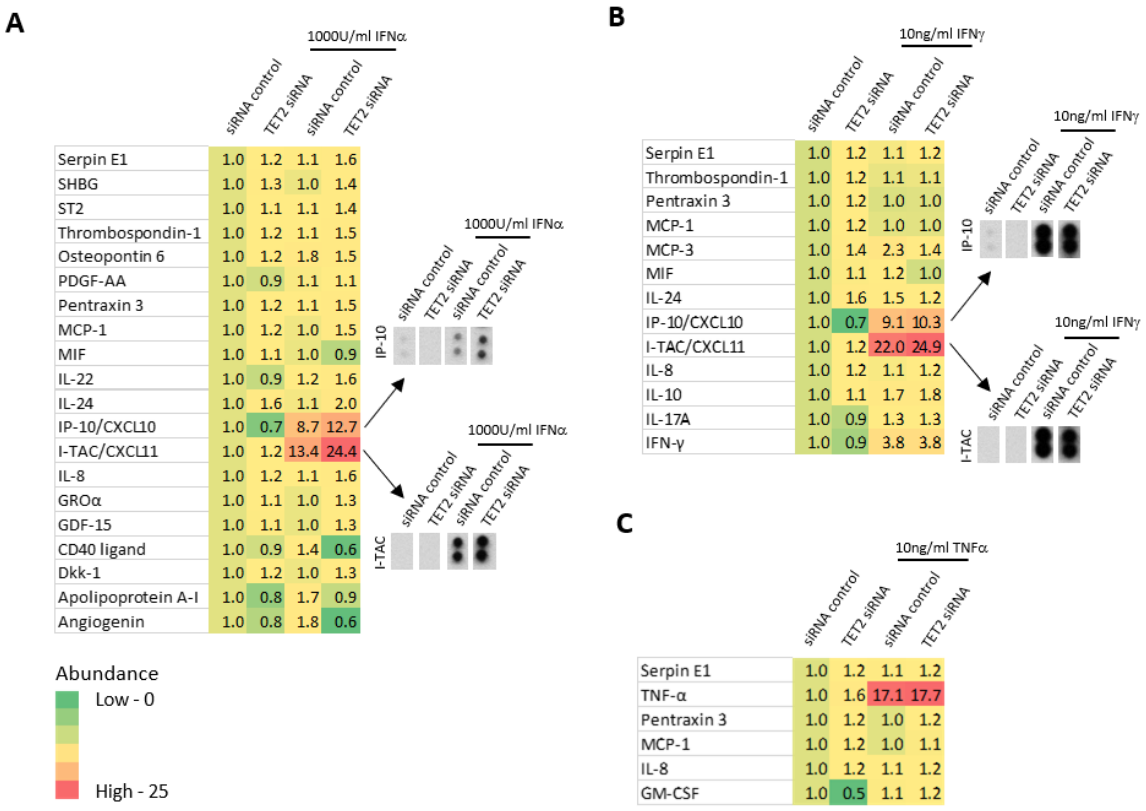

Figure 4.28: ***siRNA-mediated silencing of TET2 affects interferon-stimulated cytokine release by HUVEC.*** *Cell culture supernatants were collected from negative control siRNA-treated or TET2 siRNA-treated HUVEC and cytokine abundance was measured using a Proteome Profiler Human XL Cytokine Array. The signals from each array were quantified by densitometry and the relative cytokine abundance was calculated. Heatmaps show the subset of cytokines upregulated by IFNα (A), IFNγ (B) and TNFα (C) stimulation and their relative abundance in TET2-silenced HUVEC compared to siRNA controls.*

4.2.17 TET2 silencing does not affect leukocyte adhesion to endothelial monolayers under static conditions

It has been previously reported that TET2 silencing increases the adhesion of THP-1 cells (a monocyte-like cell line) to oxidised LDL-activated HUVEC monolayers [164]. It was questioned whether this finding is specific to the oxidised LDL stimulus, or whether leukocyte adhesion to the endothelium in response to other pro-inflammatory stimuli may similarly involve TET2. HL-60 cells (differentiated to a neutrophil-like phenotype) have been previously used in our laboratory as a model for studying TNFα-induced leukocyte recruitment to and across the endothelium [281]. As a preliminary experiment, adhesion of fluorescently-labelled HL-60 cells to HUVEC monolayers was compared in a static adhesion assay following 24h stimulation with TNFα or IFNγ (Figure 4.29). TNFα significantly increased leukocyte adhesion to the HUVEC monolayer by ~4-fold, whereas IFNγ did not affect adhesion (Figure 4.29). Next, the effect of duration of TNFα stimulation on leukocyte adhesion was determined (Figure 4.30). Maximal leukocyte adhesion was evident by 4h, so this time of exposure was used subsequently (Figure 4.30).

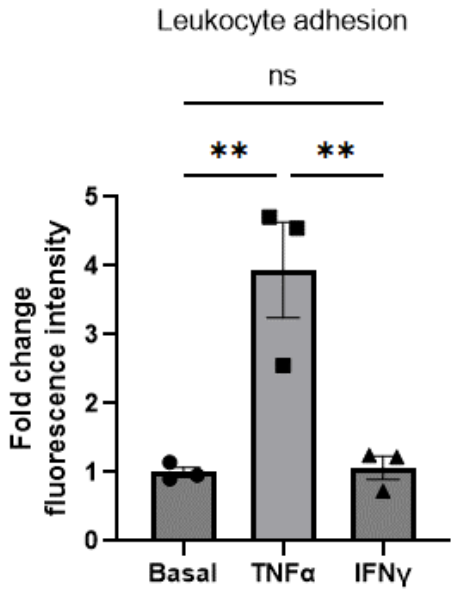

Figure 4.29: ***Adhesion of HL-60 cells to HUVEC monolayers is increased by TNFα but not IFNγ stimulation.*** *HUVEC were grown until monolayers had formed before treatment with 10ng/ml TNFα or 10ng/ml IFNγ for 24h. HL-60 cells differentiated to a neutrophil-like phenotype were fluorescently labelled with LeukoTracker™ and allowed to adhere to the monolayers for 1h. Non-adherent cells were removed by 3 gentle washes with PBS. Cells were lysed and fluorescence intensity (proportional to the number of adherent HL-60 cells) was measured using a fluorimeter. A Shapiro-Wilk test for normality was performed, followed by a one-way ANOVA and post-hoc Tukey's test. Data presented as mean ± SEM. n=3 technical replicates. ** denotes p<0.01.*

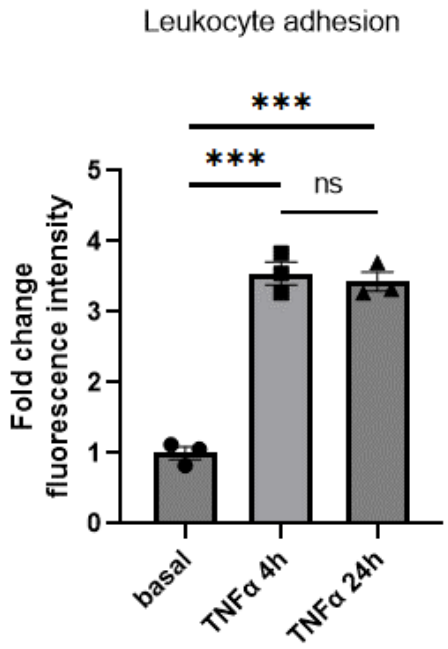

Figure 4.30: ***Adhesion of HL-60 cells to HUVEC monolayers is increased equally by 4h and 24h TNFα stimulation.*** *HUVEC were grown until monolayers had formed before treatment with 10ng/ml TNFα for 4h or 24h. HL-60 cells differentiated to a neutrophil-like phenotype were fluorescently labelled with LeukoTracker™ and allowed to adhere to the monolayers for 1h. Non-adherent cells were removed by 3 gentle washes with PBS. Cells were lysed and fluorescence intensity (proportional to the number of adherent HL-60 cells) was measured using a fluorimeter. A Shapiro-Wilk test for normality was performed, followed by a one-way ANOVA and post-hoc Tukey's test. Data presented as mean ± SEM. n=3 technical replicates. ** denotes p<0.01.*

The static adhesion assay was then conducted to compare the adhesion of HL-60 cells to siRNA control and TET2-silenced HUVEC with or without 4h TNFα treatment (Figure 4.31). TNFα treatment significantly increased leukocyte adhesion as expected (Figure 4.31). Although a slight trend towards increased adhesion was observed for TET2-silenced HUVEC, this was not statistically significant (Figure 4.31). Similarly, no significant difference in leukocyte adhesion was observed for TET2-silenced HUVEC compared to siRNA controls in response to LPS treatment (Figure 4.32). Taken together, these data suggest that TET2 is not involved in the adhesion of neutrophil-like cells to endothelial cells in response to TNFα or LPS under static conditions. Under these conditions, IFNγ alone is not sufficient to induce the adhesion of HL-60 cells to HUVEC.

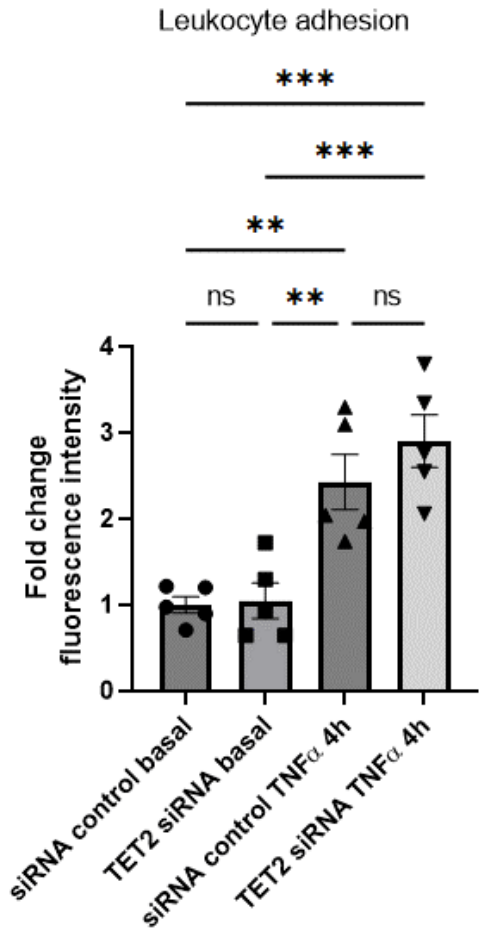

Figure 4.31: ***Basal and TNFα-stimulated adhesion of HL-60 cells to HUVEC monolayers are not altered by silencing of TET2 in HUVEC.*** *HUVEC treated with a negative control siRNA or siRNA targeting TET2 were grown until monolayers had formed before treatment with 10ng/ml TNFα for 4h. HL-60 cells differentiated to a neutrophil-like phenotype were fluorescently labelled with LeukoTracker™ and allowed to adhere to the monolayers for 1h. Non-adherent cells were removed by 3 gentle washes with PBS. Cells were lysed and fluorescence intensity (proportional to the number of adherent HL-60 cells) was measured using a fluorimeter. A Shapiro-Wilk test for normality was performed, followed by a one-way ANOVA and post-hoc Tukey's test. Data presented as mean ± SEM. n=5 independent experiments. ** denotes p<0.01. *** denotes p<0.001.*

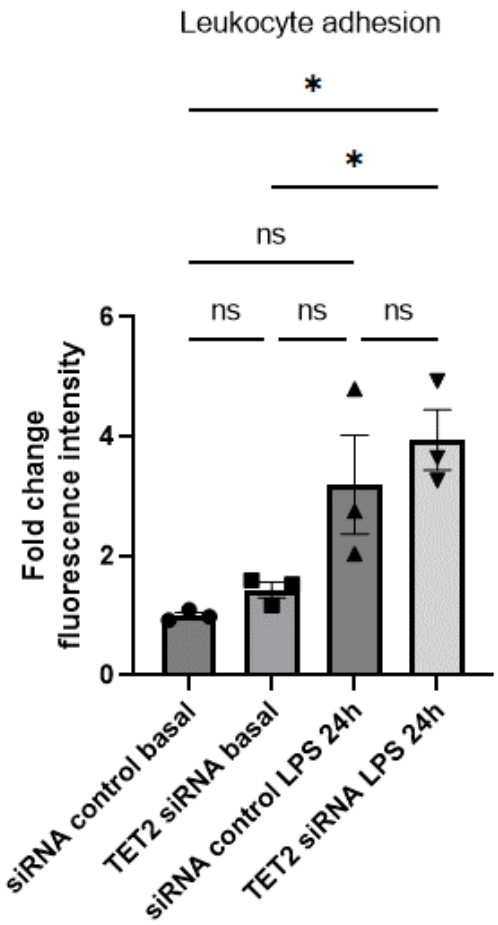

Figure 4.32: ***Basal and LPS-stimulated adhesion of HL-60 cells to HUVEC monolayers is not altered by silencing of TET2 in HUVEC.*** *HUVEC treated with a negative control siRNA or siRNA targeting TET2 were grown until monolayers had formed before treatment with 1μg/ml LPS for 24h. HL-60 cells differentiated to a neutrophil-like phenotype were fluorescently labelled with LeukoTracker™ and allowed to adhere to the monolayers for 1h. Non-adherent cells were removed by 3 gentle washes with PBS. Cells were lysed and fluorescence intensity (proportional to the number of adherent HL-60 cells) was measured using a fluorimeter. A Shapiro-Wilk test for normality was performed, followed by a one-way ANOVA and post-hoc Tukey's test. Data presented as mean ± SEM. n=3 technical replicates. ** denotes p<0.01. *** denotes p<0.001.*

4.2.18 Intermittent high glucose culture of HUVEC does not affect leukocyte adhesion to endothelial monolayers under static conditions

In previous studies, exposure of endothelial cells to either stable or intermittent high glucose concentrations has been shown to augment cytokine-induced upregulation of cell adhesion molecules involved in the recruitment of leukocytes to the endothelium [228, 266, 282-284]. The next experiment tested whether exposure of HUVEC to intermittent high glucose culture for 14 days (varying between high and low glucose every 24h) would increase leukocyte adhesion in the present static adhesion model. In response to TNFα or LPS stimulation, leukocyte adhesion was significantly increased, but no significant difference was identified between intermittent glucose and mannitol-treated cells in these experiments (Figure 4.33).

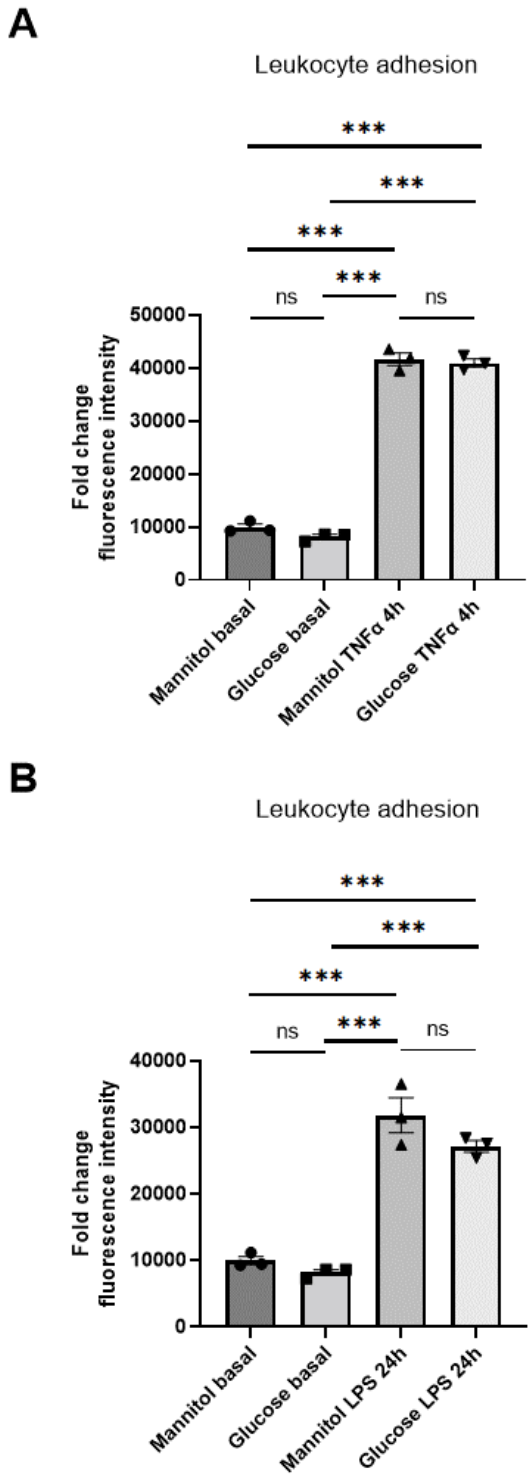

Figure 4.33: ***Basal, TNFα- and LPS-stimulated adhesion of HL-60 cells to HUVEC monolayers are not altered by intermittent high glucose culture of HUVEC.*** *HUVEC were cultured for 14 days in intermittent high glucose or mannitol before treatment with 10ng/ml TNFα for 4h (A) or 1μg/ml LPS for 24h (B). HL-60 cells differentiated to a neutrophil-like phenotype were fluorescently labelled with LeukoTracker™ and allowed to adhere to the monolayers for 1h. Non-adherent cells were removed by 3 gentle washes with PBS. Cells were lysed and fluorescence intensity (proportional to the number of adherent HL-60 cells) was measured using a fluorimeter. A Shapiro-Wilk test for normality was performed, followed by a one-way ANOVA and post-hoc Tukey's test. Data presented as mean ± SEM. n=3 technical replicates. *** denotes p<0.001.*

4.2.19 TET2 silencing has no effect on HUVEC permeability upon IFNγ or LPS stimulation

IFNγ has previously been reported to disrupt endothelial barrier function and increase endothelial permeability [38]. The homeostatic regulation of endothelial barrier integrity is vital for the proper functioning of the vascular network. In a quiescent state, the endothelium actively maintains intercellular junctions (adherens junctions and tight junctions) between adjacent cells to prevent excess plasma leakage and inappropriate extravasation of leukocytes and macromolecules from the blood into underlying tissues [36]. When activated acutely by pro-inflammatory stimuli, junctional reorganisation occurs to increase endothelial permeability transiently to enable transendothelial migration of leukocytes to reach sites of infection [36]. However, in situations of chronic inflammation, a loss of endothelial barrier integrity can occur persistently, causing excessive permeability which can contribute to disease pathogenesis [36]. For example, in atherosclerosis, loss of endothelial barrier function can contribute to intimal accumulation of LDL [285]. Given that data presented here support a role for TET2 in regulating interferon responses and cholesterol levels (see Chapter 3), both of which are associated with alterations of endothelial permeability [38, 286], it is possible that TET2 may be functionally important in modulating endothelial permeability.

Using a transwell permeability assay, the passage of fluorescently-conjugated macromolecules (FITC-dextran and TRITC-BSA) across monolayers of HUVEC were first measured in response to 4h or 24h stimulation with IFNγ (Figure 4.34). The effect of IFNγ on HUVEC permeability was previously shown to be biphasic, with the passage of FITC-conjugated dextran between 3- and 4-fold greater than unstimulated HUVEC at 4h and 24h of 10ng/ml IFNγ stimulation [38]. However, it was seen here that the increase in permeability in response to equivalent stimulation occurred to a much lesser degree (<1.5-fold) (Figure 4.34A-D). Stimulation with LPS has also previously been shown in a similar assay to increase endothelial permeability in a dose-dependent manner [287]. However, at the concentration used in the present study, LPS induced a variable <1.5-fold increase in permeability (Figure 4.34E-H).

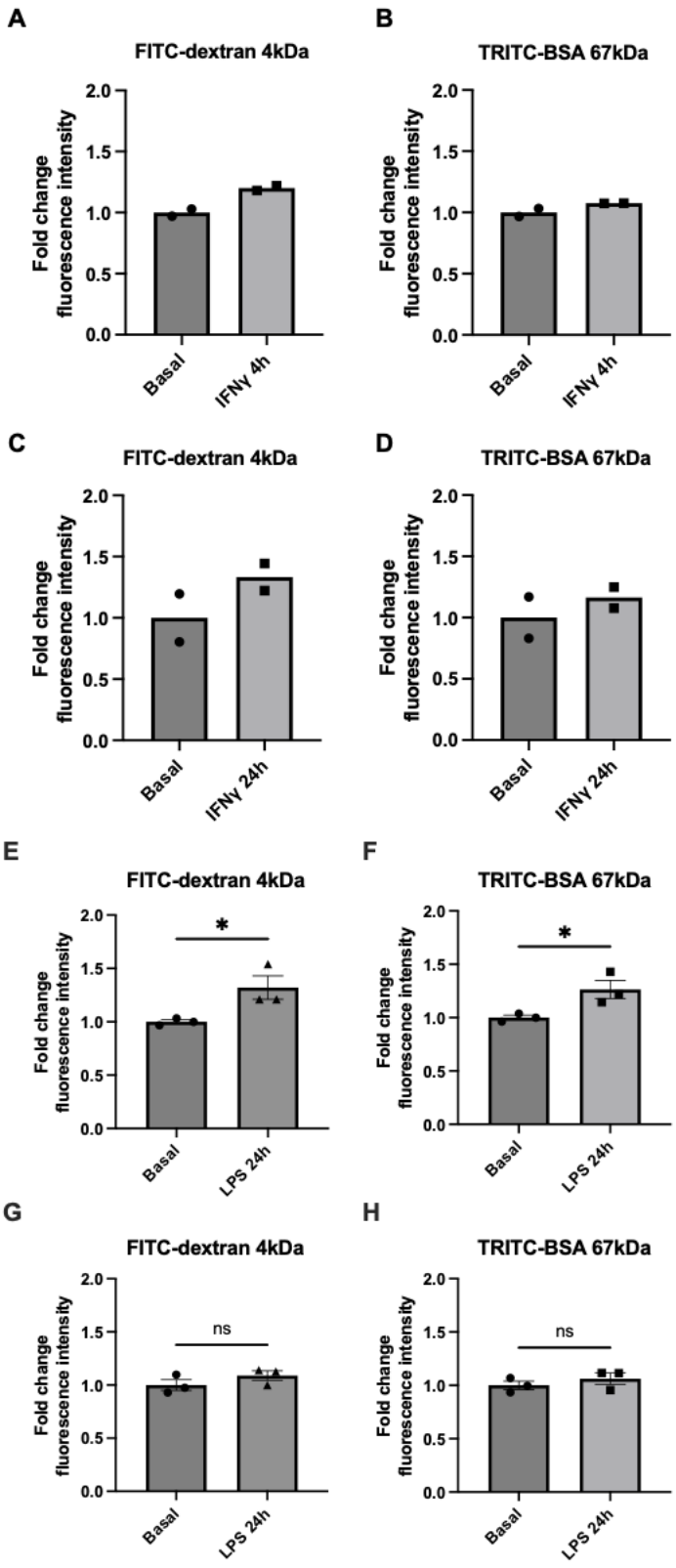

Figure 4.34: ***Permeability of HUVEC monolayers in response to IFNγ or LPS treatment.*** *HUVEC were grown on transwell inserts until monolayers had formed before stimulation with 10ng/ml IFNγ or 1μg/ml LPS. FITC-dextran and TRITC-BSA were applied to the upper chamber and after 1h, media samples from the lower chamber were taken and fluorescence intensity was measured using a fluorimeter. Data presented as individual data points (A-D) or mean ± SEM (E-H). Panels A-D n=2 technical replicates. Panels E-H n=3 technical replicates from two independent experiments (E&F and G&H). For E-H, A Shapiro-Wilk test was performed, followed by a one-way ANOVA with post-hoc Tukey's test. * denotes p<0.05.*

Nonetheless, the transwell permeability assay was performed using 24h IFNγ stimulation to investigate whether the increase in HUVEC permeability was affected by silencing TET2 (Figure 4.35). In this case, IFNγ surprisingly did not increase permeability to FITC-dextran or TRITC-BSA (Figure 4.35). Intriguingly, in unstimulated HUVEC, TET2 silencing caused a slight decrease in permeability of the endothelial monolayer (particularly to FITC-dextran) compared to negative control siRNA-treated HUVEC (Figure 4.35).

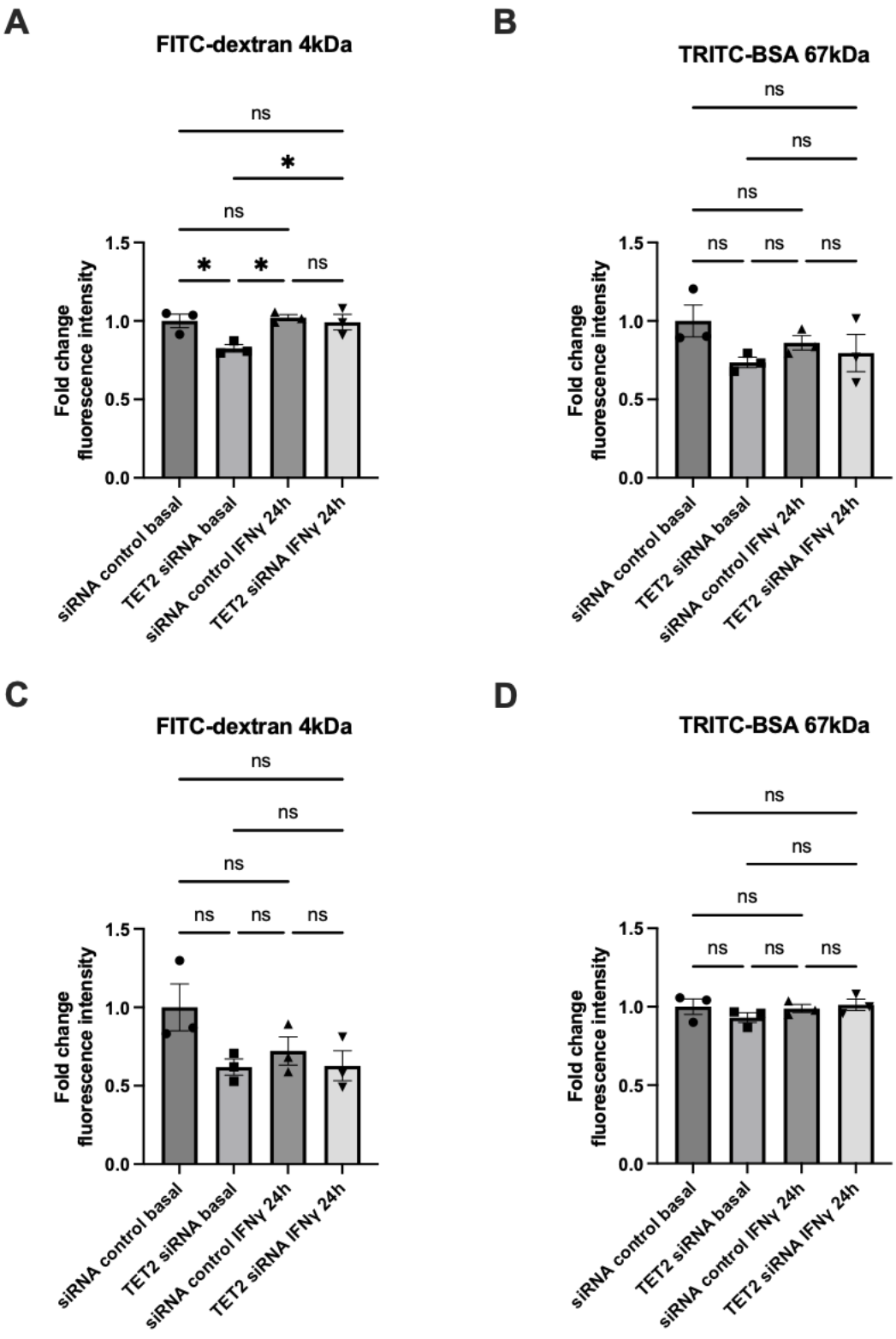

Figure 4.35: ***siRNA-mediated silencing of TET2 in HUVEC monolayers alters basal, but not IFNγ-stimulated permeability.*** *HUVEC were transfected with a negative control siRNA or siRNA targeting TET2 and grown on transwell inserts until monolayers had formed. They were stimulated with 10ng/ml IFNγ for 24h. FITC-dextran and TRITC-BSA were applied to the upper chamber and after 1h, media samples from the lower chamber were taken and fluorescence intensity was measured using a fluorimeter. Data presented as mean ± SEM. n=3 technical replicates from two independent experiments (A&B and C&D). A Shapiro-Wilk test was performed, followed by a one-way ANOVA with post-hoc Tukey's test. * denotes p<0.05.*

The assay was repeated with stimulation for 4h with 10ng/ml TNFα, a cytokine previously used in our laboratory to induce a small but significant increase in HUVEC permeability at this concentration and duration (data not shown). Surprisingly, TNFα produced no effect on permeability in siRNA control HUVEC but did appear to show a trend towards increased permeability of TET2-silenced HUVEC (Figure 4.36). In these experiments, unstimulated TET2-silenced HUVEC again showed a decrease in permeability to FITC-dextran and TRITC-BSA compared to siRNA control HUVEC (Figure 4.36).

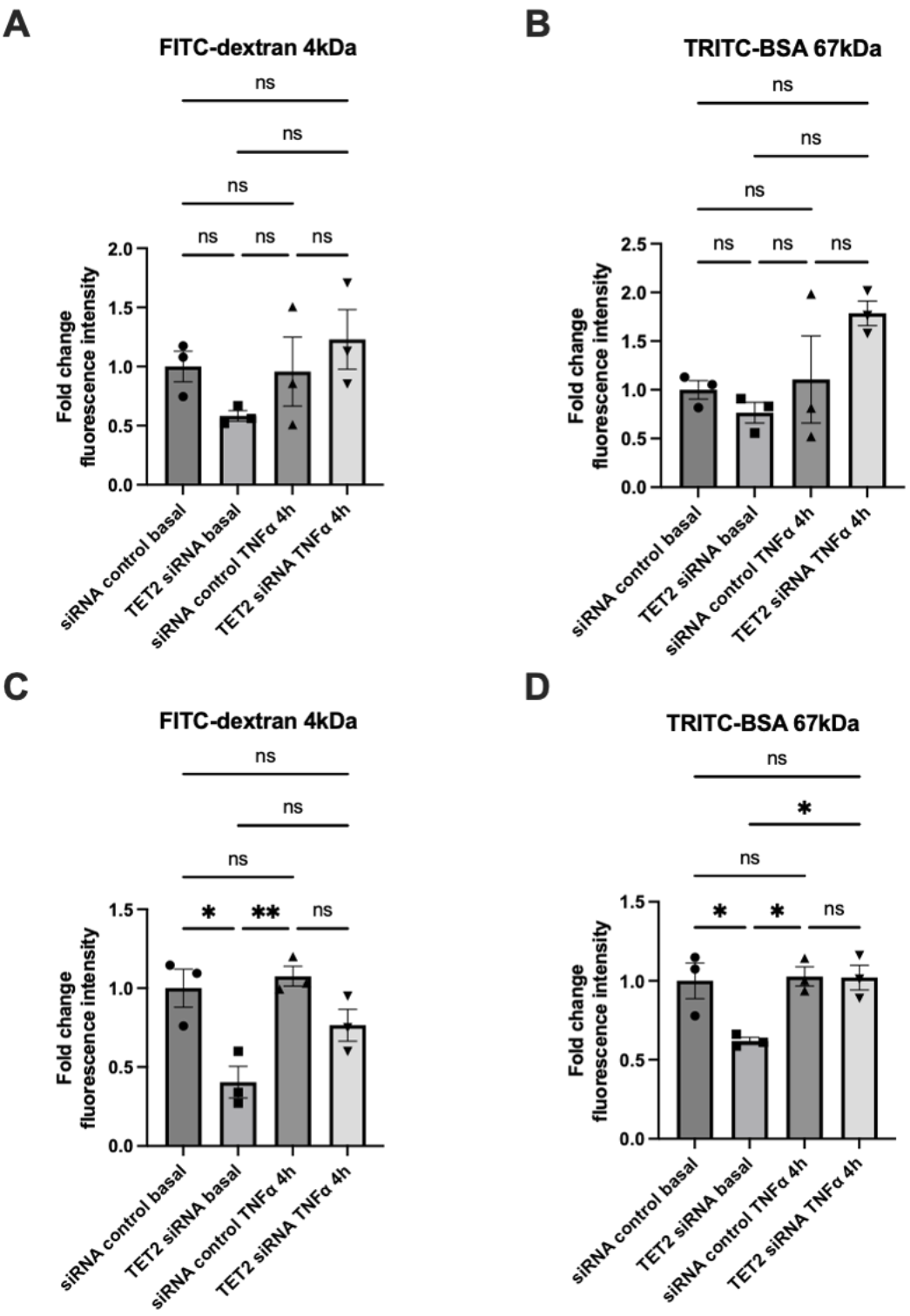

Figure 4.36: ***A trend towards increased permeability of TET2-silenced, but not negative control siRNA-treated HUVEC monolayers upon TNFα treatment.*** *HUVEC were transfected with a negative control siRNA or siRNA targeting TET2 and grown on transwell inserts until monolayers had formed. They were stimulated with 10ng/ml TNFα for 4h. FITC-dextran and TRITC-BSA were applied to the upper chamber and after 1h, media samples from the lower chamber were taken and fluorescence intensity was measured using a fluorimeter. Data presented as mean ± SEM. n=3 technical replicates from two independent experiments (A&B and C&D). A Shapiro-Wilk test was performed, followed by a one-way ANOVA with post-hoc Tukey's test. * denotes p<0.05, ** denotes p<0.01.*

4.2.20 Intermittent high glucose culture has no effect on basal, TNFα- or LPS-stimulated HUVEC permeability

Many of the microvascular complications associated with diabetes mellitus (including diabetic nephropathy, retinopathy and neuropathy) involve perturbation of endothelial barrier function, leading to hyperpermeability [288]. Hyperpermeability of the endothelium also facilitates intimal lipid accumulation in atherosclerosis, so also contributes to macrovascular disease [289]. *In vitro* studies have shown that high glucose culture increases endothelial permeability [268, 290]. The transwell assay described in the previous sections was used to determine whether the 14-day intermittent high glucose culture model would lead to measurable changes in permeability. In this setting, a trend towards increased permeability was observed upon TNFα stimulation and a significant increase in permeability was observed upon LPS stimulation (Figure 4.37). However, no change in permeability was observed between intermittent high glucose and mannitol-treated HUVEC at baseline or following TNFα or LPS stimulation (Figure 4.37).

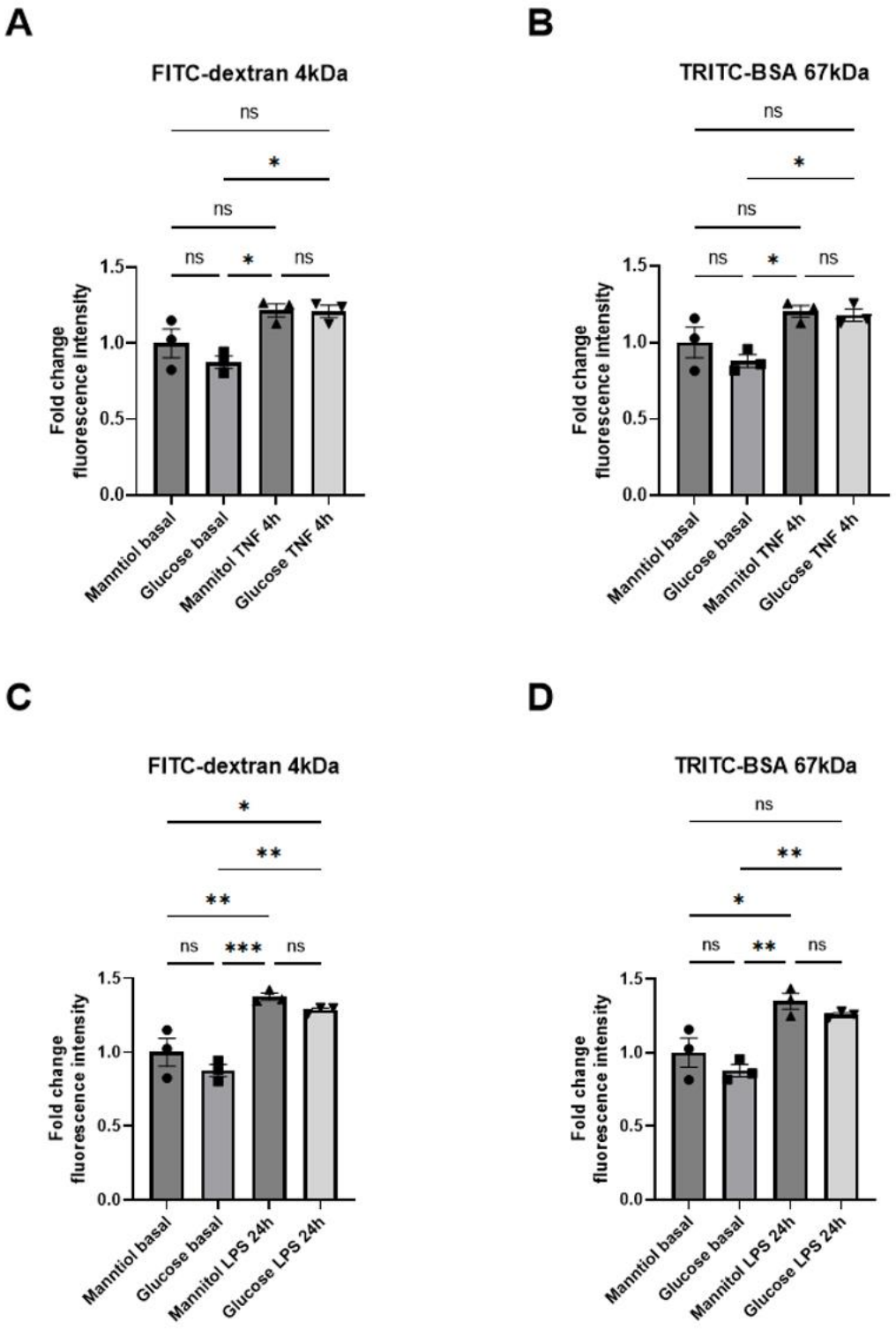

Figure 4.37: ***Intermittent high glucose culture does not affect basal, TNFα or LPS-stimulated endothelial permeability.*** *HUVEC were cultured for 14 days in intermittent high glucose or mannitol and then grown on transwell inserts until monolayers had formed. They were stimulated with 10ng/ml TNFα for 4h (A,B) or 1μg/ml LPS for 24h (C,D). FITC-dextran and TRITC-BSA were applied to the upper chamber and after 1h, media samples from the lower chamber were taken and fluorescence intensity was measured using a fluorimeter. Data presented as mean ± SEM. n=3 technical replicates. A Shapiro-Wilk test was performed, followed by a one-way ANOVA with post-hoc Tukey's test. * denotes p<0.05, ** denotes p<0.01, *** denotes p<0.001.*

4.2.21 siRNA-mediated silencing of TET2, but not TET3, in HUVEC decreases baseline endothelial monolayer permeability

The transwell permeability assay was repeated to confirm changes in permeability of TET2-silenced endothelial monolayers in the absence of cytokine stimulation. Consistently, in each experiment, silencing of TET2 decreased the permeability of endothelial monolayers to FITC-dextran (Figure 4.38). The permeability of HUVEC to the higher molecular weight macromolecule TRITC-BSA was also significantly decreased in one experiment and showed a trend towards decreased permeability in others (Figure 4.38).

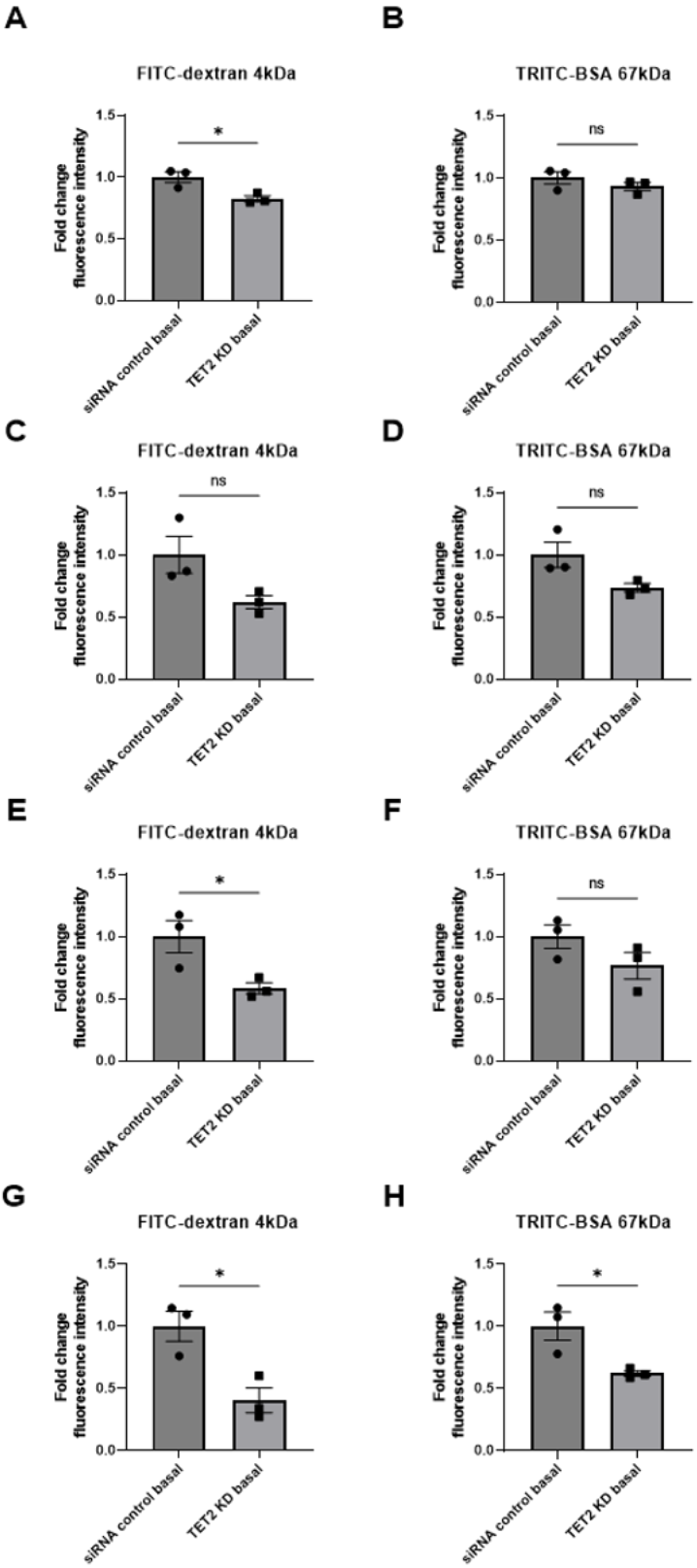

Figure 4.38: ***siRNA-mediated silencing of TET2 decreases basal HUVEC permeability.*** *HUVEC were transfected with a negative control siRNA or siRNA targeting TET2 and grown on transwell inserts until monolayers had formed. FITC-dextran (A, C, E, G) and TRITC-BSA (B, D, F, H) were applied to the upper chamber and after 1h, media samples from the lower chamber were taken and fluorescence intensity was measured using a fluorimeter. Data presented as mean ± SEM from n=3 triplicate samples. Each graph is from one of four independent experiments. A Shapiro-Wilk test was performed, followed by an unpaired t-test. * denotes p<0.05.*

To rule out the possibility that the HUVEC were not complete monolayers, leading to passage of macromolecules across the transwell unimpeded by the presence of endothelial cells in some areas, the polyester membranes were removed from the transwells after the experiment and staining with DAPI and phalloidin-488 was performed (Figure 4.39). This confirmed the presence of a monolayer and showed no obvious morphological differences between siRNA control and TET2-silenced HUVEC (Figure 4.39). Furthermore, an equal number of cells were seeded into transwells for each condition and previous data showed no difference between the viability of siRNA control and TET2-silenced HUVEC (Figure 4.26), so it is unlikely that differences in cell number or viability account for the differences in permeability observed. Taken together, these data suggest that TET2 may be involved in the regulation of endothelial permeability under basal conditions. This effect appears to be specific to TET2, since silencing of TET3 did not affect the permeability of unstimulated HUVEC (Figure 4.40).

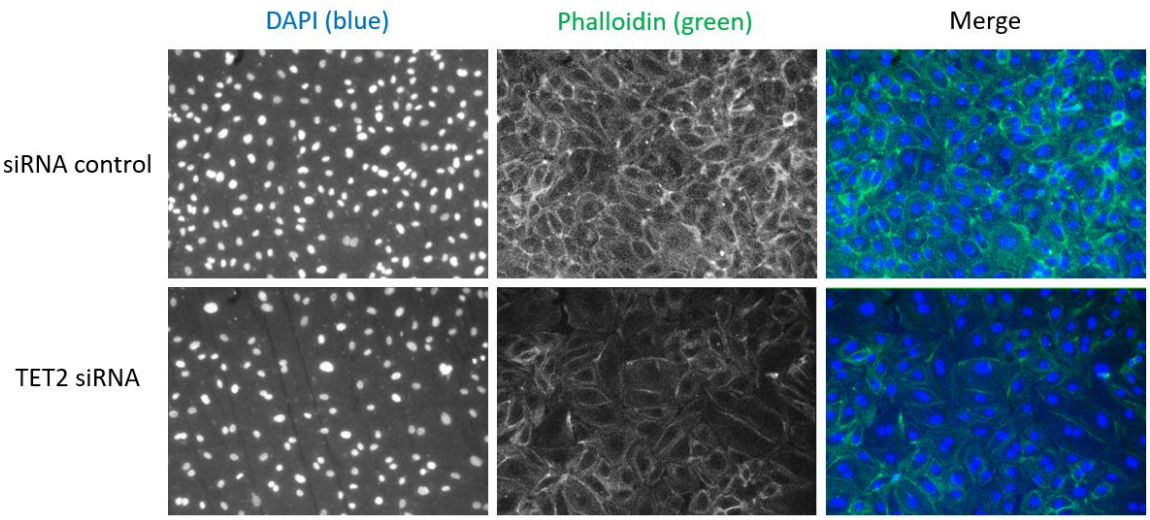

Figure 4.39: ***Confirmation of monolayer formation in siRNA control and TET2-silenced HUVEC.*** *HUVEC were transfected with a negative control siRNA or siRNA targeting TET2 and grown on transwell inserts until monolayers had formed. After permeability assays were performed, transwell polyester membranes were removed and DAPI and phalloidin-488 staining was performed.*

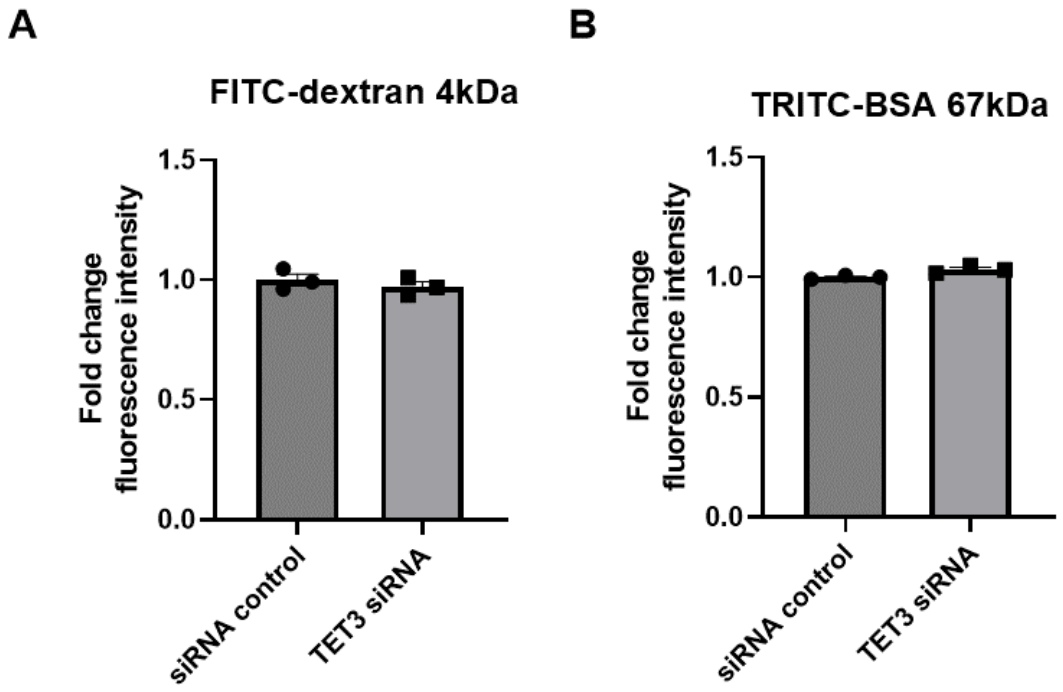

Figure 4.40: ***siRNA-mediated silencing of TET3 does not alter basal HUVEC permeability.*** *HUVEC were transfected with a negative control siRNA or siRNA targeting TET3 and grown on transwell inserts until monolayers had formed. FITC-dextran (A) and TRITC-BSA (B) were applied to the upper chamber and after 1h, media samples from the lower chamber were taken and fluorescence intensity was measured using a fluorimeter. Data presented as mean ± SEM from n=3 triplicate samples.*

4.3 Discussion

4.3.1 Summary of findings

In the first part of this chapter, the potential contribution of catalytic and non-catalytic activities of TET2 in endothelial transcriptional regulation were explored. In support of a catalytic mechanism of regulation, interferon-sensitive genes were upregulated by inhibition of DNA methylation (Figure 4.1). Upstream regulators of interferon-sensitive genes upregulated by TET2 silencing were identified, including IRF7, STAT1 and STAT2 (Figures 4.5, 4.6 & 4.7). IRF7 was identified as being subject to transcriptional regulation by DNA methylation (Figure 4.9) and differential hydroxymethylation of the gene body was identified in the absence of TET2, supporting the possibility of its regulation by TET2 catalytic activity (Figure 4.10). Non-catalytic roles were also explored, as TET2 binding of STAT1, HDAC1 and HDAC2 has previously been shown to be involved in regulating inflammatory responses [158, 197]. STAT1 protein expression was strongly increased by TET2 silencing and pSTAT1 was retained in the nucleus during the resolution of the IFNγ response in TET2-silenced HUVEC, unlike controls (Figure 4.14). This TET2-dependent pSTAT1 localisation may, in part, explain the persistently high expression of interferon-sensitive genes during the resolution phase of the interferon response in the absence of TET2 that was identified in the previous chapter (Figure 3.24). Finally, a correlation was identified between the transcriptional regulation of interferon-sensitive genes by TET2 and HDAC1 and by TET3 and HDAC2, raising the possibility that these classes of epigenetic modifier co-operate in some way to regulate interferon responses in endothelial cells (Figure 4.17).

With respect to transcriptional regulation of cholesterol biosynthesis genes by TET2, it was found that addition of 25-HC (the product of CH25H enzymatic activity) abrogated the increase in cholesterol biosynthesis gene expression in TET2-silenced HUVEC (Figure 4.20). CH25H was shown to be upregulated by pharmacological inhibition of DNMTs, suggesting that it may be regulated by DNA methylation, in

agreement with published data from other cell types (Figure 4.21) [291]. Furthermore, the enrichment of 5hmC in the gene body of CH25H was reduced by TET2 silencing (Figure 4.22). Taken together, this supports the hypothesis that regulation of cholesterol biosynthesis in HUVEC could involve catalytic activity of TET2 acting on CH25H. Consistent with the upregulation of cholesterol biosynthesis genes, intracellular cholesterol levels were increased by TET2 silencing in HUVEC (Figure 4.23). Interestingly, IFNα and IFNγ treatment impacted on free cholesterol levels, supporting the link between interferon signalling and cholesterol metabolism in endothelial cells (Figure 4.24).

In the second part of this chapter, the importance of TET2 for endothelial functions related to inflammation was explored using *in vitro* assays. The data presented here indicate that TET2 is involved in the release of cytokines by endothelial cells, most notably IFNα and IFNγ-stimulated release of CXCL10 and CXCL11, which were more abundant in the supernatants of TET2-silenced HUVEC than that of siRNA control HUVEC (Figure 4.28). Furthermore, these data indicate that TET2 may be involved in the regulation of endothelial permeability, as the passage of macromolecules across unstimulated endothelial monolayers was decreased in the absence of TET2 (Figure 4.38).

4.3.2 Catalytic and non-catalytic roles of TET2

From the data presented here, it is possible that IRF7 and CH25H may be regulated by TET2 catalytic activity, since a loss of 5hmC enrichment was observed in the gene body of IRF7 and CH25H in TET2-silenced HUVEC compared to siRNA controls (Figures 4.10 & 4.22). This is consistent with the prior finding in mouse embryonic stem cells (ESCs) that TET2 regulates 5hmC levels primarily in gene bodies of highly expressed genes (whereas TET1 primarily regulates 5hmC levels at gene promoters) [292]. In addition, TET2 has previously been shown to regulate IRF7 methylation and expression in plasmacytoid dendritic cells, leading to perturbed anti-viral responses [160]. The

deposition of 5hmC within the gene body has previously been both positively and negatively correlated with gene expression in a cell-type specific manner [293]. Therefore, a plausible mechanism of the transcriptional repression of interferon-sensitive genes is that TET2 catalytic activity causes hydroxymethylation of the IRF7 gene body, resulting in its downregulation, which in turn leads to downregulation of interferon-sensitive genes which are regulated by IRF7. Similarly, TET2 catalytic activity acting on the gene body of CH25H could be involved in its transcriptional repression. Alternatively, regulation of CH25H may occur downstream of TET2-dependent regulation of interferon signalling. The data presented here show that CH25H is an interferon-sensitive gene in HUVEC and existing literature demonstrates that CH25H is a direct target of IFN regulation, through the binding of STAT1 to its promoter [237]. Establishing causality between epigenetic modifications and gene expression is challenging and the data presented here do not address whether there is a causal relationship between hydroxymethylation of IRF7 or CH25H and their expression level in HUVEC. Nonetheless, these findings are intriguing and warrant further study.

Unlike IRF7, the upstream regulator STAT1 did not display differential hydroxymethylation in TET2-silenced HUVEC compared to controls (Figure 4.13). However, the intriguing observation was made that the level of pSTAT1 in the nucleus after removal of IFNγ was greater in TET2-silenced than control HUVEC, consistent with the idea that TET2 may be involved in the resolution of interferon responses (Figure 4.14). This preliminary finding raises many questions, such as whether nuclear retention of pSTAT1 is due to a TET2-mediated increase in total STAT1 expression, or a physical interaction with TET2 altering its localisation or preventing its degradation. It would be helpful to confirm that TET2 and STAT1 bind in endothelial cells as shown in other cell types [197], whether this is influenced by tyrosine phosphorylation of STAT1 and investigate whether the two enzymes co-localise at interferon-sensitive gene loci. Given that TET2 does not possess a CXXC DNA-binding domain and relies instead on association with DNA-binding proteins (unlike TET1 and TET3 which do possess a CXXC domain) [294], it is plausible that TET2 may be recruited to interferon-

sensitive gene promoters by an interaction with pSTAT1. At those sites, catalytic or non-catalytic activities of TET2 may be involved in transcriptional repression. One possibility is that repression may involve deacetylation of the genes by HDACs, as it has previously been shown that a complex of HDAC1, HDAC2 and TET2 repress IL-6 [158] and the data here show that silencing HDAC1 produces the same outcome for ISG15 and IFITM1 expression in HUVEC as silencing TET2 does.

4.3.4 Interferon-induced cytokine production is perturbed by silencing TET2 in endothelial cells

Interferon signalling and cholesterol metabolism, alone or in combination, have the potential to impact many endothelial cell functions. For example, interferon pathways are known to trigger the release of various cytokines [217, 218]. Similarly, the expression of cytokines has been shown to involve cholesterol metabolism in some cases, such as IL-10 expression by Th1 cells [295]. Furthermore, cholesterol accumulation can activate the NLRP3 inflammasome, which leads to activation and secretion of IL-1 cytokines [296-298]. Interestingly, TET2 mutations in clonal haematopoiesis have previously been associated with increased NLRP3 inflammasome–mediated IL-1β secretion [157], with relevance to heart failure [206], insulin resistance and obesity [205]. TET2 deficiency has also been associated with decreased production of certain cytokines by Th1 and Th17 cells [299] and increased production of cytokines, including IFNγ, by CD8+ T cells [300].

In HUVEC, it was found that interferon-stimulated release of the T-cell chemo-attractants CXCL10 and CXCL11 were increased by silencing of TET2, indicating that TET2 may act to restrain their production or secretion (Figure 4.28). CXCL10 and CXCL11 are both ligands for CXCR3 and their role in cardiovascular diseases, together with their potential as biomarkers, is increasingly becoming appreciated [301]. In a previous publication, ChIP-sequencing revealed IFNγ-dependent binding of TET2 to the promoter of CXCL10 in THP-1 cells [197]. By contrast to the findings presented

here, the authors showed that IFNγ-induced CXCL10 production was *decreased* in TET2-deficient cells [197], suggesting that TET2 may regulate this cytokine differently in immune cells and endothelial cells.

The results of the cytokine array were somewhat surprising because although TNFα was clearly abundant in the TNFα-treated samples, there was no increase in secretion of cytokines known to be induced by TNFα-activation of endothelial cells, such as Groα (CXCL1) and MCP-1, which are involved in chemoattraction of neutrophils and monocytes (Figure 4.28) [302, 303]. It may be that the duration of TNFα stimulation was not appropriate to observe changes in the abundance of these cytokines, which may occur at specific timepoints of the inflammatory response.

4.3.5 HL-60 cell adhesion to activated endothelial monolayers is not affected by siRNA-mediated silencing of TET2 or intermittent high glucose culture of HUVEC

The data presented here do not support the involvement of endothelial-expressed TET2 in leukocyte adhesion in response to TNFα stimulation of the endothelium (Figure 4.31). This is perhaps unsurprising given that previous data presented in Chapter 3 showed that TET2-silencing did not significantly alter TNFα-stimulated expression of E-selectin, ICAM-1 or VCAM-1 in HUVEC (Figure 3.28). In addition, TNFα-stimulated cytokine production was not affected by TET2 silencing (Figure 4.28). Although it was intended to explore IFNγ-mediated leukocyte adhesion, this stimulus did not increase HL-60 adhesion to the endothelium under the conditions tested (Figure 4.29). This is again perhaps unsurprising, as it has previously been published that IFNγ alone is insufficient to induce leukocyte adhesion, but instead requires co-activation of the NFκB pathway [304]. Therefore, it may be beneficial to explore the synergistic effects of TNFα and IFNγ stimulation on leukocyte adhesion to HUVEC. Furthermore, as the endothelial-released cytokines with altered abundance upon TET2 silencing were CXCL10 and CXCL11 which are T cell chemoattractants, it may be interesting to investigate the recruitment of T cells to (and across) control and TET2-

silenced HUVEC monolayers, where the absence of TET2 may be functionally more important than for recruitment of the HL-60 neutrophil-like cell line.

Although previous literature suggests that stable or intermittent high glucose culture upregulates cell adhesion molecules and promotes leukocyte-endothelial interactions [228, 266, 282-284], an increase in TNFα- or LPS-induced HL-60 adhesion to HUVEC following intermittent high glucose culture was not observed here (Figure 4.33). It is unclear whether this is due to the lack of upregulation of relevant cell adhesion molecules, or because the sensitivity of the assay used in this study is not sufficient to detect subtle differences in leukocyte recruitment. Limitations of the assay include that it was conducted under static conditions and no distinguishment was made between leukocytes that were adhered to the apical surface of the endothelium and those that had undergone transendothelial migration. In future, the physiological setting could be more accurately modelled by applying shear stress, and more detail about the dynamics of leukocyte recruitment could be obtained by quantifying the number of adherent and transmigrated leukocytes, and assessing which stage, if any, is affected by TET2 activity or high glucose concentrations.

4.3.6 TET2 may be involved in the regulation of endothelial permeability

The data here demonstrate that silencing of TET2, but not TET3, decreases HUVEC permeability in the absence of any cytokines (Figures 4.38 & 4.40). It was surprising that LPS and IFNγ treatment did not increase HUVEC permeability to the extent expected from existing literature (Figure 4.34) [38, 287] and that high glucose culture did not act here to increase endothelial permeability as has been reported previously (Figure 4.37) [268, 290]. In addition, the small increase in IFNγ-induced permeability that was observed in non-transfected HUVEC was not evident in transfected HUVEC (Figures 4.34 & 4.35). This could be explained by the activation of the interferon response by transfection itself, as discussed in chapter 3. This methodological limitation prevented the assessment of the potential involvement of TET2 in the

dynamic regulation of endothelial permeability during interferon responses, which may be interesting to pursue in subsequent studies. Since the previous findings showing that high glucose affects permeability were not replicated here (Figure 4.37) [268, 290], it was not possible to assess any contribution of dysregulation of TET2 to high glucose-induced hyperpermeability. Nonetheless, the data presented here are promising, demonstrating the functional importance of TET2 activity for regulating endothelial permeability to macromolecules under baseline conditions. In future studies, transendothelial electrical resistance (TEER) could be used to provide an additional quantitative measure of endothelial barrier integrity [305]. TEER uses electrodes to determine the electrical resistance across the endothelial monolayer, so acts as a measure of the flow of small inorganic molecules, as opposed to the passage of macromolecules which has been investigated here [305].

In summary, the data presented in this chapter provide insight into the potential catalytic and non-catalytic involvement of TET2 in the transcriptional regulation of interferon responses and cholesterol biosynthesis in endothelial cells. *In vitro* functional assays suggest that perturbation of these pathways in endothelial cells leads to disruption of interferon-induced cytokine release and baseline endothelial permeability, confirming the functional importance of TET2 in endothelial cells.

5. Results 3: The effect of endothelial-specific TET2 knockout on the vascular function of diabetic mice *in vivo*.

5.1 Introduction

In the preceding chapters, the importance of TET2 to endothelial cell transcriptional regulation and function has been explored *in vitro*. This revealed roles for TET2 in regulating interferon signalling and cholesterol homeostasis, with impacts on endothelial cytokine release and permeability. The effect of high glucose culture on endothelial cell transcription and function was also explored. The response of HUVEC to IFNγ was perturbed by intermittent high glucose culture in a similar manner to when TET2 was silenced. However, many of the other findings regarding the effects of high glucose culture on endothelial cells did not reproduce previously published data.

Existing literature has shown that peripheral blood mononuclear cells from diabetic patients have decreased levels of 5hmC, associated with perturbed TET2 activity in hyperglycaemia due to impaired AMPK-mediated phosphorylation and stabilisation of the TET2 protein [183]. This, combined with the requirement of TETs for O_2, Fe^{2+} and 2-oxoglutarate, the levels of which may be altered in hyperglycaemia [173], led to the hypothesis that TET2 may act as a cellular sensor of hyperglycaemia, altering the epigenetic and transcriptional landscape of cells in this context. By nature of their position, endothelial cells are particularly susceptible to changing blood glucose levels and hyperglycaemia is known to initiate endothelial dysfunction [9-12, 16, 67]. Therefore, it was hypothesised that endothelial dysfunction in diabetes may involve hyperglycaemia-induced dysregulation of TET2 activity in endothelial cells. In this chapter, the importance of endothelial-expressed TET2 to vascular function *in vivo* is explored in the context of diabetes by generating and characterising endothelial-specific TET2 knockout mice in normoglycaemic and hyperglycaemic conditions.

5.1.1 Aim

A hallmark of endothelial dysfunction is impaired endothelium-dependent vasodilation. Therefore, a key aim of this study was to determine whether vascular reactivity of control or diabetic mice was altered by the endothelial-specific deletion of TET2. In addition, the transcriptome of endothelial cells isolated from these mice was characterised and plasma cytokines were measured to determine whether other characteristics of endothelial dysfunction (such as a pro-inflammatory or pro-thrombotic phenotype) were evident in the diabetic mice. Comparisons were made to assess whether the any of the changes observed in the diabetic model were recapitulated in the endothelial-specific TET2 knockout mice, which could support a role for dysregulation of TET2 in hyperglycaemia-induced endothelial dysfunction.

5.2 Results

5.2.1 Body weights of WT and endothelial-specific TET2 KO mice fed a standard chow or high fat diet for 10 or 20 weeks

Endothelial-specific TET2 "knockout" mice (TET2 endo KO) were generated by crossing $TET2^{fl/fl}$ mice [149] to tamoxifen-inducible, endothelial-specific Cre-expressing mice (Cdh5-CreERT2) [207]. Male Cre^{+ve} $TET2^{fl/fl}$ mice and their male Cre^{-ve} $TET2^{fl/fl}$ littermates (as controls) were injected with tamoxifen at 6-8 weeks of age before 10 or 20 weeks of either continuation of a standard chow diet (13.6% kcal from fat) or beginning a high fat diet (HFD) (60% kcal from fat) to induce a diabetic phenotype. The body weight of Cre^{-ve} $TET2^{fl/fl}$ ("wildtype" (WT)) HFD-fed mice was significantly higher than that of WT chow-fed mice after 8 weeks (Figure 5.1), but for TET2 endo KO mice, the difference in body weights between chow-fed and HFD-fed mice was first statistically significant after 16 weeks on the diet (Figure 5.1). However, no significant difference in body weight was observed between TET2 endo KO mice and WT mice in either the chow-fed or HFD-fed groups at any timepoint.

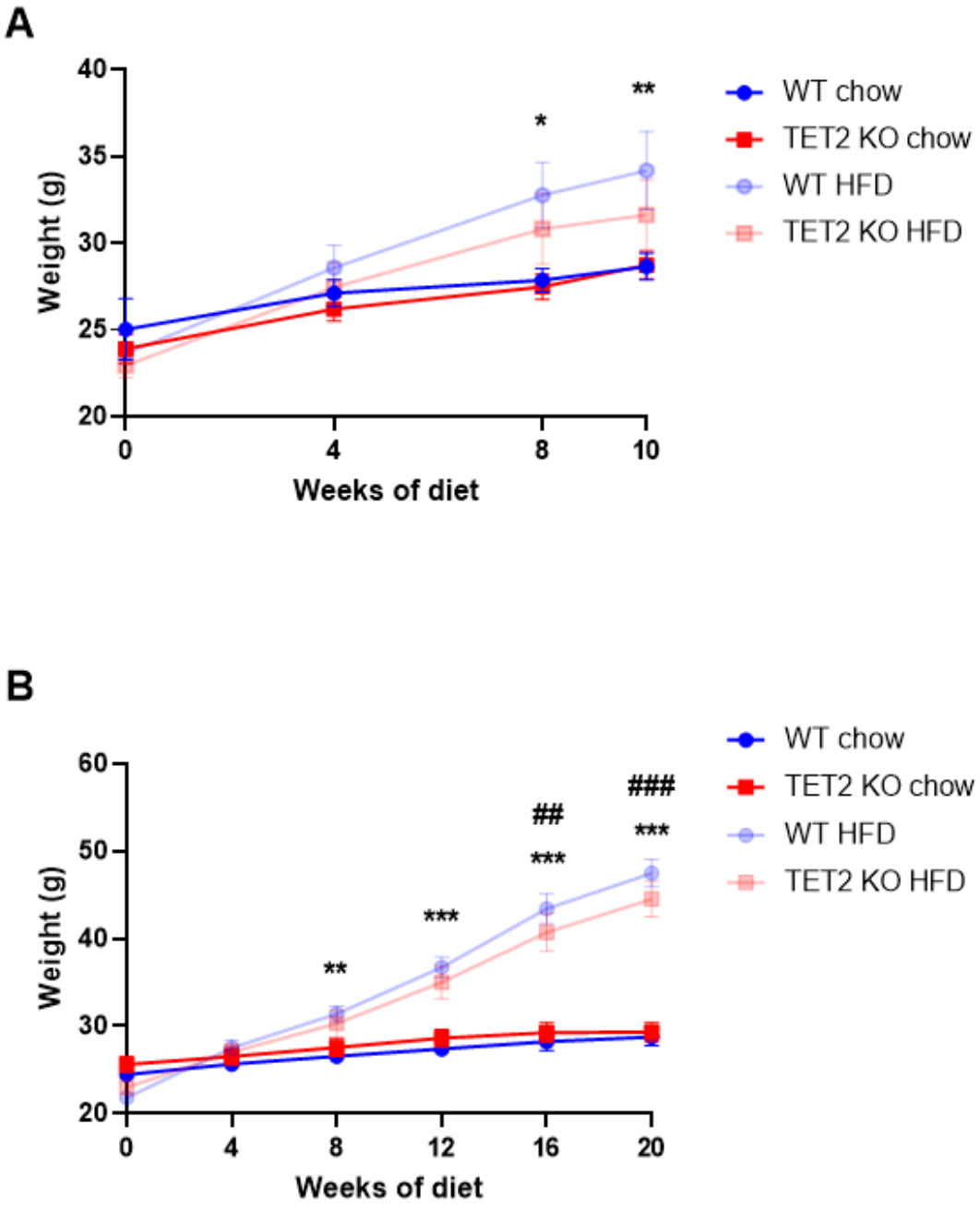

Figure 5.1: ***Body weight of WT and endothelial-specific TET2 KO mice during high fat diet feeding.*** *Male TET2$^{fl/fl}$ CDH5-CreERT2 Cre^{-ve} (WT) and Cre^{+ve} (TET2 KO) C57Bl/6J mice were weighed one week after tamoxifen injection (0 weeks) and at the indicated timepoints during standard chow diet or high fat diet (HFD) feeding ad libitum for 10 weeks n=8-11 per group (A) or 20 weeks n=8 per group (B). Data presented as mean ± SEM. A Shapiro-Wilk test for normality was conducted, followed by a one-way ANOVA and post-hoc Tukey's test comparing the four groups at each timepoint. * (p<0.05), ** (p<0.01) and *** (p<0.001) denote a statistically significant difference between WT chow and WT HFD groups. ## (p<0.01) and ### (p<0.001) denote a statistically significant difference between TET2 KO chow and TET2 KO HFD groups.*

5.2.2 HFD feeding of WT and endothelial-specific TET2 KO mice impairs glucose tolerance by 9 weeks

To confirm that the HFD induced a diabetic phenotype, a glucose tolerance test was performed after 9 weeks of standard chow or HFD feeding to monitor blood glucose concentrations before and in the 2h following intraperitoneal injection of 2mg/g D-glucose (Figure 5.2A). This confirmed that by 9 weeks, HFD-fed mice had significantly impaired glucose tolerance compared to standard chow-fed mice. Upon intraperitoneal administration of glucose, blood glucose concentrations increased to a greater extent in HFD-fed groups and failed to return to baseline levels after 2h, unlike chow-fed mice, leading to an increased area under the curve (Figure 5.2A & B). No significant difference in glucose tolerance was observed between WT and TET2 endo KO mice in either diet group. The fasting blood glucose concentration was not significantly different in the chow and HFD groups after a 4h fast, although a trend towards increased fasting blood glucose was observed in the HFD-fed groups compared to the chow-fed groups (Figure 5.2B).

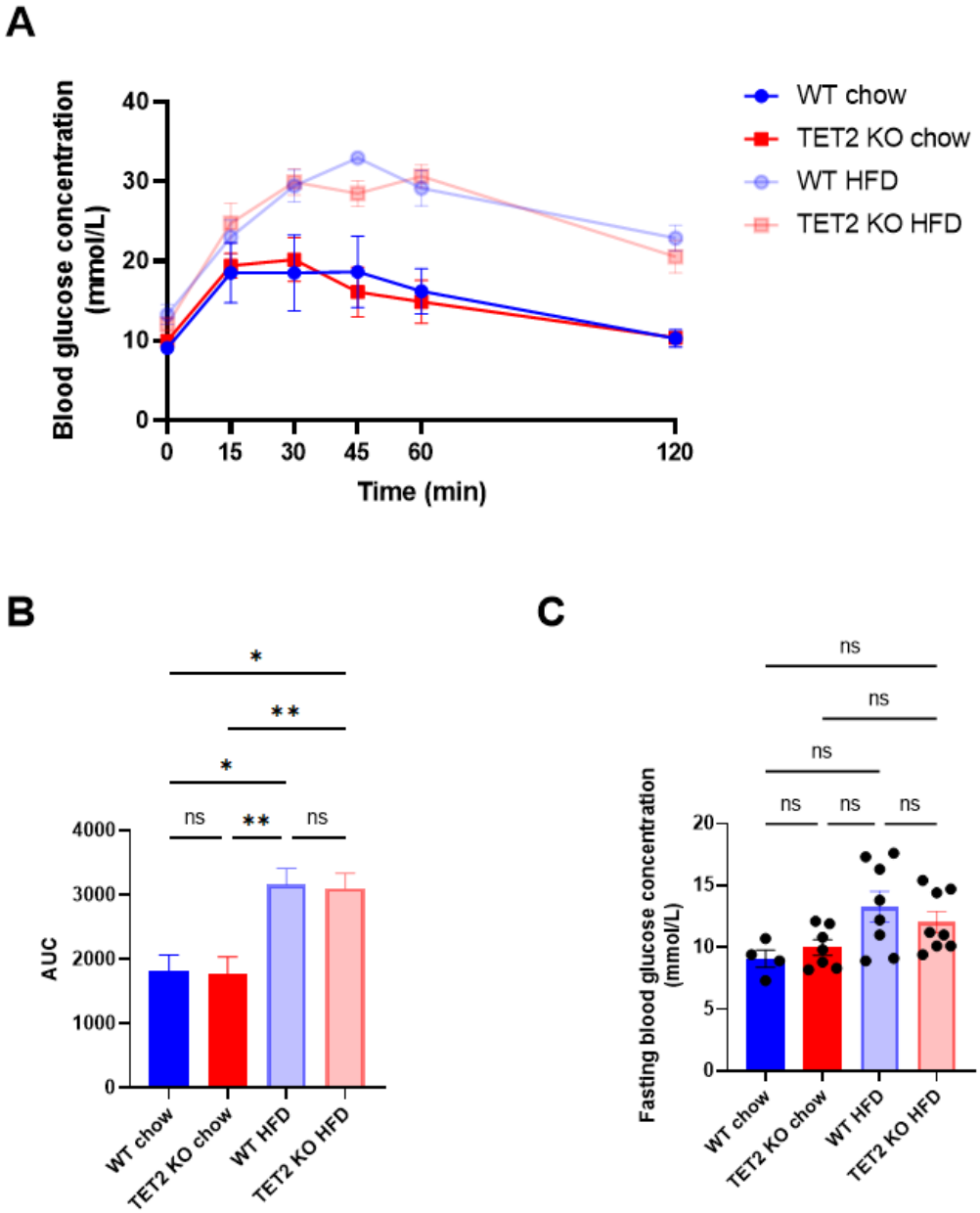

Figure 5.2: ***High fat diet impairs glucose tolerance in WT and endothelial-specific TET2 KO mice.*** *A) Glucose tolerance test performed on male TET2$^{fl/fl}$ CDH5-CreERT2 Cre^{-ve} (WT) and Cre^{+ve} (TET2 KO) tamoxifen-injected C57Bl/6J mice after 9 weeks of standard chow diet or high fat diet (HFD) feeding ad libitum for 9 weeks. Mice were fasted for 4h. Blood glucose was measured at baseline and 15, 30, 45, 60 and 120 minutes following intraperitoneal D-glucose administration (2mg/g). B) Area under the curve (AUC) of glucose tolerance test. C) Fasting blood glucose concentrations of WT and TET2 KO mice after 4h fasting. Data presented as mean ± SEM from n=4-8 per group. A Shapiro-Wilk test for normality was conducted, followed by a one-way ANOVA and post-hoc Tukey's test. * denotes p<0.05, ** denotes p<0.01.*

5.2.3 No difference in vascular reactivity after 10 weeks of HFD feeding in WT and endothelial-specific TET2 KO mice

Having confirmed that the HFD induced hyperglycaemia by 9 weeks, a study of vascular reactivity in response to vasoconstrictor and vasodilator stimuli *ex vivo* was conducted. The aim was to investigate whether the hyperglycaemic conditions had impaired vascular function and whether this was worsened by the absence of endothelial TET2. To do this, aortae were isolated from the WT and TET2 endo KO mice after 10 or 20 weeks of chow or HFD feeding and aortic sections were mounted onto parallel wires in an organ bath filled with oxygenated Kreb's solution, connected to PowerLab apparatus to enable measurement of vessel tension under isometric conditions. Aortic sections were treated with agonists to assess vasoconstrictor and vasodilatory responses (Figures 5.3 & 5.4). From existing literature, it was expected that endothelium-dependent vasodilation would be impaired and that vasoconstrictor responses would be increased in HFD-fed mice compared to chow-fed controls [15].

First, vessels were pre-constricted with a submaximal dose of phenylephrine ($3x10^{-9}$M) before application of increasing concentrations of acetylcholine from 10^{-9} to 10^{-5}M (Figure 5.3A). Phenylephrine is an α1-adrenergic receptor agonist which is known to induce contraction of vascular smooth muscle cells *via* phospholipase C-mediated IP_3 production and Ca^{2+} mobilisation [306]. Acetylcholine induces vasodilation in an endothelium-dependent manner by binding to muscarinic cholinergic receptors on endothelial cells, triggering downstream production of nitric oxide and other vasodilators such as prostacyclin and endothelium-derived hyperpolarising factor (EDHF) [20]. After 10 weeks of HFD feeding, no difference in acetylcholine-mediated vasodilation of the aortic sections was observed between chow-fed and HFD-fed mice or between WT or TET2 endo KO mice, indicating that their endothelium-dependent vasodilator function was equivalent (Figure 5.3A & B).

To assess any differences in vasoconstrictor responses, a dose-response curve was generated by applying increasing doses of phenylephrine from 10^{-9} to 10^{-5}M (Figure 5.3C). This revealed no difference in phenylephrine-mediated vasoconstriction

between diet groups after 10 weeks or between genotypes (Figure 5.3C & D). Finally, to ascertain whether the groups displayed different vascular smooth muscle relaxation responses, vessels were pre-constricted with $3x10^{-7}$M phenylephrine followed by application of increasing doses of sodium nitroprusside (SNP) from 10^{-11} to 10^{-5}M (Figure 5.3E). SNP directly activates soluble guanylyl cyclase in smooth muscle cells, bypassing the reliance on eNOS-driven NO production for relaxation. A difference in smooth muscle cell-dependent relaxation was not anticipated as a result of the TET2 endo KO, since the knockout is specific to the endothelium, and indeed no difference between genotypes was observed. Neither was there any difference in SNP-mediated relaxation between the two diet groups at this timepoint (Figure 5.3E & F).

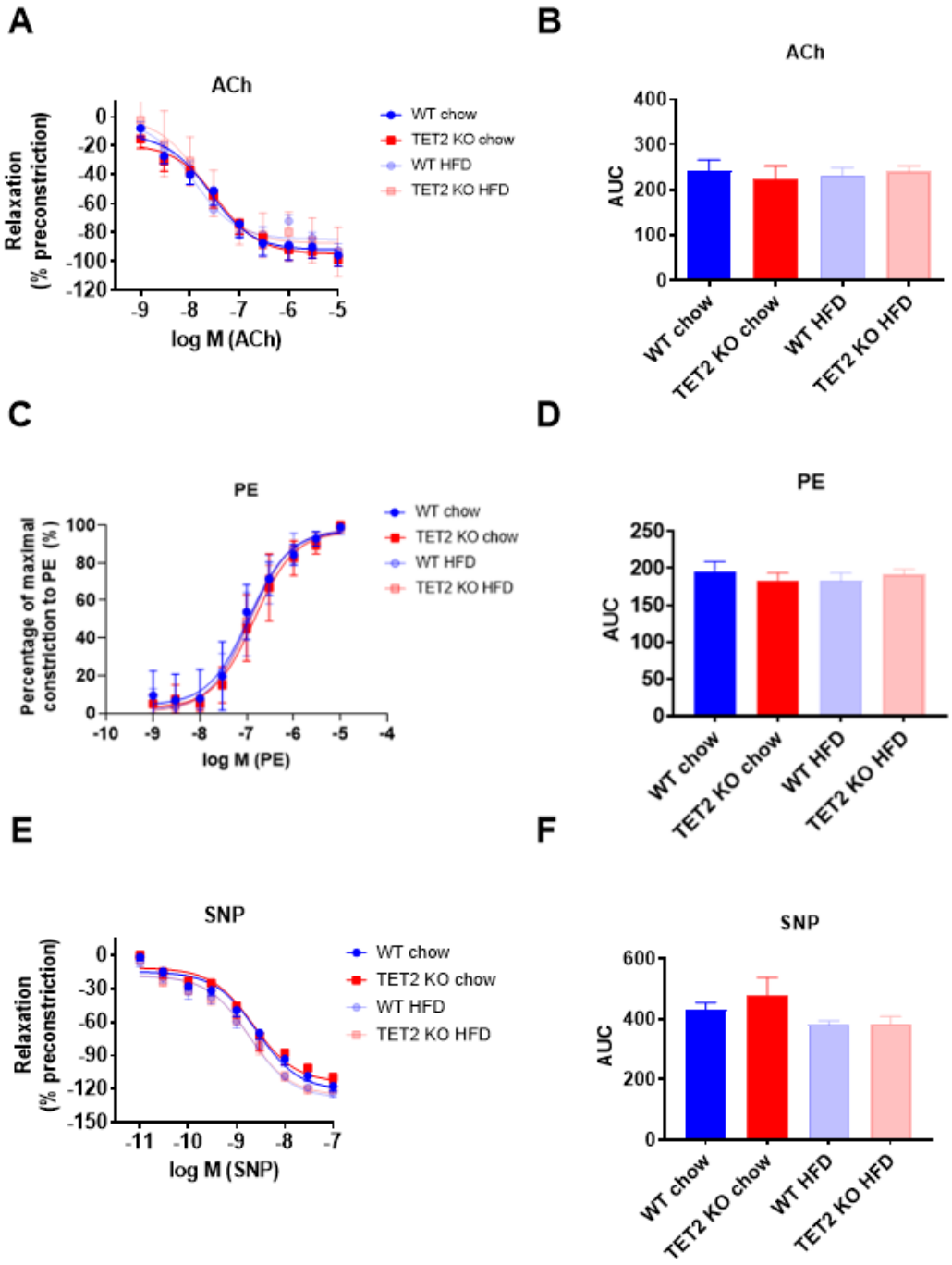

Figure 5.3: ***10 weeks of high fat diet feeding does not alter vascular reactivity in WT or TET2 KO mice.*** *Aortae were isolated from male TET2$^{fl/fl}$ CDH5-CreERT2 Cre^{-ve} (WT) and Cre^{+ve} (TET2 KO) tamoxifen-injected C57Bl/6J mice after standard chow or high fat diet (HFD) feeding ad libitum for 10 weeks. Aortic sections were suspended in organ bath chambers and dose response curves were generated for acetylcholine (ACh) (A), phenylephrine (PE) (C) and sodium nitroprusside (SNP) (E). Area under the curve (AUC) for each dose-response was calculated (B, D, F) and a one-way ANOVA was performed which showed no significant difference between groups. Data presented as mean ± SEM from n=5-9 per group.*

5.2.4 Increased SNP-mediated vasorelaxation in endothelial-specific TET2 KO mice after 20 weeks of HFD feeding

Reasoning that vascular dysfunction develops with age [307] and that an increased duration of exposure to hyperglycaemia and/or TET2 endo KO may worsen vascular function, the same measurements were performed in a second cohort at a later timepoint of 20 weeks of HFD feeding (Figure 5.4). Surprisingly, aortae from HFD-fed mice responded to acetylcholine with a slightly greater extent of vasorelaxation than chow-fed controls (Figure 5.4A), although the difference in area under the curve was not statistically significant (Figure 5.4B) and neither was the pEC50 (a measure of sensitivity to the agonist) or maximal relaxation (Figure 5.5A & B). Similarly, no difference in the sensitivity to phenylephrine-induced constriction was observed between the four groups (Figures 5.4C & D, 5.5C). Comparing the maximal response to phenylephrine, HFD-fed TET2 endo KO mice had a significantly decreased response compared to WT chow-fed mice (Figure 5.5D). Surprisingly, SNP-mediated vasorelaxation was also increased in the HFD group compared to the chow-fed controls (Figure 5.4E & F). This was particularly noticeable in the TET2 endo KO groups. A significant reduction in the area under the curve was observed in TET2 endo KO mice upon HFD feeding, which was not apparent in the WT group (Figure 5.4E). In addition, a significantly higher maximal response to SNP was observed in the TET2 endo KO compared to WT mice fed a HFD, whereas there was no difference between the groups in chow-fed mice (Figure 5.5F). This could indicate that differences in the vascular relaxation of these mice may be due to changes in smooth muscle function or release of endothelial-derived vasodilators other than nitric oxide (such as prostacyclin or EDHF), rather than eNOS-driven NO production.

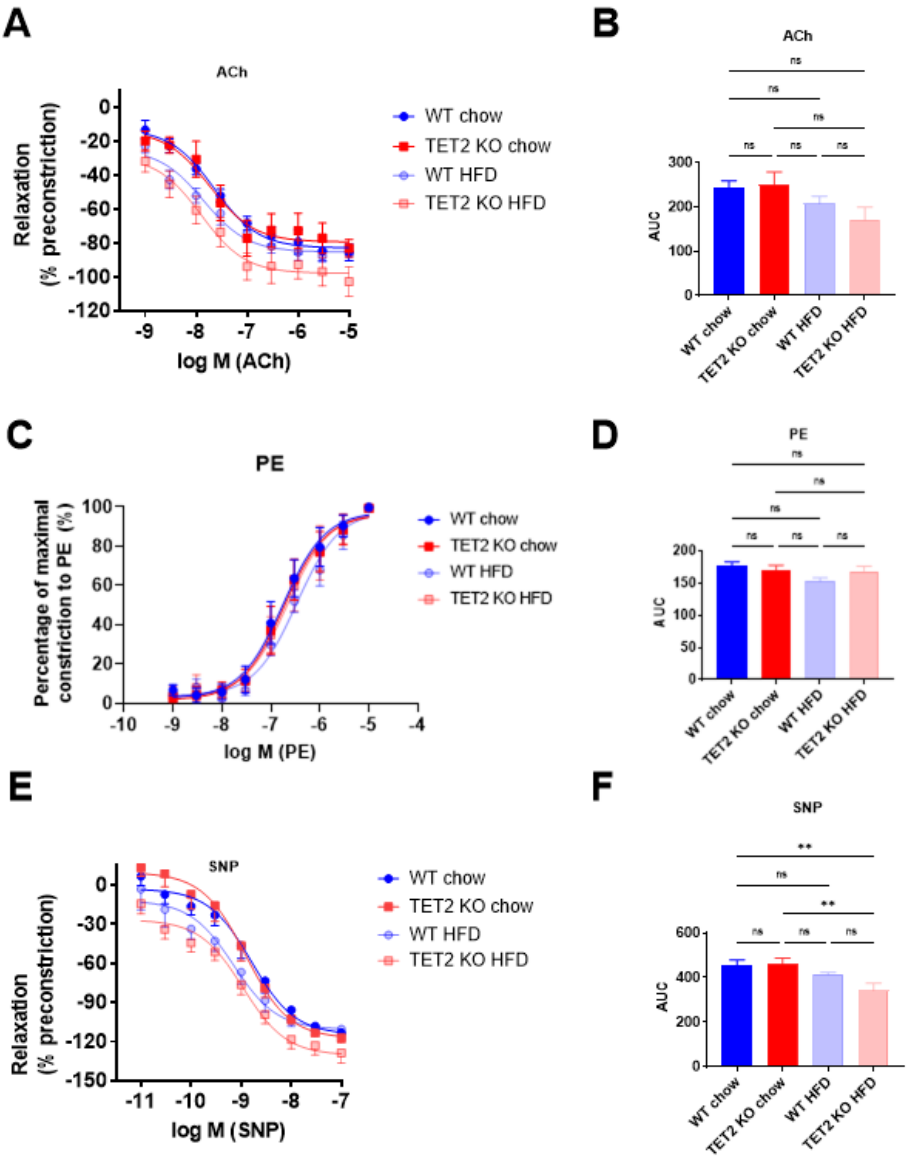

Figure 5.4: ***20 weeks of high fat diet feeding increases SNP-mediated vasorelaxation in TET2 KO mice.*** *Aortae were isolated from male TET2$^{fl/fl}$ CDH5-CreERT2 Cre^{-ve} (WT) and Cre^{+ve} (TET2 KO) tamoxifen-injected C57Bl/6J mice after standard chow or high fat diet (HFD) feeding ad libitum for 20 weeks. Aortic sections were suspended in organ bath chambers and dose response curves were generated for acetylcholine (ACh) (A), phenylephrine (PE) (C) and sodium nitroprusside (SNP) (E). Area under the curve (AUC) for each dose-response was calculated (B, D, F) and a one-way ANOVA with post-hoc Tukey's test was performed. ** denotes p<0.01. Data presented as mean ± SEM from n=8 per group.*

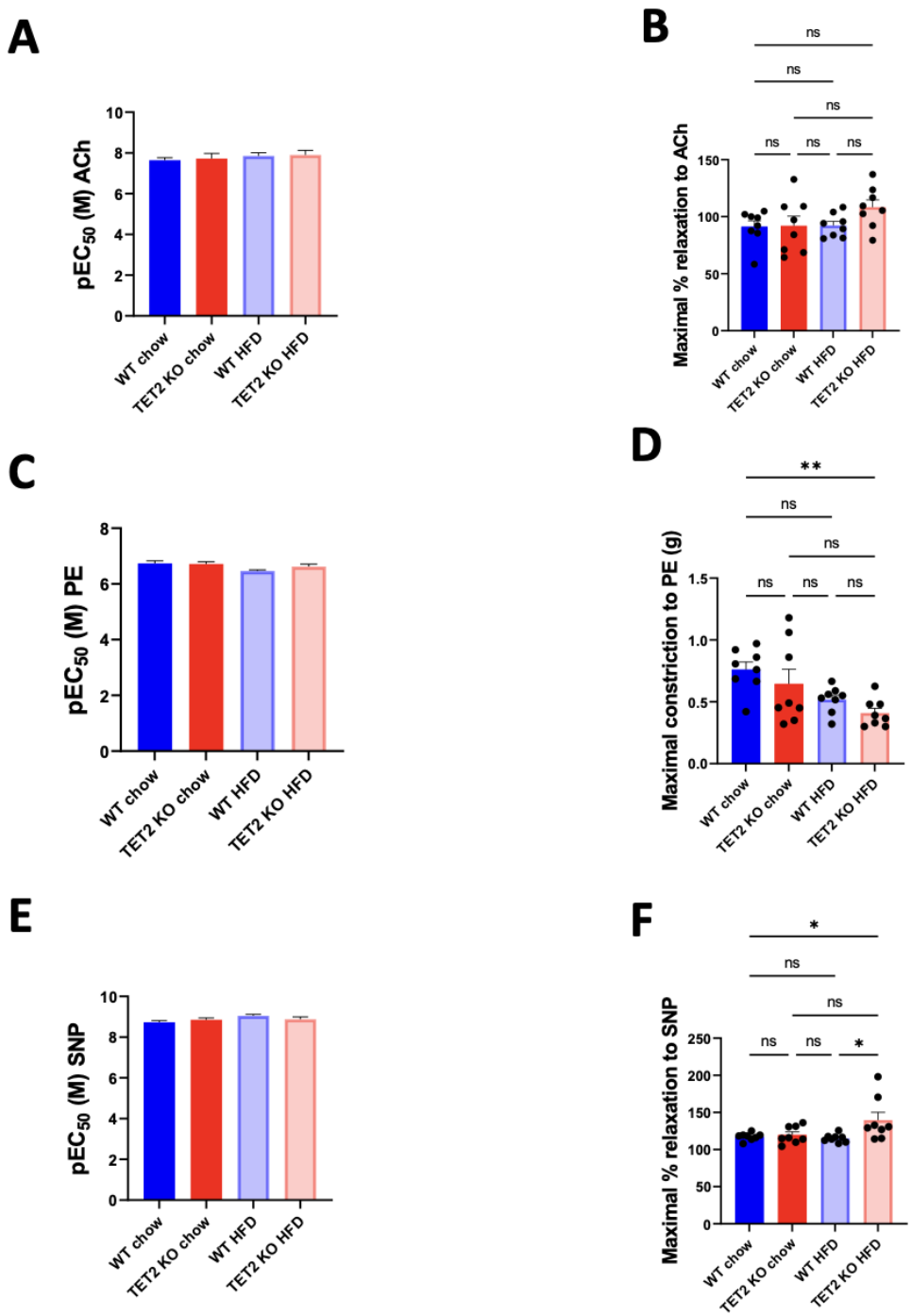

Figure 5.5: ***20 weeks of high fat diet feeding increases maximal response SNP-mediated vasorelaxation in TET2 KO mice.*** *Aortae were isolated from male TET2$^{fl/fl}$ CDH5-CreERT2 Cre^{-ve} (WT) and Cre^{+ve} (TET2 KO) tamoxifen-injected C57Bl/6J mice after standard chow or high fat diet (HFD) feeding ad libitum for 20 weeks. Aortic sections were suspended in organ bath chambers and dose response curves were generated for acetylcholine (ACh), phenylephrine (PE) and sodium nitroprusside (SNP). pEC$_{50}$ (A, C, E) and maximal response to each agonist (B, D, F) were calculated. A Shaprio-Wilk test for normality was performed, followed by a one-way ANOVA. No significant difference was observed in pEC$_{50}$ values between groups. * denotes p<0.05, ** denotes p<0.01. Data presented as mean ± SEM from n=8 per group.*

5.2.5 Plasma cytokine abundance differs between WT and endothelial-specific TET2 KO mice

In addition to impaired endothelium-dependent vasodilation, endothelial dysfunction involves a shift towards a persistent pro-inflammatory, pro-thrombotic phenotype in which endothelial cells express cell adhesion molecules and release pro-inflammatory and pro-thrombotic mediators which promote leukocyte and platelet recruitment to the vessel wall [52]. Preliminary *in vitro* data indicated that TET2 may be involved in the release of cytokines from the endothelium (Figures 4.27 & 4.28). This led to the question as to whether the plasma cytokine profile of TET2 endo KO mice differed from that of WT mice. Using a Proteome Profiler Mouse XL Cytokine Array, the abundance of a panel of cytokines was measured in plasma samples pooled (n=8) from either WT or TET2 endo KO male mice (fed either a standard chow diet or HFD for 20 weeks) (Figure 5.6). While most cytokines displayed a similar abundance in the two genotypes, some subtle changes in abundance were identified in this preliminary study.

In the chow-fed group, souble RAGE was amongst those with a decreased abundance in TET2 endo KO plasma compared to WT plasma. RAGE is associated with vascular complications of diabetes and progression of atherosclerosis due to initiation of pro-inflammatory signalling following ligand binding [308]. However, soluble RAGE appears to be atheroprotective in animal studies and high plasma soluble RAGE is associated with decreased cardiovascular risk [308]. Several cytokines were decreased in abundance, including fractalkine (a T cell and monocyte chemoattractant [309]), chemerin (an NK cell and dendritic cell chemoattractant [310]) and FLT3 ligand (a regulator of haematopoiesis [311]). Mediators involved the innate immune response (myeloperoxidase and complement C5) and adaptive immune response (IL-28A/B) were increased in abundance. Both angiopoietin-1 (which promote angiogenesis [28]) and endostatin (which inhibits angiogenesis [312]) were decreased in abundance in TET2 endo KO plasma. Interestingly, plasma leptin was substantially lower in chow-fed TET2 endo KO mice than in WT mice.

Comparisons were also made to determine how HFD consumption affects plasma cytokine abundance. A clear increase in plasma leptin was observed as a result of HFD consumption, consistent with previous research [313]. Given that the abundance of leptin was much lower in TET2 endo KO chow-fed mice compared to WT chow-fed mice, the fold-change in leptin abundance upon HFD consumption was much higher for TET2 endo KO mice than for WT mice. In WT mice, the fibrinolysis inhibitor plasminogen activator inhibitor (PAI)-1, growth factors epidermal growth factor (EGF) and fibroblast growth factor (FGF) and T cell/NK cell regulating proteins CXCL16 and IL-12 p40 were increased in abundance upon HFD consumption. These cytokines were not elevated in the plasma of HFD-fed TET2 endo KO mice (and in some cases were decreased), which could potentially indicate a role for endothelial TET2 in their regulation. Surprisingly, some cytokines typically elevated in obesity, diabetes or cardiovascular disease were *decreased* in abundance following HFD consumption, for example, retinol binding protein 4 (RBP4) [314], osteopontin [315], resistin [278] and RAGE [74, 308]. These cytokines were also decreased in abundance in TET2 KO mice upon HFD consumption, but to a lesser extent. Although some changes in cytokine abundance have been identified using this assay, validation of these findings would be necessary for firm conclusions to be drawn about the effect of HFD consumption and endothelial-specific TET2 knockout on plasma cytokine profiles.

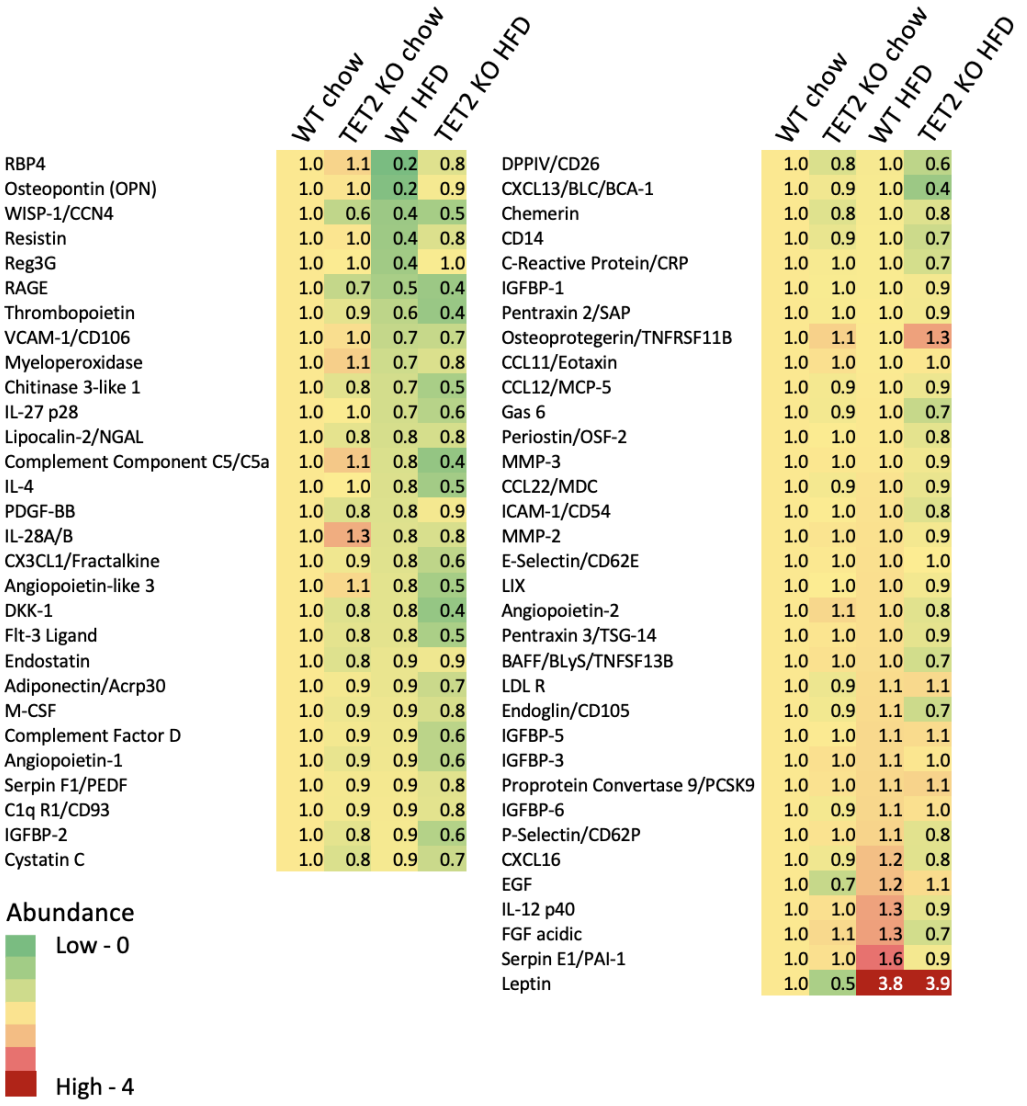

Figure 5.6: ***Plasma cytokine abundance differs between WT chow-fed and high fat diet-fed mice and endothelial-specific TET2 KO mice.*** *Plasma was collected from male TET2$^{fl/fl}$ CDH5-CreERT2 Cre^{-ve} (WT) and Cre^{+ve} (TET2 KO) tamoxifen-injected C57Bl/6J mice after standard chow or high fat diet (HFD) feeding ad libitum for 20 weeks. Plasma samples were pooled from n=8 mice per group and plasma cytokine abundance was measured using a Proteome Profiler Human XL Cytokine Array. The signals from each array were quantified by densitometry and the relative cytokine abundance was calculated. Heatmaps show the fold-change of cytokine abundance of TET2 KO, WT HFD and TET2 KO HFD mice compared to WT chow controls.*

5.2.6 Confirmation of isolation of mouse lung endothelial cells and successful cre-recombination

To explore further whether knockout of TET2 impacts endothelial function, microvascular endothelial cells were isolated from the lung tissue of TET2 endo KO and WT mice and cultured for *ex vivo* characterisation. First, successful isolation of endothelial cells was verified by assessing their morphology and confirming the presence of an endothelial marker, VE-cadherin, using immunofluorescence staining (Figure 5.7). The characteristic 'cobblestone' endothelial morphology was visible by light microscopy (Figure 5.7A) and cells formed junctions which were clearly identified by VE-cadherin expression (Figure 5.7B).

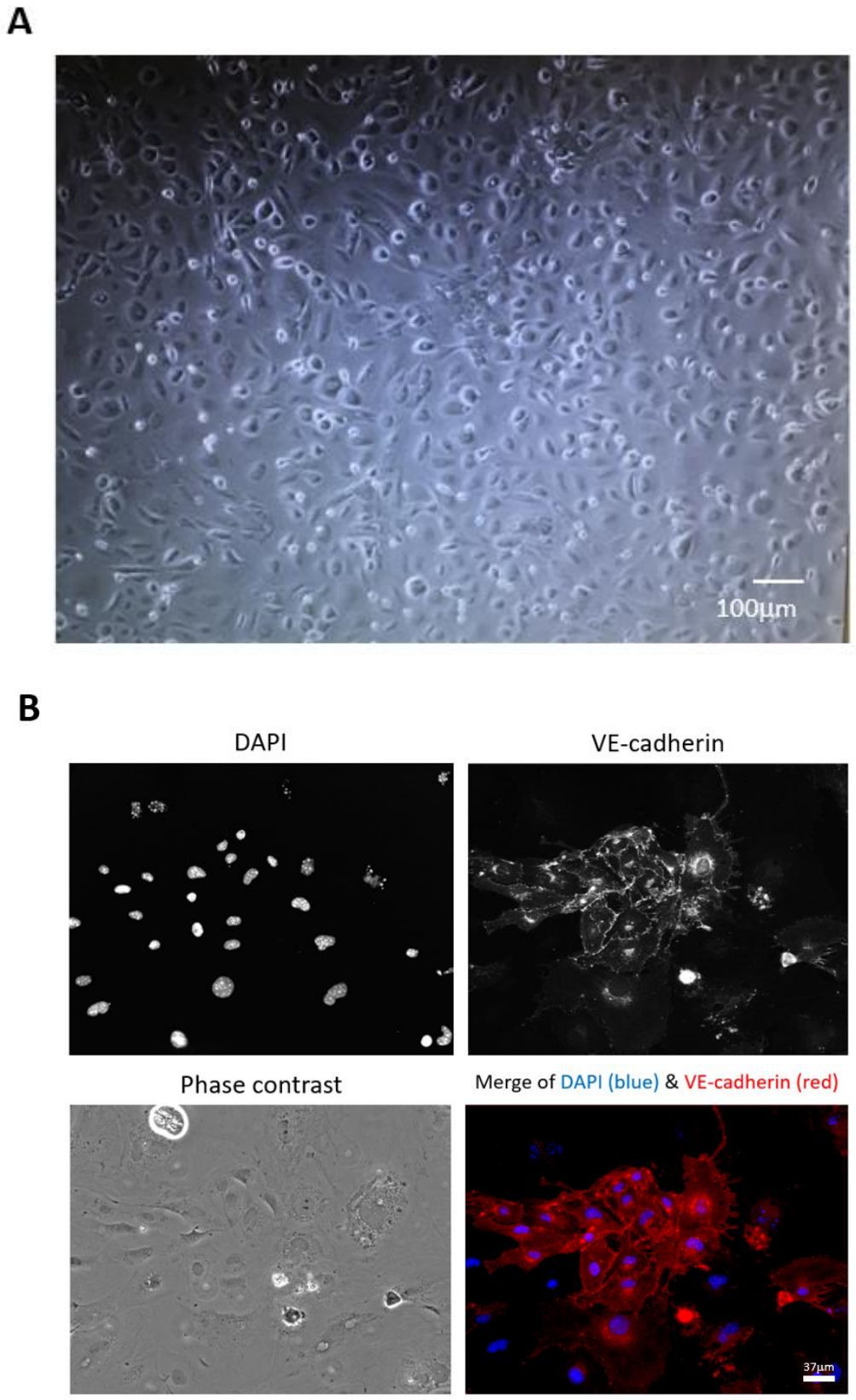

Figure 5.7: ***Confirmation of endothelial morphology and VE-cadherin expression in isolated mouse lung endothelial cells.*** *Mouse lung endothelial cells were isolated from TET2$^{fl/fl}$ CDH5-CreERT2 Cre^{-ve} C57Bl/6J mice and cultured in vitro. (A) The cells displayed a 'cobblestone' morphology. Scale bar represents 100μm. (B) Cells were fixed before staining with DAPI and an antibody targeting VE-cadherin, which was present at junctions between endothelial cells. Scale bar represents 37μm.*

Next, it was confirmed that cre-recombination was successfully induced in endothelial cells from Cre^{+ve} TET2$^{fl/fl}$ mice, either by intraperitoneal injection of tamoxifen of mice at least 1 week before isolation of endothelial cells, or by *in vitro* treatment of isolated cells with 4-hydroxytamoxifen (Figure 5.8). Using primers to amplify across the proximal LoxP site, the presence of the floxed TET2 allele was confirmed in endothelial cells from Cre^{+ve} and Cre^{-ve} mice (Figure 5.8B). Using primers to amplify across the deleted exon, it was further confirmed that recombination had occurred following tamoxifen injection or 4-hydroxytamoxifen treatment of isolated endothelial cells from Cre^{+ve} mice. The absence of recombination in 4-hydroxytamoxifen-treated endothelial cells from Cre^{-ve} mice was also confirmed (Figure 5.8C).

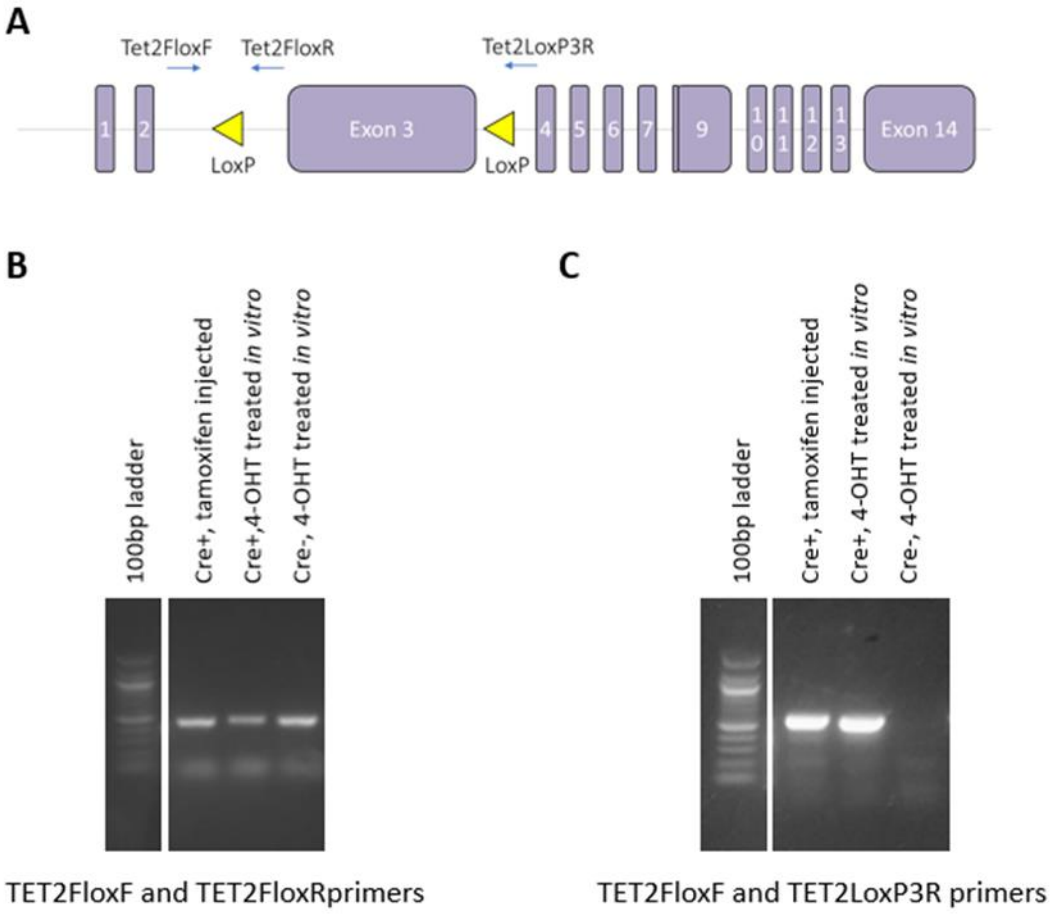

Figure 5.8: ***Confirmation of successful Cre-recombination in mouse lung endothelial cells (MLEC).*** *A) Figure adapted from [149], showing the position of LoxP sites and primers used in (B) and (C). (B) Agarose gel of PCR products from amplification of MLEC extracts using primers TET2FloxF and TET2FloxR to confirm the presence of the floxed TET2 allele in TET2$^{fl/fl}$ CDH5-CreERT2 Cre^{-ve} and Cre^{+ve} cells. (C) Agarose gel of PCR products from amplification of MLEC extracts using primers TET2FloxF and TET2LoxP3R to confirm Cre recombination in Cre+ cells after tamoxifen injection or 4-hydroxytamoxifen (4-OHT) treatment and absence of Cre recombination in Cre- cells.*

5.2.7 Adhesion of bone marrow-derived cells to monolayers of mouse lung endothelial cells is not affected by the absence of TET2

Having confirmed successful isolation of WT and TET2 endo KO mouse lung endothelial cells (MLEC), endothelial functions were assessed. Firstly, an *in vitro* static adhesion assay was used to assess whether TNFα-stimulated adhesion of mouse bone marrow-derived cells to MLEC was impacted by the absence of TET2 (Figure 5.9). However, TNFα did not significantly increase leukocyte adhesion and no difference in adhesion was observed between WT and TET2 endo KO MLEC (Figure 5.9).

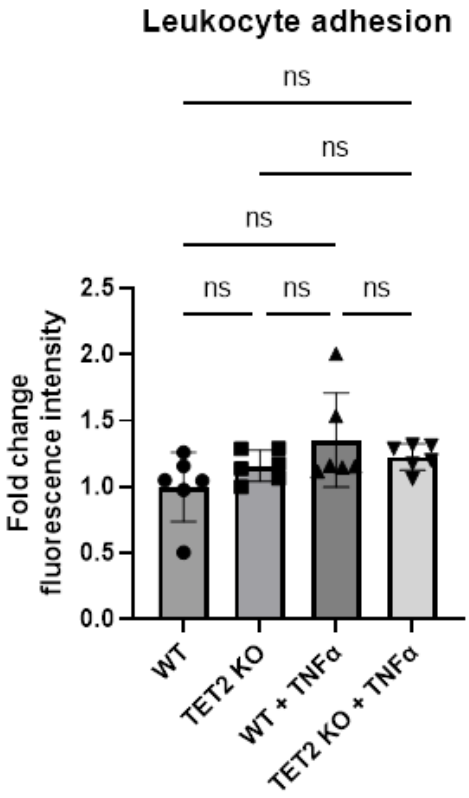

Figure 5.9: ***Adhesion of mouse bone marrow cells (BMCs) to mouse lung endothelial cells (MLEC) is not altered by endothelial-specific TET2 knockout under static conditions in vitro.*** *MLEC were isolated from TET2$^{fl/fl}$ CDH5-CreERT2 Cre^{-ve} (WT) and Cre^{+ve} (TET2 KO) tamoxifen-injected C57Bl/6J mice and cultured until monolayers had formed. Monolayers were left untreated or activated with 10ng/ml TNFα before addition of BMCs fluorescently labelled with LeukoTracker™. BMCs were allowed to adhere to the monolayers for 1h. Non-adherent cells were removed by 3 gentle washes with PBS. Cells were lysed and fluorescence intensity (proportional to the number of adherent BMCs) was measured using a fluorimeter. A Shapiro-Wilk test for normality was performed, followed by a one-way ANOVA and post-hoc Tukey's test. Data presented as mean ± SEM. n=6 technical replicates.*

5.2.8 Expression of leukocyte markers and pro-inflammatory cytokines in heart tissue is not affected by the absence of TET2 in endothelial cells

Taking a second approach to explore whether endothelial-expressed TET2 is important for leukocyte recruitment, the mRNA expression of a panel of leukocyte/inflammatory markers in heart tissue from WT and TET2 endo KO mice was measured by qPCR (Figure 5.10). No difference was observed in expression of the markers L-selectin (expressed by most circulating leukocytes [316]), CXCL10 (expressed by a variety of cells including T cells and monocytes), CD206 (expressed primarily by macrophages), or the pro-inflammatory cytokines TNFα, IL-1β or IL-6 (Figure 5.10).

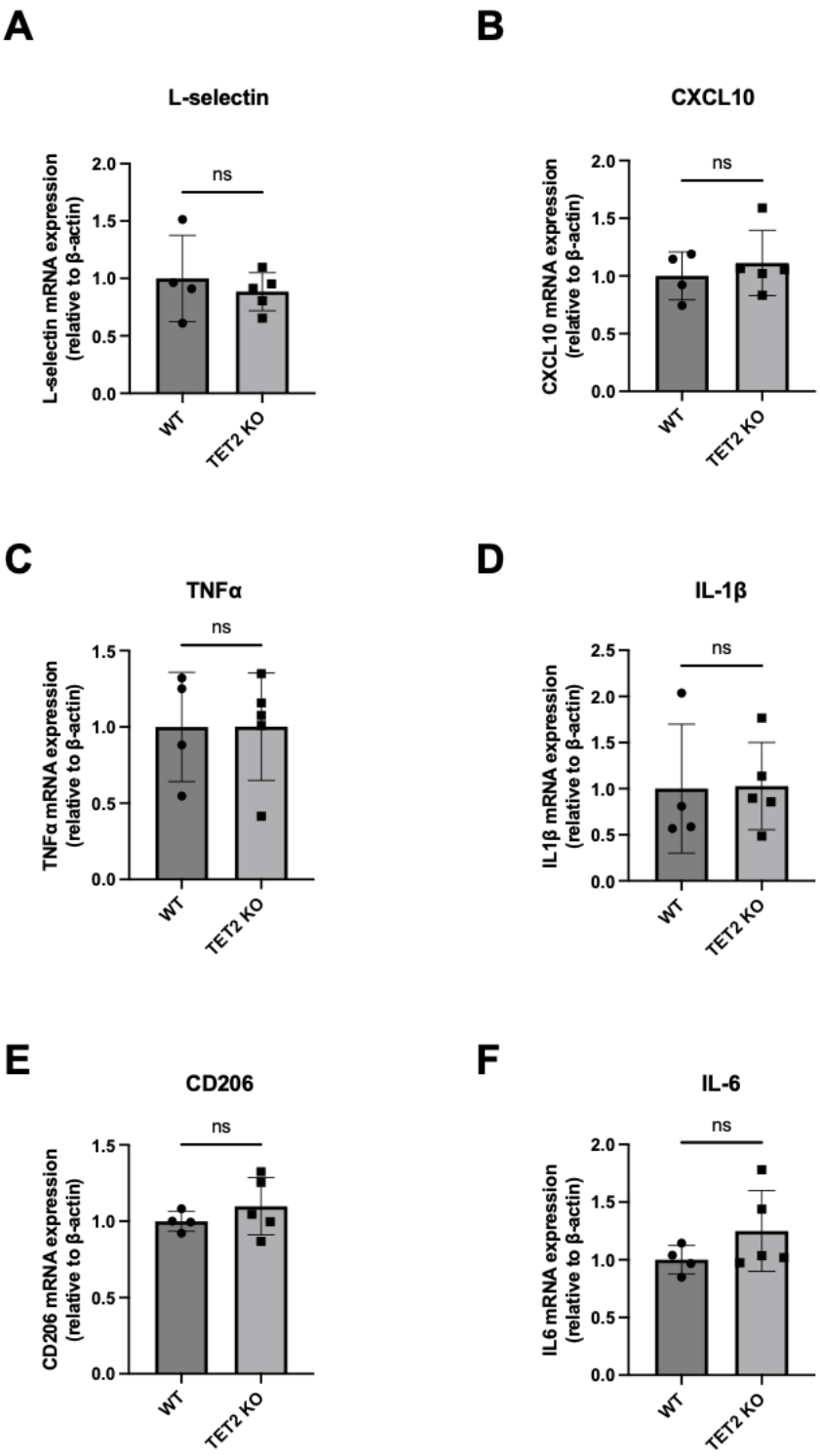

Figure 5.10: ***mRNA expression of a panel of leukocyte markers and pro-inflammatory cytokines in heart tissue is not affected by endothelial-specific TET2 KO.*** *cDNA was prepared from heart tissue from male TET2$^{fl/fl}$ CDH5-CreERT2 Cre^{-ve} (WT) and Cre^{+ve} (TET2 KO) tamoxifen-injected C57Bl/6J mice. qPCR was performed to measure relative mRNA expression of L-selectin (A), CXCL10 (B), TNFα (C), IL-1β (D), CD206 (E) and IL-6 (F), normalised to the housekeeping gene β-actin. A Shapiro-Wilk test for normality was performed, followed by an unpaired t-test. Data presented as mean $\pm$SEM. n=4-5 in each group.*

5.2.9 Permeability of mouse lung endothelial cells is not affected by the absence of TET2

The siRNA-mediated silencing of TET2 was shown here previously to decrease the permeability of HUVEC monolayers to the fluorescently-conjugated macromolecules FITC-dextran and TRITC-BSA (Figure 4.38). Next, it was assessed whether the alteration of endothelial barrier function was also evident in MLEC from WT and TET2 endo KO mice. Using the same transwell permeability assay as for HUVEC, the passage of FITC-dextran and TRITC-BSA across WT and TET2 endo KO MLEC was measured (Figure 5.11). This showed no significant difference in permeability in the absence of TET2, in contrast to the findings in HUVEC (Figure 5.11).

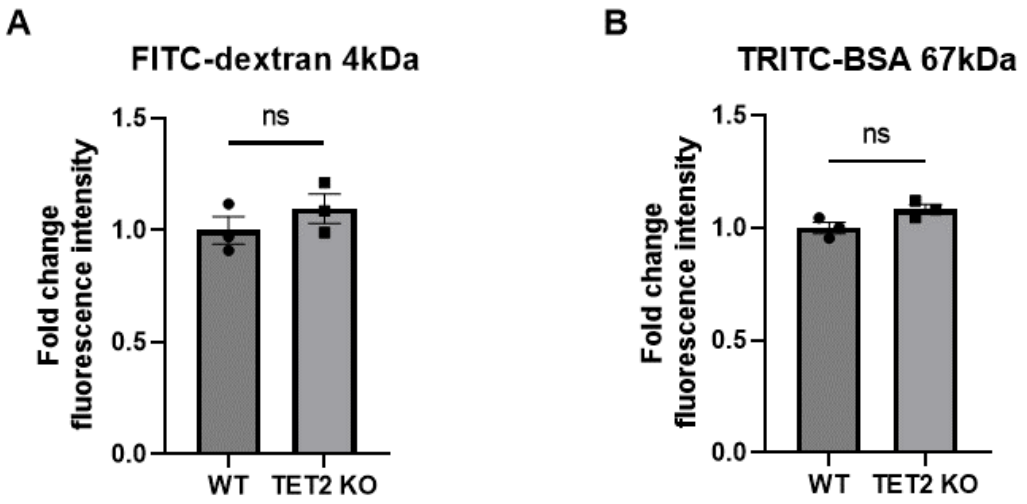

Figure 5.11: ***Permeability of mouse lung endothelial cells is not altered by TET2 knockout.*** *MLEC were isolated from TET2$^{fl/fl}$ CDH5-CreERT2 Cre^{-ve} (WT) and Cre^{+ve} (TET2 KO) tamoxifen-injected C57Bl/6J mice and grown on transwell inserts until monolayers had formed. FITC-dextran (A) and TRITC-BSA (B) were applied to the upper chamber and after 1h, media samples from the lower chamber were taken and fluorescence intensity was measured using a fluorimeter. Data presented as mean ± SEM from n=3 technical replicates. A Shapiro-Wilk test for normality was performed, followed by an unpaired t-test.*

5.2.10 A subset of genes differentially-expressed in mouse lung endothelial cells by HFD feeding are also differentially-expressed upon TET2 knockout

To explore the transcriptomic differences that result in endothelial cells due to TET2 endo KO and/or HFD consumption, RNA was prepared from n=3 MLEC samples from WT and TET2 endo KO mice fed a standard chow diet or HFD for 20 weeks and RNA sequencing was performed. Figure 5.12A displays the number of differentially-expressed genes between these conditions after applying cutoff values of Log2FoldChange>|1| and P<0.05. The magnitude and statistical significance of differentially-expressed genes are also visualised as volcano plots (Figure 5.12B-E). It is evident that HFD consumption strongly impacts the endothelial transcriptome, leading to downregulation of 2168 genes and upregulation of 1286 genes in MLEC from HFD-fed mice compared to MLEC from chow-fed mice (Figure 5.12). The absence of TET2 impacted MLEC gene expression in both chow-fed and HFD-fed mice, to varying extents (Figure 5.12). Full lists of differentially expressed genes can be accessed *via* the GEO database (GSE232888).

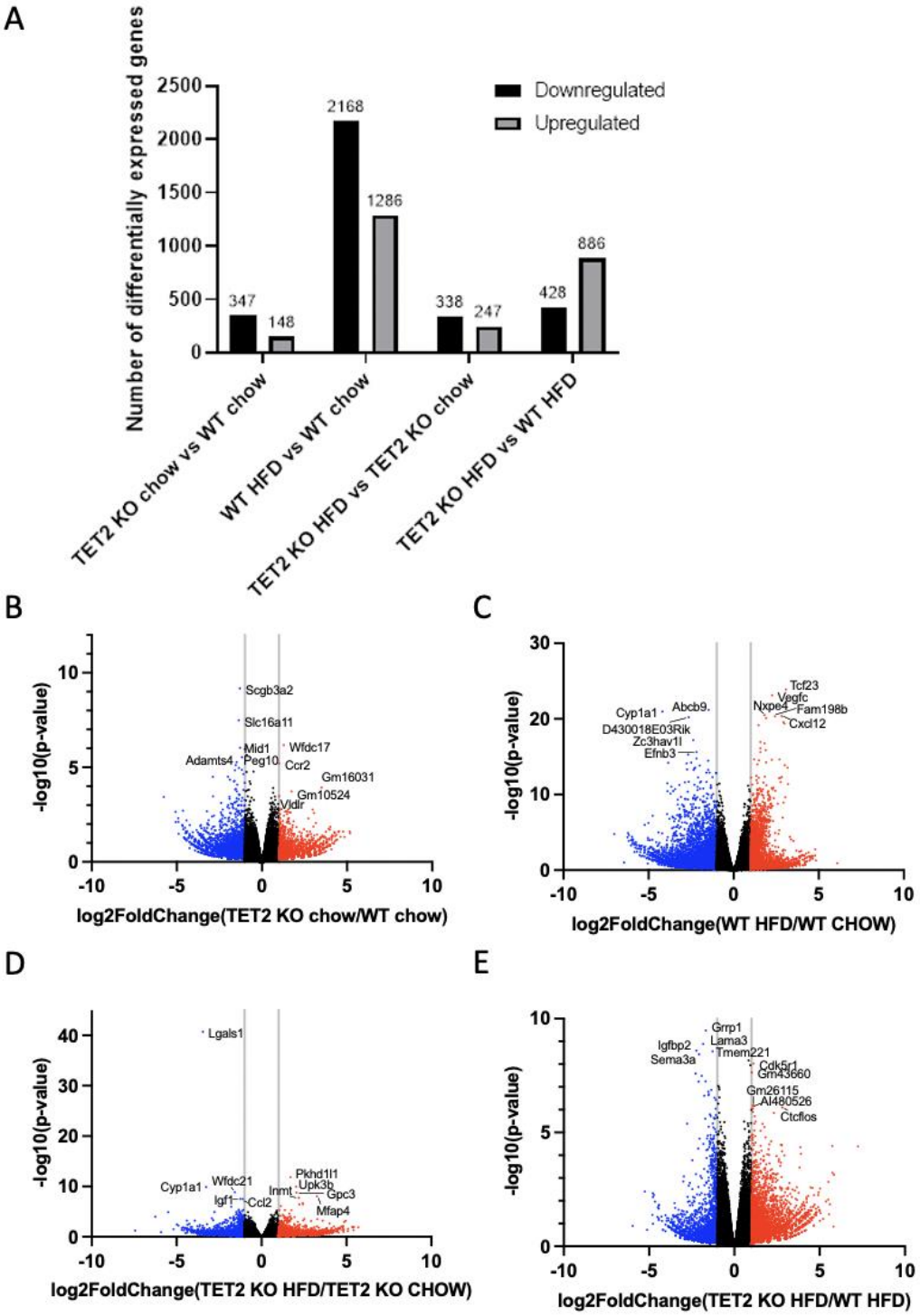

Figure 5.12: ***Number of differentially-expressed genes in mouse lung endothelial cells upregulated or downregulated between WT and endothelial-specific TET2 KO genotypes and between chow and high fat diet groups.*** *RNA sequencing was performed on mouse lung endothelial cells isolated from TET2$^{fl/fl}$ CDH5-CreERT2 Cre^{-ve} (WT) and Cre^{+ve} (TET2 KO) tamoxifen-injected C57Bl/6J mice fed a standard chow diet or high fat diet (HFD) for 20 weeks (n=3 per group). (A) Graph displaying the number of up- or down-regulated genes between indicated groups, applying cut-offs of Log2FoldChange>|1| and p<0.05. (B-E) Volcano plots showing significantly differentially expressed genes in TET2 KO vs WT chow (B), WT HFD vs WT chow (C), TET2 KO HFD vs TET2 KO chow (D) and TET2 KO HFD vs WT HFD (E) groups. The five genes with the most statistically significant upregulation and downregulation are labelled.*

Comparing the genes differentially-expressed in TET2 endo KO or following HFD consumption, an overlap was identified, consisting of 260 genes (Figure 5.13). Although this comprises only a small proportion of genes dysregulated by HFD consumption, it accounts for more than half of the genes dysregulated by TET2 endo KO.

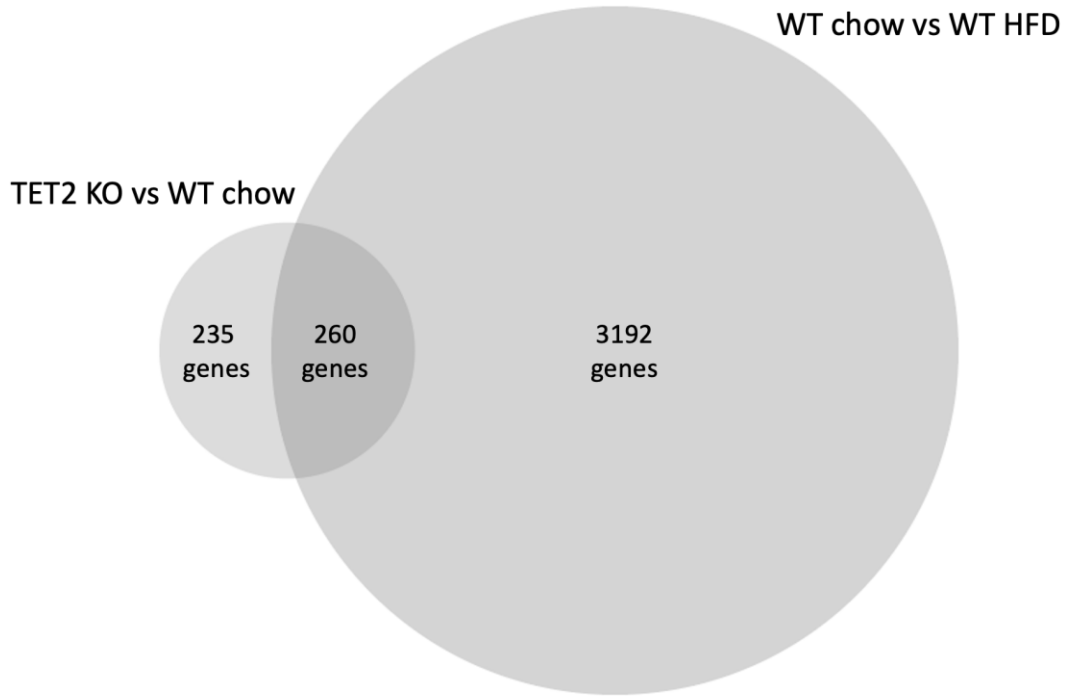

Figure 5.13: ***Genes commonly differentially-expressed in mouse lung endothelial cells by endothelial-specific TET2 KO and HFD consumption.*** *RNA sequencing was performed on mouse lung endothelial cells isolated from TET2$^{fl/fl}$ CDH5-CreERT2 Cre^{-ve} (WT) and Cre^{+ve} (TET2 KO) tamoxifen-injected C57Bl/6J mice fed a standard chow diet or high fat diet (HFD) for 20 weeks (n=3 per group). Venn diagram shows the uniquely and commonly differentially-expressed genes between indicated groups, applying cut-offs of Log2FoldChange>|1| and p<0.05.*

5.2.11 Biological pathways dysregulated in mouse lung endothelial cells as a result of TET2 knockout or HFD feeding

In the same manner as for the RNA sequencing analysis of HUVEC described in Chapter 3, IPA software was used to group differentially-expressed genes into the biological pathways with which they are associated (Figure 5.14). This was performed to assess whether there were pathways dysregulated by HFD consumption that were similarly dysregulated by TET2 endo KO, which could indicate a common mode of TET2-dependent regulation. MLEC from chow-fed mice showed significant differential

expression of genes related to immune cells (particularly increased activation of NK cell signalling) and inflammatory signalling in TET2 endo KO compared to WT cells (Figure 5.14A). The pathways containing differentially-expressed genes following HFD consumption included those associated with axonal guidance (which contains many genes overlapping with roles in angiogenesis, such as semaphorins, netrins and various proteases) [28], pulmonary fibrosis and healing, and pathways involved in leukocyte recruitment (specifically of agranulocytes) and S100 signalling which is associated with inflammation (Figure 5.14B). Genes associated with axonal guidance and pulmonary fibrosis signalling were further differentially-expressed between TET2 endo KO and WT cells from HFD-fed mice (Figure 5.14C). In TET2 endo KO mice, HFD consumption also led to differential expression of genes belonging to inflammation-related pathways, including atherosclerosis (Figure 5.14D).

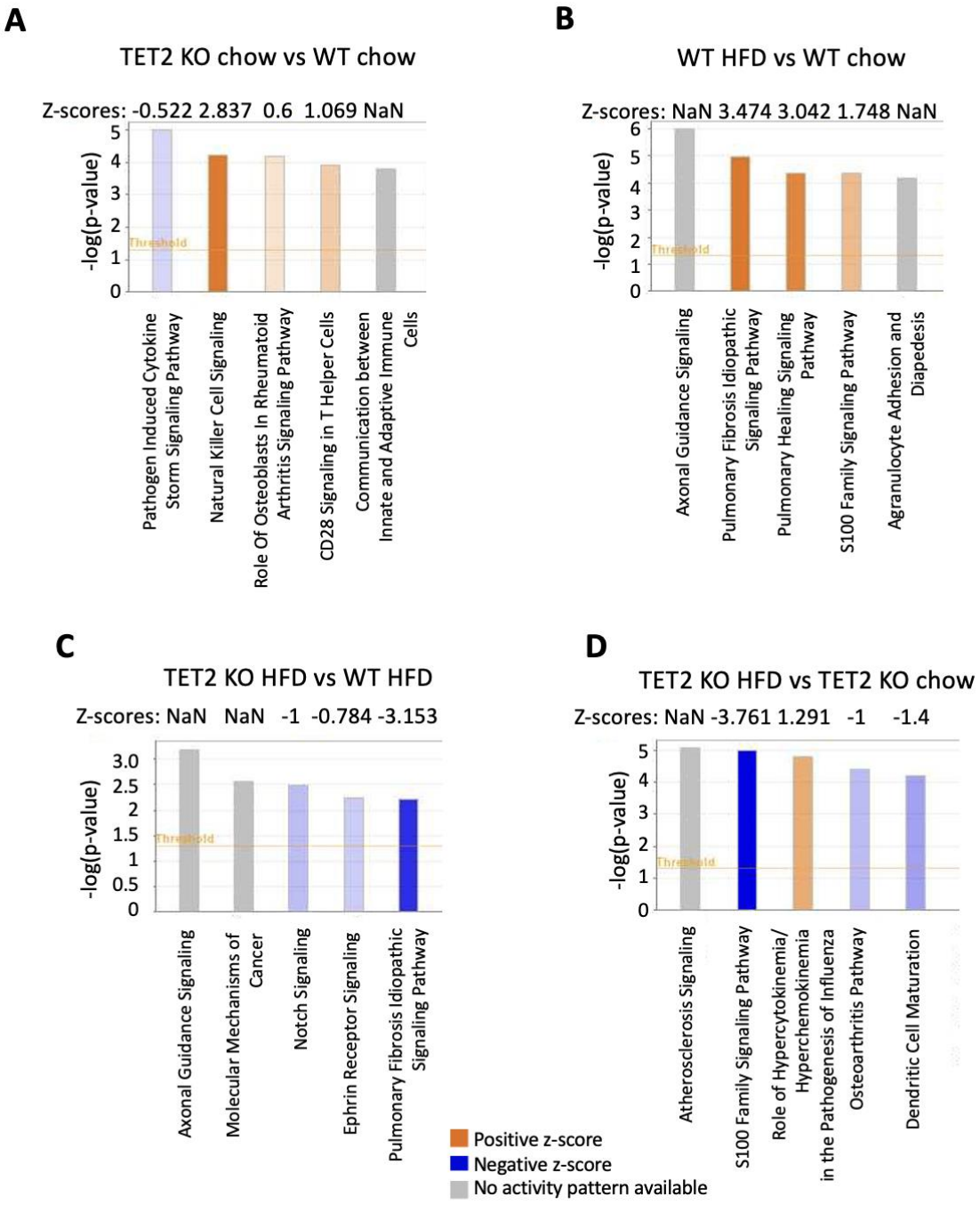

Figure 5.14: ***Pathway analysis of RNA sequencing of mouse lung endothelial cells from WT and endothelial-specific TET2 KO mice fed a standard chow or high fat diet.*** *RNA sequencing was performed on mouse lung endothelial cells isolated from TET2$^{fl/fl}$ CDH5-CreERT2 Cre^{-ve} (WT) and Cre^{+ve} (TET2 KO) tamoxifen-injected C57Bl/6J mice fed a standard chow diet or high fat diet (HFD) for 20 weeks (n=3 per group). Ingenuity Pathway Analysis software was used to identify pathways containing significantly differentially-expressed genes between groups. Orange bars denote a positive z-score, indicating the pathway is overall predicted to be activated and blue bars denote a negative z-score, indicating that the pathway is predicted to be inhibited. P-values were calculated by Fisher's Exact Test. –log(p-value)<1.3 and Z-scores <|2| are considered statistically significant.*

5.2.12 Biological functions common to genes differentially-expressed in mouse lung endothelial cells as a result of TET2 knockout or HFD feeding

To make additional comparisons between genes differentially-expressed by TET2 endo KO or HFD consumption, the IPA biological functions analysis was used (Figure 5.15). This revealed clear common features of activation of cell migration, leukocyte recruitment and inflammatory responses in both groups (Figure 5.15).

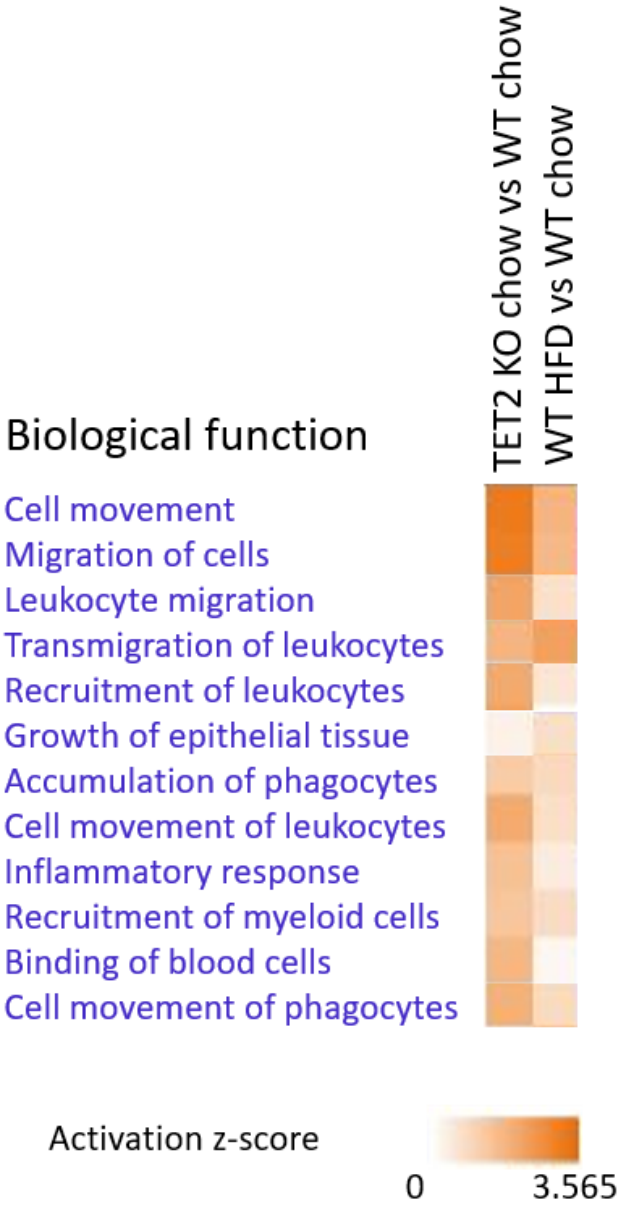

Figure 5.15: ***Biological functions associated with genes differentially-expressed in mouse lung endothelial cells (MLEC) from WT and endothelial-specific TET2 KO mice and in MLEC from WT mice fed a standard chow or high fat diet.*** *RNA sequencing was performed on MLEC isolated from TET2$^{fl/fl}$ CDH5-CreERT2 Cre^{-ve} (WT) and Cre^{+ve} (TET2 KO) tamoxifen-injected C57Bl/6J mice fed a standard chow diet or high fat diet (HFD) for 20 weeks (n=3 per group). Ingenuity Pathway Analysis software was used to identify biological functions related to the significantly differentially-expressed genes between groups. Orange colour scale denotes the z-score, indicating the extent to which the biological function is predicted to be activated.*

5.2.13 IRF7 identified as a potential upstream regulator for a subset of genes differentially-expressed as a result of TET2 knockout or HFD feeding

Another method used to identify broad similarities between genes and pathways altered by TET2 endo KO and HFD consumption was to compare the graphical summaries generated by IPA software for these groups (Figure 5.16). The graphical summary is constructed from the most significant canonical pathways, upstream regulators and biological functions identified within the dataset and the relationships between them. From this, it was identified that a core feature resulting from either TET2 endo KO or HFD consumption was the activation of interferon signalling pathways in MLEC from these mice compared to controls (Figure 5.16). Notably, this confirms the findings from RNA sequencing of TET2-silenced HUVEC and subsequent *in vitro* studies which evidenced that TET2 silencing or high glucose culture impaired interferon responses in HUVEC (Figures 3.15, 3.24 & 3.27). Furthermore, IRF7 was upregulated in both datasets compared to chow-fed controls and was identified as an upstream regulator of a subset of the differentially-expressed genes which included interferon-sensitive genes such as IFIT2, OAS2 and OASL (Figure 5.17), which were also differentially-expressed in TET2-silenced HUVEC (Figure 4.7).

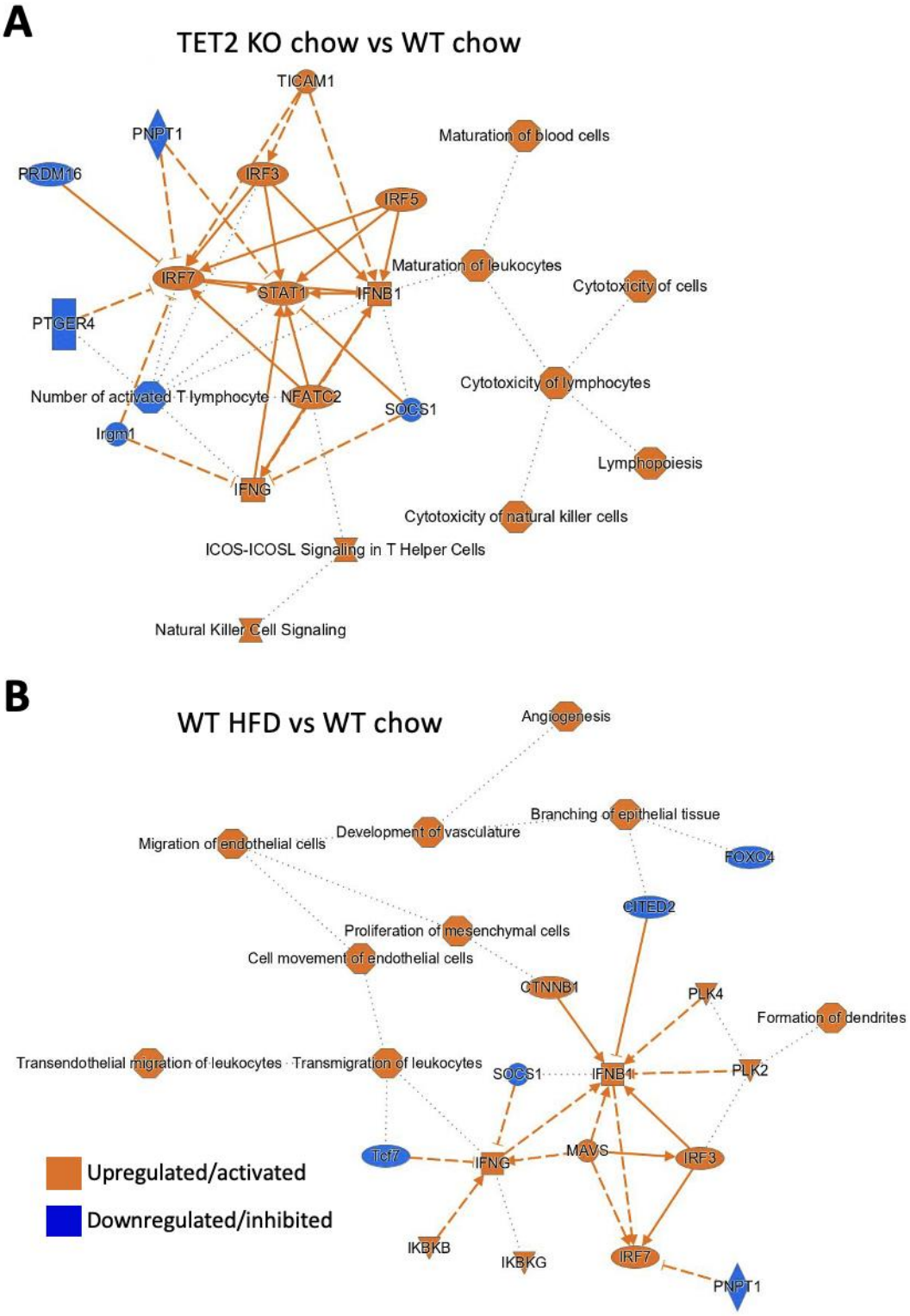

Figure 5.16: ***Graphical summary of differentially-expressed genes and their associated pathways in mouse lung endothelial cells (MLEC) from WT and endothelial-specific TET2 KO mice and in MLEC from WT mice fed a standard chow or high fat diet.*** *RNA sequencing was performed on MLEC isolated from TET2$^{fl/fl}$ CDH5-CreERT2 Cre^{-ve} (WT) and Cre^{+ve} (TET2 KO) tamoxifen-injected C57Bl/6J mice fed a standard chow diet or high fat diet (HFD) for 20 weeks (n=3 per group). Ingenuity Pathway Analysis software was used to generate a graphical summary showing the key differentially-expressed genes and biological pathways associated with differential activity in cells from TET2 KO chow compared to WT chow groups (A) and between WT HFD and WT chow groups (B). Solid lines indicate a direct relationship between the components. Dashed lines indicate an indirect relationship. Dotted lines indicate that the activation state of two components produces a similar effect on downstream molecules.*

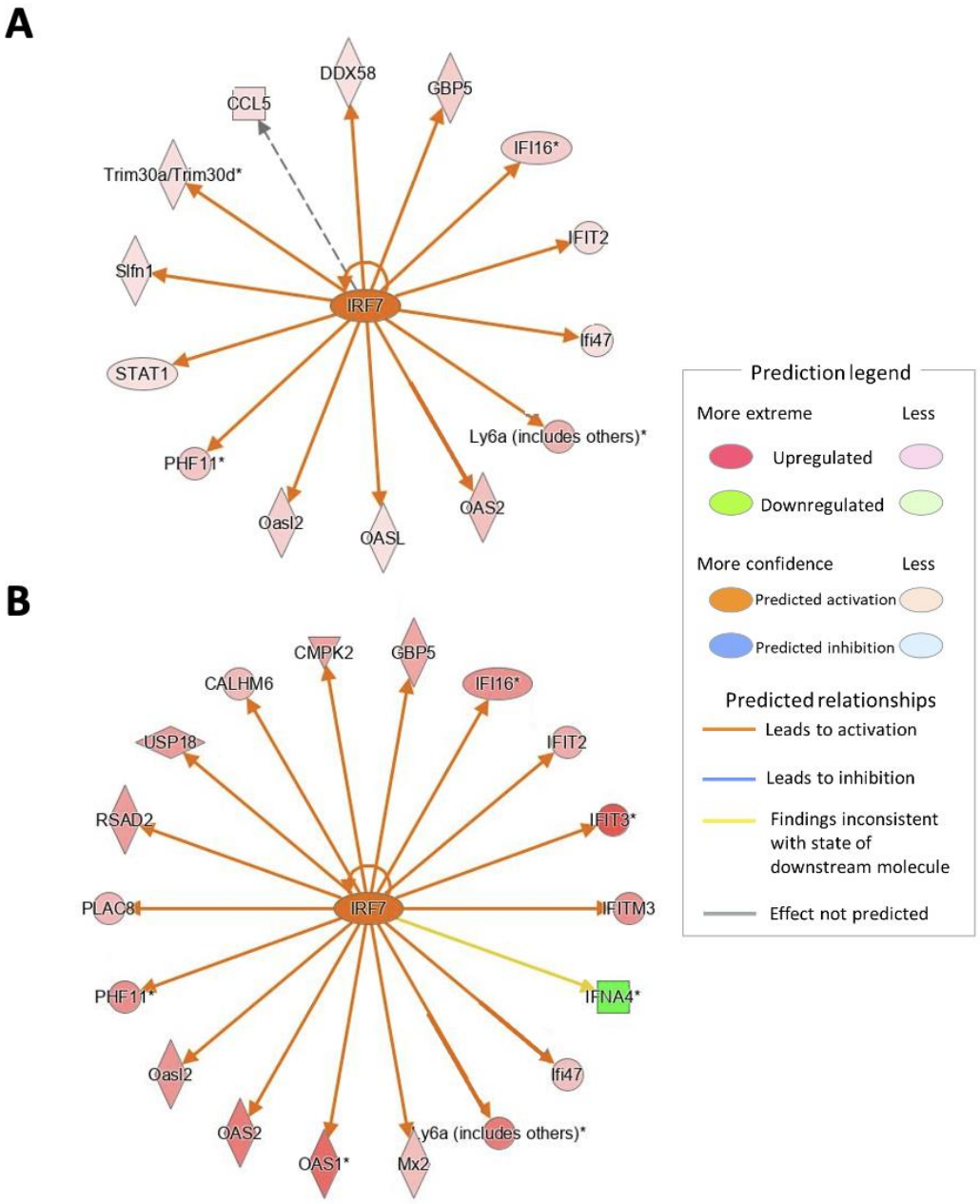

Figure 5.17: ***Ingenuity Pathway Analysis identifies IRF7 as an upstream regulator of genes differentially-expressed in mouse lung endothelial cells by endothelial-specific TET2 KO or HFD consumption.*** *RNA sequencing was performed on mouse lung endothelial cells isolated from TET2$^{fl/fl}$ CDH5-CreERT2 Cre^{-ve} (WT) and Cre^{+ve} (TET2 KO) tamoxifen-injected C57Bl/6J mice fed a standard chow diet or high fat diet (HFD) for 20 weeks (n=3 per group). Ingenuity Pathway Analysis software was used to predict upstream regulators of differentially-expressed genes, based on known interactions from existing literature. IRF7 is upregulated in MLEC from TET2 KO vs WT mice (A) and in MLEC from WT HFD-fed mice compared to WT chow-fed mice (B). Orange arrows indicate that activation of IRF7 is predicted to activate the target gene and that the target gene is also upregulated in the dataset. Yellow arrows indicate that the expression of the target gene in the dataset is inconsistent with that predicted from IRF7 activation. Grey arrows indicate that no activity pattern is available. Dotted lines indicate an indirect relationship.*

Taken together, these data indicate that HFD consumption leads to an altered microvascular endothelial transcriptome and that some of the transcriptomic changes correlate with those resulting from TET2 deletion. The commonly differentially-expressed genes have biological functions relating to leukocyte recruitment and inflammatory pathways, including interferon signalling pathways. Although not all of the changes in endothelial gene expression resulting from HFD consumption will be caused directly by exposure to hyperglycaemia (as many metabolic pathways in multiple tissues are influenced by an obesogenic diet), these findings support the hypothesis that TET2 may be functionally important in the response of endothelial cells to hyperglycaemia, particularly in the regulation of inflammatory signalling.

5.3 Discussion

5.3.1 Summary of findings

This chapter documents the generation of tamoxifen-inducible endothelial-specific TET2 KO mice and investigates the endothelial function of these mice under normoglycaemic and hyperglycaemic conditions. The data show that HFD feeding *ad libitum* significantly increases body weight compared to a standard chow diet and that glucose tolerance is impaired by HFD feeding by 9 weeks, modelling some of the features of metabolic syndrome and type 2 diabetes. No difference in aortic vasoconstriction to phenylephrine or vasorelaxation to acetylcholine or SNP was observed after 10 weeks between TET2 endo KO mice or WT mice, or between diet groups. Similarly, after 20 weeks there was no significant difference between the vascular reactivity of TET2 endo KO and WT mice under normoglycaemic or hyperglycaemic conditions. Surprisingly, after 20 weeks, SNP-mediated vasorelaxation was increased in aortae from HFD-fed TET2 endo KO mice compared to TET2 endo KO chow-fed mice. This difference was not observed between WT mice of the two diet groups. HFD consumption and TET2 endo KO both led to changes in the abundance of plasma cytokines. *In vitro* assays did not reveal any differences in leukocyte-endothelial adhesion or permeability of microvascular endothelial cells from the lungs of these mice. However, RNA sequencing identified similarities between genes and pathways dysregulated by HFD consumption or TET2 endo KO in these cells, such as leukocyte recruitment and inflammation-related pathways including interferon signalling.

5.3.2 HFD model of diabetes mellitus

Various methods are used to induce a diabetic phenotype in experimental animals: streptozotocin injection and alteration of diet to derive a higher percentage of calories from fat are two of the most used non-genetically induced diabetes models [317, 318]. Although both models induce hyperglycaemia, the former mimics type 1 diabetes by destruction of pancreatic islet β-cells and produces a rapid and severe phenotype

[318]. Streptozotocin is also associated with toxicity affecting multiple organs [318]. HFDs induce obesity, hyperglycaemia and eventual insulin resistance in rodents in a progressive manner, sharing the aetiology of human type 2 diabetes [317]. For the present study, a diet-induced model was selected based on previous findings from our laboratory that feeding male C57Bl/6J mice a diet consisting of 60% kcal from fat impaired glucose tolerance within 10 weeks (data not shown). Although it was confirmed that there was a significant increase in weight gain and impaired glucose tolerance in mice fed a 60% kcal fat diet compared to standard chow-fed controls (13% kcal from fat) (Figure 5.2), no significant change in vascular reactivity to acetylcholine, phenylephrine or SNP was observed between WT mice in these groups after 20 weeks of feeding (Figure 5.4).

A previous study by Molnar *et al.* has shown impaired acetylcholine-mediated vasorelaxation and increased phenylephrine-induced vasoconstriction in femoral arteries from C57Bl/6J mice fed a HFD [15]. However, differences are apparent between the methodology of that study and the present one. For example, the use of femoral arteries instead of aortae and the fact that the HFD consisted of 35% fat and 37% carbohydrate (primarily sucrose), as opposed to 60% and 20%, respectively, used here. It is thought that a diet high in sucrose as well as fat (often referred to as a 'western diet' or a 'cafeteria diet') causes greater impairment of vascular function than a HFD alone in C57Bl/6J mice [319]. Furthermore, in the study by Molnar *et al.*, it is not clear whether perivascular adipose tissue was removed. Perivascular adipose tissue has been shown to affect the extent of vascular dysfunction in mice following high fat/high sucrose feeding [319, 320]. Differences in vascular reactivity (impaired norepinephrine-induced vasoconstriction and impaired acetylcholine- or SNP-mediated relaxation) have also been shown in mice fed a diet comprised of 60% kcal from fat (as used here). However, these differences were apparent after 16 months, but not 8 months of feeding, indicating that a much longer duration is required for vascular dysfunction to develop using this model [321]. In hindsight, a high fat, high sucrose diet may have produced a better model of the vascular dysfunction resulting from type 2 diabetes. Not only would this potentially elicit a greater extent of vascular

dysfunction, but it also more closely resembles the human obesogenic/diabetogenic diet which typically consists of highly palatable, sugar-rich (as well as high fat) containing foods, as opposed to the 60% fat diet used here, which may have less relevance to a human diet.

Another consideration for designing animal studies include the influence of sex on cardiovascular outcomes. Male mice are typically used in studies involving HFD because they are more susceptible to hyperglycaemia from HFD than female mice [317]. Similarly, most streptozotocin models of type 1 diabetes use male mice, as female mice are less sensitive to this toxin [318]. However, as the prevalence, presentation and pathophysiology of cardiovascular diseases and diabetes differs between sexes [322, 323], it would be important for future studies to examine the influence of sex on outcomes of *in vivo* studies.

5.3.3 Differences in vascular reactivity of endothelial-specific TET2 KO mice fed a standard chow or HFD

Despite the limitations discussed, a significant increase in SNP-mediated relaxation was observed between chow-fed and HFD-fed TET2 endo KO mice which was not apparent in WT mice (Figures 5.4 & 5.5). Given that the TET2 deletion in these mice is specific to the endothelium, a difference in SNP-mediated vasorelaxation was not anticipated (particularly in the absence of any impairment of acetylcholine-mediated vasorelaxation), which is indicative of smooth muscle, rather than endothelial dysfunction. It may be that TET2 influences factors involved in endothelial-smooth muscle cell cross-talk other than NO, such as prostacyclin or EDHF. Alternatively, in the absence of a physiological explanation for this, it is possible that physical damage to the vascular smooth muscle during tissue preparation or mounting of the vessels may have occurred and that TET2 depletion may cause the tissue to be differentially prone to this, which could account for the differences observed. From the data presented in this chapter, it can be concluded that in the absence of hyperglycaemia,

WT and TET2 endo KO mice exhibit similar vascular reactivity. There was also no significant difference between the vascular reactivity of WT HFD-fed and TET2 endo KO HFD-fed mice. Future studies could use an alternative model of type 2 diabetes to investigate further whether deletion of TET2 in the endothelium exacerbates dysfunction or improves the vascular reactivity of diabetic mice, which may lead to a better understanding of the mechanisms underlying hyperglycaemia-induced endothelial dysfunction.

5.3.4 Altered abundance of cytokines in the plasma of WT and endothelial-specific TET2 KO mice

Type 2 diabetes is associated with low-grade chronic inflammation and various cytokines have been linked to metabolic dysfunction and the initiation and progression of diabetic vascular complications [324, 325]. Alterations in circulating cytokine levels can even precede the onset of type 2 diabetes, such as in the case of elevated IL-6 and IL-1β [326]. Notably, these two cytokines have previously been shown to be subject to transcriptional regulation by TET2 [158, 159]. The *in vitro* data presented in chapters 3 and 4 suggest that TET2 may be involved in the release of cytokines from endothelial cells and that interferon signalling pathways may involve TET2-mediated regulation. It was therefore questioned whether the abundance of cytokines in plasma may differ between WT and TET2 endo KO mice.

Plasma cytokine levels are determined by their release from numerous cell types and therefore cytokines released from endothelial cells are unlikely to be a major determinant of these levels. Thus endothelial-specific TET2 deletion may not strongly affect their abundance in plasma. Indeed, in chow-fed mice, levels of only five cytokines differed by >20% fold change in TET2 endo KO mice compared to WT controls (Figure 5.6). Those with a decreased abundance were associated with roles in immunity, inflammation and angiogenesis, potentially supporting a role for endothelial TET2 in the regulation of these processes. Interestingly, plasma from

chow-fed TET2 endo KO mice had a lower abundance of leptin than that of chow-fed WT mice (Figure 5.6). Leptin is a hormone produced by adipocytes and its concentration in the plasma is correlated with body fat percentage [327]. Although no difference in body mass was observed between the two genotypes (Figure 5.1), it is possible that differences in fat mass could account for this finding. In *ex vivo* rodent studies of aortic or mesenteric vascular reactivity, leptin has been shown to induce vasorelaxation in an endothelium-dependent manner [328, 329]. However, no difference in acetylcholine-induced aortic relaxation was observed between WT and TET2 endo KO mice in the present study and neither was a difference observed between chow-fed and HFD-fed mice after 20 weeks (Figures 5.4 & 5.5), as discussed above.

The plasma of HFD-fed WT mice showed elevated levels of PAI-1, FGF, CXCL16 and IL-12 p40 compared to chow-fed controls, which were not elevated in the plasma of HFD-fed TET2 endo KO mice (Figure 5.6). Whilst further validation would be necessary to confirm these findings, the altered abundance of cytokines related to inflammation, thrombosis, proliferation, angiogenesis and immune responses in the absence of endothelial TET2 is intriguing and suggests its functional importance *in vivo*, with possible relevance to diabetes and its vascular complications. The potential involvement of TET2 in cytokine release is also supported by RNA sequencing data comparing WT and TET2 endo KO MLEC in which the 'pathogen induced cytokine storm signalling pathway' contained a significant number of differentially-expressed genes (Figure 5.14), as well as *in vitro* data showing that siRNA-mediated silencing of TET2 affected cytokine release from HUVEC (Figures 4.27 & 4.28).

5.3.5 Functional assays of mouse lung endothelial cells from WT and endothelial-specific TET2 KO mice

The *in vitro* data from HUVEC suggested that TET2 may be involved in the regulation of endothelial permeability (Figure 4.38). Using the same assay, no difference was observed in the permeability of MLEC isolated from WT or TET2 endo KO mice (Figure

5.11). Species differences or the phenotypic differences between macrovascular (HUVEC) and microvascular (MLEC) endothelial cells could account for these differences. However, as well as this assay not being highly powered, it was challenging to culture equally confluent monolayers of MLEC from each condition and it is likely that (perhaps varying levels of) fibroblasts or other non-endothelial cells were also present in the cultures. These limitations make it challenging to draw firm conclusions about a potential role for TET2 in the regulation of endothelial permeability from these data. In future, a more physiologically relevant model of vascular permeability could be studied in WT and TET2 endo KO mice by using the *in vivo* Miles assay. This method involves the intravenous injection of Evan's blue dye, which binds to albumin, followed by intradermal administration of a stimulus known to affect permeability, and a vehicle control, on opposite flanks [330, 331]. At the region where the stimulus is applied, endothelial permeability increases and albumin (and therefore Evan's blue dye) can extravasate into the surrounding tissue, which can be visualised as blue colouration in the skin after culling. The dye can also be extracted from the skin for quantitative measurement and comparison between the stimulus and vehicle control [330, 331]. This assay enables the assessment of intact blood vessels as opposed to endothelial monolayers and is relatively simple and inexpensive to perform, so may be a useful model for assessing the role of endothelial TET2 in regulating vascular permeability *in vivo*.

The low statistical power and difficulty in culturing equally confluent MLEC monolayers should also be taken into consideration for the *in vitro* leukocyte adhesion assay (Figure 5.9), in addition to the limitations of this assay discussed in chapter 4. This assay showed no difference in leukocyte adhesion between WT and TET2 endo KO MLEC (Figure 5.9) and neither was there a difference in mRNA expression of a small panel of leukocyte and pro-inflammatory markers in heart tissue from these mice (Figure 5.10). However, RNA sequencing MLEC from WT and TET2 endo KO mice revealed differential expression of many genes involved in cytokine signalling, leukocyte recruitment and leukocyte transmigration (Figures 5.14 & 5.15). Therefore, the hypothesis that endothelial TET2 may be involved in leukocyte recruitment may

be interesting to pursue further. Initially, this could be explored by immunofluorescent staining of leukocyte markers in tissues collected from WT and TET2 endo KO mice to compare their abundance and localisation.

5.3.6 Transcriptomic comparison of mouse lung endothelial cells from chow- and HFD-fed WT and endothelial-specific TET2 KO mice

Abnormalities of angiogenesis are a feature of microvascular and macrovascular diabetic complications [332]. Indeed, RNA sequencing revealed differential expression of genes involved in angiogenesis, development of vasculature and migration of endothelial cells in MLEC from HFD-fed mice compared to chow-fed mice (Figure 5.16). These functions were not associated with differential expression in MLEC from TET2 endo KO compared to WT mice, suggesting that TET2 is not necessarily involved in their regulation (Figure 5.16). This is consistent with RNA sequencing of TET-silenced HUVEC in which no alteration in gene expression in angiogenesis-related pathways was observed (Figure 3.9).

Amongst the pathways in MLEC commonly dysregulated by both TET2 endo KO and HFD consumption were those associated with leukocyte recruitment and transmigration (Figure 5.15). Future research could explore whether the expression of genes belonging to these pathways involves transcriptional regulation by TET2 and whether immune responses in diabetes are worsened or improved in the absence of TET2. Interestingly, interferon signalling was a key feature of altered gene expression in MLEC by both TET2 endo KO and HFD consumption (Figure 5.16). This is consistent with the *in vitro* data which suggested a role for TET2 in repressing or resolving interferon responses in HUVEC (Figures 3.23 & 3.24) and that the response of HUVEC to IFNγ was similarly dysregulated by intermittent high glucose culture (Figure 3.27). In chapter 4, the idea was posited that transcriptional regulation of IRF7 by TET2 could explain the altered expression of interferon-sensitive genes. This idea is further supported here, since IRF7 was among the upstream regulators of genes dysregulated

in MLEC by TET2 endo KO or HFD consumption and was itself upregulated in the absence of TET2 (Figure 5.17).

5.3.7 Methods available to assess TET2 activity in hyperglycaemia

A limitation of this study of MLEC is that the hypothesis that hyperglycaemia alters TET2 activity in endothelial cells has not been explicitly tested. Methods are available to measure global 5hmC levels quantitatively, such as dot blotting and mass spectrometry and qualitatively, such as by immunofluorescent staining. However, it is challenging to obtain enough genomic DNA from MLEC for these types of quantitative analyses (*i.e.* 1-2μg) and functionally important TET2 activity may not necessarily alter global levels of 5hmC, but might rather effect locus-specific changes in (hydroxy)methylation patterns. To study this, hydroxymethylated DNA immunoprecipitation sequencing or oxybisulphite sequencing can be used, however, these methods also require relatively high levels of starting material. Furthermore, as some activities of TET2 are non-catalytic, these methods do not address these aspects. Nonetheless, the data presented in Chapter 3 (Figure 3.5) support the hypothesis that TET activity is altered by high glucose levels, leading to changes in hydroxymethylation patterns in HUVEC. In this chapter, correlations have been shown between genes dysregulated by both HFD consumption and TET2 endo KO, with functions relevant to the inflammatory processes that are associated with the vascular dysfunction frequently seen in diabetes. Although the extent to which hyperglycaemia-induced alteration of TET2 activity in endothelial cells is responsible for the transcriptional changes following HFD consumption has not been fully explored, it is possible that some of these changes may involve altered TET2 activity.

In summary, TET2 does not appear to affect endothelial-dependent vasorelaxation of mice under normoglycaemic or hyperglycaemic conditions. However, other aspects of endothelial dysfunction known to be involved in diabetes may be regulated by TET2. These may include inflammatory processes such as cytokine release and the recruitment of leukocytes to and across the endothelium. Interferon signalling in endothelial cells is perturbed by both HFD consumption and by TET2 endo KO, which

could potentially be explained by TET2-mediated transcriptional regulation of IRF7, in agreement with the previous findings described here.

6. General discussion

6.1 Introduction

The data presented in this thesis provide evidence for the functional importance of TET2 in the regulation of interferon signalling, cholesterol homeostasis, cytokine release and permeability of endothelial cells. Using *in vitro* and *in vivo* approaches, comparisons have been made between high glucose-induced and TET2-mediated changes in gene expression and endothelial function, which revealed some common features. These findings will now be discussed in the context of existing literature and the broader implications of this work will be considered.

6.2 Hyperglycaemia and endothelial dysfunction

Hyperglycaemia is well-documented to induce endothelial dysfunction, including perturbations to the regulation of permeability, leukocyte adhesion and vascular tone [14, 15, 49, 50]. However, data presented here did not show any difference in TNFα- or LPS-stimulated HUVEC permeability (Figure 4.37) or TNFα- or LPS-stimulated adhesion of HL-60 (neutrophil-like) cells to HUVEC monolayers when cultured under high glucose conditions (Figure 4.33). Nor was a difference observed in the phenylephrine-induced constriction or acetylcholine-induced relaxation of aortic rings from control (chow-fed) or hyperglycaemic (HFD-fed) mice. Nonetheless, differences in gene expression were evident in HUVEC and MLEC as a result of high glucose culture or HFD consumption (Figures 3.11 & 5.14). This encompassed altered transcription of genes related to mitochondrial function and oxidative phosphorylation, angiogenesis, leukocyte recruitment and inflammation (Figures 3.11 & 5.14).

6.3 Hyperglycaemia and altered TET activity

DNA methylation changes have been observed in various tissues from diabetic patients compared to healthy controls [122-128]. Additionally, studies have shown altered DNA methylation and gene expression in endothelial cells cultured under (stable or intermittent) high glucose conditions [133, 134, 136, 137, 224-229]. Owing to changes in metabolic flux, O_2 availability and cellular redox in endothelial cells in hyperglycaemia [173], as well as the documented AMPK-mediated phosphorylation of TET2 in a glucose concentration-dependent manner in diabetic PBMCs [183], it was hypothesised that the activity of TET enzymes in endothelial cells may be altered by hyperglycaemia. Although no change in the global level of 5hmC was observed in HUVEC cultured under high glucose conditions for 48h (Figure 3.4), an altered pattern of 5hmC enrichment across the genome was observed following high glucose culture of HUVEC for 2 weeks (Figure 3.5). Furthermore, intermittent high glucose culture for 2 weeks increased the IFNγ-induced expression of interferon-sensitive genes and delayed their return to baseline levels following removal of IFNγ (Figure 3.27), similar to that observed when TET2 was silenced (Figure 3.24). Similarities were observed between RNA sequencing datasets examining the effect of TET2endoKO or HFD consumption on the MLEC transcriptome compared to controls (Figures 5.15 & 5.16). In particular, interferon signalling was identified as a feature common to both, noting that the differential expression of IRF7, as an upstream regulator, could account for the expression patterns observed in both datasets (Figure 5.17) (in agreement with that observed in TET2-silenced HUVEC (Figure 4.7)). Notably, IRF7 is a known target of TET2 catalytic activity in plasmacytoid dendritic cells [160] and data presented here support the potential regulation of IRF7 expression in endothelial cells by DNA methylation and TET2 catalytic activity (Figures 4.9 & 4.10). Interestingly, the expression of IRF7 in PBMCs of diabetic patients is known to correlate with blood glucose levels [333], indicating that the interferon response of these cells may be augmented by hyperglycaemia. Given that TET2 is known to be destabilised by hyperglycaemia in diabetic PBMCs (due to loss of AMPK-mediated phosphorylation of the protein), leading to a decrease in its activity [183], it may be speculated that a loss of TET2-mediated suppression of IRF7 is responsible for this observation.

6.4 Relationship between TET activity and altered gene expression

TET enzymes catalyse the successive oxidation of 5mC to 5hmC, 5fC and 5caC. These intermediate modified forms of cytosine can be lost passively during DNA replication, as they are not recognised by DNMT1 as methylated and therefore not maintained in daughter strands [334]. Active DNA demethylation occurs when the final two intermediates, 5caC or 5fC, are excised by thymine DNA glycosylase and replaced with unmethylated cytosine by base excision repair machinery [335]. Typically, the presence of 5mC within CpG islands of promoter regions is associated with transcriptional repression [336]. Removal of 5mC, or the presence of catalytic intermediates like 5hmC (the most stable of the intermediates), is often associated with transcriptional activation [336]. However, in the RNA sequencing datasets described here, it was interesting to note that over one third of genes showing differential expression upon TET1- or TET2- silencing were upregulated rather than downregulated and an even greater proportion (62%) were upregulated upon TET3 silencing (Figure 3.7). If TET activity is associated with transcriptional activation, then it may be expected that their silencing would lead to maintained methylation and therefore downregulation of genes. These findings could therefore indicate two levels of regulation. For example, if the TET enzyme activates a transcriptional repressor, then silencing the TET could decrease its activity and lead to upregulation of other genes.

Alternatively, the upregulation of genes following TET silencing could be explained by a more nuanced understanding of how TETs mediate transcriptional regulation. Williams *et al.* reported that inhibition of TET1 expression in mouse embryonic stem (ES) cells led to a higher fraction of differentially-expressed genes being upregulated than downregulated [337]. The authors suggest that TET1-mediated transcriptional repression is independent of its catalytic activity, as the transcriptional effects of TET1 silencing were also evident when TET1 was silenced in ES cells lacking DNMTs [337]. Instead, the mechanism of repression proposed was recruitment of the SIN3A co-repressor complex by TET1 [337]. The dual function of TET1 as a transcriptional

repressor as well as an activator was simultaneously reported by another group, who showed that recruitment of polycomb-repressor complex 2 (PRC2) by TET1 contributed to repression of developmental regulators in mouse ESCs [265].

More recently, TET2 has also been shown to be involved in transcriptional repression, in this case repressing a number of pro-inflammatory mediators in innate myeloid cells [158]. Among them was IL-6, which was shown to be repressed during the resolution of the cellular response to LPS by the recruitment of HDAC2 to the IL-6 promoter by TET2 [158]. Accordingly, it was reasoned that involvement of HDACs could explain the TET2-mediated transcriptional repression of interferon-sensitive genes observed in the present study. Indeed, silencing of HDAC1 or TET2 produced similar effects on IFITM1 and ISG15 expression (Figures 4.16 & 4.17). Non-catalytic roles for TETs in mediating transcriptional repression could explain the high proportion of upregulated genes upon TET silencing that was observed in HUVEC by RNA sequencing (Figure 3.7). The differences in proportion of up- and downregulated genes following silencing of the three TETs may be attributable to varying contributions of non-catalytic and catalytic activities to the functions of each enzyme.

Another possibility is that TET catalytic activity is involved in the regulation of these genes but that 5mC is not always a repressive mark and/or that 5hmC, 5fC and 5caC are not always activating marks. Approximately 5% of cytosine residues in the genome are estimated to be 5mC and less than 1% estimated to be 5hmC. 5fC and 5caC abundance is much lower; approximately 10-1000 fold less than that of 5hmC [139, 143]. Although 5mC is typically associated with transcriptional downregulation, it has been reported that 5mC may not always be a repressive mark [338, 339]. In a recent bioinformatic analysis comparing prostate cancer and healthy tissues, a strong association was found between promoter hypermethylation and increased gene expression (as well as the canonical association between promoter hypermethylation and decreased gene expression) [338]. This is in agreement with a previous study of

differentially-methylated and differentially-expressed genes in mouse retina and brain samples, showing a positive, as well as negative association between DNA methylation and gene expression [339]. The finding that some transcription factors preferentially bind methyl-CpG islands over unmethylated CpGs could, at least in part, explain this observation [340, 341]. It is understandable therefore, that removal of 5mC by TET-mediated demethylation could cause gene repression in some instances.

The relationship between 5hmC and gene expression is also complex. 5hmC is the most stable, abundant and well-characterised catalytic intermediate of 5mC demethylation. 5hmC is often found within gene bodies, where, in some reports, 5hmC levels correlate positively with gene expression [342, 343]. However, this appears to be dependent on cell type, as Tan *et al*. found that 5hmC deposition over the gene body correlated positively with gene expression in mouse ES cells, but negatively with gene expression in neural progenitor cells [293]. 5hmC can also be highly enriched at the transcriptional start site of developmental regulators known to be repressed by TET1/polycomb repressive complex 2, again demonstrating that 5hmC abundance does not always correlate with gene activation [293]. Understanding whether causal relationships exist between specific epigenetic modifications and gene expression is a major challenge in the field, particularly as they may be cell type-specific. Comparisons can be made between transcriptomic and epigenomic datasets such as the RNA sequencing and hMeDIPseq datasets generated here for HUVEC. Recent advances have made it possible to manipulate the epigenome using the clustered regularly interspaced short palindromic repeat- (CRISPR-) associated protein 9 (Cas9) system to guide epigenetic modifiers to specific genetic loci [344]. The use of this technology could help to unveil the precise activity of TET2 in endothelial cells and its relationship to gene expression.

Despite their relatively low abundance, it has become increasingly appreciated that as well as being intermediates of 5mC demethylation, 5fC and 5caC themselves may have unique functions, which are not yet fully understood [345-347]. The existence of

proteins which selectively bind 5fC or 5caC also gives credence to their potential as epigenetic marks in their own right [348-350], although owing to the low abundance of these modifications and their propensity for further processing, this is a challenging area of study. As such, the nature of their relationship to gene expression is not fully understood, but there is evidence that 5fC and 5caC in gene bodies reduce the rate of RNA polymerase II transcription elongation, which could, in theory, influence gene expression [347]. Adding a further level of complexity, it has been suggested that the TET enzymes have different propensities to catalyse each step of the successive oxidation of 5mC, with TET2 contributing more to the conversion of 5hmC to 5fC than TET1 does in mouse ES cells and epiblast-like stem cells (independent of which TET is more highly expressed) [210]. It could be speculated that upon individual silencing of TETs, the formation of each catalytic intermediate may differ, leading to different outcomes for gene expression. This, among other diverse mechanisms discussed here, demonstrate the complexity of TET-mediated regulation of gene expression underlying the findings presented. A summary of the possible mechanisms of gene repression involving TET enzymes are displayed below (Figure 6.1).

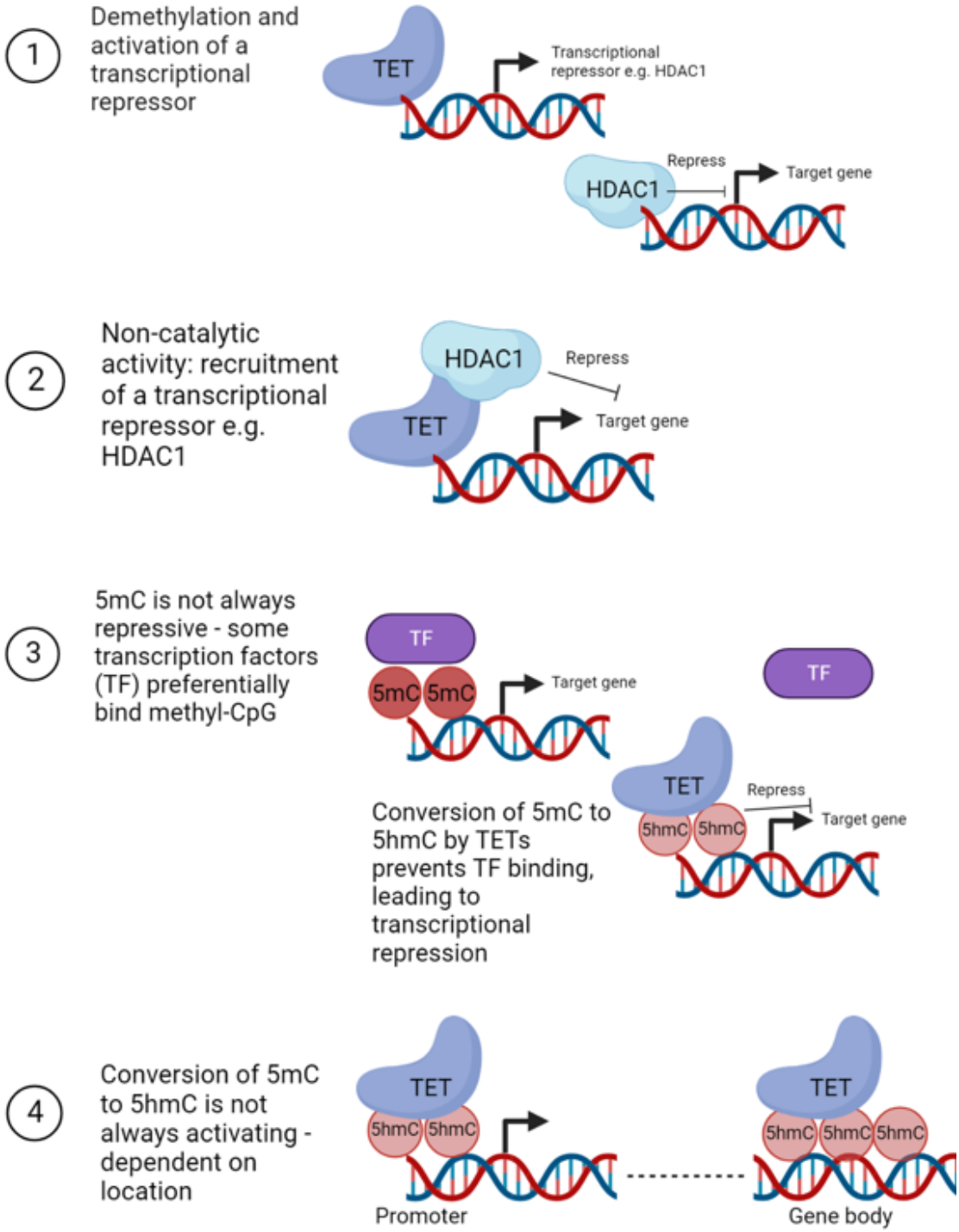

Figure 6.1: ***Mechanisms of TET-mediated gene repression****. Repression of a target gene could occur indirectly by TET-mediated activation of a repressor (1) or by TET-mediated recruitment of a repressor (2) such as histone deacetylase 1 (HDAC1). Given that some transcription factors (TF) preferentially bind methyl-CpGs, conversion of 5mC to 5hmC by TETs may prevent TF binding and lead to transcriptional repression (3). The presence of 5hmC may be associated with transcriptional activation or repression depending on whether it is located within a promoter or a gene body (4).*

6.5 The relationship of TET2 with immunity and inflammation

Since the identification of TETs as cytosine demethylases in 2009, an increasing number of publications have made a link between TETs and roles in inflammation and immunity [158-162]. In particular, TET2 is associated with immune cells because of its important role in the differentiation of haematopoietic stem cells (HSCs) and myelopoiesis [149]. In the absence of TET2, increased self-renewal of HSCs and skewing towards myeloid lineages is observed [149]. Accordingly, somatic mutations in TET2 are common in acute myeloid leukaemia, chronic myelomonocytic leukaemia, myelodysplastic syndromes and other myeloid malignancies [351]. Functions for TET2 in innate immune cells include the repression of IL-6 and IL-1β for the resolution of inflammatory activation in macrophages and dendritic cells [158, 159], the regulation of mast cell differentiation and proliferation [161] and regulation of the antiviral response of plasmacytoid dendritic cells [160]. TET2 also has roles in adaptive immunity, for example, TET2 and TET3 co-operatively repress CD86 to prevent B cell hyperactivity and autoimmunity [162].

A relationship between TET2 and interferon signalling was reported in plasmacytoid dendritic cells, where it was shown that CXXC5 recruits TET2 to maintain hypomethylation of a CpG island within the IRF7 promoter, enabling activation of antiviral responses in response to TLR7/9 signalling [160]. Inhibition of TET2 expression led to attenuated interferon production and rendered $TET2^{-/-}$ mice more susceptible to viral infection [160]. In the present study, IRF7 was identified as a potential upstream regulator accounting for the upregulation of interferon-sensitive genes upon TET2 silencing in HUVEC (Figure 4.7). This was also the case in the RNA sequencing analysis of MLEC from TET2endoKO mice compared to those from WT mice (Figure 5.17). The findings presented here support the possibility of TET2-mediated regulation of the methylation status of IRF7, with two regions of the gene body becoming hypo-hydroxymethylated upon silencing of TET2 (Figure 4.10). However, this was associated with *upregulation* of IRF7 and other interferon-sensitive genes, suggesting that in endothelial cells (unlike in plasmacytoid dendritic cells), TET2

acts to repress, rather than activate, interferon responses. Repression of interferon signalling by TET2, in concert with DNMT3a, has recently been reported in macrophages [352]. In their study, TET2 binding was not apparent at interferon-sensitive genes. Instead, the upregulation of interferon-sensitive genes in the absence of TET2 or DNMT3a was attributed to regulation of TFAM (a mitochondrial DNA transcription factor), release of mitochondrial DNA into the cytoplasm and triggering of an interferon response *via* cGAS signalling (a cytoplasmic DNA sensing pathway) [352]. This raises a possible indirect mechanism by which TET2 can regulate interferon responses, which could similarly exist in endothelial cells.

6.6 TET2 and interferon signalling in atherosclerosis

TET2 has been implicated in the chronic inflammatory condition atherosclerosis, through its involvement in clonal haematopoiesis which is a risk factor for atherosclerosis [157]. Clonal haematopoiesis, the benign expansion of HSCs, particularly the myeloid compartment, occurs during ageing and is frequently associated with somatic mutations in TET2 [353]. In atherosclerosis-prone $LDLR^{-/-}$ mice, the presence of TET2-deficient bone marrow HSCs led to clonal haematopoiesis and increased atherosclerotic plaque size [157]. Aggravation of atherosclerosis was attributed, at least in part, to enhanced NLRP3 inflammasome activity promoting expression of proinflammatory cytokines including IL-1β by TET2-deficient macrophages [157]. Interestingly, although increased proliferation is observed in HSCs with TET2 loss-of-function mutations, siRNA-mediated silencing of TET2 (or indeed individual silencing of any of the three TET enzymes) in HUVEC did not alter their proliferation (Figure 4.26). The potential involvement of TET2 in atherosclerosis and inflammatory signalling has been studied less in endothelial cells than in myeloid cells. However, TET2 has been shown to be important in preventing endothelial dysfunction and improve autophagy induced by oxidised LDL treatment of HUVEC [164, 165]. The expression of TET2 and the abundance of 5hmC have been observed to decrease in the vessel during the progression of the atherosclerosis and overexpression of TET2 in $ApoE^{-/-}$ mice reduced the formation of atherosclerotic plaques [164].

IFNγ is a key pro-inflammatory mediator in atherosclerotic lesions produced primarily by CD4+ and CD8+ T cells which acts on the endothelium and causes them to express adhesion molecules and chemokines which contribute to monocyte recruitment to the endothelium [230, 246]. Individuals with autoimmune conditions such as systemic lupus erythematosus (SLE), characterised by raised circulating type I interferon levels, are predisposed to atherosclerosis and early cardiovascular disease mortality [354]. This has been attributed, in part, to endothelial dysfunction exacerbated by the chronic inflammatory environment, including high IFNα levels, to which the endothelium is exposed [355]. Furthermore, multiple studies have reported the involvement of IFNγ and JAK-STAT signalling in endothelial dysfunction and the vascular complications of diabetes [251-254]. Given that perturbed interferon signalling is involved in vascular diseases, it is important for endothelial cells to regulate the expression of interferon-sensitive genes appropriately during the activation and resolution of an inflammatory response. The data presented here suggest that TET2 may be important for these regulatory mechanisms. Since TET2 protects against endothelial dysfunction in the context of other pro-inflammatory stimuli involved in atherosclerosis [165], it is tempting to speculate that TET2-mediated suppression of interferon responses in endothelial cells may play an important protective role in atherosclerosis.

Increased interferon-stimulated release of CXCL10 and CXCL11 was observed in TET2-silenced HUVEC relative to controls (Figure 4.28). High levels of these cytokines have been observed in atherosclerotic plaques and a high abundance of CXCL10 is associated with plaque instability [356, 357]. An increased abundance of these cytokines could contribute to T cell accumulation within atherosclerotic plaques, particularly CD8+ and Th1 cells as they abundantly express the CXCR3 receptor for which these cytokines are ligands [358]. Furthermore, IFNγ-driven CXCL10 release from smooth muscle cells has been shown to inhibit endothelial recovery following arterial injury, so could contribute to the persistent endothelial dysfunction in atherosclerosis [359]. Genetic deletion of CXCL10 in $ApoE^{-/-}$ mice or pharmacological inhibition of CXCR3 in $LDLR^{-/-}$ mice has been shown to reduce the development of

atherosclerotic lesions [360, 361]. Increasingly, studies demonstrate the importance of CXCR3 and its ligands in the pathogenesis of atherosclerosis and other cardiovascular diseases [362]. Perhaps, by limiting interferon-induced expression of CXCL10 and CXCL11, TET2 plays a protective role.

No difference in adhesion of neutrophil-like cells was observed between monolayers of control and TET2-silenced HUVEC (Figures 4.31 & 4.32). Nor was there a difference in adhesion of BMCs to monolayers of WT and TET2endoKO MLEC using *in vitro* assays (Figure 5.9). However, cytokine signalling, leukocyte recruitment and leukocyte transmigration were amongst the biological functions related to genes that were differentially-expressed by both TET2 endo KO and HFD consumption (Figures 5.14 & 5.15). Perhaps differences in leukocyte recruitment in the absence of endothelial TET2 may be apparent for specific leukocyte subtypes such as macrophages or T cells, under flow conditions and/or in the presence of multiple pro-inflammatory mediators.

It has been reported that IFNγ-stimulation of endothelial cells elicits a persistent pro-inflammatory phenotype (involving chemokine release, adhesion molecule upregulation, co-stimulatory molecule expression and antigen presentation) which takes longer to resolve than that of TNFα [363]. Whereas removal of the TNFα stimulus triggered resolution of the response and restoration of homeostasis in endothelial cells, the effects of IFNγ-stimulation lasted at least two days after its removal [363]. This is in agreement with the data presented here, showing that the expression of ISG15 and IFITM1 remained higher than baseline 24h after removal of IFNγ, even in control cells (Figure 3.24). This delayed recovery was exacerbated in the absence of TET2 (Figure 3.24). Interestingly, a recent study has suggested that whilst the acute effects of TNFα on the endothelium are mediated by NFκB signalling, the later and more prolonged effects of TNFα are rather driven by IRF/STAT-mediated transcription [364]. Since the effects of IRF/STAT are sustained and less readily resolved [363, 364], this places interferon signalling as a crucial mediator of chronic activation of endothelial cells (*i.e.* endothelial dysfunction) which is known to be

detrimental in vascular diseases. It may be speculated that similar to the phenomenon of 'hyperglycaemic memory', inflammatory stimuli may produce a memory in endothelial cells that sustains their dysfunction even in the absence of the initiating stimulus. Such a memory could involve epigenetic mechanisms and from the data presented here, TET2-dependent regulation of interferon signalling is a possible candidate.

The importance of TET2 in the resolution of interferon responses in endothelial cells could therefore represent a possible therapeutic target for chronic inflammatory conditions such as atherosclerosis where the prolonged effects of interferon signalling contribute to endothelial dysfunction and disease progression. Changes to the metabolic flux, cellular redox and O_2 availability within endothelial cells as a result of cardiovascular disease risk factors such as diabetes, obesity, smoking and hypertension could alter TET2 activity (*e.g.* by increased ROS production altering the redox balance and decreasing Fe^{2+} availability, required for TET activity [173]) and lead to aberrant interferon signalling, contributing to prolonged endothelial dysfunction and amplification of inflammatory/immune responses. Furthermore, given that somatic mutations in TET2 which cause HSC expansion in clonal haematopoiesis (and are associated with atherosclerosis [157, 353]) have also been observed in mature circulating endothelial cells (suggestive of a common precursor cell) [365], it is plausible that loss-of-function mutations in TET2 in endothelial cells (as well as those affecting the myeloid compartment) may play a role in atherogenesis. However, the identification, origin and importance of endothelial progenitor cells remains controversial [366].

6.7 Cholesterol homeostasis in atherosclerosis

Hypercholesterolaemia is one of the primary risk factors for atherosclerotic cardiovascular disease [50]. Intimal accumulation of LDL is a major event in the initiation of atherosclerosis, leading to the formation of foam cells by the uptake of oxidised LDL primarily by macrophages as well as smooth muscle cells [50, 255].

Although endothelial cells express lipoprotein receptors and can allow entry of lipoproteins *via* endocytosis, they do not accumulate cholesterol to the same extent as macrophages and smooth muscle cells [255]. This has been suggested to be due to tight regulation of cholesterol homeostasis by decreased cholesterol biosynthesis and LDLR expression and increased cholesterol efflux by endothelial cells in response to elevated extracellular cholesterol levels [255]. However, the precise mechanisms underlying endothelial cholesterol homeostasis have not been extensively studied. Herein, evidence is provided for the first time that TET2 may be involved in regulating cellular cholesterol levels (Figure 4.23). This is mechanistically explained by transcriptional regulation of cholesterol biosynthesis genes in endothelial cells (Figure 3.30), possibly involving TET2-dependent changes to the methylation status and expression of CH25H (Figures 3.32, 4.21 & 4.22). However, it is surprising, given the negative regulation of cholesterol biosynthesis genes by 25-HC (Figure 4.20), that TET2 silencing upregulates both CH25H and biosynthetic enzymes (Figures 3.30 & 3.32). Further research is warranted to explore this complex relationship.

Recently, some insights have been gained about the potential contribution of endothelial cell cholesterol metabolism to early stages of atherogenesis [367]. In response to high levels of LDL *in vitro*, endothelial cells generated cholesterol crystals, which are pro-inflammatory and perturb endothelial function [367]. *In vivo*, cholesterol crystals were observed in the sub-endothelial space following only short-term exposure of LDLR-/- mice to hypercholesterolaemic conditions, which *preceded* macrophage infiltration and neointima formation [367]. This indicates that perturbed cholesterol handling by endothelial cells may play an early role in the pathogenesis of atherosclerosis, leading to intimal cholesterol deposition independent of that deposited by macrophages. To summarise the points discussed above, suggestions of the potential effects of altered TET2 activity in the endothelium on the development of an atherosclerotic plaque are displayed as a schematic diagram (Figure 6.2).

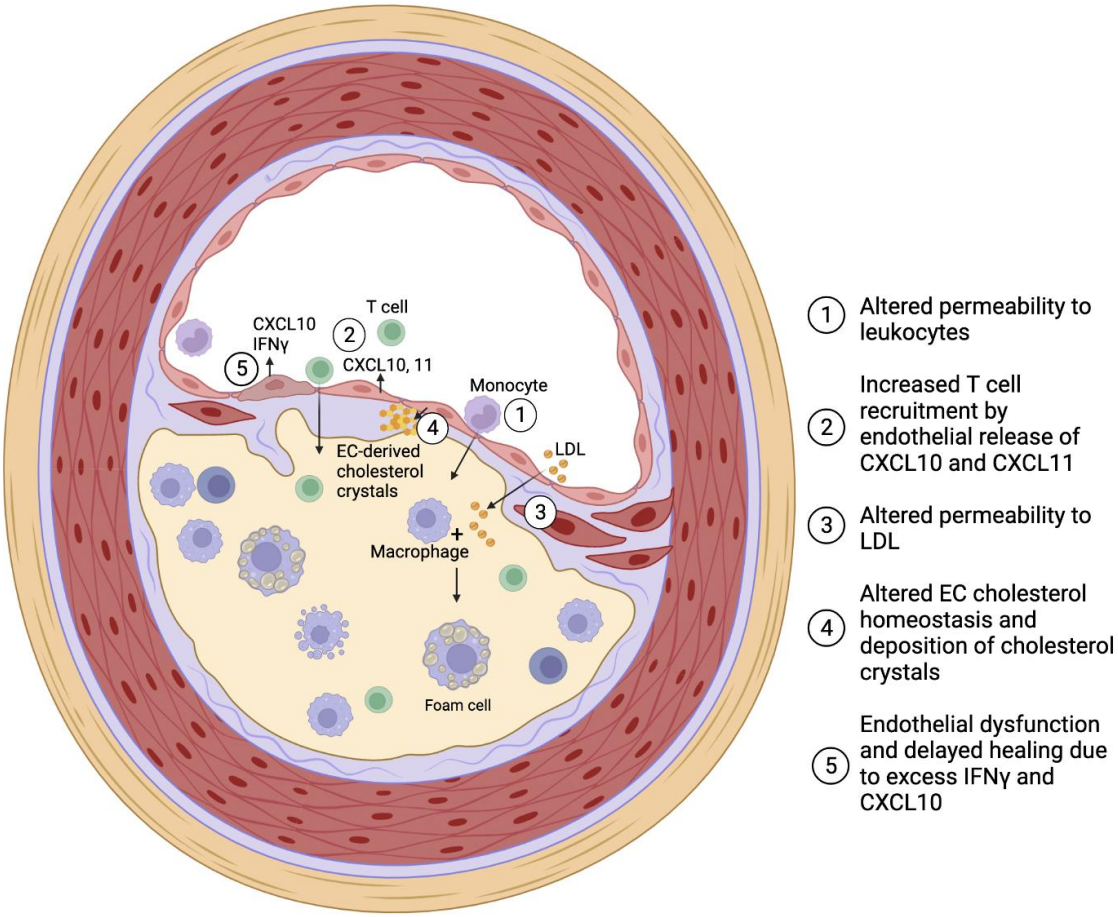

Figure 6.2: ***Potential effects of impaired endothelial TET2 activity on the development of an atherosclerotic plaque.*** *Data presented here suggests that TET2 silencing in the endothelium affects interferon signalling, cholesterol homeostasis, permeability and CXCL10 and CXCL11 release. In the context of atherosclerosis, this may induce endothelial dysfunction, alter the presence of endothelial cell (EC)-derived cholesterol crystals and affect the accumulation of leukocytes and low-density lipoprotein (LDL) in the intima.*

6.8 TET2, interferon signalling and cholesterol homeostasis in endothelial cells

In innate immune cells, it has previously been suggested that downregulation of cholesterol synthesis in response to pathogen sensing acts as a host defence mechanism [235]. This is thought to be because pathogens may utilise host cell energy sources for their own growth and replication, so the host cell decreases the available pool of cholesterol to prevents this [235]. To prevent this, signalling *via* TLRs and IFNs regulate cholesterol handling at various levels. For example, by downregulation of biosynthetic enzymes [368], increased production of 25HC [238, 259] and re-distribution of free cholesterol to an esterified cholesterol pool [369]. Although the relationship between inflammatory processes and cholesterol homeostasis is less

studied in endothelial cells, a recent publication has shown that TNFα and IL-1β, signalling *via* NFκB, alter the distribution of cholesterol and trigger SREBP-2-mediated upregulation of cholesterol biosynthesis genes in endothelial cells [370]. Data presented here, although preliminary, suggest that in endothelial cells, IFNγ decreases free intracellular cholesterol (Figure 4.24). IFNα, by contrast, acts to increase free intracellular cholesterol levels (Figure 4.24). A small but not statistically significant increase in esterified cholesterol levels was observed upon stimulation with IFNα or IFNγ (Figure 4.24). At baseline, TET2 silencing in HUVEC increases both free and esterified cholesterol levels, in agreement with the data showing upregulation of cholesterol biosynthesis genes (Figures 3.30 & 4.23). However, after IFN treatment, no difference in the esterified cholesterol level was observed between siRNA controls and TET2-silenced HUVEC, abolishing the differences seen at baseline (Figure 4.25). TET2 may therefore be involved in regulating cellular cholesterol esterification in response to interferons in endothelial cells. In agreement with this, one of the two main enzymes responsible for intracellular cholesterol esterification, ACAT2, was upregulated in TET2-silenced HUVEC compared to controls in the RNA sequencing dataset (Figure 3.29). These data suggest opposing actions of type I and type II interferon on endothelial cell cholesterol levels which may involve regulation by TET2.

The relationship between TET2 and cholesterol biosynthesis in endothelial cells is a novel finding. Existing studies support the involvement of DNA methylation in the regulation of cholesterol homeostasis [291, 371-373]. CH25H, which was found to be upregulated and show altered gene body hydroxymethylation upon TET2 silencing in the present study (Figures 3.32 & 4.22), has previously been shown to be regulated by DNA methylation [291]. Additionally, epigenome-wide association studies (EWAS) have demonstrated differential-methylation of various genes involved in cholesterol homeostasis (such as the reverse cholesterol transporter ATP-binding cassette sub-family G member 1 (ABCG1) and the transcription factor SREBF1) correlated with HDL, LDL and triglyceride levels in the blood, measures of adiposity and cardiovascular events [371-373].

6.9 TET2 and endothelial permeability

In vitro findings suggest that TET2 regulates the baseline permeability of endothelial cells (Figure 4.38). This may be important to maintain the appropriate degree of permeability of the endothelial barrier under homeostatic conditions. Given that plasma membrane cholesterol levels dictate the fluidity and rigidity of membranes [234], one possibility is that the in the absence of TET2, the increase in cholesterol levels causes stiffening of the lipid bilayer, which could impact the tightness of intercellular junctions leading to the decrease in permeability that was observed. However, casting doubt on this idea, it has previously been found that although depletion of membrane cholesterol typically makes cell membranes less rigid, the opposite has been observed in bovine aortic endothelial cells [374, 375]. Nonetheless, there is evidence to suggest that cholesterol can influence endothelial permeability. Cholesterol crystals (which have been documented to be of endothelial origin in some cases [367]) disrupted adherens junctions and increased the permeability of human aortic endothelial cells *in vitro* [286]. Treatment of HUVEC with LDL increased the passage of high molecular weight dextrans *via* the transcellular route in a cholesterol-dependent manner [376]. Furthermore, treatment of HUVEC or human pulmonary artery endothelial cells with simvastatin improved their barrier function (although this is not necessarily attributable to the cholesterol-lowering effect of statins) [377, 378].

It may also be hypothesised that TET2 directly regulates components of endothelial tight junctions or adherens junctions at the transcriptional level. Differential mRNA expression of genes encoding the main components of tight junctions (claudins, occludin, junctional adhesion molecules and zonula occludens [33]) or adherens junctions (catenins and VE-cadherin [33]) was not observed in the RNA sequencing dataset comparing TET2-silenced and siRNA control HUVEC. However, the interferon-sensitive gene IFITM1 has been identified as a tight junction protein which interacts with occludin in hepatocytes to inhibit viral entry [379]. Moreover, this interaction has been confirmed in endothelial cells, where IFITM1 appears to be required for the formation of cell-cell contacts during angiogenesis [244]. This raises the possibility that

TET2-mediated regulation of IFITM1 expression may regulate the proper formation of tight junctions in endothelial cells, which in turn could account for the decrease in permeability observed in TET2-silenced HUVEC.

Given that endothelial hyperpermeability is a feature of vascular diseases including diabetic retinopathy and atherosclerosis, it is clearly essential to maintain proper control of endothelial barrier function. However, whilst TET2 may be hypothesised to play a protective role in limiting excessive interferon signalling, if TET2 activity increases endothelial permeability, this could be damaging in the context of vascular disease, for example, by favouring intimal LDL accumulation in atherogenesis. Silencing or overexpression of TET2 and IFITM1 in combination with transwell and transendothelial electrical resistance (TEER) *in vitro* permeability assays and immunofluorescent imaging may help to elucidate the roles of these proteins in regulating endothelial permeability. This study could also be extended to an *in vivo* setting using the Miles assay. Whether or not endothelial TET2 exacerbates or improves atherosclerotic plaque burden could be assessed in high cholesterol-fed $ApoE^{-/-}$ or $LDLR^{-/-}$ mice with an endothelial-specific TET2 deletion. However, TET2-dependent alterations of endothelial cholesterol homeostasis may be challenging to investigate in this setting, as both mouse models involve altered cholesterol transport.

6.10 Considerations and future directions

In addition to the limitations mentioned throughout this thesis, it is important to note that the heterogeneity of endothelial cells across the vascular network is considerable [17] and that findings described here in HUVEC and MLEC may not apply to other endothelial cells. Furthermore, the nature of shear stress (laminar or oscillatory) is known to alter the transcriptome and epigenome of endothelial cells and accounts for the preferential development of atherosclerosis at regions of the vascular tree that encounter disturbed blood flow [380]. The lack of incorporation of shear stress during cell culture experiments is likely to cause deviation from the (patho)physiological setting, as well as the lack of mural cells and extracellular milieu.

To build on the findings of this work, future studies could explore the precise mechanisms underlying TET2-mediated regulation of interferon signalling, for example, by locating TET2-bound regions of the genome, assessing the cytosine modifications present, identifying any binding partners involved and exploring the temporal regulation of these interactions during the cellular response to interferon. The impact of altered cholesterol homeostasis upon the endothelial cell membrane fluidity, cholesterol-dependent signalling pathways and vascular permeability could also be investigated. In addition, the relationship between interferon signalling and cholesterol homeostasis in endothelial cells warrants further study. The formation of foam cells from macrophages and vascular smooth muscle cells and the release of IFNγ by T cells, contribute to atherogenesis [230, 246, 255]. Given that data presented here supports the involvement of TET2 in the regulation of cholesterol homeostasis and interferon signalling in endothelial cells, exploring the involvement of TET2 in the regulation of these pathways in other cell types may be of additional value.

References

1. Zimmet, P., K.G. Alberti, and J. Shaw, *Global and societal implications of the diabetes epidemic.* Nature, 2001. **414**(6865): p. 782-7.
2. Zheng, Y., S.H. Ley, and F.B. Hu, *Global aetiology and epidemiology of type 2 diabetes mellitus and its complications.* Nat Rev Endocrinol, 2018. **14**(2): p. 88-98.
3. Gaede, P., et al., *Multifactorial intervention and cardiovascular disease in patients with type 2 diabetes.* N Engl J Med, 2003. **348**(5): p. 383-93.
4. Kannel, W.B. and D.L. McGee, *Diabetes and cardiovascular disease. The Framingham study.* JAMA, 1979. **241**(19): p. 2035-8.
5. de Ferranti, S.D., et al., *Type 1 diabetes mellitus and cardiovascular disease: a scientific statement from the American Heart Association and American Diabetes Association.* Diabetes Care, 2014. **37**(10): p. 2843-63.
6. Leybovitz-Haleluya, N., et al., *Maternal gestational diabetes mellitus and the risk of subsequent pediatric cardiovascular diseases of the offspring: a population-based cohort study with up to 18 years of follow up.* Acta Diabetol, 2018. **55**(10): p. 1037-1042.
7. Moore, T.R., *Fetal exposure to gestational diabetes contributes to subsequent adult metabolic syndrome.* Am J Obstet Gynecol, 2010. **202**(6): p. 643-9.
8. UK, D. *The Cost of Diabetes Report*. 2014; Available from: https://www.diabetes.org.uk/resources-s3/2017-11/diabetes%20uk%20cost%20of%20diabetes%20report.pdf.
9. Srinivasan, S., et al., *Hyperglycaemia-induced superoxide production decreases eNOS expression via AP-1 activation in aortic endothelial cells.* Diabetologia, 2004. **47**(10): p. 1727-34.
10. Piga, R., et al., *Short-term high glucose exposure induces monocyte-endothelial cells adhesion and transmigration by increasing VCAM-1 and MCP-1 expression in human aortic endothelial cells.* Atherosclerosis, 2007. **193**(2): p. 328-34.
11. Yu, C.H., et al., *High glucose induced endothelial to mesenchymal transition in human umbilical vein endothelial cell.* Exp Mol Pathol, 2017. **102**(3): p. 377-383.
12. Iwasaki H, O.R., Kato S, Konishi K, Mizutani H, Yamada N, Isaka N, Nakano T, Ito M, *High glucose induces plasminogen activator inhibitor-1 expression through Rho/Rho-kinase-mediated NF-κB activation in bovine aortic endothelial cells.* Atherosclerosis, 2008. **196**: p. 22-28.
13. Ho FM, L.S., Liau CS, Huang PJ, Lin-Shiau SY., *High glucose-induced apoptosis in human endothelial cells is mediated by sequential activations of c-JUN NH2-terminal kinase and caspase-3.* Circulation, 2000. **101**: p. 2618-24.
14. Takenouchi, Y., et al., *Gender differences in vascular reactivity of aortas from streptozotocin-induced diabetic mice.* Biol Pharm Bull, 2010. **33**(10): p. 1692-7.
15. Molnar, J., et al., *Diabetes induces endothelial dysfunction but does not increase neointimal formation in high-fat diet fed C57BL/6J mice.* Circ Res, 2005. **96**(11): p. 1178-84.
16. Loader, J., et al., *Acute Hyperglycemia Impairs Vascular Function in Healthy and Cardiometabolic Diseased Subjects: Systematic Review and Meta-Analysis.* Arterioscler Thromb Vasc Biol, 2015. **35**(9): p. 2060-72.

17. Aird, W.C., *Phenotypic heterogeneity of the endothelium: I. Structure, function, and mechanisms.* Circ Res, 2007. **100**(2): p. 158-73.
18. Michiels, C., *Endothelial cell functions.* J Cell Physiol, 2003. **196**(3): p. 430-43.
19. Komarova, Y.A., et al., *Protein Interactions at Endothelial Junctions and Signaling Mechanisms Regulating Endothelial Permeability.* Circ Res, 2017. **120**(1): p. 179-206.
20. Sandoo, A., et al., *The endothelium and its role in regulating vascular tone.* Open Cardiovasc Med J, 2010. **4**: p. 302-12.
21. Yau, J.W., H. Teoh, and S. Verma, *Endothelial cell control of thrombosis.* BMC Cardiovasc Disord, 2015. **15**: p. 130.
22. Eelen, G., et al., *Basic and Therapeutic Aspects of Angiogenesis Updated.* Circ Res, 2020. **127**(2): p. 310-329.
23. Shao, Y., et al., *Vascular Endothelial Cells and Innate Immunity.* Arterioscler Thromb Vasc Biol, 2020. **40**(6): p. e138-e152.
24. Ley, K., et al., *Getting to the site of inflammation: the leukocyte adhesion cascade updated.* Nat Rev Immunol, 2007. **7**(9): p. 678-89.
25. Neubauer, K. and B. Zieger, *Endothelial cells and coagulation.* Cell Tissue Res, 2022. **387**(3): p. 391-398.
26. Gu, C., et al., *Comprehensive analysis of angiogenesis-related genes and pathways in early diabetic retinopathy.* BMC Med Genomics, 2020. **13**(1): p. 142.
27. Maas, J.W., et al., *Endometrial angiogenesis throughout the human menstrual cycle.* Hum Reprod, 2001. **16**(8): p. 1557-61.
28. Adams, R.H. and K. Alitalo, *Molecular regulation of angiogenesis and lymphangiogenesis.* Nat Rev Mol Cell Biol, 2007. **8**(6): p. 464-78.
29. Sedding, D.G., et al., *Vasa Vasorum Angiogenesis: Key Player in the Initiation and Progression of Atherosclerosis and Potential Target for the Treatment of Cardiovascular Disease.* Front Immunol, 2018. **9**: p. 706.
30. Blanco, R. and H. Gerhardt, *VEGF and Notch in tip and stalk cell selection.* Cold Spring Harb Perspect Med, 2013. **3**(1): p. a006569.
31. Flournoy, J., S. Ashkanani, and Y. Chen, *Mechanical regulation of signal transduction in angiogenesis.* Front Cell Dev Biol, 2022. **10**: p. 933474.
32. Munoz-Chapuli, R., A.R. Quesada, and M. Angel Medina, *Angiogenesis and signal transduction in endothelial cells.* Cell Mol Life Sci, 2004. **61**(17): p. 2224-43.
33. Cong, X. and W. Kong, *Endothelial tight junctions and their regulatory signaling pathways in vascular homeostasis and disease.* Cell Signal, 2020. **66**: p. 109485.
34. Kevil, C.G., et al., *Expression of zonula occludens and adherens junctional proteins in human venous and arterial endothelial cells: role of occludin in endothelial solute barriers.* Microcirculation, 1998. **5**(2-3): p. 197-210.
35. Hirase, T., et al., *Occludin as a possible determinant of tight junction permeability in endothelial cells.* J Cell Sci, 1997. **110 (Pt 14)**: p. 1603-13.
36. Claesson-Welsh, L., E. Dejana, and D.M. McDonald, *Permeability of the Endothelial Barrier: Identifying and Reconciling Controversies.* Trends Mol Med, 2021. **27**(4): p. 314-331.
37. Ferrero, E., et al., *The platelet endothelial cell adhesion molecule-1 (PECAM1) contributes to endothelial barrier function.* FEBS Lett, 1995. **374**(3): p. 323-6.

38. Ng, C.T., et al., *Interferon-Gamma Increases Endothelial Permeability by Causing Activation of p38 MAP Kinase and Actin Cytoskeleton Alteration.* J Interferon Cytokine Res, 2015. **35**(7): p. 513-22.
39. Burke-Gaffney, A. and A.K. Keenan, *Modulation of human endothelial cell permeability by combinations of the cytokines interleukin-1 alpha/beta, tumor necrosis factor-alpha and interferon-gamma.* Immunopharmacology, 1993. **25**(1): p. 1-9.
40. Komarova, Y. and A.B. Malik, *Regulation of endothelial permeability via paracellular and transcellular transport pathways.* Annu Rev Physiol, 2010. **72**: p. 463-93.
41. Muller, W.A., *Transendothelial migration: unifying principles from the endothelial perspective.* Immunol Rev, 2016. **273**(1): p. 61-75.
42. Woodfin, A., et al., *The junctional adhesion molecule JAM-C regulates polarized transendothelial migration of neutrophils in vivo.* Nat Immunol, 2011. **12**(8): p. 761-9.
43. Feng, D., et al., *Neutrophils emigrate from venules by a transendothelial cell pathway in response to FMLP.* J Exp Med, 1998. **187**(6): p. 903-15.
44. Konradt, C. and C.A. Hunter, *Pathogen interactions with endothelial cells and the induction of innate and adaptive immunity.* Eur J Immunol, 2018. **48**(10): p. 1607-1620.
45. Mai, J., et al., *An evolving new paradigm: endothelial cells--conditional innate immune cells.* J Hematol Oncol, 2013. **6**: p. 61.
46. Leeuwenberg, J.F., et al., *Effects of tumor necrosis factor on the interferon-gamma-induced major histocompatibility complex class II antigen expression by human endothelial cells.* Eur J Immunol, 1988. **18**(9): p. 1469-72.
47. Lozanoska-Ochser, B. and M. Peakman, *Level of major histocompatibility complex class I expression on endothelium in non-obese diabetic mice influences CD8 T cell adhesion and migration.* Clin Exp Immunol, 2009. **157**(1): p. 119-27.
48. Kadl, A. and N. Leitinger, *The role of endothelial cells in the resolution of acute inflammation.* Antioxid Redox Signal, 2005. **7**(11-12): p. 1744-54.
49. Rezzola, S., et al., *Angiogenesis-Inflammation Cross Talk in Diabetic Retinopathy: Novel Insights From the Chick Embryo Chorioallantoic Membrane/Human Vitreous Platform.* Front Immunol, 2020. **11**: p. 581288.
50. Libby, P., et al., *Atherosclerosis.* Nat Rev Dis Primers, 2019. **5**(1): p. 56.
51. Bonetti, P.O., L.O. Lerman, and A. Lerman, *Endothelial dysfunction: a marker of atherosclerotic risk.* Arterioscler Thromb Vasc Biol, 2003. **23**(2): p. 168-75.
52. Tabit, C.E., et al., *Endothelial dysfunction in diabetes mellitus: molecular mechanisms and clinical implications.* Rev Endocr Metab Disord, 2010. **11**(1): p. 61-74.
53. Chen, P.Y., et al., *Endothelial-to-mesenchymal transition drives atherosclerosis progression.* J Clin Invest, 2015. **125**(12): p. 4514-28.
54. Lind, L., et al., *Endothelial function in resistance and conduit arteries and 5-year risk of cardiovascular disease.* Circulation, 2011. **123**(14): p. 1545-51.
55. Huang, A.L., et al., *Predictive value of reactive hyperemia for cardiovascular events in patients with peripheral arterial disease undergoing vascular surgery.* Arterioscler Thromb Vasc Biol, 2007. **27**(10): p. 2113-9.
56. Yeboah, J., et al., *Predictive value of brachial flow-mediated dilation for incident cardiovascular events in a population-based study: the multi-ethnic study of atherosclerosis.* Circulation, 2009. **120**(6): p. 502-9.

57. Bierhansl, L., et al., *Central Role of Metabolism in Endothelial Cell Function and Vascular Disease.* Physiology (Bethesda), 2017. **32**(2): p. 126-140.
58. Du, X.L., et al., *Hyperglycemia-induced mitochondrial superoxide overproduction activates the hexosamine pathway and induces plasminogen activator inhibitor-1 expression by increasing Sp1 glycosylation.* Proc Natl Acad Sci U S A, 2000. **97**(22): p. 12222-6.
59. Sasaki, N., et al., *Augmentation of vascular remodeling by uncoupled endothelial nitric oxide synthase in a mouse model of diabetes mellitus.* Arterioscler Thromb Vasc Biol, 2008. **28**(6): p. 1068-76.
60. Hink, U., et al., *Mechanisms underlying endothelial dysfunction in diabetes mellitus.* Circ Res, 2001. **88**(2): p. E14-22.
61. Hamada, Y., et al., *Role of polyol pathway in nonenzymatic glycation.* Nephrol Dial Transplant, 1996. **11 Suppl 5**: p. 95-8.
62. Goldin, A., et al., *Advanced glycation end products: sparking the development of diabetic vascular injury.* Circulation, 2006. **114**(6): p. 597-605.
63. Muniyappa, R. and J.R. Sowers, *Role of insulin resistance in endothelial dysfunction.* Rev Endocr Metab Disord, 2013. **14**(1): p. 5-12.
64. Takeda, Y., et al., *Endothelial Dysfunction in Diabetes.* Biomedicines, 2020. **8**(7).
65. Montagnani, M., et al., *Inhibition of phosphatidylinositol 3-kinase enhances mitogenic actions of insulin in endothelial cells.* J Biol Chem, 2002. **277**(3): p. 1794-9.
66. Ghosh, A., et al., *Role of free fatty acids in endothelial dysfunction.* J Biomed Sci, 2017. **24**(1): p. 50.
67. El-Osta, A., et al., *Transient high glucose causes persistent epigenetic changes and altered gene expression during subsequent normoglycemia.* J Exp Med, 2008. **205**(10): p. 2409-17.
68. Guzik, T.J., et al., *Mechanisms of increased vascular superoxide production in human diabetes mellitus: role of NAD(P)H oxidase and endothelial nitric oxide synthase.* Circulation, 2002. **105**(14): p. 1656-62.
69. Matsumoto, S., et al., *Confirmation of superoxide generation via xanthine oxidase in streptozotocin-induced diabetic mice.* Free Radic Res, 2003. **37**(7): p. 767-72.
70. Pangare, M. and A. Makino, *Mitochondrial function in vascular endothelial cell in diabetes.* J Smooth Muscle Res, 2012. **48**(1): p. 1-26.
71. Schmidt AM, H.O., Chen JX, Li JF, Crandall J, Zhang J, Cao R, Yan SD, Brett J, Stern D., *Advanced glycation endproducts interacting with their endothelial receptor induce expression of vascular cell adhesion molecule-1 (VCAM-1) in cultured human endothelial cells and in mice: A potential mechanism for the accelerated vasculopathy of diabetes.* J Clin Invest., 1995. **96**: p. 1395-1403.
72. Hirose A, T.T., Mori H, Okada Y, Tanaka Y., *Advanced glycation end products increase endothelial permeability through the RAGE/Rho signaling pathway.* FEBS Lett., 2010. **584**: p. 61-6.
73. Esposito, C., et al., *Long-term exposure to high glucose up-regulates VCAM-induced endothelial cell adhesiveness to PBMC.* Kidney Int, 2001. **59**(5): p. 1842-9.
74. Bierhaus A, I.T., Kasper M, Luther T, Quehenberger P, Tritschler H, Wahl P, Ziegler R, Müller M, Nawroth PP., *Advanced glycation end product (AGE)-mediated induction of tissue factor in cultured endothelial cells is dependent on RAGE.* Circulation, 1997. **96**: p. 2262-71.

75. Quehenberger P, B.A., Fasching P, Muellner C, Klevesath M, Hong M, Stier G, Sattler M, Schleicher E, Speiser W, et al., *Endothelin 1 transciption is controlled by nuclear factor-κB in AGE-stimulated cultured endothelial cells.* Diabetes, 2000. **49**: p. 1561-70.
76. Bucala, R., K.J. Tracey, and A. Cerami, *Advanced glycosylation products quench nitric oxide and mediate defective endothelium-dependent vasodilatation in experimental diabetes.* J Clin Invest, 1991. **87**(2): p. 432-8.
77. Federici M, M.R., Mauriello A, Hribal ML, Ferrelli F, Lauro D, Sbraccia P, Spagnoli LG, Sesti G, Lauro R., *Insulin-dependent activation of endothelial nitric oxide synthase is impaired by O-linked glycosylation modification of signaling proteins in human coronary endothelial cells.* Circulation, 2002. **106**: p. 466-72.
78. Shrikhande, G.V., et al., *O-glycosylation regulates ubiquitination and degradation of the anti-inflammatory protein A20 to accelerate atherosclerosis in diabetic ApoE-null mice.* PLoS One, 2010. **5**(12): p. e14240.
79. Zhang, Z., et al., *High glucose inhibits glucose-6-phosphate dehydrogenase via cAMP in aortic endothelial cells.* J Biol Chem, 2000. **275**(51): p. 40042-7.
80. Action to Control Cardiovascular Risk in Diabetes Study, G., et al., *Effects of intensive glucose lowering in type 2 diabetes.* N Engl J Med, 2008. **358**(24): p. 2545-59.
81. Kirkman, M.S., H. Mahmud, and M.T. Korytkowski, *Intensive Blood Glucose Control and Vascular Outcomes in Patients with Type 2 Diabetes Mellitus.* Endocrinol Metab Clin North Am, 2018. **47**(1): p. 81-96.
82. Engerman, R.L. and T.S. Kern, *Progression of incipient diabetic retinopathy during good glycemic control.* Diabetes, 1987. **36**(7): p. 808-12.
83. Kowluru, R.A., *Effect of reinstitution of good glycemic control on retinal oxidative stress and nitrative stress in diabetic rats.* Diabetes, 2003. **52**(3): p. 818-23.
84. Kowluru, R.A., S.N. Abbas, and S. Odenbach, *Reversal of hyperglycemia and diabetic nephropathy: effect of reinstitution of good metabolic control on oxidative stress in the kidney of diabetic rats.* J Diabetes Complications, 2004. **18**(5): p. 282-8.
85. Kelstrup, L., et al., *Insulin resistance and impaired pancreatic beta-cell function in adult offspring of women with diabetes in pregnancy.* J Clin Endocrinol Metab, 2013. **98**(9): p. 3793-801.
86. Tam, W.H., et al., *In Utero Exposure to Maternal Hyperglycemia Increases Childhood Cardiometabolic Risk in Offspring.* Diabetes Care, 2017. **40**(5): p. 679-686.
87. Guillemette, L., et al., *Intrauterine exposure to diabetes and risk of cardiovascular disease in adolescence and early adulthood: a population-based birth cohort study.* CMAJ, 2020. **192**(39): p. E1104-E1113.
88. Yu, Y., et al., *Maternal diabetes during pregnancy and early onset of cardiovascular disease in offspring: population based cohort study with 40 years of follow-up.* BMJ, 2019. **367**: p. l6398.
89. Pathirana, M.M., et al., *Cardiovascular risk factors in offspring exposed to gestational diabetes mellitus in utero: systematic review and meta-analysis.* J Dev Orig Health Dis, 2020. **11**(6): p. 599-616.
90. Holemans, K., et al., *Streptozotocin diabetes in the pregnant rat induces cardiovascular dysfunction in adult offspring.* Diabetologia, 1999. **42**(1): p. 81-9.

91. Samuelsson, A.M., et al., *Diet-induced obesity in female mice leads to offspring hyperphagia, adiposity, hypertension, and insulin resistance: a novel murine model of developmental programming.* Hypertension, 2008. **51**(2): p. 383-92.
92. Bhatt, M.P., et al., *C-peptide protects against hyperglycemic memory and vascular endothelial cell apoptosis.* J Endocrinol, 2016. **231**(1): p. 97-108.
93. Ihnat, M.A., et al., *Reactive oxygen species mediate a cellular 'memory' of high glucose stress signalling.* Diabetologia, 2007. **50**(7): p. 1523-31.
94. Roy, S., et al., *Overexpression of fibronectin induced by diabetes or high glucose: phenomenon with a memory.* Proc Natl Acad Sci U S A, 1990. **87**(1): p. 404-8.
95. Targosz-Korecka, M., et al., *Stiffness memory of EA.hy926 endothelial cells in response to chronic hyperglycemia.* Cardiovasc Diabetol, 2013. **12**: p. 96.
96. Pirola, L., et al., *Epigenetic phenomena linked to diabetic complications.* Nat Rev Endocrinol, 2010. **6**(12): p. 665-75.
97. Waddington, C.H., *The epigenotype. 1942.* Int J Epidemiol, 2012. **41**(1): p. 10-3.
98. Nicoglou, A., *Waddington's epigenetics or the pictorial meetings of development and genetics.* Hist Philos Life Sci, 2018. **40**(4): p. 61.
99. Waddington, C.H., *The strategy of the genes*. 1957, London: George Allen & Unwin LTD.
100. Wu, C. and J.R. Morris, *Genes, genetics, and epigenetics: a correspondence.* Science, 2001. **293**(5532): p. 1103-5.
101. Saksouk, N., E. Simboeck, and J. Dejardin, *Constitutive heterochromatin formation and transcription in mammals.* Epigenetics Chromatin, 2015. **8**: p. 3.
102. Jaenisch, R. and A. Bird, *Epigenetic regulation of gene expression: how the genome integrates intrinsic and environmental signals.* Nat Genet, 2003. **33 Suppl**: p. 245-54.
103. Tahiliani, M., et al., *Conversion of 5-methylcytosine to 5-hydroxymethylcytosine in mammalian DNA by MLL partner TET1.* Science, 2009. **324**(5929): p. 930-5.
104. Hubner, M.R., M.A. Eckersley-Maslin, and D.L. Spector, *Chromatin organization and transcriptional regulation.* Curr Opin Genet Dev, 2013. **23**(2): p. 89-95.
105. Bannister, A.J. and T. Kouzarides, *Regulation of chromatin by histone modifications.* Cell Res, 2011. **21**(3): p. 381-95.
106. Ntorla, A. and J.R. Burgoyne, *The Regulation and Function of Histone Crotonylation.* Front Cell Dev Biol, 2021. **9**: p. 624914.
107. Anand, R. and R. Marmorstein, *Structure and mechanism of lysine-specific demethylase enzymes.* J Biol Chem, 2007. **282**(49): p. 35425-9.
108. Klose, R.J., E.M. Kallin, and Y. Zhang, *JmjC-domain-containing proteins and histone demethylation.* Nat Rev Genet, 2006. **7**(9): p. 715-27.
109. Gangwar, R.S., et al., *Noncoding RNAs in Cardiovascular Disease: Pathological Relevance and Emerging Role as Biomarkers and Therapeutics.* Am J Hypertens, 2018. **31**(2): p. 150-165.
110. Stratton, M.S., F.M. Farina, and L. Elia, *Epigenetics and vascular diseases.* J Mol Cell Cardiol, 2019. **133**: p. 148-163.
111. Pathania, A.S., et al., *The emerging role of non-coding RNAs in the epigenetic regulation of pediatric cancers.* Semin Cancer Biol, 2022. **83**: p. 227-241.
112. Yao, Q., Y. Chen, and X. Zhou, *The roles of microRNAs in epigenetic regulation.* Curr Opin Chem Biol, 2019. **51**: p. 11-17.

113. Hernando-Herraez, I., et al., *DNA Methylation: Insights into Human Evolution.* PLoS Genet, 2015. **11**(12): p. e1005661.
114. Deaton, A.M. and A. Bird, *CpG islands and the regulation of transcription.* Genes Dev, 2011. **25**(10): p. 1010-22.
115. Sproul, D. and R.R. Meehan, *Genomic insights into cancer-associated aberrant CpG island hypermethylation.* Brief Funct Genomics, 2013. **12**(3): p. 174-90.
116. Li, E., T.H. Bestor, and R. Jaenisch, *Targeted mutation of the DNA methyltransferase gene results in embryonic lethality.* Cell, 1992. **69**(6): p. 915-26.
117. Okano, M., et al., *DNA methyltransferases Dnmt3a and Dnmt3b are essential for de novo methylation and mammalian development.* Cell, 1999. **99**(3): p. 247-57.
118. Subramaniam, D., et al., *DNA methyltransferases: a novel target for prevention and therapy.* Front Oncol, 2014. **4**: p. 80.
119. Jjingo, D., et al., *On the presence and role of human gene-body DNA methylation.* Oncotarget, 2012. **3**(4): p. 462-74.
120. Xie, S. and C. Qian, *The Growing Complexity of UHRF1-Mediated Maintenance DNA Methylation.* Genes (Basel), 2018. **9**(12).
121. Siegfried, Z. and H. Cedar, *DNA methylation: a molecular lock.* Curr Biol, 1997. **7**(5): p. R305-7.
122. Dayeh T, V.P., Salö S, Hall E, Nilsson E, Olsson AH, Kirkpatrick CL, Wollheim CB, Eliasson L, Rönn T, et al., *Genome-Wide DNA Methylation Analysis of Human Pancreatic Islets from Type 2 Diabetic and Non-Diabetic Donors Identifies Candidate Genes That Influence Insulin Secretion.* PloS Genetics, 2014. **10**: p. 1004160.
123. Zhao J, G.J., Bremner JD, Vaccarino V, *Global DNA methylation is associated with insulin resistance: A monozygotic twin study.* Diabetes, 2012. **61**: p. 542-6.
124. Hall, E., et al., *DNA methylation of the glucagon-like peptide 1 receptor (GLP1R) in human pancreatic islets.* BMC Med Genet, 2013. **14**: p. 76.
125. Florath, I., et al., *Type 2 diabetes and leucocyte DNA methylation: an epigenome-wide association study in over 1,500 older adults.* Diabetologia, 2016. **59**(1): p. 130-138.
126. Barajas-Olmos, F., et al., *Altered DNA methylation in liver and adipose tissues derived from individuals with obesity and type 2 diabetes.* BMC Med Genet, 2018. **19**(1): p. 28.
127. Kirchner, H., et al., *Altered DNA methylation of glycolytic and lipogenic genes in liver from obese and type 2 diabetic patients.* Mol Metab, 2016. **5**(3): p. 171-183.
128. Martin-Nunez, G.M., et al., *Type 2 diabetes mellitus in relation to global LINE-1 DNA methylation in peripheral blood: a cohort study.* Epigenetics, 2014. **9**(10): p. 1322-8.
129. Malipatil, N., et al., *Assessment of global long interspersed nucleotide element-1 (LINE-1) DNA methylation in a longitudinal cohort of type 2 diabetes mellitus (T2DM) individuals.* Int J Clin Pract, 2018: p. e13270.
130. Pearce MS, M.J., Potter C, Barrett LM, Parker L, Mathers JC, Relton CL, *Global LINE-1 DNA methylation is associated with blood glycaemic and lipid profiles.* Int J Epidemiol., 2012(41): p. 210-7.
131. Morgan, H.D., et al., *Epigenetic inheritance at the agouti locus in the mouse.* Nat Genet, 1999. **23**(3): p. 314-8.

132. Wolff, G.L., et al., *Maternal epigenetics and methyl supplements affect agouti gene expression in Avy/a mice.* FASEB J, 1998. **12**(11): p. 949-57.
133. Biswas S, F.B., Thomas A, Chen S, Aref-Eshghi E, Sadikovic B, Chakrabarti S., *Endothelin-1 regulation is entangled in a complex web of epigenetic mechanisms in diabetes.* Physiological Research, 2018. **67**: p. 115-25.
134. Tewari, S., et al., *Mitochondria DNA replication and DNA methylation in the metabolic memory associated with continued progression of diabetic retinopathy.* Invest Ophthalmol Vis Sci, 2012. **53**(8): p. 4881-8.
135. Zhao, J., et al., *Transient High Glucose Causes Persistent Vascular Dysfunction and Delayed Wound Healing by the DNMT1-Mediated Ang-1/NF-kappaB Pathway.* J Invest Dermatol, 2021. **141**(6): p. 1573-1584.
136. Pirola, L., et al., *Genome-wide analysis distinguishes hyperglycemia regulated epigenetic signatures of primary vascular cells.* Genome Res, 2011. **21**(10): p. 1601-15.
137. Pepin, M.E., et al., *The human aortic endothelium undergoes dose-dependent DNA methylation in response to transient hyperglycemia.* Exp Cell Res, 2021. **400**(2): p. 112485.
138. Aref-Eshghi, E., et al., *Glucose-induced, duration-dependent genome-wide DNA methylation changes in human endothelial cells.* Am J Physiol Cell Physiol, 2020. **319**(2): p. C268-C276.
139. Ito S, S.L., Dai Q, Wu SC, Collins LB, Swenberg JA, He C, Zhang Y., *Tet proteins can convert 5-methylcytosine to 5-formylcytosine and 5-carboxylcytosine.* Science, 2011. **333**: p. 1300-3.
140. Skvortsova, K., et al., *Comprehensive evaluation of genome-wide 5-hydroxymethylcytosine profiling approaches in human DNA.* Epigenetics Chromatin, 2017. **10**: p. 16.
141. He, B., et al., *Tissue-specific 5-hydroxymethylcytosine landscape of the human genome.* Nat Commun, 2021. **12**(1): p. 4249.
142. Yu, M., et al., *Base-resolution analysis of 5-hydroxymethylcytosine in the mammalian genome.* Cell, 2012. **149**(6): p. 1368-80.
143. Song, C.X., C. Yi, and C. He, *Mapping recently identified nucleotide variants in the genome and transcriptome.* Nat Biotechnol, 2012. **30**(11): p. 1107-16.
144. Song, C.X. and C. He, *Potential functional roles of DNA demethylation intermediates.* Trends Biochem Sci, 2013. **38**(10): p. 480-4.
145. Rasmussen, K.D. and K. Helin, *Role of TET enzymes in DNA methylation, development, and cancer.* Genes Dev, 2016. **30**(7): p. 733-50.
146. Ko, M., et al., *Modulation of TET2 expression and 5-methylcytosine oxidation by the CXXC domain protein IDAX.* Nature, 2013. **497**(7447): p. 122-6.
147. Dawlaty, M.M., et al., *Tet1 is dispensable for maintaining pluripotency and its loss is compatible with embryonic and postnatal development.* Cell Stem Cell, 2011. **9**(2): p. 166-75.
148. Zhang, R.R., et al., *Tet1 regulates adult hippocampal neurogenesis and cognition.* Cell Stem Cell, 2013. **13**(2): p. 237-45.
149. Moran-Crusio, K., et al., *Tet2 loss leads to increased hematopoietic stem cell self-renewal and myeloid transformation.* Cancer Cell, 2011. **20**(1): p. 11-24.
150. Kang, J., et al., *Simultaneous deletion of the methylcytosine oxidases Tet1 and Tet3 increases transcriptome variability in early embryogenesis.* Proc Natl Acad Sci U S A, 2015. **112**(31): p. E4236-45.
151. Gu, T.P., et al., *The role of Tet3 DNA dioxygenase in epigenetic reprogramming by oocytes.* Nature, 2011. **477**(7366): p. 606-10.

152. Dawlaty, M.M., et al., *Combined deficiency of Tet1 and Tet2 causes epigenetic abnormalities but is compatible with postnatal development.* Dev Cell, 2013. **24**(3): p. 310-23.
153. Tan, L. and Y.G. Shi, *Tet family proteins and 5-hydroxymethylcytosine in development and disease.* Development, 2012. **139**(11): p. 1895-902.
154. Li, X., et al., *Neocortical Tet3-mediated accumulation of 5-hydroxymethylcytosine promotes rapid behavioral adaptation.* Proc Natl Acad Sci U S A, 2014. **111**(19): p. 7120-5.
155. Feng, Y., et al., *TET2 Function in Hematopoietic Malignancies, Immune Regulation, and DNA Repair.* Front Oncol, 2019. **9**: p. 210.
156. Jaiswal, S., et al., *Clonal Hematopoiesis and Risk of Atherosclerotic Cardiovascular Disease.* N Engl J Med, 2017. **377**(2): p. 111-121.
157. Fuster, J.J., et al., *Clonal hematopoiesis associated with TET2 deficiency accelerates atherosclerosis development in mice.* Science, 2017. **355**(6327): p. 842-847.
158. Zhang Q, Z.K., Shen Q,Han Y, Gu Y, Li X, Zhao D, Liu Y, Wang C, Zhang X, Su X, Liu J, Ge W, Levine RL, Li N, Cao X, *Tet2 is required to resolve inflammation by recruiting Hdac2 to specifically repress IL-6.* Nature, 2015. **525**(7569): p. 389-393.
159. Cull, A.H., et al., *Tet2 restrains inflammatory gene expression in macrophages.* Exp Hematol, 2017. **55**: p. 56-70 e13.
160. Ma, S., et al., *Epigenetic regulator CXXC5 recruits DNA demethylase Tet2 to regulate TLR7/9-elicited IFN response in pDCs.* J Exp Med, 2017. **214**(5): p. 1471-1491.
161. Montagner, S., et al., *TET2 Regulates Mast Cell Differentiation and Proliferation through Catalytic and Non-catalytic Activities.* Cell Rep, 2016. **15**(7): p. 1566-1579.
162. Tanaka, S., et al., *Tet2 and Tet3 in B cells are required to repress CD86 and prevent autoimmunity.* Nat Immunol, 2020. **21**(8): p. 950-961.
163. Liu, R., et al., *Ten-eleven translocation-2 (TET2) is a master regulator of smooth muscle cell plasticity.* Circulation, 2013. **128**(18): p. 2047-57.
164. Peng, J., et al., *Tet methylcytosine dioxygenase 2 inhibits atherosclerosis via upregulation of autophagy in ApoE-/- mice.* Oncotarget, 2016. **7**(47): p. 76423-76436.
165. Peng, J., et al., *TET2 Protects against oxLDL-Induced HUVEC Dysfunction by Upregulating the CSE/H2S System.* Front Pharmacol, 2017. **8**: p. 486.
166. Niu, Y., et al., *Oxidative stress alters global histone modification and DNA methylation.* Free Radic Biol Med, 2015. **82**: p. 22-8.
167. Minor, E.A., et al., *Ascorbate induces ten-eleven translocation (Tet) methylcytosine dioxygenase-mediated generation of 5-hydroxymethylcytosine.* J Biol Chem, 2013. **288**(19): p. 13669-74.
168. Yin, R., et al., *Ascorbic acid enhances Tet-mediated 5-methylcytosine oxidation and promotes DNA demethylation in mammals.* J Am Chem Soc, 2013. **135**(28): p. 10396-403.
169. Laukka, T., et al., *Fumarate and Succinate Regulate Expression of Hypoxia-inducible Genes via TET Enzymes.* J Biol Chem, 2016. **291**(8): p. 4256-65.
170. Xu, W., et al., *Oncometabolite 2-hydroxyglutarate is a competitive inhibitor of alpha-ketoglutarate-dependent dioxygenases.* Cancer Cell, 2011. **19**(1): p. 17-30.

171. Burr S, C.A., Chong M, Beretta M, Metcalf S, Hancock M, Arno M, Balu S, Leon Kropf V, Mistry RK, Shah AM, Mann GE, Brewer AC., *Oxygen gradients can determine epigenetic asymmetry and cellular differentiation via differential regulation of Tet activity in embryonic stem cells.* Nucleic Acids Research, 2018. **46**(3): p. 1210-1226.
172. Lamadema, N., S. Burr, and A.C. Brewer, *Dynamic regulation of epigenetic demethylation by oxygen availability and cellular redox.* Free Radic Biol Med, 2019. **131**: p. 282-298.
173. Green, H.L.H. and A.C. Brewer, *Dysregulation of 2-oxoglutarate-dependent dioxygenases by hyperglycaemia: does this link diabetes and vascular disease?* Clin Epigenetics, 2020. **12**(1): p. 59.
174. Dobrina, A. and F. Rossi, *Metabolic properties of freshly isolated bovine endothelial cells.* Biochim Biophys Acta, 1983. **762**(2): p. 295-301.
175. Sada, K., et al., *Hyperglycemia Induces Cellular Hypoxia through Production of Mitochondrial ROS Followed by Suppression of Aquaporin-1.* PLoS One, 2016. **11**(7): p. e0158619.
176. La Selva, M., et al., *Thiamine corrects delayed replication and decreases production of lactate and advanced glycation end-products in bovine retinal and human umbilical vein endothelial cells cultured under high glucose conditions.* Diabetologia, 1996. **39**(11): p. 1263-8.
177. Sonveaux, P., et al., *Targeting the lactate transporter MCT1 in endothelial cells inhibits lactate-induced HIF-1 activation and tumor angiogenesis.* PLoS One, 2012. **7**(3): p. e33418.
178. Intlekofer, A.M., et al., *Hypoxia Induces Production of L-2-Hydroxyglutarate.* Cell Metab, 2015. **22**(2): p. 304-11.
179. Alarcon, C., et al., *Succinate is a preferential metabolic stimulus-coupling signal for glucose-induced proinsulin biosynthesis translation.* Diabetes, 2002. **51**(8): p. 2496-504.
180. Zheng, H., et al., *Protein Modifications as Manifestations of Hyperglycemic Glucotoxicity in Diabetes and Its Complications.* Biochem Insights, 2016. **9**: p. 1-9.
181. Camarena, V., et al., *cAMP signaling regulates DNA hydroxymethylation by augmenting the intracellular labile ferrous iron pool.* Elife, 2017. **6**.
182. Deb, D.K., R. Bao, and Y.C. Li, *Critical role of the cAMP-PKA pathway in hyperglycemia-induced epigenetic activation of fibrogenic program in the kidney.* FASEB J, 2017. **31**(5): p. 2065-2075.
183. Wu, D., et al., *Glucose-regulated phosphorylation of TET2 by AMPK reveals a pathway linking diabetes to cancer.* Nature, 2018. **559**(7715): p. 637-641.
184. Neri, F., et al., *Genome-wide analysis identifies a functional association of Tet1 and Polycomb repressive complex 2 in mouse embryonic stem cells.* Genome Biol, 2013. **14**(8): p. R91.
185. Hrit, J., et al., *OGT binds a conserved C-terminal domain of TET1 to regulate TET1 activity and function in development.* Elife, 2018. **7**.
186. Vella, P., et al., *Tet proteins connect the O-linked N-acetylglucosamine transferase Ogt to chromatin in embryonic stem cells.* Mol Cell, 2013. **49**(4): p. 645-56.
187. Zhu, F., et al., *Sin3a-Tet1 interaction activates gene transcription and is required for embryonic stem cell pluripotency.* Nucleic Acids Res, 2018. **46**(12): p. 6026-6040.

188. Yildirim, O., et al., *Mbd3/NURD complex regulates expression of 5-hydroxymethylcytosine marked genes in embryonic stem cells.* Cell, 2011. **147**(7): p. 1498-510.
189. Tsai, Y.P., et al., *TET1 regulates hypoxia-induced epithelial-mesenchymal transition by acting as a co-activator.* Genome Biol, 2014. **15**(12): p. 513.
190. Wang, Y., et al., *WT1 recruits TET2 to regulate its target gene expression and suppress leukemia cell proliferation.* Mol Cell, 2015. **57**(4): p. 662-673.
191. de la Rica, L., et al., *PU.1 target genes undergo Tet2-coupled demethylation and DNMT3b-mediated methylation in monocyte-to-osteoclast differentiation.* Genome Biol, 2013. **14**(9): p. R99.
192. Chen, Q., et al., *TET2 promotes histone O-GlcNAcylation during gene transcription.* Nature, 2013. **493**(7433): p. 561-4.
193. Deplus R, D.B., Schwinn MK, Defrance M, Méndez J, Murphy N, Dawson MA, Volkmar M, Putmans P, Calonne E, Shih AH, Levine RL, Bernard O, Mercher T, Solary E, Urh M, Daniels DL, Fuks F, *TET2 and TET3 regulate GlcNAcylation and H3K4 methylation through OGT and SET1/COMPASS.* EMBO, 2013. **32**(5): p. 645-55.
194. Chu, Y., et al., *Tet2 Regulates Osteoclast Differentiation by Interacting with Runx1 and Maintaining Genomic 5-Hydroxymethylcytosine (5hmC).* Genomics Proteomics Bioinformatics, 2018. **16**(3): p. 172-186.
195. Chen, L.L., et al., *SNIP1 Recruits TET2 to Regulate c-MYC Target Genes and Cellular DNA Damage Response.* Cell Rep, 2018. **25**(6): p. 1485-1500 e4.
196. Jiao, J., et al., *AID and TET2 co-operation modulates FANCA expression by active demethylation in diffuse large B cell lymphoma.* Clin Exp Immunol, 2019. **195**(2): p. 190-201.
197. Xu, Y.P., et al., *Tumor suppressor TET2 promotes cancer immunity and immunotherapy efficacy.* J Clin Invest, 2019. **129**(10): p. 4316-4331.
198. Zhang, Y.W., et al., *Acetylation Enhances TET2 Function in Protecting against Abnormal DNA Methylation during Oxidative Stress.* Mol Cell, 2017. **65**(2): p. 323-335.
199. Jeong, J.J., et al., *Cytokine-Regulated Phosphorylation and Activation of TET2 by JAK2 in Hematopoiesis.* Cancer Discov, 2019. **9**(6): p. 778-795.
200. Li, X., et al., *Ten-eleven translocation 2 interacts with forkhead box O3 and regulates adult neurogenesis.* Nat Commun, 2017. **8**: p. 15903.
201. Perera, A., et al., *TET3 is recruited by REST for context-specific hydroxymethylation and induction of gene expression.* Cell Rep, 2015. **11**(2): p. 283-94.
202. Guan, W., et al., *Methylcytosine dioxygenase TET3 interacts with thyroid hormone nuclear receptors and stabilizes their association to chromatin.* Proc Natl Acad Sci U S A, 2017. **114**(31): p. 8229-8234.
203. Xue, S., et al., *TET3 Inhibits Type I IFN Production Independent of DNA Demethylation.* Cell Rep, 2016. **16**(4): p. 1096-1105.
204. Jaiswal, S., et al., *Age-related clonal hematopoiesis associated with adverse outcomes.* N Engl J Med, 2014. **371**(26): p. 2488-98.
205. Fuster, J.J., et al., *TET2-Loss-of-Function-Driven Clonal Hematopoiesis Exacerbates Experimental Insulin Resistance in Aging and Obesity.* Cell Rep, 2020. **33**(4): p. 108326.
206. Sano S, O.K., Wang Y, MacLauchlan S, Katanasaka Y, Sano M, Zuriaga MA, Yoshiyama M, Goukassian D, Cooper MA, Fuster JJ, Walsh K., *Tet2-mediated Clonal Hematopoiesis Accelerates Heart Failure through a Mechanism*

Involving the IL-1β/NLRP3 Inflammasome. J Am Coll Cardiol, 2019. **71**(8): p. 875–886.
207. Sag, C.M., et al., *Distinct Regulatory Effects of Myeloid Cell and Endothelial Cell NAPDH Oxidase 2 on Blood Pressure.* Circulation, 2017. **135**(22): p. 2163-2177.
208. Li, C., et al., *Overlapping Requirements for Tet2 and Tet3 in Normal Development and Hematopoietic Stem Cell Emergence.* Cell Rep, 2015. **12**(7): p. 1133-43.
209. Cakouros, D., et al., *Specific functions of TET1 and TET2 in regulating mesenchymal cell lineage determination.* Epigenetics Chromatin, 2019. **12**(1): p. 3.
210. Mulholland, C.B., et al., *Distinct and stage-specific contributions of TET1 and TET2 to stepwise cytosine oxidation in the transition from naive to primed pluripotency.* Sci Rep, 2020. **10**(1): p. 12066.
211. Yan, H., et al., *Distinct roles for TET family proteins in regulating human erythropoiesis.* Blood, 2017. **129**(14): p. 2002-2012.
212. Piccolo, F.M., et al., *Different roles for Tet1 and Tet2 proteins in reprogramming-mediated erasure of imprints induced by EGC fusion.* Mol Cell, 2013. **49**(6): p. 1023-33.
213. Melamed, P., et al., *Tet Enzymes, Variants, and Differential Effects on Function.* Front Cell Dev Biol, 2018. **6**: p. 22.
214. Hossian, A., et al., *Advanced bioinformatic analysis and pathway prediction of NSCLC cells upon cisplatin resistance.* Sci Rep, 2021. **11**(1): p. 6520.
215. Shao, Z., et al., *Ingenuity pathway analysis of differentially expressed genes involved in signaling pathways and molecular networks in RhoE geneedited cardiomyocytes.* Int J Mol Med, 2020. **46**(3): p. 1225-1238.
216. Wek, R.C., H.Y. Jiang, and T.G. Anthony, *Coping with stress: eIF2 kinases and translational control.* Biochem Soc Trans, 2006. **34**(Pt 1): p. 7-11.
217. Lee, A.J. and A.A. Ashkar, *The Dual Nature of Type I and Type II Interferons.* Front Immunol, 2018. **9**: p. 2061.
218. McNab, F., et al., *Type I interferons in infectious disease.* Nat Rev Immunol, 2015. **15**(2): p. 87-103.
219. Platanias, L.C., *Mechanisms of type-I- and type-II-interferon-mediated signalling.* Nat Rev Immunol, 2005. **5**(5): p. 375-86.
220. Yang, E. and M.M.H. Li, *All About the RNA: Interferon-Stimulated Genes That Interfere With Viral RNA Processes.* Front Immunol, 2020. **11**: p. 605024.
221. Jia, H., et al., *Endothelial cell functions impaired by interferon in vitro: Insights into the molecular mechanism of thrombotic microangiopathy associated with interferon therapy.* Thromb Res, 2018. **163**: p. 105-116.
222. Battle TE, L.R., Frank DA, *Signal transducer and activator of transcription 1 activation in endothelial cells is a negative regulator of angiogenesis.* Cancer Research, 2006. **66**(7): p. 3649-57.
223. Javanmard, S.H. and N. Dana, *The effect of interferon gamma on endothelial cell nitric oxide production and apoptosis.* Adv Biomed Res, 2012. **1**: p. 69.
224. Ciechanowska, A., et al., *The Effect of High and Variable Glucose on the Viability of Endothelial Cells Co-Cultured with Smooth Muscle Cells.* Int J Mol Sci, 2022. **23**(12).
225. Risso, A., et al., *Intermittent high glucose enhances apoptosis in human umbilical vein endothelial cells in culture.* Am J Physiol Endocrinol Metab, 2001. **281**(5): p. E924-30.

226. Quagliaro, L., et al., *Intermittent high glucose enhances apoptosis related to oxidative stress in human umbilical vein endothelial cells: the role of protein kinase C and NAD(P)H-oxidase activation.* Diabetes, 2003. **52**(11): p. 2795-804.
227. Piconi, L., et al., *Intermittent high glucose enhances ICAM-1, VCAM-1, E-selectin and interleukin-6 expression in human umbilical endothelial cells in culture: the role of poly(ADP-ribose) polymerase.* J Thromb Haemost, 2004. **2**(8): p. 1453-9.
228. Quagliaro, L., et al., *Intermittent high glucose enhances ICAM-1, VCAM-1 and E-selectin expression in human umbilical vein endothelial cells in culture: the distinct role of protein kinase C and mitochondrial superoxide production.* Atherosclerosis, 2005. **183**(2): p. 259-67.
229. Schisano, B., et al., *Glucose oscillations, more than constant high glucose, induce p53 activation and a metabolic memory in human endothelial cells.* Diabetologia, 2011. **54**(5): p. 1219-26.
230. Moss, J.W. and D.P. Ramji, *Interferon-gamma: Promising therapeutic target in atherosclerosis.* World J Exp Med, 2015. **5**(3): p. 154-9.
231. McKellar, G.E., et al., *Role for TNF in atherosclerosis? Lessons from autoimmune disease.* Nat Rev Cardiol, 2009. **6**(6): p. 410-7.
232. Luo, J., H. Yang, and B.L. Song, *Mechanisms and regulation of cholesterol homeostasis.* Nat Rev Mol Cell Biol, 2020. **21**(4): p. 225-245.
233. Ikonen, E., *Cellular cholesterol trafficking and compartmentalization.* Nat Rev Mol Cell Biol, 2008. **9**(2): p. 125-38.
234. Hong, Z., et al., *How cholesterol regulates endothelial biomechanics.* Front Physiol, 2012. **3**: p. 426.
235. Cardoso, D. and E. Perucha, *Cholesterol metabolism: a new molecular switch to control inflammation.* Clin Sci (Lond), 2021. **135**(11): p. 1389-1408.
236. Trindade, B.C., et al., *The cholesterol metabolite 25-hydroxycholesterol restrains the transcriptional regulator SREBP2 and limits intestinal IgA plasma cell differentiation.* Immunity, 2021. **54**(10): p. 2273-2287 e6.
237. Blanc, M., et al., *The transcription factor STAT-1 couples macrophage synthesis of 25-hydroxycholesterol to the interferon antiviral response.* Immunity, 2013. **38**(1): p. 106-18.
238. Liu, S.Y., et al., *Interferon-inducible cholesterol-25-hydroxylase broadly inhibits viral entry by production of 25-hydroxycholesterol.* Immunity, 2013. **38**(1): p. 92-105.
239. Anggakusuma, et al., *Interferon-inducible cholesterol-25-hydroxylase restricts hepatitis C virus replication through blockage of membranous web formation.* Hepatology, 2015. **62**(3): p. 702-14.
240. Kremer, E.A., et al., *Interplay between TETs and microRNAs in the adult brain for memory formation.* Sci Rep, 2018. **8**(1): p. 1678.
241. Cheng, J., et al., *An extensive network of TET2-targeting MicroRNAs regulates malignant hematopoiesis.* Cell Rep, 2013. **5**(2): p. 471-81.
242. Cui, Y., et al., *miR-29 regulates Tet1 expression and contributes to early differentiation of mouse ESCs.* Oncotarget, 2016. **7**(40): p. 64932-64941.
243. Pober, J.S., *Endothelial activation: intracellular signaling pathways.* Arthritis Res, 2002. **4 Suppl 3**: p. S109-16.
244. Popson, S.A., et al., *Interferon-induced transmembrane protein 1 regulates endothelial lumen formation during angiogenesis.* Arterioscler Thromb Vasc Biol, 2014. **34**(5): p. 1011-9.

245. Gonzalez-Amor, M., et al., *Interferon stimulated gene 15 pathway is a novel mediator of endothelial dysfunction and aneurysms development in angiotensin II infused mice through increased oxidative stress.* Cardiovasc Res, 2021.
246. Lee, L.Y., et al., *Interferon-gamma Impairs Human Coronary Artery Endothelial Glucose Metabolism by Tryptophan Catabolism and Activates Fatty Acid Oxidation.* Circulation, 2021. **144**(20): p. 1612-1628.
247. Koziel, A., et al., *The influence of high glucose on the aerobic metabolism of endothelial EA.hy926 cells.* Pflugers Arch, 2012. **464**(6): p. 657-69.
248. Neri, F., et al., *TET1 is controlled by pluripotency-associated factors in ESCs and downmodulated by PRC2 in differentiated cells and tissues.* Nucleic Acids Res, 2015. **43**(14): p. 6814-26.
249. Monnier, L., et al., *Activation of oxidative stress by acute glucose fluctuations compared with sustained chronic hyperglycemia in patients with type 2 diabetes.* JAMA, 2006. **295**(14): p. 1681-7.
250. Torimoto, K., et al., *Relationship between fluctuations in glucose levels measured by continuous glucose monitoring and vascular endothelial dysfunction in type 2 diabetes mellitus.* Cardiovasc Diabetol, 2013. **12**: p. 1.
251. Manea, S.A., A. Manea, and C. Heltianu, *Inhibition of JAK/STAT signaling pathway prevents high-glucose-induced increase in endothelin-1 synthesis in human endothelial cells.* Cell Tissue Res, 2010. **340**(1): p. 71-9.
252. Marrero, M.B., et al., *Role of the JAK/STAT signaling pathway in diabetic nephropathy.* Am J Physiol Renal Physiol, 2006. **290**(4): p. F762-8.
253. Banes-Berceli, A.K., et al., *Angiotensin II and endothelin-1 augment the vascular complications of diabetes via JAK2 activation.* Am J Physiol Heart Circ Physiol, 2007. **293**(2): p. H1291-9.
254. Saez, J.C., et al., *Interferon-gamma and high glucose-induced opening of Cx43 hemichannels causes endothelial cell dysfunction and damage.* Biochim Biophys Acta Mol Cell Res, 2020. **1867**(8): p. 118720.
255. Hassan, H.H., et al., *Cellular cholesterol homeostasis in vascular endothelial cells.* Can J Cardiol, 2006. **22 Suppl B**: p. 35B-40B.
256. Drzewinska, J., A. Walczak-Drzewiecka, and M. Ratajewski, *Identification and analysis of the promoter region of the human DHCR24 gene: involvement of DNA methylation and histone acetylation.* Mol Biol Rep, 2011. **38**(2): p. 1091-101.
257. Nunes, M.J., et al., *Okadaic acid inhibits the trichostatin A-mediated increase of human CYP46A1 neuronal expression in a ERK1/2-Sp3-dependent pathway.* J Lipid Res, 2012. **53**(9): p. 1910-9.
258. Poirier, S., et al., *The epigenetic drug 5-azacytidine interferes with cholesterol and lipid metabolism.* J Biol Chem, 2014. **289**(27): p. 18736-51.
259. Dang, E.V., et al., *Oxysterol Restraint of Cholesterol Synthesis Prevents AIM2 Inflammasome Activation.* Cell, 2017. **171**(5): p. 1057-1071 e11.
260. Xiang, Y., et al., *Identification of Cholesterol 25-Hydroxylase as a Novel Host Restriction Factor and a Part of the Primary Innate Immune Responses against Hepatitis C Virus Infection.* J Virol, 2015. **89**(13): p. 6805-16.
261. Gantier, M.P. and B.R. Williams, *The response of mammalian cells to double-stranded RNA.* Cytokine Growth Factor Rev, 2007. **18**(5-6): p. 363-71.
262. Meng, Z. and M. Lu, *RNA Interference-Induced Innate Immunity, Off-Target Effect, or Immune Adjuvant?* Front Immunol, 2017. **8**: p. 331.

263. Li, Z., et al., *Lipofectamine 2000/siRNA complexes cause endoplasmic reticulum unfolded protein response in human endothelial cells.* J Cell Physiol, 2019. **234**(11): p. 21166-21181.
264. Li, Y., et al., *Cationic liposomes induce cytotoxicity in HepG2 via regulation of lipid metabolism based on whole-transcriptome sequencing analysis.* BMC Pharmacol Toxicol, 2018. **19**(1): p. 43.
265. Wu, H., et al., *Dual functions of Tet1 in transcriptional regulation in mouse embryonic stem cells.* Nature, 2011. **473**(7347): p. 389-93.
266. Morigi M, A.S., Imberti B, Donadelli R, Micheletti G, Figliuzzi M, Remuzzi A, Zoja C, Remuzzi G, *Leukocyte-endothelial interaction is augmented by high glucose concentrations and hyperglycemia in a NF-kB-dependent fashion.* Journal of Clinical Investigation, 1998. **101**(9): p. 1905-15.
267. Pezhman, L., A. Tahrani, and M. Chimen, *Dysregulation of Leukocyte Trafficking in Type 2 Diabetes: Mechanisms and Potential Therapeutic Avenues.* Front Cell Dev Biol, 2021. **9**: p. 624184.
268. Hempel, A., et al., *High glucose concentrations increase endothelial cell permeability via activation of protein kinase C alpha.* Circ Res, 1997. **81**(3): p. 363-71.
269. Shirodkar, A.V., et al., *A mechanistic role for DNA methylation in endothelial cell (EC)-enriched gene expression: relationship with DNA replication timing.* Blood, 2013. **121**(17): p. 3531-40.
270. Mogensen, T.H., *IRF and STAT Transcription Factors - From Basic Biology to Roles in Infection, Protective Immunity, and Primary Immunodeficiencies.* Front Immunol, 2018. **9**: p. 3047.
271. Istvan, E.S., *Structural mechanism for statin inhibition of 3-hydroxy-3-methylglutaryl coenzyme A reductase.* Am Heart J, 2002. **144**(6 Suppl): p. S27-32.
272. Kunimoto, H. and H. Nakajima, *TET2: A cornerstone in normal and malignant hematopoiesis.* Cancer Sci, 2021. **112**(1): p. 31-40.
273. Buscarlet, M., et al., *DNMT3A and TET2 dominate clonal hematopoiesis and demonstrate benign phenotypes and different genetic predispositions.* Blood, 2017. **130**(6): p. 753-762.
274. Zhong, Y., X. Zhang, and W. Chong, *Interleukin-24 Immunobiology and Its Roles in Inflammatory Diseases.* Int J Mol Sci, 2022. **23**(2).
275. Li, X., et al., *Ten-eleven translocation 2 demethylates the MMP9 promoter, and its down-regulation in preeclampsia impairs trophoblast migration and invasion.* J Biol Chem, 2018. **293**(26): p. 10059-10070.
276. Yabluchanskiy, A., et al., *Matrix metalloproteinase-9: Many shades of function in cardiovascular disease.* Physiology (Bethesda), 2013. **28**(6): p. 391-403.
277. Janssens, R., S. Struyf, and P. Proost, *The unique structural and functional features of CXCL12.* Cell Mol Immunol, 2018. **15**(4): p. 299-311.
278. Jamaluddin, M.S., et al., *Resistin: functional roles and therapeutic considerations for cardiovascular disease.* Br J Pharmacol, 2012. **165**(3): p. 622-32.
279. Hamilton, J.A., *GM-CSF in inflammation.* J Exp Med, 2020. **217**(1).
280. Metzemaekers, M., et al., *Overview of the Mechanisms that May Contribute to the Non-Redundant Activities of Interferon-Inducible CXC Chemokine Receptor 3 Ligands.* Front Immunol, 2017. **8**: p. 1970.
281. Rahman, I., et al., *L-selectin regulates human neutrophil transendothelial migration.* J Cell Sci, 2021. **134**(3).

282. Azcutia V, A.-T.M., Romacho T, Vázquez-Bella M, Matesanz N, Luscinskas FW, Rodríguez-Mañas L, Jesús Sanz M, Sánchez-Ferrer CF, Peiró C, *Inflammation Determines the Pro-Adhesive Properties of High Extracellular D-Glucose in Human Endothelial Cells In Vitro and Rat Microvessels In Vivo.* PloS One, 2010. **5**(4): p. e10091.
283. Kim JA, B.J., Natarajan RD, Nadler JL, *Evidence that glucose increases monocyte binding to human aortic endothelial cells.* Diabetes, 1994. **43**(9): p. 1103-7.
284. Altannavch TS, R.K., Kucera P, Andel M, *Effect of high glucose concentrations on expression of ELAM-1, VCAM-1 and ICAM-1 in HUVEC with and without cytokine activation.* Physiological Research, 2004. **53**(1): p. 77-82.
285. Mundi, S., et al., *Endothelial permeability, LDL deposition, and cardiovascular risk factors-a review.* Cardiovasc Res, 2018. **114**(1): p. 35-52.
286. Mani, A.M., et al., *Cholesterol crystals increase vascular permeability by inactivating SHP2 and disrupting adherens junctions.* Free Radic Biol Med, 2018. **123**: p. 72-84.
287. Chen, Q., et al., *Aminophylline modulates the permeability of endothelial cells via the Slit2-Robo4 pathway in lipopolysaccharide-induced inflammation.* Exp Ther Med, 2021. **22**(3): p. 1042.
288. Yuan, S.Y., et al., *Microvascular permeability in diabetes and insulin resistance.* Microcirculation, 2007. **14**(4-5): p. 363-73.
289. Simionescu, M., *Implications of early structural-functional changes in the endothelium for vascular disease.* Arterioscler Thromb Vasc Biol, 2007. **27**(2): p. 266-74.
290. Zhao, X.Y., et al., *Effects of high glucose on human umbilical vein endothelial cell permeability and myosin light chain phosphorylation.* Diabetol Metab Syndr, 2015. **7**: p. 98.
291. Tsujioka, T., et al., *Five-aza-2'-deoxycytidine-induced hypomethylation of cholesterol 25-hydroxylase gene is responsible for cell death of myelodysplasia/leukemia cells.* Sci Rep, 2015. **5**: p. 16709.
292. Huang, Y., et al., *Distinct roles of the methylcytosine oxidases Tet1 and Tet2 in mouse embryonic stem cells.* Proc Natl Acad Sci U S A, 2014. **111**(4): p. 1361-6.
293. Tan, L., et al., *Genome-wide comparison of DNA hydroxymethylation in mouse embryonic stem cells and neural progenitor cells by a new comparative hMeDIP-seq method.* Nucleic Acids Res, 2013. **41**(7): p. e84.
294. Joshi, K., et al., *Mechanisms that regulate the activities of TET proteins.* Cell Mol Life Sci, 2022. **79**(7): p. 363.
295. Perucha, E., et al., *The cholesterol biosynthesis pathway regulates IL-10 expression in human Th1 cells.* Nat Commun, 2019. **10**(1): p. 498.
296. Westerterp, M., et al., *Cholesterol Efflux Pathways Suppress Inflammasome Activation, NETosis, and Atherogenesis.* Circulation, 2018. **138**(9): p. 898-912.
297. de la Roche, M., et al., *Trafficking of cholesterol to the ER is required for NLRP3 inflammasome activation.* J Cell Biol, 2018. **217**(10): p. 3560-3576.
298. Duewell, P., et al., *NLRP3 inflammasomes are required for atherogenesis and activated by cholesterol crystals.* Nature, 2010. **464**(7293): p. 1357-61.
299. Ichiyama, K., et al., *The methylcytosine dioxygenase Tet2 promotes DNA demethylation and activation of cytokine gene expression in T cells.* Immunity, 2015. **42**(4): p. 613-26.

300. Carty, S.A., et al., *The Loss of TET2 Promotes CD8(+) T Cell Memory Differentiation.* J Immunol, 2018. **200**(1): p. 82-91.
301. Szentes, V., et al., *The Role of CXCR3 and Associated Chemokines in the Development of Atherosclerosis and During Myocardial Infarction.* Front Immunol, 2018. **9**: p. 1932.
302. Sawant, K.V., et al., *Chemokine CXCL1 mediated neutrophil recruitment: Role of glycosaminoglycan interactions.* Sci Rep, 2016. **6**: p. 33123.
303. Murao, K., et al., *TNF-alpha stimulation of MCP-1 expression is mediated by the Akt/PKB signal transduction pathway in vascular endothelial cells.* Biochem Biophys Res Commun, 2000. **276**(2): p. 791-6.
304. De Caterina, R., et al., *Induction of endothelial-leukocyte interaction by interferon-gamma requires coactivation of nuclear factor-kappaB.* Arterioscler Thromb Vasc Biol, 2001. **21**(2): p. 227-32.
305. Bednarek, R., *In Vitro Methods for Measuring the Permeability of Cell Monolayers.* Methods Protoc, 2022. **5**(1).
306. Amberg, G.C. and M.F. Navedo, *Calcium dynamics in vascular smooth muscle.* Microcirculation, 2013. **20**(4): p. 281-9.
307. Herrera, M.D., et al., *Endothelial dysfunction and aging: an update.* Ageing Res Rev, 2010. **9**(2): p. 142-52.
308. Grauen Larsen, H., et al., *High Plasma sRAGE (Soluble Receptor for Advanced Glycation End Products) Is Associated With Slower Carotid Intima-Media Thickness Progression and Lower Risk for First-Time Coronary Events and Mortality.* Arterioscler Thromb Vasc Biol, 2019. **39**(5): p. 925-933.
309. Bazan, J.F., et al., *A new class of membrane-bound chemokine with a CX3C motif.* Nature, 1997. **385**(6617): p. 640-4.
310. Parolini, S., et al., *The role of chemerin in the colocalization of NK and dendritic cell subsets into inflamed tissues.* Blood, 2007. **109**(9): p. 3625-32.
311. Tsapogas, P., et al., *The Cytokine Flt3-Ligand in Normal and Malignant Hematopoiesis.* Int J Mol Sci, 2017. **18**(6).
312. Walia, A., et al., *Endostatin's emerging roles in angiogenesis, lymphangiogenesis, disease, and clinical applications.* Biochim Biophys Acta, 2015. **1850**(12): p. 2422-38.
313. Lin, S., et al., *Development of high fat diet-induced obesity and leptin resistance in C57Bl/6J mice.* Int J Obes Relat Metab Disord, 2000. **24**(5): p. 639-46.
314. Yang, Q., et al., *Serum retinol binding protein 4 contributes to insulin resistance in obesity and type 2 diabetes.* Nature, 2005. **436**(7049): p. 356-62.
315. Kahles, F., H.M. Findeisen, and D. Bruemmer, *Osteopontin: A novel regulator at the cross roads of inflammation, obesity and diabetes.* Mol Metab, 2014. **3**(4): p. 384-93.
316. Ivetic, A., H.L.H. Green, and S.J. Hart, *L-selectin: A Major Regulator of Leukocyte Adhesion, Migration and Signaling.* Front Immunol, 2019. **10**: p. 1068.
317. Heydemann, A., *An Overview of Murine High Fat Diet as a Model for Type 2 Diabetes Mellitus.* J Diabetes Res, 2016. **2016**: p. 2902351.
318. Furman, B.L., *Streptozotocin-Induced Diabetic Models in Mice and Rats.* Curr Protoc Pharmacol, 2015. **70**: p. 5 47 1-5 47 20.
319. Lang, P., et al., *Effects of different diets used in diet-induced obesity models on insulin resistance and vascular dysfunction in C57BL/6 mice.* Sci Rep, 2019. **9**(1): p. 19556.

320. Victorio, J.A., et al., *Effects of High-Fat and High-Fat/High-Sucrose Diet-Induced Obesity on PVAT Modulation of Vascular Function in Male and Female Mice.* Front Pharmacol, 2021. **12**: p. 720224.
321. Calligaris, S.D., et al., *Mice long-term high-fat diet feeding recapitulates human cardiovascular alterations: an animal model to study the early phases of diabetic cardiomyopathy.* PLoS One, 2013. **8**(4): p. e60931.
322. Pinho-Gomes, A.C., et al., *Sex differences in prevalence, treatment and control of cardiovascular risk factors in England.* Heart, 2020.
323. de Ritter, R., et al., *Sex differences in the risk of vascular disease associated with diabetes.* Biol Sex Differ, 2020. **11**(1): p. 1.
324. Shi, J., et al., *Cytokines and Abnormal Glucose and Lipid Metabolism.* Front Endocrinol (Lausanne), 2019. **10**: p. 703.
325. Goldberg, R.B., *Cytokine and cytokine-like inflammation markers, endothelial dysfunction, and imbalanced coagulation in development of diabetes and its complications.* J Clin Endocrinol Metab, 2009. **94**(9): p. 3171-82.
326. Spranger, J., et al., *Inflammatory cytokines and the risk to develop type 2 diabetes: results of the prospective population-based European Prospective Investigation into Cancer and Nutrition (EPIC)-Potsdam Study.* Diabetes, 2003. **52**(3): p. 812-7.
327. Considine, R.V., et al., *Serum immunoreactive-leptin concentrations in normal-weight and obese humans.* N Engl J Med, 1996. **334**(5): p. 292-5.
328. Jamroz-Wisniewska, A., et al., *Leptin-induced endothelium-dependent vasorelaxation of peripheral arteries in lean and obese rats: role of nitric oxide and hydrogen sulfide.* PLoS One, 2014. **9**(1): p. e86744.
329. Benkhoff, S., et al., *Leptin potentiates endothelium-dependent relaxation by inducing endothelial expression of neuronal NO synthase.* Arterioscler Thromb Vasc Biol, 2012. **32**(7): p. 1605-12.
330. Radu, M. and J. Chernoff, *An in vivo assay to test blood vessel permeability.* J Vis Exp, 2013(73): p. e50062.
331. Brash, J.T., C. Ruhrberg, and A. Fantin, *Evaluating Vascular Hyperpermeability-inducing Agents in the Skin with the Miles Assay.* J Vis Exp, 2018(136).
332. Tahergorabi, Z. and M. Khazaei, *Imbalance of angiogenesis in diabetic complications: the mechanisms.* Int J Prev Med, 2012. **3**(12): p. 827-38.
333. Hu, R., et al., *Effect of high glucose on cytokine production by human peripheral blood immune cells and type I interferon signaling in monocytes: Implications for the role of hyperglycemia in the diabetes inflammatory process and host defense against infection.* Clin Immunol, 2018. **195**: p. 139-148.
334. Valinluck, V. and L.C. Sowers, *Endogenous cytosine damage products alter the site selectivity of human DNA maintenance methyltransferase DNMT1.* Cancer Res, 2007. **67**(3): p. 946-50.
335. He, Y.F., et al., *Tet-mediated formation of 5-carboxylcytosine and its excision by TDG in mammalian DNA.* Science, 2011. **333**(6047): p. 1303-7.
336. Cui, X.L., et al., *A human tissue map of 5-hydroxymethylcytosines exhibits tissue specificity through gene and enhancer modulation.* Nat Commun, 2020. **11**(1): p. 6161.
337. Williams, K., et al., *TET1 and hydroxymethylcytosine in transcription and DNA methylation fidelity.* Nature, 2011. **473**(7347): p. 343-8.

338. Rauluseviciute, I., F. Drablos, and M.B. Rye, *DNA hypermethylation associated with upregulated gene expression in prostate cancer demonstrates the diversity of epigenetic regulation.* BMC Med Genomics, 2020. **13**(1): p. 6.
339. Wan, J., et al., *Characterization of tissue-specific differential DNA methylation suggests distinct modes of positive and negative gene expression regulation.* BMC Genomics, 2015. **16**: p. 49.
340. Yin, Y., et al., *Impact of cytosine methylation on DNA binding specificities of human transcription factors.* Science, 2017. **356**(6337).
341. Hu, S., et al., *DNA methylation presents distinct binding sites for human transcription factors.* Elife, 2013. **2**: p. e00726.
342. Nestor, C.E., et al., *Tissue type is a major modifier of the 5-hydroxymethylcytosine content of human genes.* Genome Res, 2012. **22**(3): p. 467-77.
343. Wu, H., et al., *Genome-wide analysis of 5-hydroxymethylcytosine distribution reveals its dual function in transcriptional regulation in mouse embryonic stem cells.* Genes Dev, 2011. **25**(7): p. 679-84.
344. Lavender, P., et al., *CRISPR-based reagents to study the influence of the epigenome on gene expression.* Clin Exp Immunol, 2018. **194**(1): p. 9-16.
345. Zhu, C., et al., *Single-Cell 5-Formylcytosine Landscapes of Mammalian Early Embryos and ESCs at Single-Base Resolution.* Cell Stem Cell, 2017. **20**(5): p. 720-731 e5.
346. Eleftheriou, M., et al., *5-Carboxylcytosine levels are elevated in human breast cancers and gliomas.* Clin Epigenetics, 2015. **7**: p. 88.
347. Kellinger, M.W., et al., *5-formylcytosine and 5-carboxylcytosine reduce the rate and substrate specificity of RNA polymerase II transcription.* Nat Struct Mol Biol, 2012. **19**(8): p. 831-3.
348. Spruijt, C.G., et al., *Dynamic readers for 5-(hydroxy)methylcytosine and its oxidized derivatives.* Cell, 2013. **152**(5): p. 1146-59.
349. Iurlaro, M., et al., *A screen for hydroxymethylcytosine and formylcytosine binding proteins suggests functions in transcription and chromatin regulation.* Genome Biol, 2013. **14**(10): p. R119.
350. Fu, T., et al., *Thymine DNA glycosylase recognizes the geometry alteration of minor grooves induced by 5-formylcytosine and 5-carboxylcytosine.* Chem Sci, 2019. **10**(31): p. 7407-7417.
351. Ko, M., et al., *Impaired hydroxylation of 5-methylcytosine in myeloid cancers with mutant TET2.* Nature, 2010. **468**(7325): p. 839-43.
352. Cobo, I., et al., *DNA methyltransferase 3 alpha and TET methylcytosine dioxygenase 2 restrain mitochondrial DNA-mediated interferon signaling in macrophages.* Immunity, 2022. **55**(8): p. 1386-1401 e10.
353. Busque, L., et al., *Recurrent somatic TET2 mutations in normal elderly individuals with clonal hematopoiesis.* Nat Genet, 2012. **44**(11): p. 1179-81.
354. Chen, H.J., S.W. Tas, and M.P.J. de Winther, *Type-I interferons in atherosclerosis.* J Exp Med, 2020. **217**(1).
355. Jones Buie, J.N. and J.C. Oates, *Role of interferon alpha in endothelial dysfunction: insights into endothelial nitric oxide synthase-related mechanisms.* Am J Med Sci, 2014. **348**(2): p. 168-75.
356. Zernecke, A., E. Shagdarsuren, and C. Weber, *Chemokines in atherosclerosis: an update.* Arterioscler Thromb Vasc Biol, 2008. **28**(11): p. 1897-908.
357. Segers, D., et al., *Atherosclerotic Plaque Stability Is Affected by the Chemokine CXCL10 in Both Mice and Humans.* Int J Inflam, 2011. **2011**: p. 936109.

358. Saigusa, R., H. Winkels, and K. Ley, *T cell subsets and functions in atherosclerosis.* Nat Rev Cardiol, 2020. **17**(7): p. 387-401.
359. Lupieri, A., et al., *Smooth muscle cells-derived CXCL10 prevents endothelial healing through PI3Kgamma-dependent T cells response.* Cardiovasc Res, 2020. **116**(2): p. 438-449.
360. Heller, E.A., et al., *Chemokine CXCL10 promotes atherogenesis by modulating the local balance of effector and regulatory T cells.* Circulation, 2006. **113**(19): p. 2301-12.
361. van Wanrooij, E.J., et al., *CXCR3 antagonist NBI-74330 attenuates atherosclerotic plaque formation in LDL receptor-deficient mice.* Arterioscler Thromb Vasc Biol, 2008. **28**(2): p. 251-7.
362. Altara, R., et al., *Emerging importance of chemokine receptor CXCR3 and its ligands in cardiovascular diseases.* Clin Sci (Lond), 2016. **130**(7): p. 463-78.
363. Valenzuela, N.M., *IFNgamma, and to a Lesser Extent TNFalpha, Provokes a Sustained Endothelial Costimulatory Phenotype.* Front Immunol, 2021. **12**: p. 648946.
364. Valenzuela, N.M., *Late phase endothelial cell inflammation is characterized by interferon response genes and driven by JAK/STAT, not NFkappaB.* Vascul Pharmacol, 2022. **146**: p. 107090.
365. Farina, M., et al., *Comparative Mutational Profiling of Hematopoietic Progenitor Cells and Circulating Endothelial Cells (CECs) in Patients with Primary Myelofibrosis.* Cells, 2021. **10**(10).
366. Chambers, S.E.J., et al., *Current concepts on endothelial stem cells definition, location, and markers.* Stem Cells Transl Med, 2021. **10 Suppl 2**(Suppl 2): p. S54-S61.
367. Baumer, Y., et al., *Hyperlipidemia-induced cholesterol crystal production by endothelial cells promotes atherogenesis.* Nat Commun, 2017. **8**(1): p. 1129.
368. Blanc, M., et al., *Host defense against viral infection involves interferon mediated down-regulation of sterol biosynthesis.* PLoS Biol, 2011. **9**(3): p. e1000598.
369. Zhou, Q.D., et al., *Interferon-mediated reprogramming of membrane cholesterol to evade bacterial toxins.* Nat Immunol, 2020. **21**(7): p. 746-755.
370. Fowler, J.W.M., et al., *Inflammatory stress signaling via NF-kB alters accessible cholesterol to upregulate SREBP2 transcriptional activity in endothelial cells.* Elife, 2022. **11**.
371. Hedman, A.K., et al., *Epigenetic Patterns in Blood Associated With Lipid Traits Predict Incident Coronary Heart Disease Events and Are Enriched for Results From Genome-Wide Association Studies.* Circ Cardiovasc Genet, 2017. **10**(1): p. e001487.
372. Pfeiffer, L., et al., *DNA methylation of lipid-related genes affects blood lipid levels.* Circ Cardiovasc Genet, 2015. **8**(2): p. 334-42.
373. Campanella, G., et al., *Epigenome-wide association study of adiposity and future risk of obesity-related diseases.* Int J Obes (Lond), 2018. **42**(12): p. 2022-2035.
374. Sun, M., et al., *The effect of cellular cholesterol on membrane-cytoskeleton adhesion.* J Cell Sci, 2007. **120**(Pt 13): p. 2223-31.
375. Byfield, F.J., et al., *Cholesterol depletion increases membrane stiffness of aortic endothelial cells.* Biophys J, 2004. **87**(5): p. 3336-43.
376. Magalhaes, A., et al., *LDL-Cholesterol Increases the Transcytosis of Molecules through Endothelial Monolayers.* PLoS One, 2016. **11**(10): p. e0163988.

377. van Nieuw Amerongen, G.P., et al., *Simvastatin improves disturbed endothelial barrier function.* Circulation, 2000. **102**(23): p. 2803-9.
378. Chen, W., et al., *Endothelial cell barrier protection by simvastatin: GTPase regulation and NADPH oxidase inhibition.* Am J Physiol Lung Cell Mol Physiol, 2008. **295**(4): p. L575-83.
379. Wilkins, C., et al., *IFITM1 is a tight junction protein that inhibits hepatitis C virus entry.* Hepatology, 2013. **57**(2): p. 461-9.
380. Dunn, J., et al., *Flow-dependent epigenetic DNA methylation regulates endothelial gene expression and atherosclerosis.* J Clin Invest, 2014. **124**(7): p. 3187-99.